Towards Voltage-Gated Ion Channels Synthesized by Solid-Phase Organic Synthesis

by

Horace Luong
B.Sc., Dalhousie University, 2003

A Dissertation Submitted in Partial Fulfillment of the

Requirements for the Degree of

DOCTOR OF PHILOSOPHY

in the Department of Chemistry

Supervisory Committee

Towards Voltage-Gated Ion Channels Synthesized by Solid-Phase Organic Synthesis

by

Horace Luong
B.Sc., Dalhousie University, 2003

Supervisory Committee

Dr. Tom Fyles (Department of Chemistry)

Supervisor

Dr. Robin Hicks (Department of Chemistry)

Departmental Member

Dr. Matt Moffitt (Department of Chemistry)

Departmental Member

Dr. Alisdair Boraston (Department of Biochemistry and Microbiology)

Outside Member

Dr. Jeffery Davis (University of Maryland, Department of Chemistry and Biochemistry)

External Examiner

Supervisory Committee
Dr. Tom Fyles (Department of Chemistry)
Supervisor
Dr. Robin Hicks (Department of Chemistry)
Departmental Member
Dr. Matt Moffitt (Department of Chemistry)
Departmental Member
Dr.Alisdair Boraston (Department of Biochemistry and Microbiology)
Outside Member
Dr. Jeffery Davis (University of Maryland, Department of Chemistry and Biochemistry)
External Examiner

Abstract

The goal of this thesis was to develop a method for efficiently synthesizing a large suite of asymmetric oligoester ion channel-forming compounds. A solid-phase organic synthesis (SPOS) approach on Wang resin was used to generate the ion channel candidates. A follow-on goal is to survey the compounds produced to uncover structure-related controls on ion transport activity.

Two classes of building blocks were used to generate the oligoesters – head groups and cores. The core building blocks were three ω-hydroxy acid derivatives six, eight and twelve carbons in length and the alcohol protected as a tetrahydropyranyl ether. The head group building blocks were either a glutaric acid monoester derivative of varying lipophilicity (12 to 16 carbon long alkyl tail) or a β-hydroxy acid derivative; these building blocks used a *tert*-butyldimethylsilyl ether for alcohol protection.

Optimized conditions for building block coupling, deprotection, and product cleavage were first established by the generation of dimeric and trimeric products. The building blocks were coupled using diisopropylcarbodiimide/ dimethylaminopyridine conditions. The deprotection of the tetrahydropyranyl ether group from the alcohol used a dilute acid solution in methanol and dichloromethane. A fluoride solution (from tetrabutylammonium fluoride) in tetrahydrofuran was used to deprotect the *tert*-butyldimethylsilyl ether group. Cleavage of the product synthesized on Wang resin was achieved by treatment with a trifluoroacetic acid/dichloromethane or ethereal hydrogen chloride solution. The products were then isolated by gel filtration. Mass spectrometry

was used to identify the minor impurities which were quantified by proton nuclear magnetic resonance integrations.

With the nine building blocks, many tetrameric and pentameric structures can be made, but a directed-library approach was used to address structure-activity related questions. Three pentameric oligoester products were the largest products synthesized to determine the scope and limitations of the SPOS methodology.

The oligoester ion channel candidates were tested for ion transport activity using a 8-hydroxypyrene-1,3,6-trisulfonic acid trisodium salt fluorescence vesicle assay. For each compound a pseudo-first order rate constant was derived at a particular concentration. A more useful normalized rate constant was calculated for an interpolated transporter concentration which allowed for transport activity comparison between compounds. The results from the fluorescence assay showed that some compounds and some isomers were substantially more active than others. There appeared to be an optimal core length and lipophilicity for relatively high activity. The aggregation of the compounds in buffer solution was probed using a pyrene fluorescence experiment.

The solid-phase methodology was extended to include coupling of amino acids. A tryptophan derivative was made from one of the most active SPOS oligoester ion channel-forming compounds. The integrity of the molecules synthesized by SPOS which contain the tryptophan group could then be determined by high performance liquid chromatography. The fluorescence of the indole is quenched by acrylamide. By first equilibrating the vesicles with the tryptophan-containing oligoesters and then adding a fluorescence quencher, the resulting indole fluorescence was monitored as a function of quencher concentration. A Stern-Volmer plot was derived based on the quenching data which reported the possible orientations of the tryptophan-containing oligoester within the vesicle.

Table of Contents

List of Tables

List of Figures

List of Schemes

List of Abbreviations

ANTS	8-aminonaphthalene-1,3,6-trisulfonic acid
BPAA	4-biphenylacetic acid
br	broad
CF	5(6)-carboxyfluorescein
d	doublet
DHP	3,4 dihydro-2H-pyran
DIC	diisopropylcarbodiimide
DMAP	4-dimethylaminopyridine
DPX	*p*-xylene-bis-pyridinium bromide
Fmoc	9-fluorenylmethyl carbamate
FT	fourier transform
HPLC	high performance liquid chromatography
HPTS	8-hydroxy-1,3,6-pyrene trisulfonate
HREIMS	high resolution electron ionization mass spectrum
HRLSIMS	high resolution liquid secondary ion mass spectrum
IR	infrared
k	rate constant
$k_{32\ \mu M}$	normalized rate constant at 32 µM
$k_{[x]}$	rate constant for a particular concentration of transporter x
LSIMS	liquid secondary ion mass spectrum
LUV	large unilamellar vesicle
m	multiplet
m_s	slope of a linear function
m-CPBA	*meta*-chloroperoxybenzoic acid
MALDI	matrix-assisted laser desorption/ionization
MeOH	methanol
MS	mass spectrum
NMR	nuclear magnetic resonance

mNBA	*m*-nitrobenzyl alcohol
m/z	mass to charge ratio
PA	phosphatidic acid
PC	phosphatidyl choline
s	singlet
SPOS	solid-phase organic synthesis
t	triplet
TBAF	tetrabutylammonium fluoride
TBDMS	*tert*-butyl dimethylsilyl
TFA	trifluoroacetic acid
THF	tetrahydrofuran
THP	tetrahydropyranyl
TLC	thin layer chromatography
Tr	ion transporter
Trp	tryptophan
p-TsOH	*p*-toluenesulfonic acid
p-TsCl	*p*-toluenesulfonyl chloride
UV	ultraviolet
[x]	a particular concentration of transporter x

List of Numbered Compounds

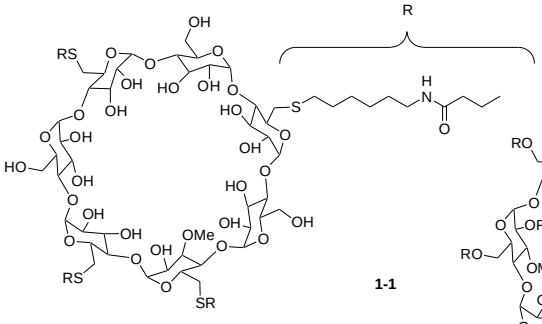

1-1

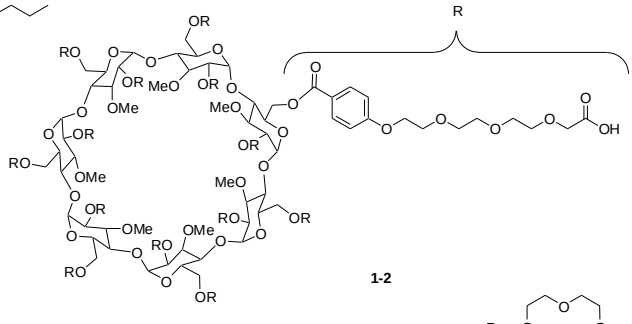

1-2

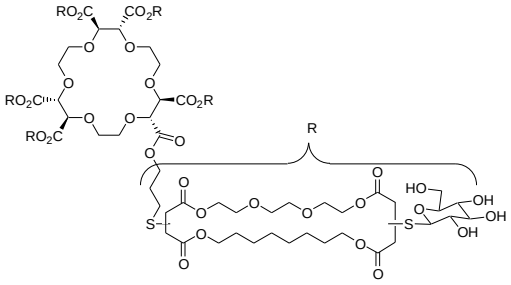

1 - 4

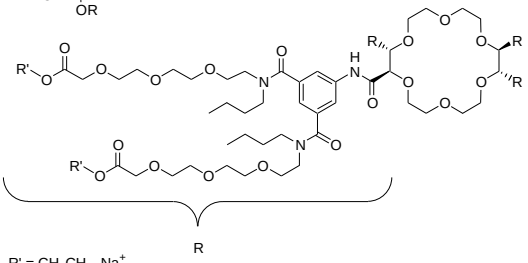

R' = CH_2CH_3, Na^+

1-3

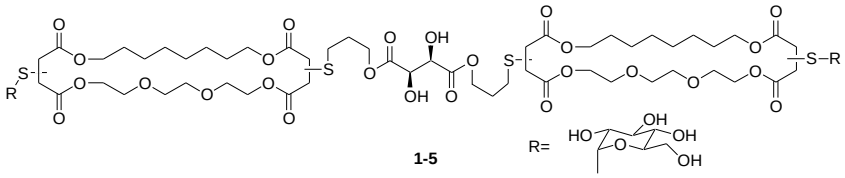

1-5

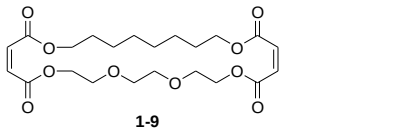

1-9

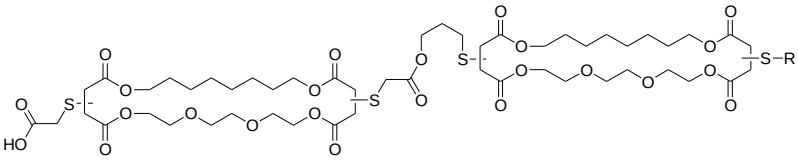

R= CO_2H NMe_2

1- 6 **1- 8** **1-7**

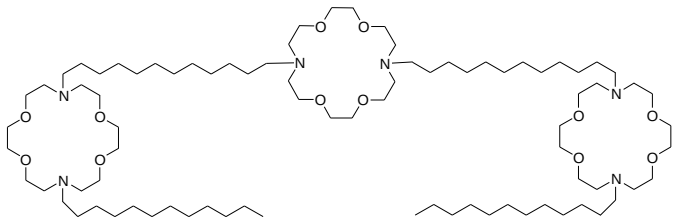

1 - 10

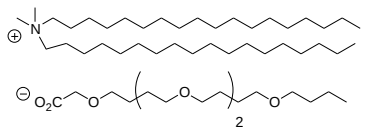

1-13

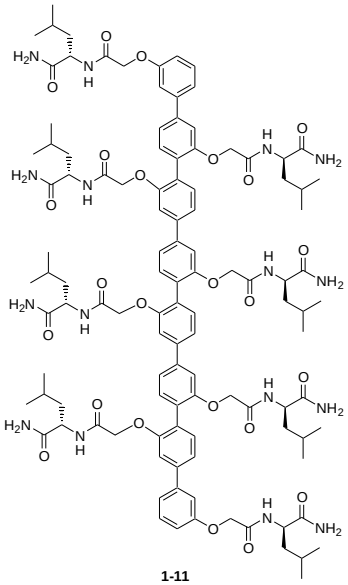

1-11

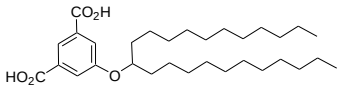

1-14

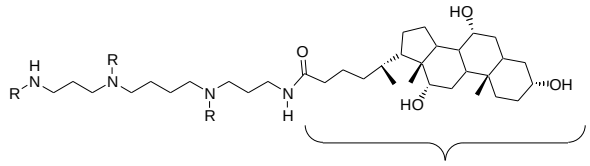

1-15

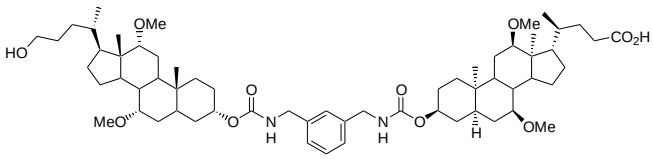

1- 16

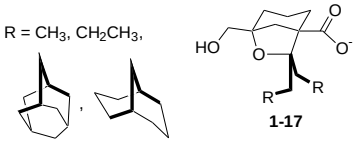

1-17

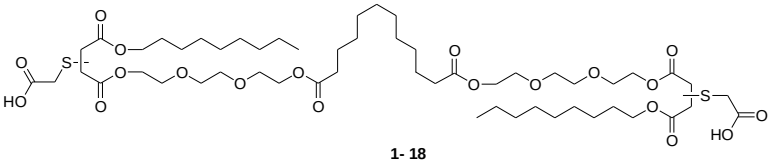

1- 18

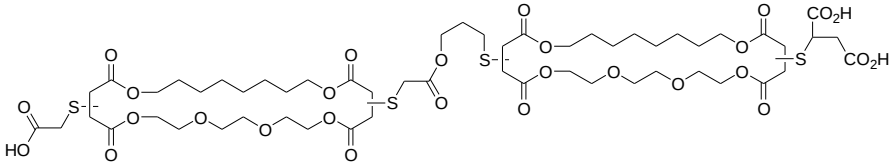

1- 19

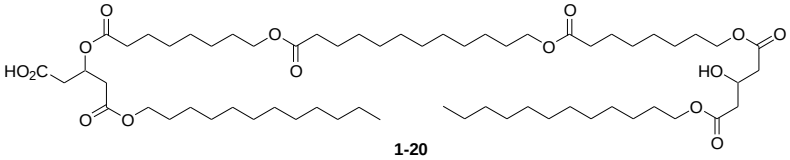

1-20

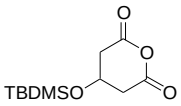

2-1

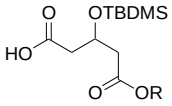

	R
2-2	$C_{10}H_{21}$
2-3	$C_{12}H_{25}$
2-4	$C_{14}H_{29}$
2-5	$C_{16}H_{33}$

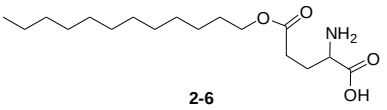

2-6

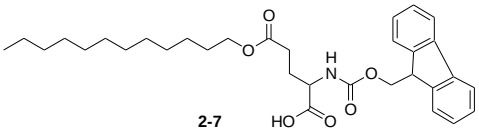

2-7

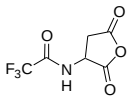

2-8

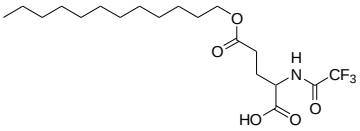

2-11

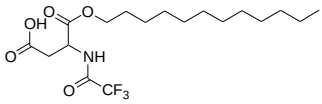

2-9

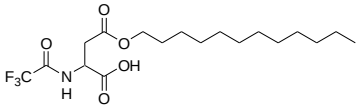

2-10

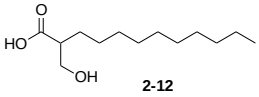

2-12

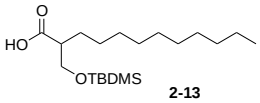

2-13

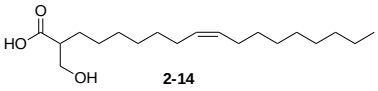

2-14

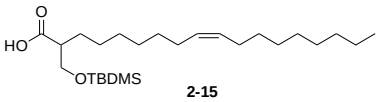

2-15

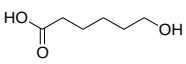

2-16

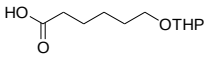

2-17

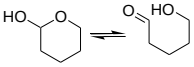

2-18

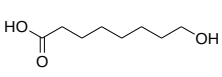

2-19

2-20

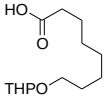

2-21

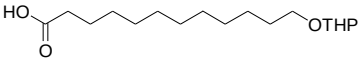

2-22

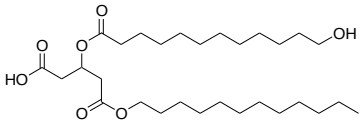

2-23

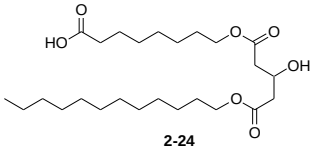

2-24

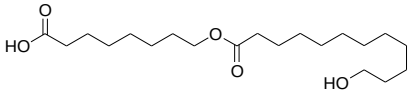

2-25

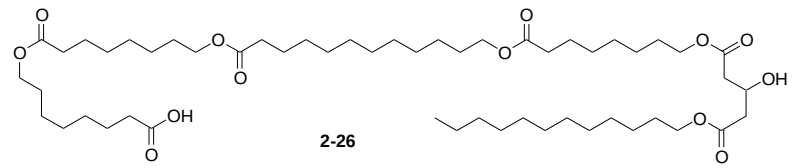

2-26

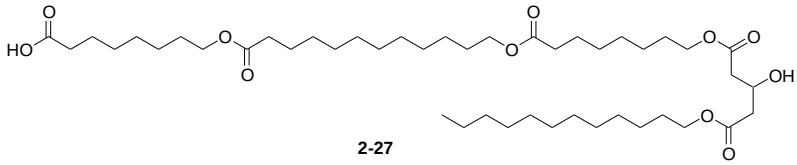

2-27

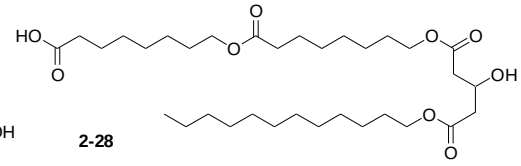

2-28

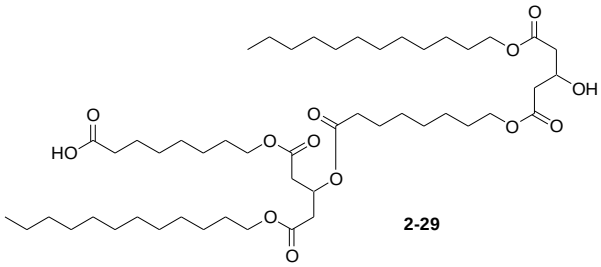

2-29

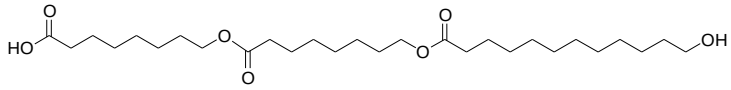

2-30

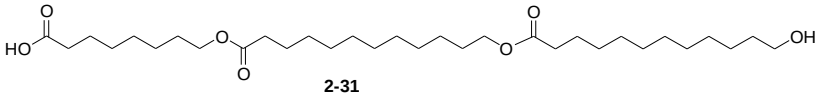

2-31

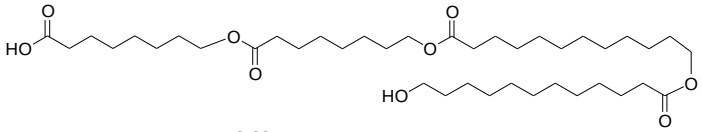

2-32

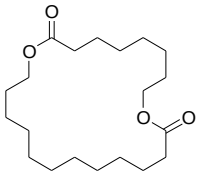

2-33

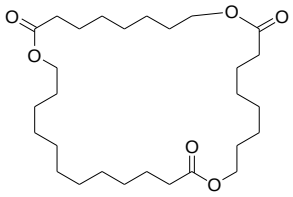

2-34

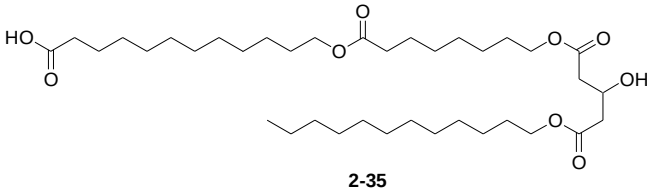

2-35

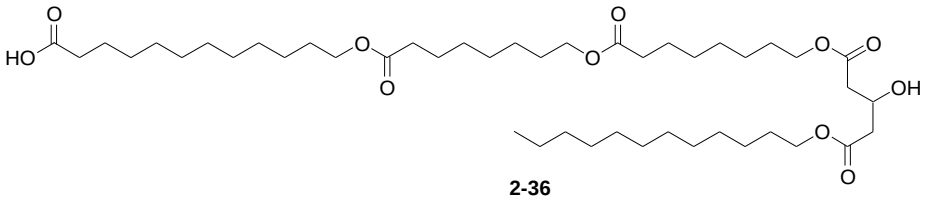

2-36

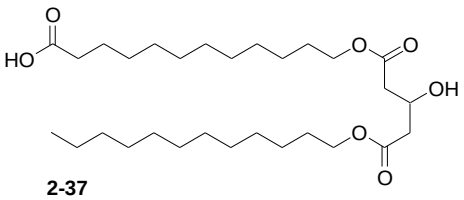

2-37

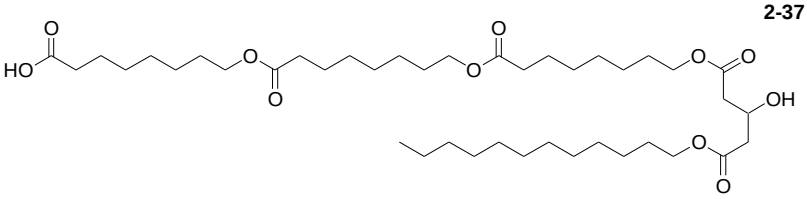

2-38

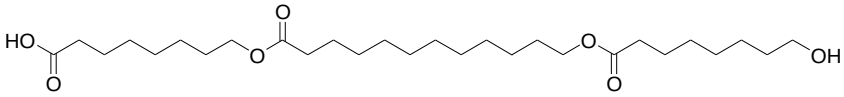

2-39

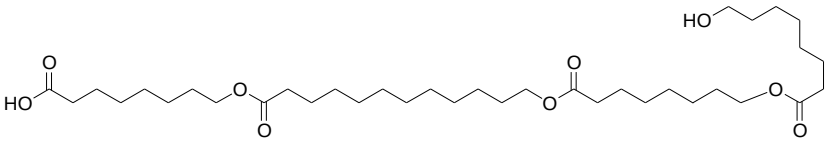

2-40

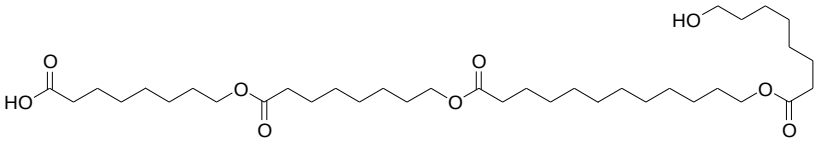

2-41

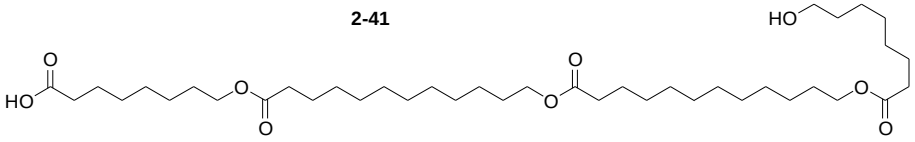

2-42

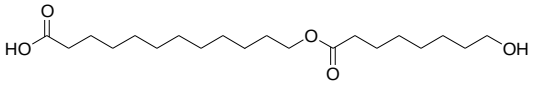

2-43

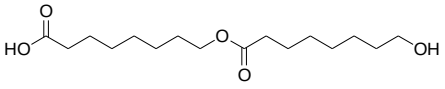

2-44

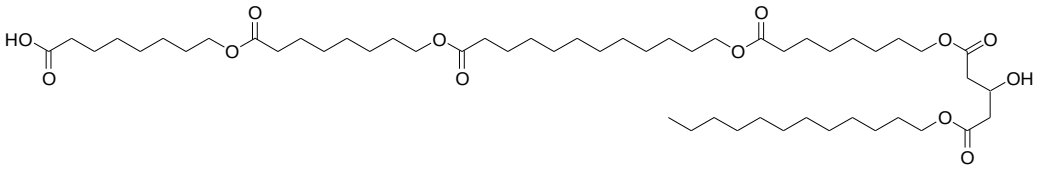

2-45

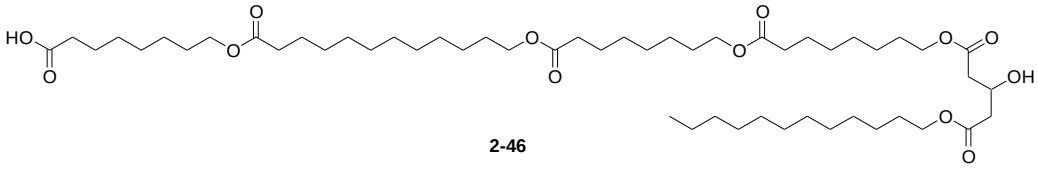

2-46

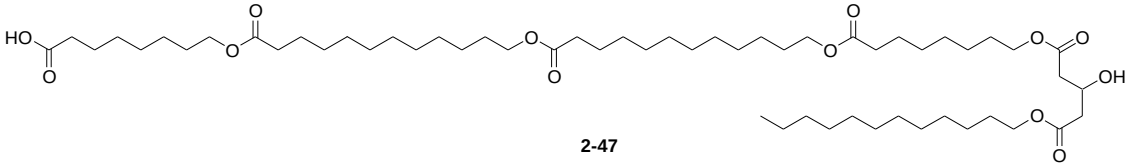

2-47

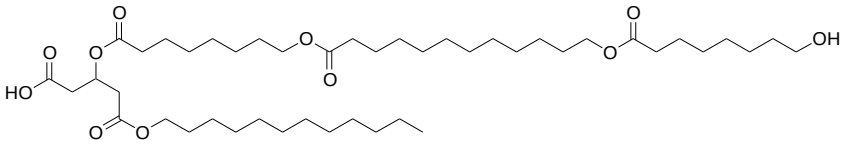

2-48

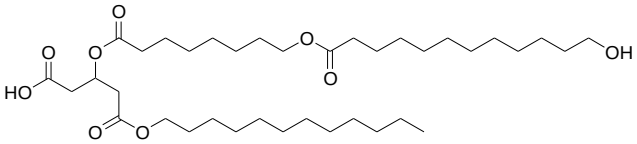

2-49

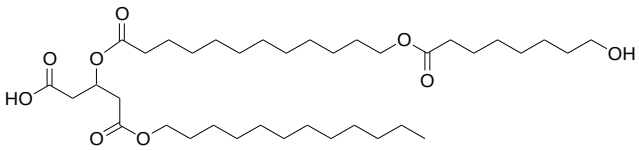

2-50

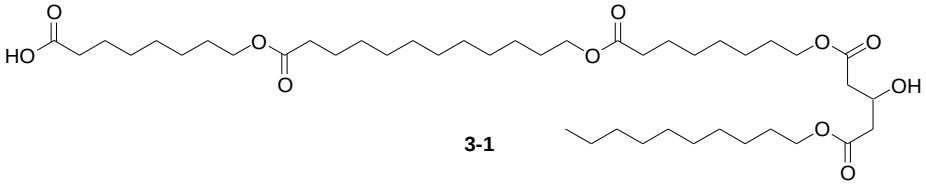

3-1

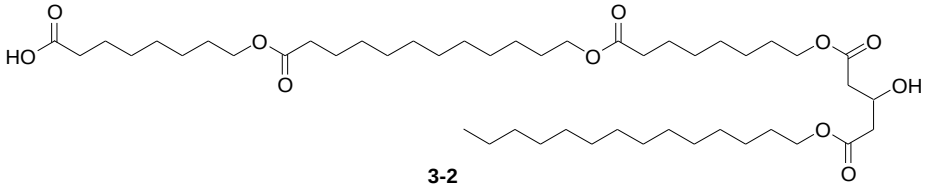

3-2

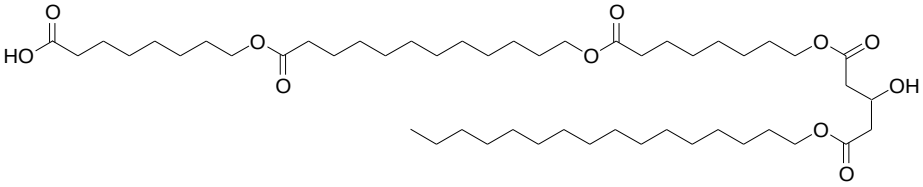

3-3

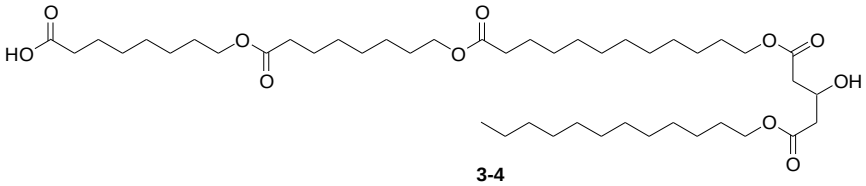

3-4

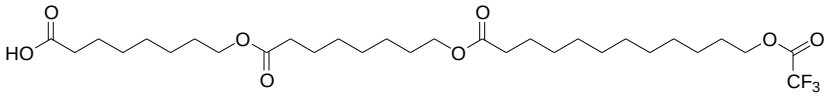

3-5

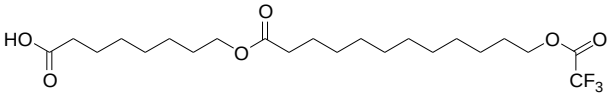

3-6

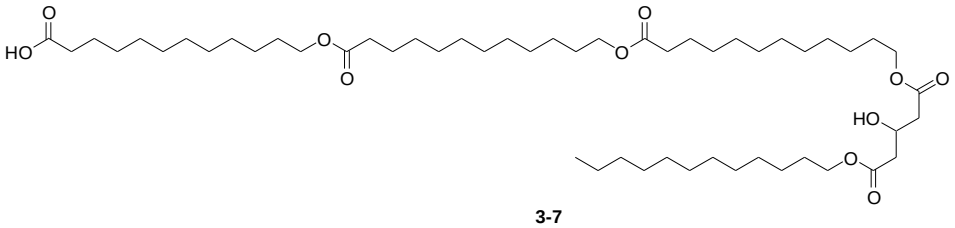

3-7

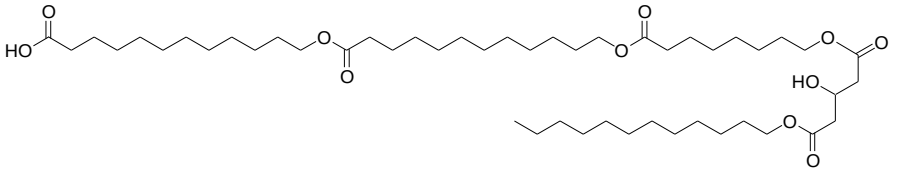

3-8

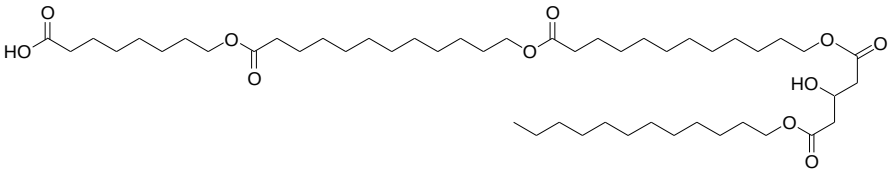

3-9

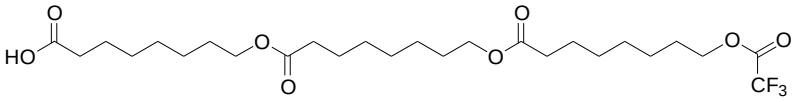

3-10

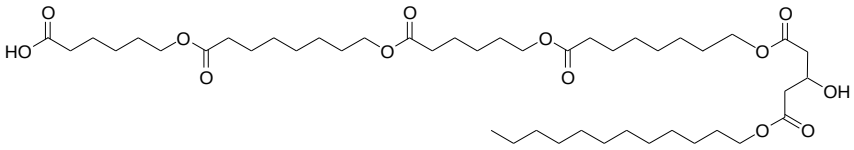

3-11

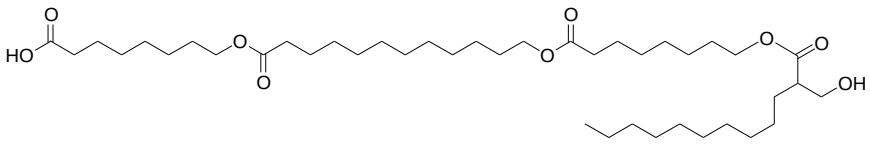

3-12

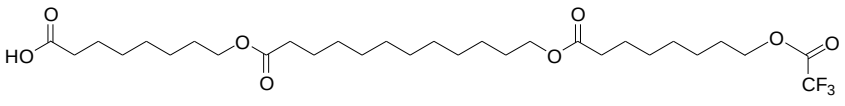

3-13

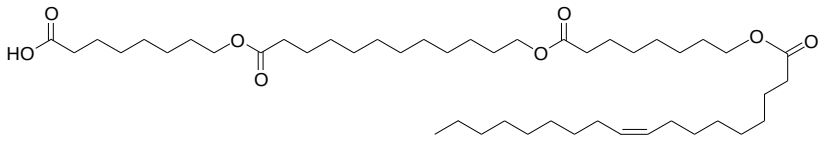

3-14

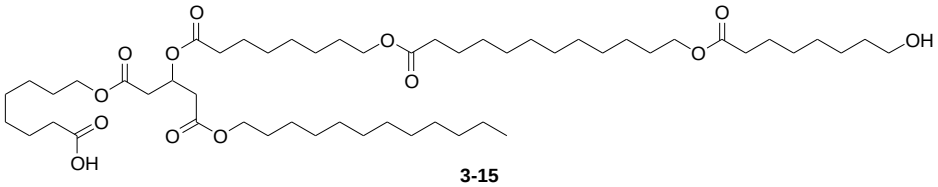

3-15

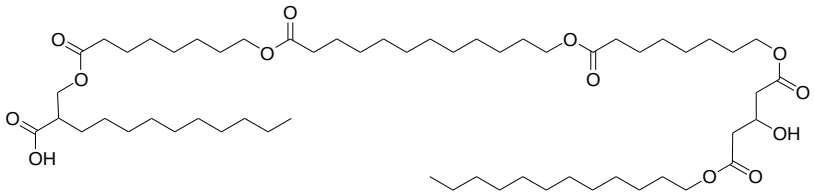

3-16

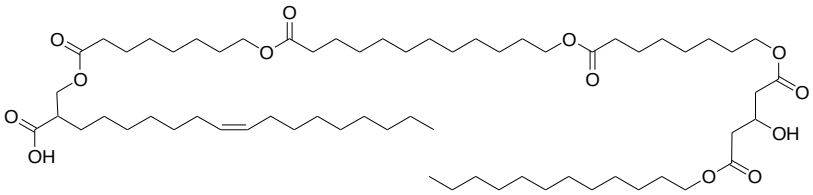

3-17

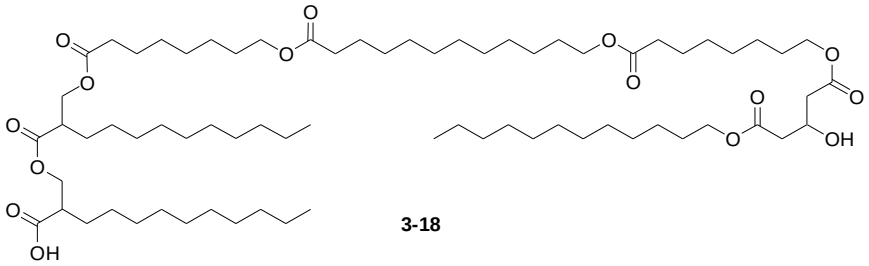

3-18

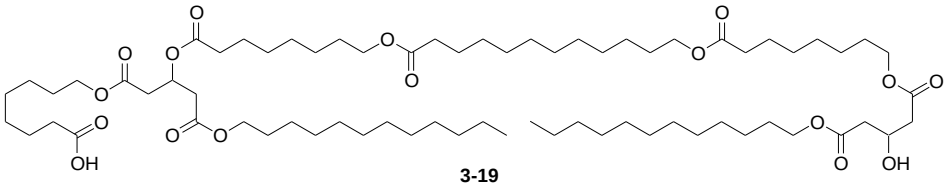

3-19

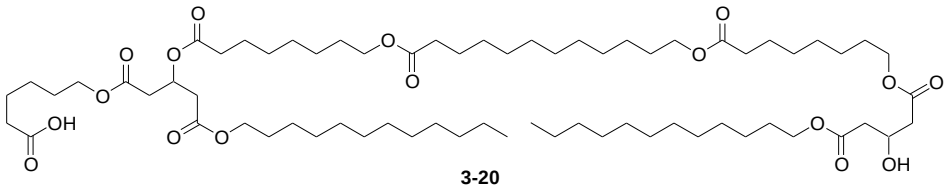

3-20

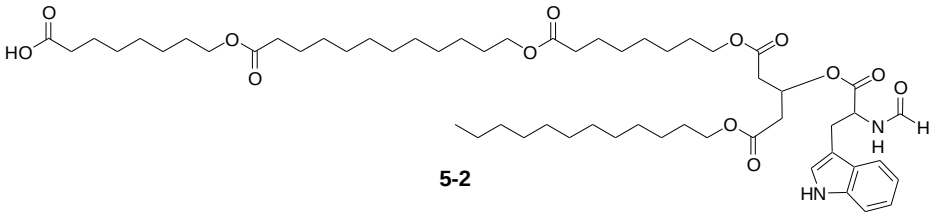

5-2

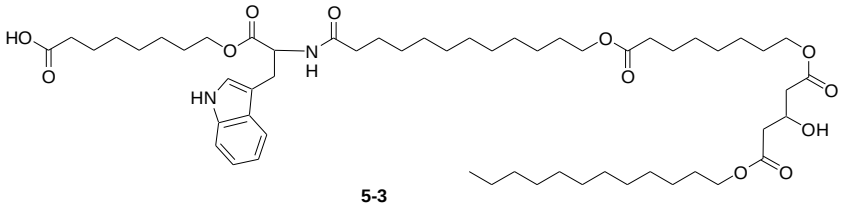

5-3

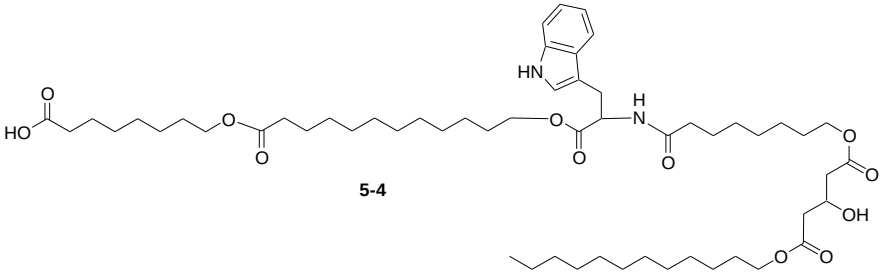

5-4

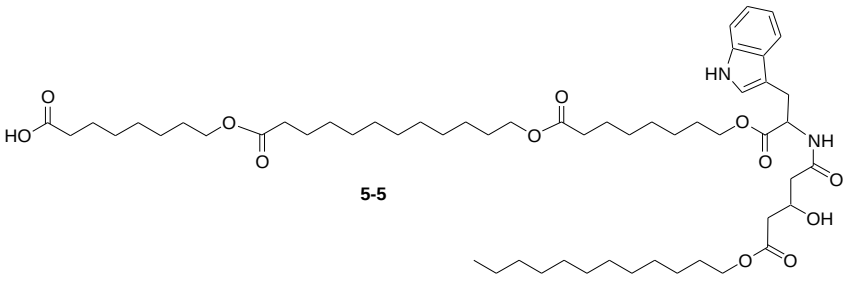

5-5

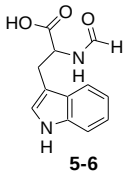

5-6

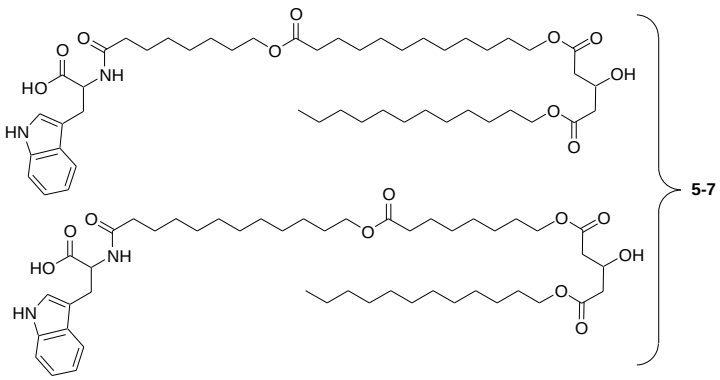

5-7

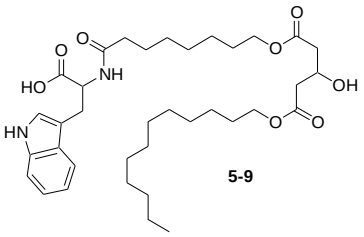

5-9

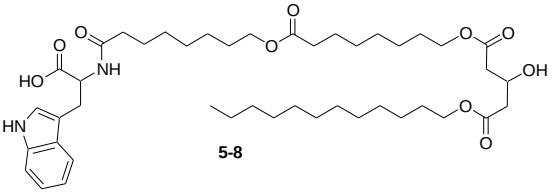

5-8

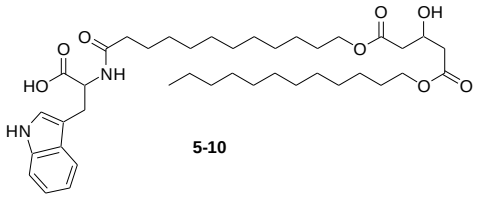

5-10

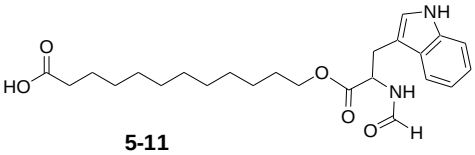

5-11

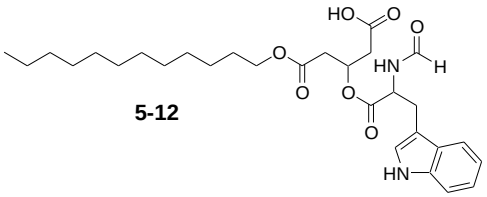

5-12

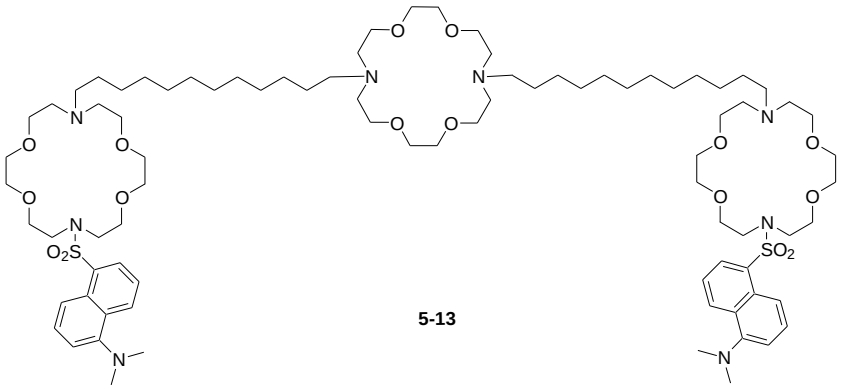

5-13

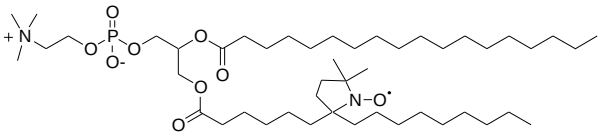

5-14

Acknowledgments

I have received much support and encouragement from many individuals over my academic studies. I would like to take this opportunity to thank those who contributed.

Writing this thesis has truly revealed to me how lucky I am to have a wonderful, ***patient*** and supportive supervisor – Tom! He has always been an inspirational teacher and juggler of many hats, definitely a superb role model!

The Fyles group (Jonathan Chui, Joanne Moszynski and Andrew Dambenieks) have always been there to have some useful chemistry discussions.

Joe Gilroy is a fellow grad student whom I have admired during all of my time at UVic. His dedication to research, success in the lab and overall great demeanor is truly motivating and inspirational.

A significant fraction of time spent on this dissertation went towards teaching in the labs. I have had two very supportive senior lab instructors – Kelli Fawkes and Nichole Taylor. Thanks ladies for being patient with me and letting me teach for you.

Dr. Cornelia Bohne has helped me understand many of the fluorescence experiments and shared with me her vast knowledge on the topic. Thanks as well to Tamara Pace and Effie Li for training me on the fluorimeter!

Much of the spectroscopic analysis and spectrometric data were collected by the hands of the skilled technicians Ms. Christine Greenwood and Dr. Dave McGillivray. Thank you both for helping me collect data on the 50+ compounds!

Thanks Dr. Bryan Koivisto and Dr. Christine Tong for all of the wonderful trips that we have shared together. Not to mention all the painfully-full yet pleasurable food/sushi adventures!

Almost every morning a small group of friends practice tai chi with me and definitely these people – Jane Browning, Shelley Henuset, Lisa Lau and Stefan Atalick deserve a big thank you for their dedication in the morning and keeping me balanced.

My family have always been very supportive in all of my pursuits and I do wish to thank them for their continued support.

Finally, I am grateful for the generous financial support that I have received from UVic and donors.

Chapter 1 Introduction

All cells in Nature are defined by their membranes. The cell membrane is comprised of mostly lipid molecules arranged in a bilayer. The driving force for bilayer formation is the hydrophobic effect; the tails of the lipid amphiphile prefer to be in a non-aqueous environment whereas the polar head groups of the amphiphile favor the aqueous environment (Figure 1-1). The connecting section between the hydrophobic and hydrophilic area is known as the mid-polar acyl region and is comprised of the lipid ester groups. The bilayer structure is then defined by polar (hydrophilic), mid-polar, and non-polar (hydrophobic) regions. The complexity of the bilayer lipid membrane allows it to function as an ion barrier and therefore assists in the regulation of cellular ion distribution between the extracellular and intracellular matrix.[1,2]

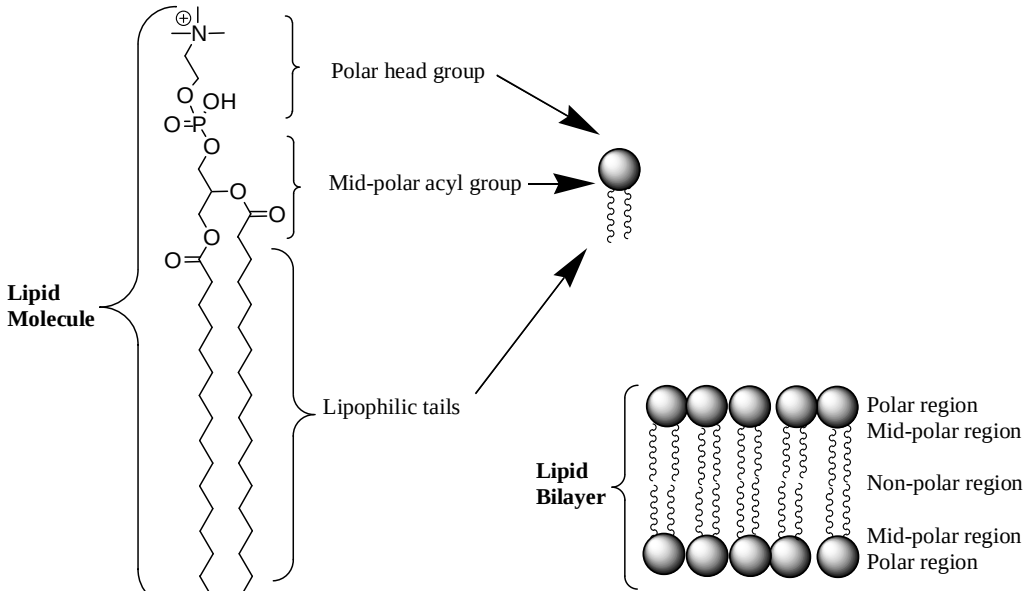

Figure 1-1. General structure of lipid and lipid bilayer.

For the regulation of some cellular functions, ions are transported through the cell membrane using proteins known as ion channels. These natural ion channels are normally large proteins which penetrate through the membrane bilayer depth. The ability of an ion channel to regulate the flow of ions through a membrane could make a potentially useful molecular device for molecular recognition/sensory[3-6], drug-delivery[7], and antimicrobial[8] applications. Natural ion transporters work very efficiently, so the purpose of creating synthetic ion channels is not so much to do better, but to make transporters which can be tailored to do things that natural channels cannot do or to allow some control over channel activities.

Natural ion channels have many specific functions and consequently their structures are diverse. Over the past several decades, much effort has been put towards deducing the structure and function of many natural ion channel-forming compounds. Recently a natural protein channel, (KcsA) K^+ channel, structure was deduced by X-ray crystallography.[9]

Two well-studied peptides that show some features of protein channels are gramicidin and alamethicin.[10] Gramicidin is a natural pentadecapeptide[11] and possibly the most well characterized channel-forming compound. There is a substantial amount of information on the elucidation of the active structure gramicidin. Many of the references are cited in an excellent review by Woolley and Wallace.[10] The linear sequence of amino acids actually forms a helical structure in the monolayer. The ion conducting state for gramicidin forms when two monomers head-to-head dimerize in the membrane. The ion conducting structure of gramicidin allows the ions to flow through the internal helical

core and down the helical axis (Figure 1-2A). Gramicidin is interesting and inspirational to the synthetic chemist because of the simple, yet fully-functional structure.

Alamethicin is a nonadecapeptide toxin and the interesting property of this compound is the ability to be voltage-gated.[10] The mechanism is discussed in section 1.1. Unlike gramicidin, the alamethicin peptide is long enough to span a bilayer membrane. Similar to gramicidin, the active ion conducting state is not just one alamethicin molecule but is the aggregation of several alamethicin molecules. Consequently the ions flow along the helical bundle similar to the transport mechanism of protein ion channels (Figure 1-2B).

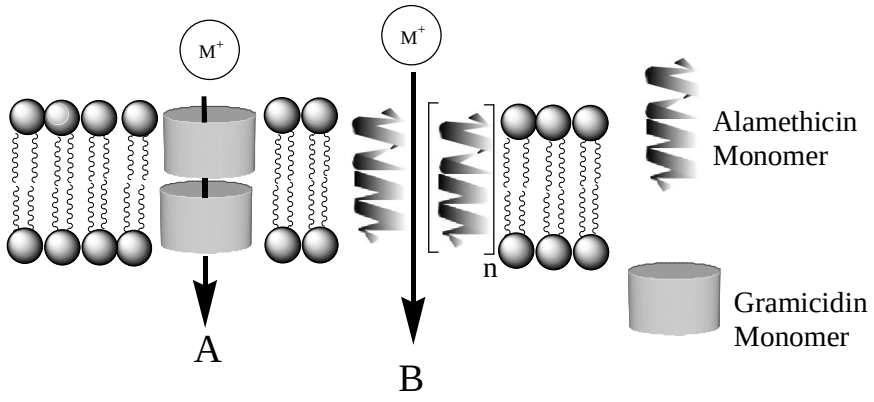

Figure 1-2. Transport mechanism of gramicidin (A) and alamethicin (B).

Finally, an ion channel that has received much attention recently is the (KcsA) K^+ channel (a natural potassium ion channel). One reason why ion channel structures are so hard to deduce is that the protein structures are dynamic in a membrane and trying to grow suitable crystals is difficult. However, Dr. Roderick Mackinnon received the Nobel Prize in 2003 for his work on the (KcsA) K^+ channel.[12] Within his work he was able to get X-ray crystal structures of the channel by removing large parts of the channel that lie outside of the membrane. One major finding from the X-ray crystal structures was that a

selectivity filter was found, which gives rise to the potassium selectivity of these ion channels.[13]

Scientists have mimicked the activities of natural ion channels by synthesizing compounds which are structurally less complex than natural ion channels. The first example of a synthetic ion channel, a cyclodextrin derivative (**1-1**), dates back to 1982 by Tabushi and co-workers.[14]

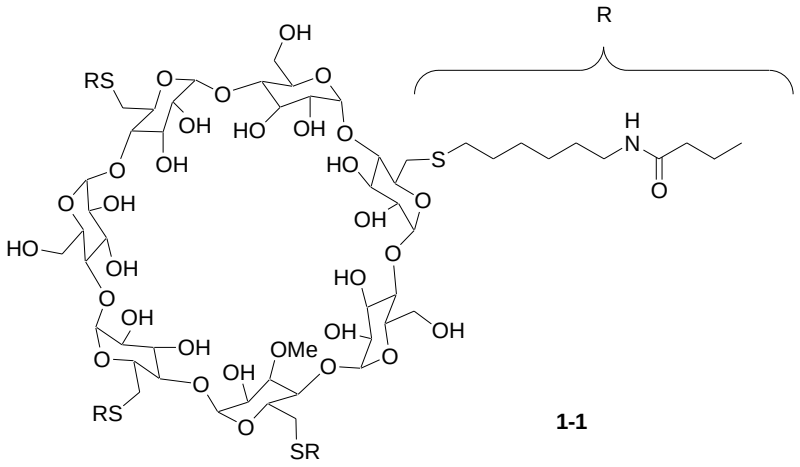

1-1

This cyclodextrin derivative took about one week to synthesize from the tetraiodo-β-cyclodextrin[15] and sodium 6-n-butyrylamino-n-hexyl-1-mercaptide in a low 6.3% yield. This cyclodextrin derivative was designed to span half a bilayer membrane and thus it would be necessary for at least two of these components to form an active transporter. The transport activity was analyzed by incorporating **1-1** into an artificial liposome with encapsulated Tiron (a dye sensitive to cobalt (II) and copper (II)) and the absorption changes of the dye was monitored over time. The cobalt (II) concentration inside the liposome increased when ion transport occurred resulting in a change of absorption of the Tiron. The authors found that these compounds are more transport active than ion carriers (18-azacrown-N_6) under the same experimental conditions.

Since this initial report there have been many examples of synthetic ion channels which have diverse structures and function. Rather than presenting an exhaustive review of all the current structures, only a selected few are discussed in this thesis. There have been several recent in-depth reviews discussing synthetic ion channels.[1,7,16-19]

1.1 Transport Mechanisms

Three modes of transport for ions across a membrane bilayer are by carrier, channel, and membrane disruption mechanisms (Figure 1-3).[20] When ions are transported by carriers, ions on one side of the membrane complex with the carrier and the carrier-ion complex migrates across the membrane (collapse the chemical potential gradient of the ion); the ion is released once the complex reaches the other side of the membrane (Figure 1-3A). In contrast, ion channels are structures which span the bilayer and remain stationary while the ions diffuse through the channel (Figure 1-3B) as a result of the chemical potential gradient of the ion. In Figure 1-3C, the mechanism described is a membrane disruption mechanism where the compound disrupts the order of the membrane structure and ions are transported intermittently through leaks in the membrane structure.

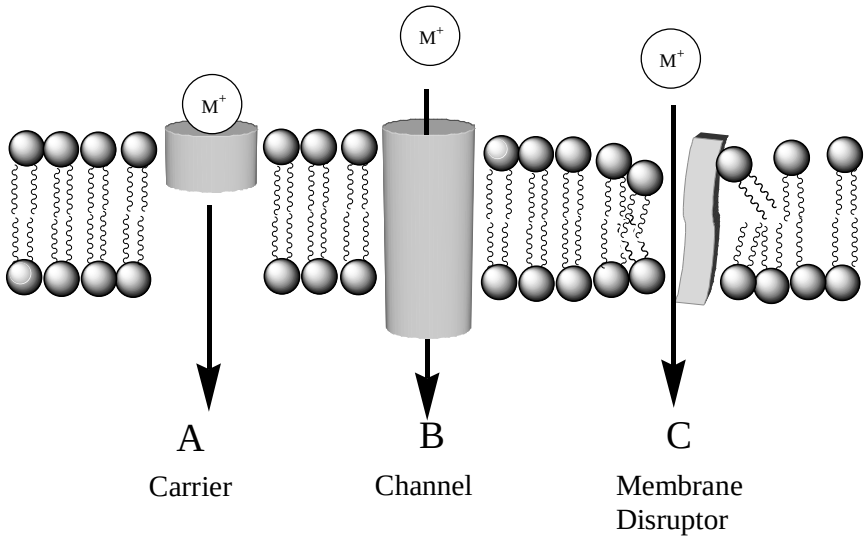

Figure 1-3. Ion transport mechanisms.

Natural ion channels have two functions - ion selectivity and gating. The ion selectivity of natural channels arises from the channel's molecular shape and exposed functional groups which interact with the ions.[1] For example, some channels are selective for anions over cations or some may be selective for one cation over another. A different task for the ion channel is the gating function, which is the ability of the channel to regulate ion transport in response to a stimulus. In the natural environment, ligand-gating (small molecule or ion stimulus) and voltage-gating (sign and magnitude of the membrane potential) are the two main types of gating stimuli. One example of voltage-gated ion channels are the potassium ion channels which form the basis of a nerve impulse. These channels undergo a conformational change when they experience a change in the membrane potential. The change in shape allows the ions to flow through above a threshold value of the membrane potential.[12]

As an inspiration from the natural world, chemists have wanted to create synthetically efficient, selective ion transporters which can rapidly move ions through a

bilayer membrane. To further enhance the function, it would be beneficial that the activity can be controlled, that is gated, by some means (ligand, voltage, etc.)

With the three modes of ion transport (channel, carrier, and membrane disruptor), the membrane disruptor is the least desired mode because of the irregular and unreliable transport process. As well, the disruption of the membrane organization to allow the permeation of ions is unlikely to give any ion selectivity. In contrast, ion channels extend through a membrane bilayer and facilitate ion transport by providing coordination sites for the ions as they diffuse through the membrane bilayer. The transport activity for ion channels could be regulated if appropriate functional groups were used. Therefore with ion channels it is potentially possible to control the selectivity and gating of the ion channel. For this reason, many research groups focus on the synthesis of ion channels. On the other hand, ion carriers are not as interesting for technological purposes because carriers tend to be much slower in the transport rate (by a factor of 1000 or 10000) and it is rather difficult to "gate" a carrier mechanism (control whether ions are being transported or not).[21]

There are several proposed mechanisms for the voltage-gating properties of alamethicin.[10] These mechanistic models are described in detail by Woolley and Wallace.[10] Three mechanisms are described below in brief. In one type of mechanism suggested, the molecular dipole is said to control the permeability by orientating the monomer in the membrane bilayer in one direction (when inactive) (Figure 1-4A) and then when a sufficient transmembrane potential is applied, monomer reorientation occurs to force the monomer to lie parallel to the applied potential. Then several of these tilted monomers aggregate together to make the active ion transporting structure. This

mechanism derives from the surface to transbilayer reorientation suggested by Baumann and Mueller.[22] In the aggregation model (Figure 1-4B), the monomers of alamethicin partition into the bilayer membrane and these monomers are non-conducting but upon the application of a voltage, these monomers associate and the aggregate conducts. In another mechanism, the alamethicin molecules are associated in the membrane in an anti-parallel fashion (Figure 1-4C). Upon application of a potential (E), the monomers flip so that they are inline with the potential. This model is known as the flip-flop mechanism. Regardless of which model is more appropriate to describe the voltage-gating process, one common feature to all the models is that the monomer must contain a macroscopic dipole and it is the aggregation of the monomers which provides a conductive state.

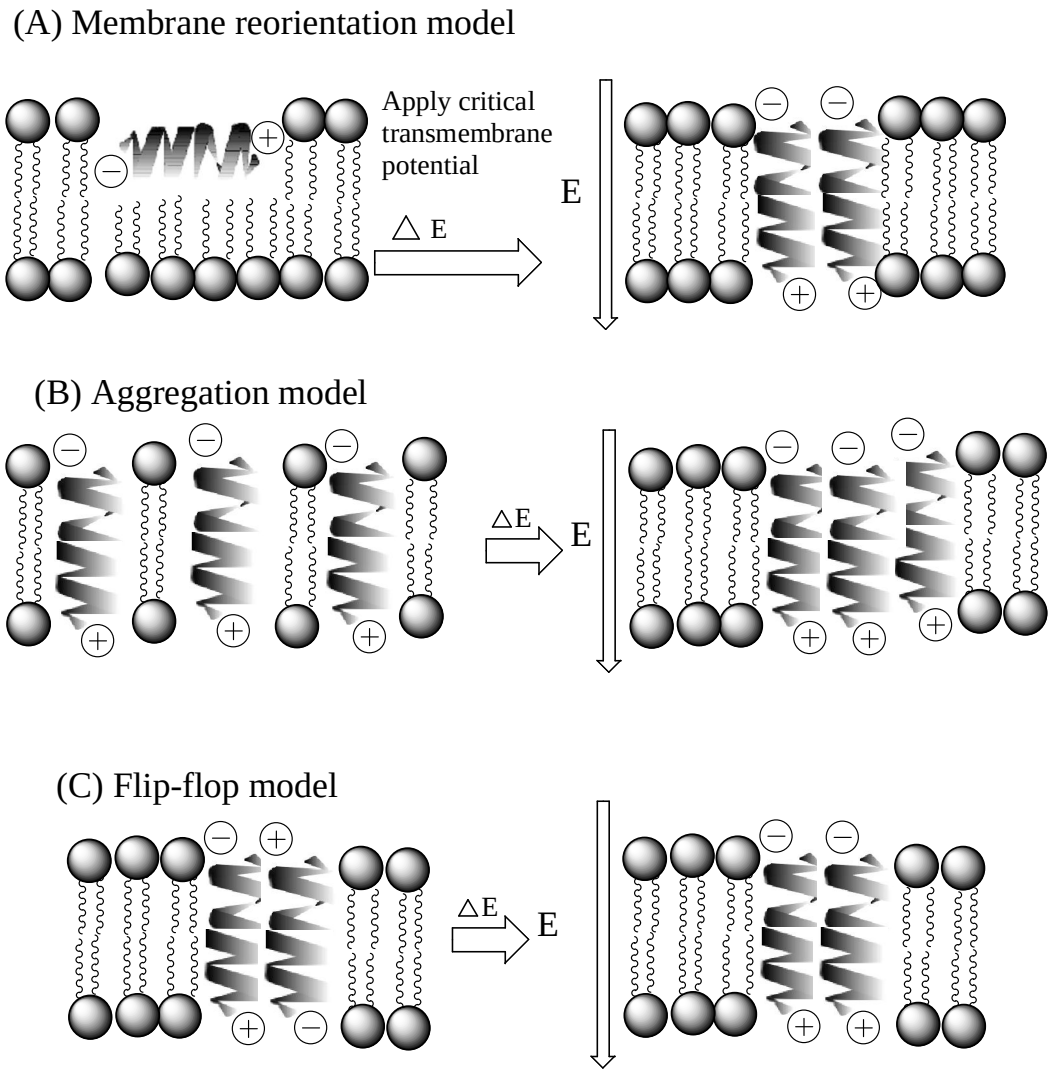

Figure 1-4. Illustration of a voltage-gated mechanism in the bilayer membrane.

1.2 Evaluating Transport Activity

The transport activity of synthetic ion channel candidates are tested by one (or more) of three general methods: vesicle assays, bilayer clamp experiments, or biological experiments. The choice of the experimenter will ultimately depend on the availability of instruments and the relative ease of experiments performed on the ion channel candidates.

There is current literature reviewing all of the most common methods for characterizing ion transport activity.[23]

1.2.1 Vesicle Assay

Vesicles are excellent models for cells because they are bound by a bilayer membrane and are roughly the same shape: typical prokaryotic and eukaryotic cells are between 1-10 μm and 3-30 μm in diameter, respectively.[24] Vesicles are generally useful (easy to make and relatively stable) in diameters between 0.025-2.5 μm.[2] The vesicles can be made to encapsulate a range of ions and/or dyes inside the vesicle. Vesicles can be purified so that the internal ions or dyes are found only within the vesicle and not in the exterior environment (external buffer). This difference in components on either side of the vesicle bilayer leads to a transmembrane chemical potential gradient. When an ion transporter is introduced, the internal components respond to the collapse of the chemical gradient and transport occurs. This change can be detected through the change in an indicator within or outside the vesicle.

Sodium NMR spectroscopy is one method used to monitor the transport process. Sodium ions can be entrapped within the vesicle at the same concentration as the outside. A transporter passes the sodium ions through the membrane in both directions. A paramagnetic relaxation agent outside the vesicle interacts with the sodium and this interaction with the relaxing agent gives rise to chemical shift differences between sodium inside and sodium outside of the vesicle. Analysis of the line widths and peak shape can deduce the exchange rate constants for transport through the channel.[1]

Another practical method for monitoring the transport process is by using an ion selective electrode (for example electrodes selective for chloride, sodium, or protons). In

a pH-stat experiment, a pH electrode can be used to measure the pH of the external buffer which is maintained at a certain pH. Typically the outside is basic (pH 7.4) relative to the inside buffer (pH 6.6). As well, the concentration of a metal-ion is typically higher in the external buffer. The opposing pH to metal ion gradient is equilibrated with the addition of an ion transporter. The flux of "exiting" protons neutralized by base in order to maintain a constant external pH and the volume of base added as a function of time is recorded.[25] The pH-stat method is commonly used for determining the kinetic order and initial proton transport rate.[26] Typically the normalized rates are discussed because variables such as transporter concentration and kinetic order are factored in.

Fluorescence spectroscopy is one of the most sensitive forms of spectroscopy and it is a very practical method for vesicle experiments. The internal probes that are commonly used for fluorescence assays for measuring proton flux are 8-hydroxypyrene-1,3,6-trisulfonic acid (HPTS), 8-aminonaphthalene-1,3,6-trisulfonic acid/ *p*-xylene-bis-pyridinium bromide (ANTS/DPX), and 5(6)-carboxyfluorescein (CF). A pH gradient can be established across the membrane and when the transporter is active, protons or hydroxides are transported. The pH can be monitored with a vesicle-entrapped pH sensitive dye (HPTS or CF). HPTS has two different excitation spectra – one for each of the acid and conjugate base form. When the pH increases, the conjugate base dominates, and so the emission from the excitation of the conjugate base form increases relative to the emission by excitation of the acid form of HPTS. In comparison, protons quench the CF emission so this assay is done at a single excitation wavelength.

To probe for large pores, the dyes ANTS/DPX are co-encapsulated in the vesicles at high enough concentrations such that DPX quenches the fluorescence of ANTS. If

large pores form, then these dyes will leak from the vesicle and be diluted in the external buffer. Upon dilution, the DPX quenching is reduced and the ANTS fluorescence increases. Similarly, at high concentrations carboxyfluorescein self-quenches so when large pores form, the dye diffuses out of the vesicle and the fluorescence signal will no longer be suppressed by the self-quenching.[23]

In summary, the two advantages in using vesicle assays are: the relative ease to conduct the experiments (vesicles are easy to make with the appropriate equipment and the fluorescence experiments are straightforward), and the ion transporters can be tested rapidly for activity. As previously mentioned there are several types of fluorescent dyes and with the appropriate experiment certain questions can be answered such as: are the ion channel candidate compounds active (HPTS)? Are the holes formed big or small (carboxyfluorescein or ANTS/DPX)? Do the channels show some form of ion selectivity (using different alkali salts in the internal and external buffer)? One pitfall associated with vesicle assays is the batch-to-batch variability; the average size may be constant but the background leakage may differ. The variability makes for a difficult comparison at times between experiments. If ion selectivity is to be examined, a batch of vesicles with a particular salt needs to be made for each ion tested. Since the concentration of lipid varies between experiments, even though the stock transporter concentration can be kept constant, the effective transporter concentration may vary. To control this variation, transporter concentration is usually reported as a mole percent relative to the lipid concentration ([transporter]/[lipid] %). Another shortcoming is that a macroscopic overview of the activities is observed using these vesicle methods. Since a macroscopic observation is made, it is difficult to identify if ion transport occurs by an ion channel,

carrier or membrane disruption mechanism. Vesicle assays reveal if an ion channel candidate is an active transporter, the size of the pores (if formed) can be estimated using appropriate fluorescent dyes, and the ion selectivities of the transporters can be determined.

1.2.2 Planar Bilayer Clamp

Another method for the characterization of ion transport different from the vesicle assay is the planar bilayer method. The planar bilayer experimental setup (Figure 1-5) is an experiment where two electrodes (grey lines) are placed in two vessels containing an electrolyte solution. A small hole connects the two solutions but normally in a planar bilayer experiment this hole is blocked by "painting" a lipid bilayer and in essence the electrodes are insulated from each other.[27] An electrical potential is applied to the membrane and without ion transporters no current is observed. Generally ion transporters are introduced to the membrane bilayer once the membrane has stabilized. Transport activity results in the observation of electric currents which are recorded over time.[23] If discrete ion channels are made, step-wise jumps or drops in the current are observed when these channels are closed (i=0 pA) or open ($i \neq 0$ pA); whether i is greater or less than 0 pA depends on the polarity of the applied electrical potential. Each jump in observed current (level) is representative of a particular type of channel opening (single channel opening); when more than one channel opens (multi-channel openings), multi-levels are observed (labeled as 1, 2 and 3 in the i versus time plot in Figure 1-5). The channels remain open as long as the channel structure is stable and the measurement of the time span for the opening of each channel is called the lifetime.

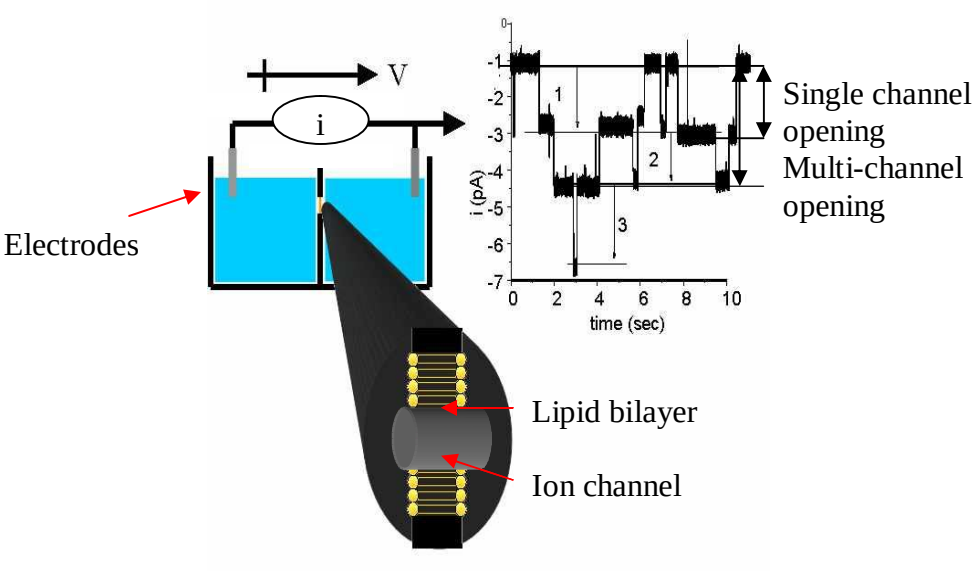

Figure 1-5. Planar bilayer experimental configuration.

Discrete jumps are not observed for a carrier mechanism because under such a mechanism, ion transport will not cease until the ion gradient has collapsed. Consequently, under a carrier mechanism, a constant current is observed for a fixed potential.

When a membrane disruptor is inserted into the membrane, neither the discrete jumps in conductance nor a drift in the conductance are observed. Membrane disruptors function by causing leaks through the membrane bilayer and therefore the ion transport is very random and unregulated. Consequently short bursts in conductance are observed when membrane disruption occurs.

When single channels are observed, bilayer clamp experiments can provide a lot of information: the channel conductance, the lifetime and the open probability.[23] The channel conductance (calculated as the ratio of the observed current/applied voltage) reveals how big the channel openings are, the lifetime is the average opening time of a channel and is related to stability of the open structure, and the open probability is the

probability of observing an open channel which is determined by counting the open and closed states.[23]

One disadvantage in using planar bilayer experiments is that it takes a while to setup the experiments and only one channel candidate can be tested with one setup. Therefore for the testing of many compounds, this is a very inefficient method. As well, an entire experiment hinges on the stability of one membrane bilayer; if the membrane rips prior to the complete collection of the data, then that data set may not be useful. Similar to a disadvantage of the vesicle assays, bilayer clamp experiments are difficult to reproduce at times; the transport activities may not always be observed.

1.2.3 Microbial Testing

Ion channels transport ions from one side of the membrane to the other and they serve to collapse activity and voltage gradients. In nature, the contents of a cell are usually different from what is extracellular. Cell death is inevitable when essential metabolites are removed from the internal cell matrix.[28] Several natural ion channels (such as amphotericin[28-30] and alamethicin[31]) are used as antimicrobial agents because these compounds create channels or pores which are large enough to release the internal cell contents and lead to cell death.

To mimic the cellular effects of alamethicin and amphotericin, synthetic ion channels can be used to collapse a chemical gradient in a bacterial cell. This assay is performed by placing disks soaked with compound onto an agar plate charged with bacteria. An inhibition of growth by the plate would suggest that the compound has antibiotic affects.[16] If various compound concentrations are used to test the inhibitory effects, then the minimum inhibitory concentration can be determined.

Several researchers have employed this as a characterization method such as Ghadiri and coworkers with their peptide nanotubes[32], Voyer and coworkers with their crown-peptides[33], and hydraphiles made by the Gokel group[34].

The advantage of microbial testing is that it is a relatively easy assay (compared to vesicle assays and planar bilayer clamp experiments) to do in order to determine if the channel candidates are active transporters. The shortcoming of microbial testing is that nothing can be said about the transport kinetics, the size of the channels or even if the compound follows under an ion transport mechanism as opposed to affecting some other cell function.

1.3 Design of Synthetic Ion Channels

The lipid bilayer is comprised of three regions: polar head group, mid-polar acyl group, and the hydrophobic nonpolar core which arise from the structure of the lipid (Figure 1-1). The polar head group can be zwitterionic, cationic or anionic depending on which lipid is used. The midpolar region is the ester component of the lipid (from the glycerol backbone). The hydrophobic nonpolar core is the region where lipophilic alkyl tails interdigitate. In order to properly construct an ion channel, these regions must be taken into account.

Ion channels are distinct structures from ion carriers because they are usually long enough to span the depth of a membrane bilayer. A primary design consideration of ion channels is that they can exist as a unimolecular structure or aggregate as a supermolecule to function (Figure 1-6).

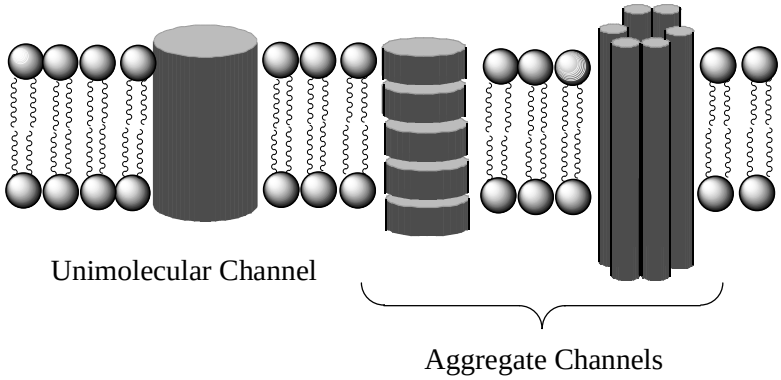

Figure 1-6. Ion channel models.

For ion channels which are embedded and span the lipid bilayer, the channel structure generally consists of three components: a head group, a lipophilic component, and functionalities which can coordinate with the ions. The lipophilic component and coordination sites constitute what is called the core (Figure 1-7).

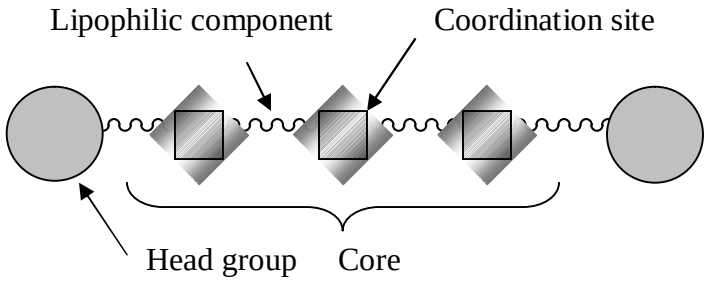

Figure 1-7. Basic structure of an ion channel.

The head group of the channel is envisioned to position itself within the lipid polar head groups or mid-polar acyl groups. It is reported from structural evidence that the midpolar region is where natural protein channels anchor into the membrane bilayer.[21] The head group would serve as an anchor through hydrogen bonding and Coulombic attractions with lipid molecules to orient the molecule perpendicular to the membrane bilayer. It would be expected that the polar head group on the channel would have little affinity to reside in the lipophilic layer. Design consideration must be put

towards the size and functional groups present (sulphates, carboxylates, etc.) of the head group. The charge on the head group affects the selectivity of the ion channel, for example, head groups with an overall cationic charge can most likely repel cations and attract anions. If the ion channels are designed as unimolecular transporters, then the head group must have a portal large enough to permit the entry of a hydrated ion.

Since the core of the ion channel is mostly comprised of coordination sites and lipophilic components, then the core should reside between the midpolar regions of the lipid bilayer. The lipophilic component on the ion channel should interact weakly with the lipid tails through weak van der Waals forces. The overall orientation of the channel responds to the hydrophobic effect that drives the lipophilic components into the lipophilic region in the lipid bilayer.

In the past, many synthetic ion channels have been targeted towards transporting cations, but recently there are more anion transporters being introduced. From a synthetic perspective, addressing the transport of cations is easier than anion transport as there are many more structural features which one can employ. In the design of cation transporters, it is essential that there are Lewis base (donor) functional groups such as ethers or carbonyls which help coordinate the ions and can potentially provide some form of selectivity if size is considered. Typical donor groups in the core of the channels are ethers, which are good donors for alkali metals. Crown ethers were initially popular because of their distinct selectivity for certain ions depending on their size.[35] Normally the ions in solution are solvated by water molecules and it is expected to be highly unfavorable for the solvated species to move through the hydrophobic interior. To totally

desolvate the ions as they enter the bilayer is energetically unfavorable, so the ions are most likely to contain some degree of hydration.[35]

In the designing of the functional ion channel, balance of attractive and repulsive forces between the head group/coordination sites and the ions must be considered. If the attractive forces are too strong, then the molecule may associate with the ion and remain stagnant.

Triton, a commercial surfactant, is capable of forming discrete channel-like openings together with membrane disrupting bursts as detected by bilayer clamp experiments when used in low concentrations.[36] The descriptions of an ion channel (possession of a polar head group and lipophilic core/tail) match those of many commercial detergents. Most ion channels are considered as surfactants[1] because they are amphiphilic and should reside at the interface between the hydrophilic and hydrophobic regions. Much consideration needs to be put towards the design of a molecule whereby it will act as an ion channel and be able to transport ions regularly with some defined activity versus that of a detergent where membrane disruption occurs and the mechanism is ill-defined. Structurally, there is an ill-defined line where a compound may exhibit defined transport activity to those which act more detergent-like and it is always the challenge for synthetic chemists to synthesize the former compounds. It is important for ion transport applications that the ion transporters produce well behaved channels.

1.3.1 Complex Synthetic Ion Channels

In the 1980's when synthetic ion channel development was occurring, many of the designs then incorporated crown ethers. There are many examples in the literature where

an extensive synthesis is used to generate a membrane active compound. To give a comprehensive survey of the structures is not needed as there are many excellent recent reviews. [1,7,16-19] Instead, a small range of compounds are discussed below to show the diversity in the synthetic ion channel area, and to focus on the synthetic aspects that control the availability of these types of compounds

1.3.1.1 Crown-Ether and Cyclodextrin-Based Bouquets

Lehn's group in the early 1990's reported bouquet-like channel compounds with a central, ridged core and long side chains (**1-2**[37,38] and **1-3**[39]). These molecules are called bouquets because of the resemblance of the molecular shape to a bouquet – a core of either β-cyclodextrin or a tartaric acid crown ether and "bundles" of amide-linked arms are attached to **1-3** or esterified on **1-2**. In molecule **1-2**, these molecules contain a cyclodextrin portal and required at least seven synthetic steps to synthesize in yields of about 13%. In comparison, **1-3** has a crown ether interior filter and is synthesized in ten steps from the crown ether with an overall yield of about 4%. Both molecules **1-2** and **1-3** have side chains of either alkyl or ethylene glycol units to help with the stabilization of cations inside a proposed channel.

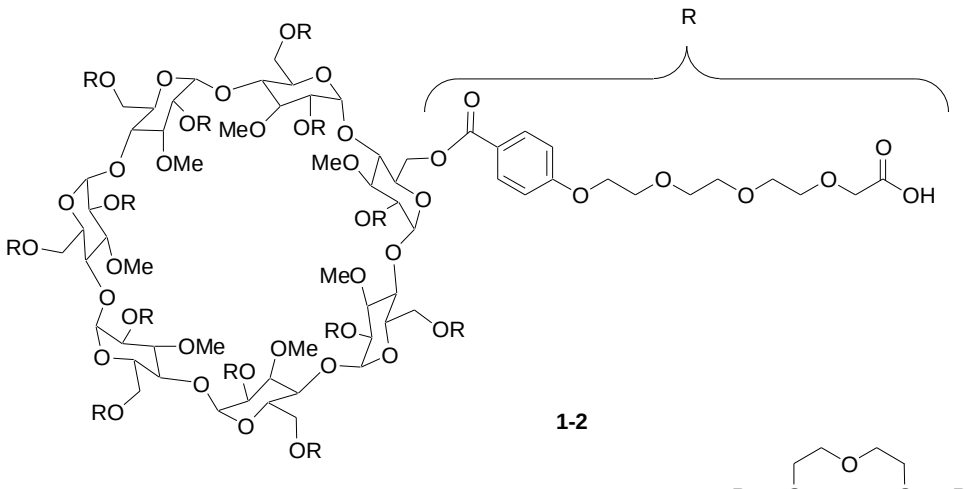

1-2

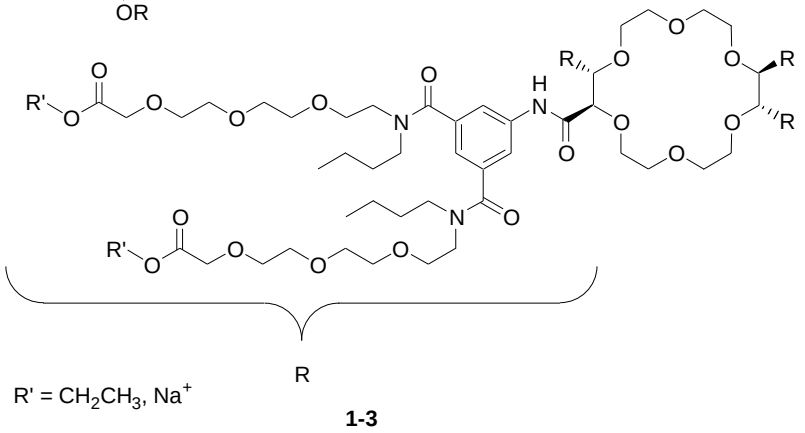

R' = CH_2CH_3, Na^+

1-3

The active structure is proposed to have the macrocyclic core between the bilayer leaflets and the carboxylates at the head groups in a membrane-spanning configuration. Compounds **1-2** and **1-3** were shown to transport sodium and lithium ions in a ^{23}Na and ^{7}Li NMR vesicle assay respectively.[39] These compounds collapsed opposing gradients of ions (i.e. counter transport – a one-for-one exchange of Na^+ for Li^+). The transport rate constants for the compounds were found to be very low; rate constant of 8.3 x 10^{-5} s^{-1} for **1-3** at a mol % concentration of 0.03% and 4.7 x 10^{-5} s^{-1} for **1-2** at a mol % concentration of 0.02%. The synthetic efforts of these compounds do not outweigh their transport properties.

1.3.1.2 Crown Ether-Based Bolaamphiphiles

Another crown ether derived ion channel (**1-4**) was reported by the Fyles group.[26,40] Since there are three variable segments to this class of molecules - core, wall, and head; compound **1-4** is just one example of 25 molecules reported[41] by Fyles. These compounds are made in about 8-12% after six steps from the crown ether.

The transport activity of **1-4** was examined using a pH-stat assay.[26] At a transporter concentration of 20 μM, the normalized rate of proton flux (in the presence of K^+) was found to be 1.3 x 10^{-9} mol H^+ s^{-1}.[26]

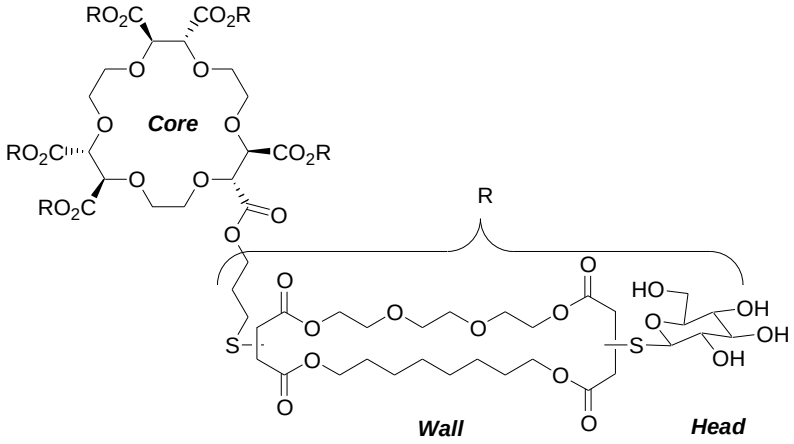

1 - 4

The design evolution of the **1-4** structure eventually lead to the development of **1-5**[42], **1-6, 1-7,** and **1-8**.[43] Compounds **1-5**[42], **1-6**, **1-7** and **1-8**[43] are made within 1-4% yields from the macrocyclic starting material **1-9**. The advanced structures have maintained the presence of the polar head groups (although the head groups have evolved to carboxylic acid and amine functionalities as well) and macrocyclic wall (from using the common starting material **1-9**) but the crown ether core is removed.

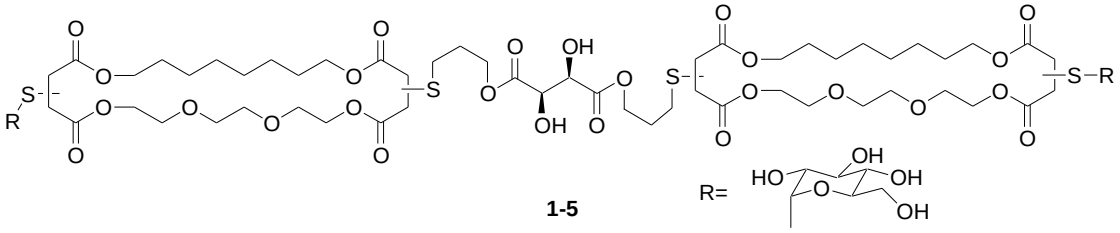

1-5

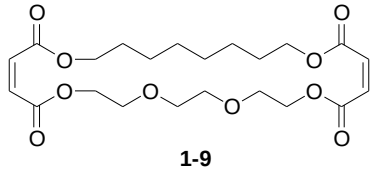

1-9

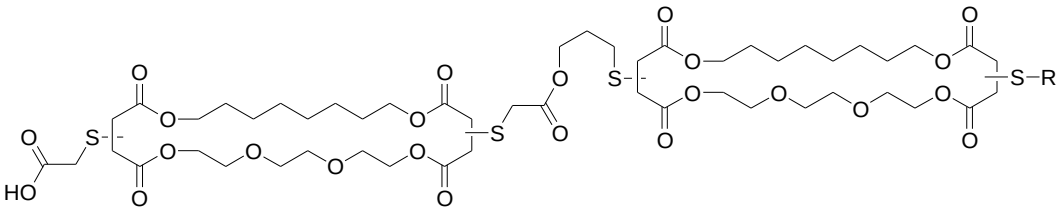

1- 6 **1- 8** **1-7**

The transport activities of **1-5**, **1-6, 1-7,** and **1-8** were examined using pH-stat vesicle experiments.[42,43] The pH-stat transport data for **1-6, 1-7,** and **1-8** showed normalized rates for K^+ which were 25-80 times faster than the transport rates for **1-5** under the same experimental conditions.[43] The structural difference between **1-5** and **1-4** is the absence of the crown ether core; such an absence leads to a channel structure which is much less active than **1-4**. The normalized rate for **1-5**[43] was 0.06 x 10^{-9} mol H^+ s^{-1} while **1-4**[26] was 1.3 x 10^{-9} mol H^+ s^{-1}. However, compounds **1-6**, **1-7** and **1-8**, differ in head group composition but maintain a constant core structure, have normalized rates[43] which are about double that of **1-4**. The transport rates observed for the vesicle assay showed that the rates differ slightly and therefore it was concluded that the effect of head groups is very minor in determining activity.[43]

Planar bilayer clamp experiments were used to study the ion selectivities of **1-6, 1-7,** and **1-8**.[43] It was found that **1-7** is cation over anion selective and the postulated reason is the presence of the dicarboxylate head group. In general, a bilayer clamp experiment for these compounds suggested weak selectivity for $Cs^+ > K^+ > Na^+$.[43] The possibility of compound aggregation in the membrane to form the active structure was also addressed using bilayer clamp experiments. When multiple channels open for gramicidin, stepwise jumps in conductances are observed at equal height for each opening. In contrast alamethicin is known to form various sized aggregates in the membrane bilayer ultimately leading to different conductance states[44] which show a non-linear increase in conductance upon addition of monomers to the ion channel aggregate. From the bilayer clamp results for **1-7** the multiple channel openings are of about equal conductance similar to gramicidin and therefore the data is consistent with a number of similar aggregates active at one time. The data are not consistent with an alamethicin-like bundle model.

1.3.1.3 Hydraphiles

Along with the development of the crown ether compounds, Gokel's cation conductors – the hydraphiles (**1-10**) - were among the early crown ether compounds introduced in the early 1990's which demonstrated ion transport.[45,46] These trismacrocycles were named hydraphiles[35] because of the resemblance of the structure to the *hydra* which is a freshwater polyp (simple marine animal with a cylindrical body and an oral opening surrounded by tentacles).

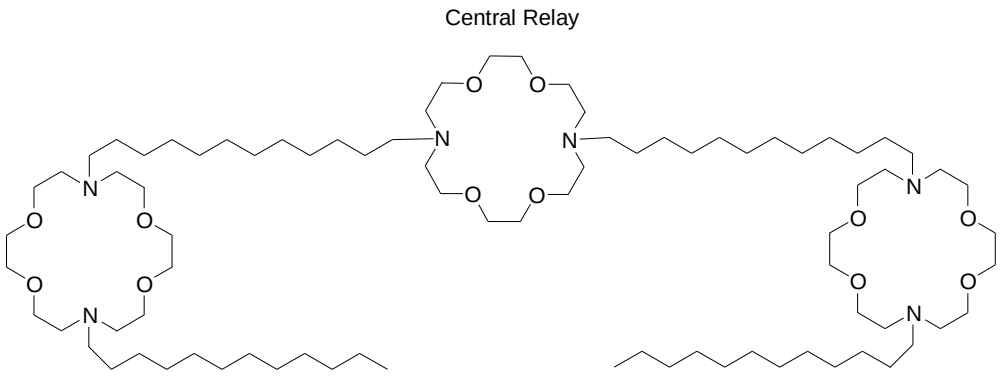

1 - 10

This family of compounds has a relatively simple structure with three convergent steps from the diazo-18-crown-6 polyether to every derivative. The yield for **1-10** from the diaza-18-crown-6 was 23%.[47]

The overall structure of the hydraphiles is different from that of previously mentioned ion channels (crown-ether and cyclodextrin-based channels). The two macrocycles (diaza-18-crown-6 polyether) located at either end of the structure are designed to act as an ion filter and also act as the head group. Unlike the crown-ether and cyclodextrin-based channels, the lipophilic component is not intermixed with coordination sites (ethers) but instead there is a centre macrocycle, known as the central relay, where it is believed that the ions receive some polar stabilization from the donor groups.[48]

Hydraphile **1-10** was tested for ion transport ability initially using ^{23}Na NMR spectroscopy.[46] It was reported that at equal concentrations (40 μM) to gramicidin, the rates for Na^+ transport in vesicles was 100 fold better for gramicidin than the hydraphile. The active structure of **1-10** in the bilayer membrane was originally proposed to have the central relay positions parallel to the bilayer plane but on a derivative of **1-10** it was subsequently found to be parallel.[49] This conclusion was found from the result of varying

the central relay ring size and replacing the central relay with a $O(CH_2CH_2O)_3$ chain. These independent variations did not stop the transport activity but did reduce it.[49] If the ions were to flow through the central relay, then it would be anticipated that the activity not diminish when the ring size decreases and increase when the ring size increases. However, since transport activity decreases for increasing and decreasing ring size, then the cations are proposed to run by and not through the central relay. [35]

Gokel noted that a cell has high K^+ and low Na^+ concentration within the cell relative to the extracellular matrix. Since the hydraphiles are centro-symmetric then ions can potentially move in either direction through the channel. Therefore if these compounds are incorporated into the cell membrane of a microbe, then the ion gradients would collapse and the microbes would die.[16] Compound **1-10** was tested for antimicrobial activity against *E. coli*. The minimum inhibitory concentration (MIC) found for **1-10** against *E. coli* is 2.1 μM[50]; compared with the reported MIC for penicillin, 8 μM. It is encouraging to note that these hydraphile ion channels are a more effective antibiotic than conventional penicillin.[16]

1.3.1.4 *p*-Octiphenyl Rigid Rod Staves

The Matile group has an interesting ion channel design consisting of a *p*-octiphenyl backbone with dangling short peptide strands from the aryl rings. The original structure of the first compound made in this class is **1-11**.[51] These molecules are proposed to self-assemble in the bilayer to an active pore structure in the barrel-stave form (**1-12**) by interdigitation of the peptide strands held by complementary inter-strand hydrogen bonding (Figure 1-8).

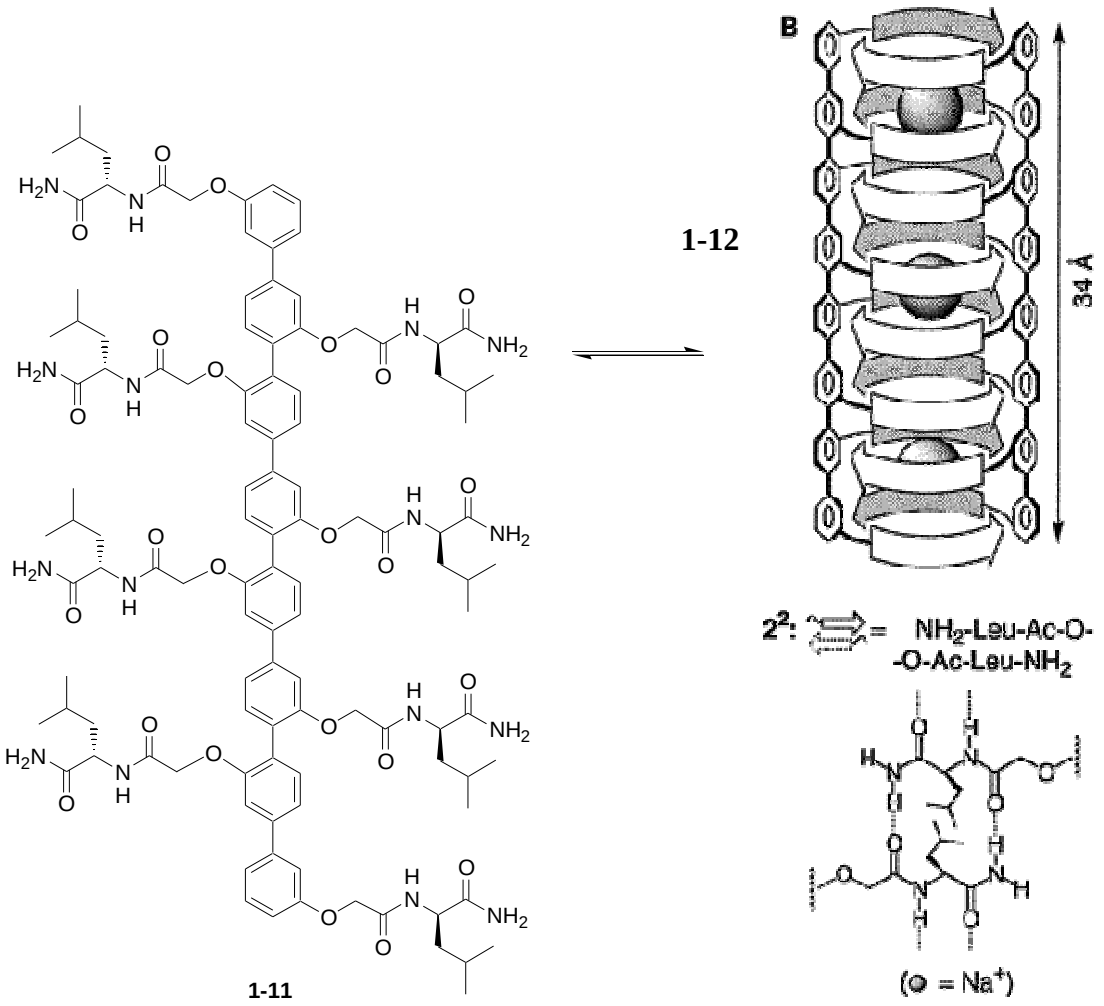

Figure 1-8. Proposed self-assembled dimerization of **1-11** to yield **1-12**. Image on right is reprinted with permission from reference 51. Copyright 1999 American Chemical Society.

Synthetically, these compounds were a challenge to make as the *p*-octiphenyl backbone required extensive solution phase synthesis.[52] Once the backbone was made, then through organic transformations, two amino acid residues were appended to give a yield of about 2% from the rigid rod backbone. Compound **1-11** has a short amino acid side chain and it is speculated that the molecules dimerizes to form the active structure. The dimerization or intermolecular formation is proposed based on solution analysis of the oligomer **1-11** using NMR and circular dichroism spectroscopy. Mass spectrometry

data also suggested the formation of dimers ($[2M+xNa^+]^{x+}$, x = 2,3,4,6) in the gas phase and not trimers or any other higher oligomers. [51]

Vesicles with HPTS entrapped were used to study the ion transport by these rigid-rod ion transporters. It was found using the fluorescence assay that nanomolar concentrations of the compound were sufficient to collapse the pH gradient to the same extent as natural peptide melittin at about a third of the concentration.[51]

Matile further developed these rigid-rod structures so that the amino acid side chains were longer and contained a combination of several amino acids.[53] By lengthening the amino acid side chains, leucine separates every amino acid in the side chain. Leucine is an important amino acid because it satisfies the lipophilic component to aid in membrane partitioning and it is proposed to point the alkyl tail external to the barrel.[53] The other amino acid component in the side chain is usually a polar amino acid (such as histidine, aspartic acid and arginine). It is postulated that these polar amino acids supply the donor sites for coordination to the hydrated ions. Upon lengthening of the side chains, it was found that mostly large pores are formed, based on current measurements (0.3-3.6 nS) in bilayer clamp experiments and the release of 5(6)-carboxyfluorescein in vesicle assays, and that the pores that form are fairly stable structures, based on long lifetimes (greater than 1000 ms) measured in bilayer clamp experiments. [53,54,55] These large pores can be blocked by a variety of molecules.[56,55]

One structural feature which distinguishes these rigid-rod channels from the previously mentioned ones is the lack of any polar head group. In the previous structures, the head group is proposed to serve as an anchor in the membrane. With these rigid-rod structures, the supermolecule or monomer is inflexible and consequently once they insert

into the bilayer membrane, two general orientations are possible – parallel or perpendicular to the bilayer membrane. Matile wrote a detailed review on the possible orientations of the oligomer and supermolecule.[53] In short, the conducting state of the channel must be in the 'perpendicular' form. Matile proposed that the active structure is an aggregate which forms first in solution and then partitions into the membrane.[57] Therefore by definition, these rigid-rod structures act as unimolecular ion channels because the solution-formed aggregate partitions into the membrane which results in transport activity.

1.3.2 Simple Ion Channels

Most of the complex ion channels discussed in section 1.3.1 function as unimolecular ion channels. By working with such large molecules, there are several disadvantages such as low yields from the synthesis, difficulty in characterization and most importantly, low compound solubility in aqueous solutions. One way of getting around these issues is by making aggregate ion channels which are the result from the assembly of a supermolecule from several smaller molecules.

Months of synthetic work is still required to generate some of the ion channel-forming compounds such as the hydraphiles and rigid-rod staves. Currently many research groups are heading to simpler channel designs for ease of synthesis and hoping to maintain or enhance the activity relative to compounds already synthesized.

In this thesis the definition of a "simple" synthetic ion channel is one which is prepared in only a few synthetic steps or has a low molecular weight (<1500 g/mol).[1] It is generally agreed that complex transport processes do not necessarily require complex ion channels.[58] In the literature, these supramolecular ion channels come in many

structural forms and sizes. A few of these molecules are discussed in this thesis to show the types of aggregates possible; several recent reviews are available. [5,12-16]

1.3.2.1 Amphiphilic Aggregates

One of the earliest types of simple ion channel forming compounds was reported by Kobuke *et. al.* **1-13** was synthesized in low yield (about 7%) over four steps.[59]

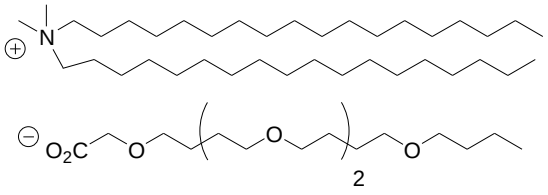

1-13

The oligoether tail on these amphiphiles is expected to have little affinity for the bilayer membrane but as the ion pair with the ammonium salt, more lipophilic character is introduced to the structure and therefore the affinity increases. Once partitioned into the bilayer membrane, the supermolecule is proposed to have the oligoether tail pointing into the channel while the lipophilic tail is on the channel periphery (Figure 1-9).

The transport activity of these compounds was demonstrated using bilayer clamp experiments and show long-lived but highly variable channel openings of conductance values of 10-10^3 pS. The oligoether amphiphiles are designed so that they are long enough to span only about half a bilayer (24 Å) (Figure 1-9). The authors proposed that the amphiphiles aggregate (in undefined numbers) in each leaflet of the bilayer and when the aggregations on either side meet up, then conductance is observed. At the time they were reported, these compounds were very interesting because the conductance by these channels rivals that of synthetic polypeptide channels which is evidence that peptides are not required for ion transport.[59]

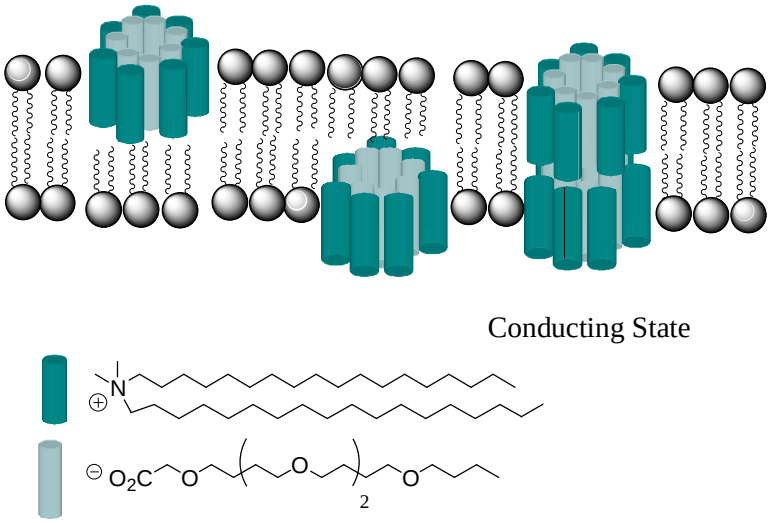

Figure 1-9. Proposed amphiphile aggregate ion channel.

1.3.2.2 Isophthalic Acid Derivatives

The Fyles group modified isophthalic acid derivatives (such as **1-14**) to generate ion channel aggregates with cation selectivity ($Cs^+ > K^+ > Na^+$).[58] Compound **1-14** was made in about 41% yield after four steps.

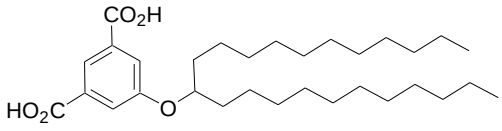

1-14

The transport activities observed for **1-14** were stable openings with lifetimes in the second timeframe and conductances of 9.2±0.1 to 31.0±0.1 pS depending on the cation. To put these conductance values into perspective, under similar experimental conditions, the conductances for **1-14** and gramicidin are 9.2±0.1 pS and 14.5 pS, respectively.[60] Therefore this class of compound can form ion channel aggregates with some membrane activity.

Compound **1-14** is interesting in that, when a pair of methylenes is added to or removed from the alkyl tails (such that there are 9 or 11 methylene units), the transport

activity in the planar bilayers for these derivatives disappears using the same experimental conditions as for **1-14**.[58]

The active channel structure of **1-14** is still unknown. With a short monomer length, it would be expected that large pores could form, but the low conductances refute any ideas about large pore formation.

1.3.2.3 Sterol Aggregates

The Regen group has demonstrated one of the easiest syntheses of an ion transporter, by condensing spermine and cholic acid (both naturally occurring products).[61,62] The condensation of spermine and cholic acid was done with dicyclohexylcarbodiimide and *N*-3-hydroxy-1,2,3-benzotriazine-4(3H)-one and yielded **1-15** in 76% yield.[61] One of the advantages to the sterol conjugates (**1-15**) is that despite the large structure, the synthesis is facile (one step from the natural products). Regen proposed that the active channel structure has all of the cholate groups parallel to one another in the bilayer membrane.

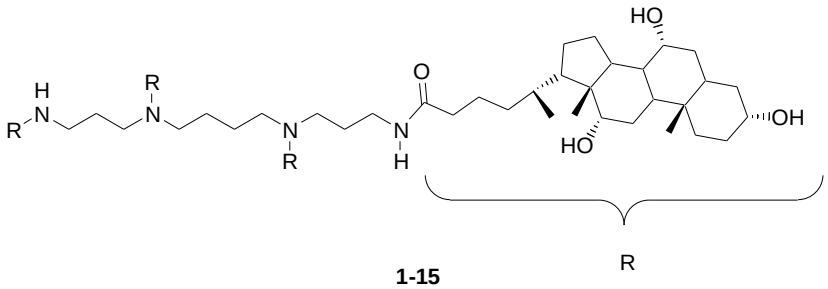

1-15

The transport activity of **1-15** was measured using ^{23}Na NMR spectroscopy with vesicles. The measured rate constants mean very little in terms of how active these compounds are, as there was no comparison to a standard ion channel. However, it was found that the activity of these compounds is highly dependent on the bilayer membrane thickness. In varying the bilayer membrane thickness by changing the lipids used to

make the bilayer, optimal transport activity was observed when the compound was four methylene units shorter than the membrane bilayer thickness.[62] This was an interesting result for optimizing transport rates as consideration will need to be made for the bilayer thickness.

The proposed active ion channel aggregate for the sterol derivatives is in a barrel stave form (Figure 1-10).[63] Unlike the other simple ion channels, which are proposed to form by smaller molecules aggregating together through intermolecular forces, the active channel form of **1-15** is proposed to be a dimer with the sterols defining the walls of the channel. The evidence of dimer formation stems from the analysis of the pseudo first-order rate constants found in ^{23}Na NMR spectroscopy that show a kinetic order of two.[61-63] The walls of the channel are proposed to be made of the cholyl components (long cylinders in Figure 1-10). The amphiphilic nature of the cholyl group implies that hydrophobic group defines the external core of the barrel while the hydrophilic core points towards the core.[63]

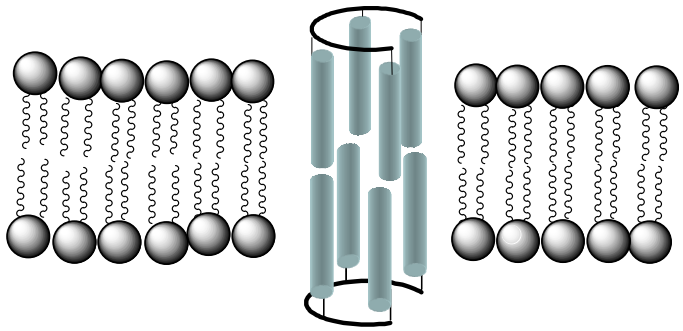

Figure 1-10. Proposed sterol barrel stave ion channel.

Other than the amphiphilic aggregates, the Kobuke group also synthesized ion channel-forming compounds made from cholic acid derivatives (**1-16**). **1-16** was synthesized by the Kobuke group from cholic acid in 0.8% yield after five synthetic steps.[64] Compound **1-16** is one of the very few examples of synthetic voltage-gated ion

channels. The compound is asymmetric and asymmetric structures have a permanent molecular dipole and therefore are suspected to be voltage-gated ion channels. The assumption is made that when the channel forming compounds are inserted into the bilayer membrane the molecules give rise to parallel or anti-parallel alignment with the applied potential; which potentially can lead to voltage dependent aggregates.

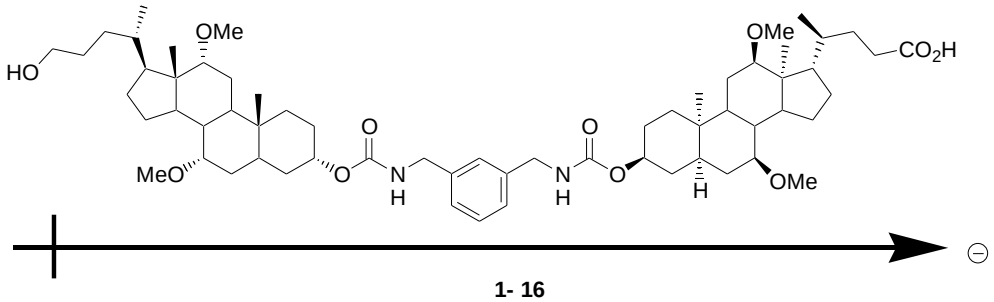

1- 16

Figure 1-11. Cholic acid derivative as a synthetic voltage-gated ion channel.

1.3.2.4 Hydroxyacid Aggregates

Perez's research is focused on bicyclic hydroxyacids (**1-17**). In the solid state, found in the X-ray crystal structure, this compound along with six water molecules forms a hexameric aggregate.[65,66] This class of compound is synthesized in about five steps with a yield of approximately 86%.[65]

Dynamic ^{23}Na NMR spectroscopy was used to assess the ion transport and it was found that all of the derivatives listed for **1-17** are active transporters.

The exact mechanism is still under development, but the current proposed active structure is that each hexameric structure stack together to form the ion channel aggregate (barrel rosette) in the membrane bilayer (Figure 1-12).

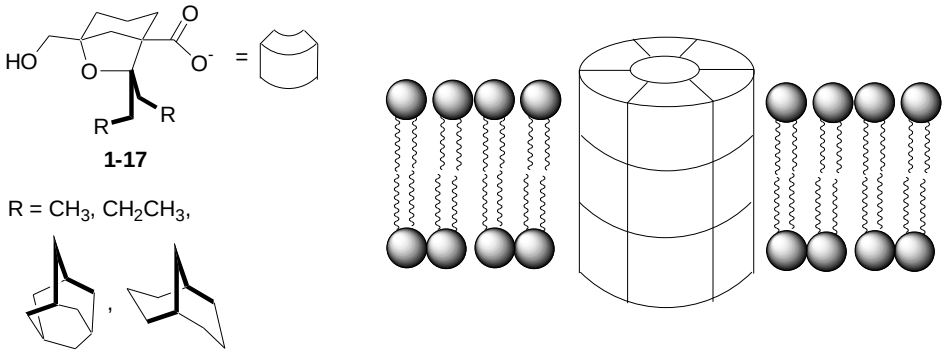

Figure 1-12. Proposed barrel rosette structure of **1-17**.

1.3.2.5 Oligoester and Acyclic Aggregates

Compound **1-7** was shown to be active but the macrocyclic nature makes the synthesis rather tedious. The Fyles group then devised another molecule (**1-18**) which is very similar in functional groups as **1-7** but the macrocycles are cleaved. Compound **1-18** was made in 46% yield from five synthetic steps.

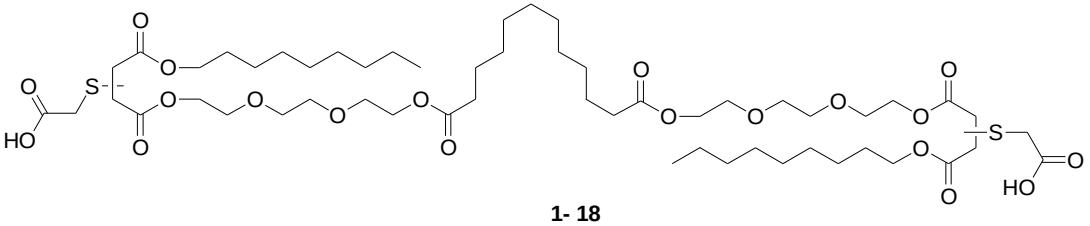

1- 18

Through pH-stat experiments, **1-18** was found to transport protons and cations. The kinetic order derived for **1-18** was similar to what was found for **1-7**. By planar bilayer clamp experiments, this compound was found to transport ions via an aggregate channel mechanism. The currents observed for **1-7** and **1-18** were 15.0 pS[43] and 13.7±0.7 pS[67], respectively, under the same bilayer clamp conditions. Hence, **1-18** is an easier molecule to synthesize and it maintained the functions that were apparent for **1-7**. The other major conclusion from this result is that macrocycles are not necessary in order to generate functional ion channels.

A potentially useful property of synthetic ion channels is having the ability to open and close in response to a transmembrane potential. The Fyles group was interested in building a membrane active compound which was asymmetric and therefore further developed the oligoester **1-7** to an asymmetric structure **1-19**. The Fyles group synthesized the voltage-gated ion channel, **1-19** in under 6% yield using solution chemistry from **1-9**.[68] The synthesis is similar for the preparation for **1-7**, **1-8**, and **1-6**.

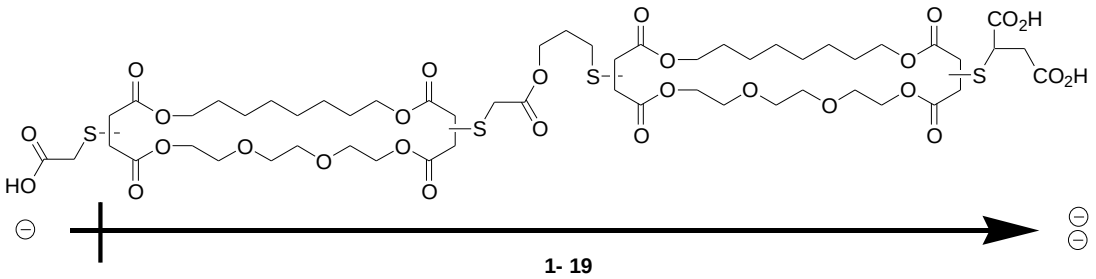

Figure 1-13. Bis-macrocycle bolaamphiphile example of a synthetic voltage-gated ion channel.

A method of building molecules asymmetrically with improved yield is by employing solid phase synthesis technology. Riguera and co-workers reported[69] solid-phase synthesis of oligoesters on Wang resin. The methods of using certain protecting groups and coupling conditions were adopted from Riguera with some modifications for condition optimization. Further development of the **1-19** structure lead to the linear **1-20** product. Hu described in detail the rationale for how the structure for **1-20** was decided upon.[25] In contrast to all of the previously mentioned solution-phase synthesized channel forming structures, **1-20** is made by solid phase methodologies on Wang resin in 82% yield.[25] The single synthesis of **1-20** gave a compound that was partly characterized and preliminary data showed that **1-20** was an active ion transporter using a bilayer clamp assay.[25]

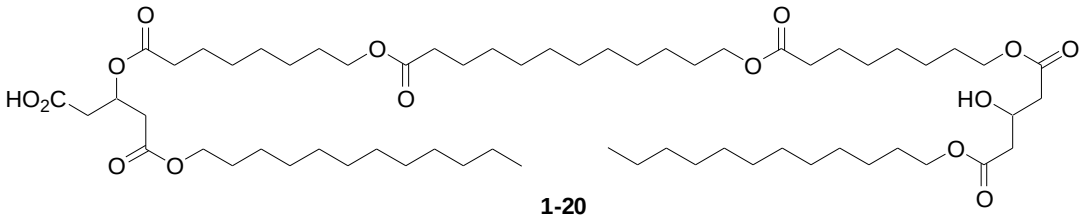

1-20

In essence, the solid support acts as a protecting group with which the molecule is built upon (Figure 1-14). The building blocks which are coupled onto the solid support must have at least two functional groups for the continuation of structure. Depending on the functional groups present, one of the functional groups might need to be protected, which would imply that following a coupling step in the sequence, a deprotection step is inevitable. The channel compound is released from the solid support at the end when all of the desired building blocks are connected.

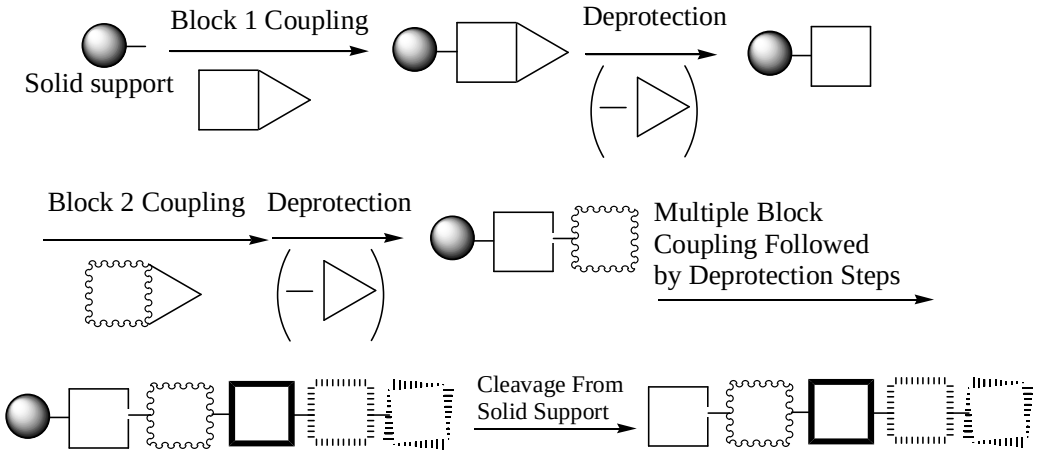

Figure 1-14. Solid support methodology with building block coupling and deprotection steps and a final release of product from solid support.

The advantage in using a solid support for synthesis is that a vast array of products can be synthesized in potentially minimal efforts and the purifications are relatively easy (because of the biphasic nature of the reactions.) Therefore, using a solid support approach to synthesis will allow for a more facile synthesis of asymmetric ion channel candidates.

Many of the simple channels are made in a linear synthesis and therefore minor modifications to the structure for structure-activity determination studies will require starting from the first step and carrying the reaction forward. If a method can be found where it is easy to synthetically modify the structure, and as a result create a large array of membrane active structures, this would be ideal for studying the structure effects of the channel compounds on the activity.

1.4 Goals of Thesis

The major goal of the thesis is to develop a method for efficiently generating asymmetric molecules which can have potential voltage gating properties. The asymmetric molecules are expected to aggregate to form "simple" ion channels. Simple ion channels are defined by either the monomers of the channels will have relatively few synthetic steps or the monomer unit has a molecular weight less than 1500 g/mol. As well, a method needs to be developed for the evaluation of the ability to transport ions through bilayer membranes by these asymmetric compounds.

Since many natural voltage-gated ion channels have asymmetric structures it would be of interest to generate compounds which are asymmetric. In the voltage-gated channel structure design used in the synthesis of **1-16** and **1-19**, it is common to find that either one or two negative charges from the carboxylate functional group are used to create the dipole. Although it has been noted that functional groups such as carboxylates, monosaccharides and ammonium when used as a single head group on bolaamphiphiles can still penetrate the bilayer such that there is no preference in membrane orientation for symmetric structures.[43] Therefore we may need to create a bigger dipole by using stronger anionic charges.

In order to generate an asymmetric ion channel in a linear synthesis, a protecting group must be used. With most types of solid support, the solid-phase resin is essentially a protecting group for carboxylic acids and alcohols. Provided that the building blocks for SPOS are end differentiated, then the final product will be end differentiated and possess an overall dipole. The Fyles group developed **1-20** because it would be asymmetric and expected to possess voltage-gating abilities. When Dr. Chi-Wei Hu embarked on the synthesis of **1-20** using solid-phase methodologies, his goal was to synthesize this target molecule but not consider optimizing the conditions.

To fully develop a methodology for building simple molecules, one of the first goals of this thesis is to optimize the solid-phase methodology. In Chapter 2, the synthesis of the building blocks as well as their coupling and decoupling on Wang resin is demonstrated.

The beauty of solid-phase synthesis is that a large array of compounds can be made efficiently, so another goal of the thesis was to generate a large group of oligoester compounds. In Chapter 3, a targeted library of compounds was made for the purpose of studying the structure-activity relationship for these oligoester ion channel-forming compounds. The rapid SPOS of a library can produce impurities. Therefore one aspect of this chapter is the focused characterization of the impurities formed in the SPOS.

By studying the large array of compounds, it might be possible to deduce structures which are selective for certain ions or be able to control the lifetime of the channel. Chapter 4 describes the use of an HPTS fluorescence assay to evaluate the transport process of the oligoester ion channel-forming compounds. A transport model is

proposed based on relative transport activities and aggregation studies of the oligoester compounds.

Chapter 5 extends the SPOS methodology to include the coupling of an amino acid (tryptophan) to the oligoester compound in order to demonstrate the generation of a molecule with a macroscopic dipole. As well, the indole is a useful fluorescent label and the fluorescence can be quenched. In applying the fluorescent label to purification methods, the integrity of the tryptophan-containing oligoester will be discussed. In order to get voltage-gating properties in the bilayer membrane, the asymmetric compounds must insert into the membrane asymmetrically, that is, there is preferential alignment of the macroscopic dipoles of the ion channel monomers in the bilayer membrane in the conducting state. SPOS gives asymmetric molecules but it is ambiguous if the SPOS compounds insert asymmetrically. Therefore Chapter 5 explains how the tryptophan-derived oligoester insert into the membrane bilayer based on fluorescence-quenching experiments.

Finally, Chapter 6 delivers the general conclusions for this research and proposes future experiments that can be conducted.

Chapter 2 Solid-Phase Organic Synthesis Methodology Development

One practical method for generating an asymmetric molecule for the synthesis of voltage-gated ion channel candidates is by using solid-phase organic synthesis (SPOS). SPOS is time efficient because for a multi-step reaction, purification only occurs at the end. In comparison, purification should occur after every intermediate step in solution phase chemistry to remove excess reagents and byproducts. Despite the high efficiency of SPOS, this method is material wasteful because an excess of reagents must be used to drive the reactions forward. Therefore in building a relatively lengthy molecule by SPOS, it would be convenient and efficient to find starting materials (building blocks) which have sufficient length to limit the number of reaction steps. These building blocks should also be easily derived from commercially available starting materials via simple organic transformations.

The advantage of SPOS is that once these building blocks are defined, various combinations of the building blocks can be used to generate a library of compounds. The purpose in generating such a large selection with permutations in the structure would help in understanding the structure-activity relationship of these potential ion channel-forming compounds.

A shortcoming of SPOS is that not all syntheses by SPOS will be efficient. For smaller products (up to about six synthetic steps) SPOS is a good method to perform the synthesis because a sufficient difference in molecular weights exists between the products and impurities. In generating much longer products the value of SPOS becomes

less apparent because of a proportional decrease in the weight difference between the impurities and the target molecule, making product separation difficult.

In this chapter three sections are discussed: 1) design and synthesis of the building blocks, 2) the loading and deprotection of the building blocks on the solid support, and 3) the coupling of building blocks to generate dimers and trimers as a proof of principle in the methodology.

One key functional group common to the bolaamphiphile ion channels synthesized in the past are the ester linkages used to join structural components. To mimic the bolaamphiphile structures, the target SPOS structures should also use esters to link the structural components. Therefore the building blocks for SPOS must consist of a carboxylic acid and alcohol functionality. A general target structure is shown in Figure 2-1. The target is composed of several building blocks connected by ester linkages and on either ends of the product are hydroxyl and carboxylic acid functional groups. The number of building blocks in the target can vary depending on the desired total molecule length and lipophilicity.

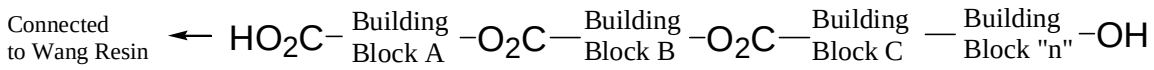

Figure 2-1. Proposed SPOS target development.

2.1 Synthesis of Building Blocks

There are many solid supports with a variety of functional groups to choose from for SPOS.[70,71] Attaching the building blocks to the solid support would involve either coupling at the carboxylic acid or alcohol end. Examples of commercially available resins for coupling the carboxylic acid and alcohol are Wang and trityl (Figure 2-2). The solid support must be insoluble in most organic and aqueous solvents in order to be used

in SPOS. Therefore the bulk of the resin is a polystyrene backbone cross-linked with divinylbenzene.

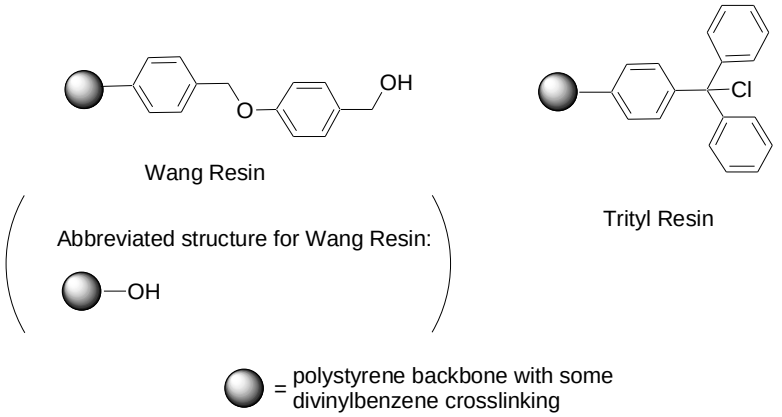

Figure 2-2. Wang and trityl resin structures used for protection of alcohols and carboxylic acids in SPOS.

The chloride on the trityl resin is prone to substitution so any nucleophilic functional group on the building blocks such as alcohols and carboxylic acids can be loaded onto the resin. Wang resin is different from trityl resin because the hydroxyl group is not a very good leaving group so instead the resin acts as a nucleophile which couples to electrophilic building blocks. Therefore most of the time carboxylic acids on building blocks are coupled onto Wang resin.

Two disadvantages of the trityl resin compared to Wang resin are the acid lability of the trityl resins and the fact that trityl resins are more expensive than Wang resins. Therefore the Wang support was used for all SPOS reactions which defined the direction that the structures must be built on the resin – coupling of the carboxylic acid end onto the resin and extension of the hydroxyl end. This direction is common in the area of solid-phase synthesis of peptides, so methods can be adapted from that area of research if needed. As well, the methodology developed for esters should also allow the use of amino acids as building blocks to increase product diversity.

The channel structure was broken down into two general components in Chapter 1 as “head group” and “core”. The head group is the part of the ion channel that is expected to anchor itself in the polar region of the bilayer membrane. Therefore the head group must have some polar component. Hu has described in detail the design criteria for the head group design.[25]

For SPOS to be efficient, the head group treated as one building block should satisfy three criteria. Since Wang resin is used as the solid support, the first criterion is that the head group should have a carboxylic acid functionality for coupling. Secondly, there should be an intrinsic lipophilic tail component to help the ion channel candidate with membrane partitioning. Finally, another functional group must exist for further coupling of building blocks such as an amine or alcohol.

The “core” components should have designs similar to the head group. That is, the building blocks must have points of connectivity so carboxylic acid and alcohol functional groups must be present for product extension on the solid support. The core building blocks should also have some degree of lipophilicity to allow for membrane partitioning. Consideration must also be given to the length of the core building block because the sum of the core components in an ion channel candidate ultimately defines the overall length of the structure.

2.1.1 Head Group Library

The head group should be made from simple chemical transformations and satisfy the three criteria previously mentioned (a graphical version is shown in Figure 2-3).

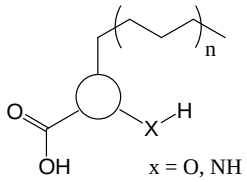

Figure 2-3. Head group design criteria: carboxylic acid functionality for coupling, nucleophilic group such as an alcohol or amine for coupling, and a lipophilic tail for aid in membrane partitioning.

The compounds made were characterized by ^{1}H and ^{13}C NMR spectroscopy as well as mass spectrometry. Elemental analyses were performed on some of the building blocks to determine compound purity. For all of the building blocks that we use for SPOS, there is a lack of any useful chromophore, so HPLC using a UV-VIS detector is not relevant for determining purity. Instead ^{1}H NMR integrations were extremely helpful for quantifying purity.

2.1.1.1 Block 1: Glutaric Acid Derivatives

Hu previously reported a commercially available TBDMS-protected glutaric anhydride (**2-1**) which undergoes alcoholysis upon the addition of an alkyl alcohol.[25] In Hu's thesis[25] 12-dodecanol was used to do the alcoholysis of **2-1** to yield **2-3**. In this thesis several other alcohols with varying numbers of carbon are utilized (10-decanol, 14-tetradecanol, 16-hexadecanol). The resulting esters **2-2**, **2-4**, and **2-5** are synthesized in a range of yields. In reference to the SPOS products and simplicity, these building blocks are known as G10 (**2-2**), G12 (**2-3**), G14 (**2-4**), G16 (**2-5**).

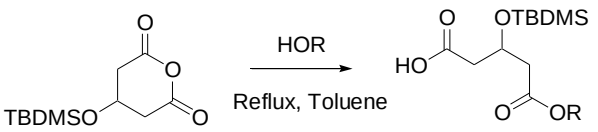

2-1

	R	Yields
2-2	$C_{10}H_{21}$	93%
2-3	$C_{12}H_{25}$	Quanitative
2-4	$C_{14}H_{29}$	71%
2-5	$C_{16}H_{33}$	33%

Scheme 2-1 Synthesis of glutaric acid derivatives

The identification of **2-2**, **2-4**, and **2-5** was made by ^{1}H NMR, ^{13}C NMR and mass spectrometry (MS). Evidence for the formation of esters is given by a multiplet with an integration of 2 at about 4 ppm which represents H_b (Figure 2-4). Since the structures of **2-2**, **2-4** and **2-5** are very similar with only a difference of some methylene units in the alkyl tail, the multiplicities and chemical shifts in the ^{1}H NMR spectra do not vary significantly; therefore only one ^{1}H NMR spectrum is shown below (Figure 2-4). The mass spectrum shows the molecular ion for the sodium complexes of **2-2**, **2-4**, and **2-5** at *m/z* 425.3, 481.3, and 487.4, respectively.

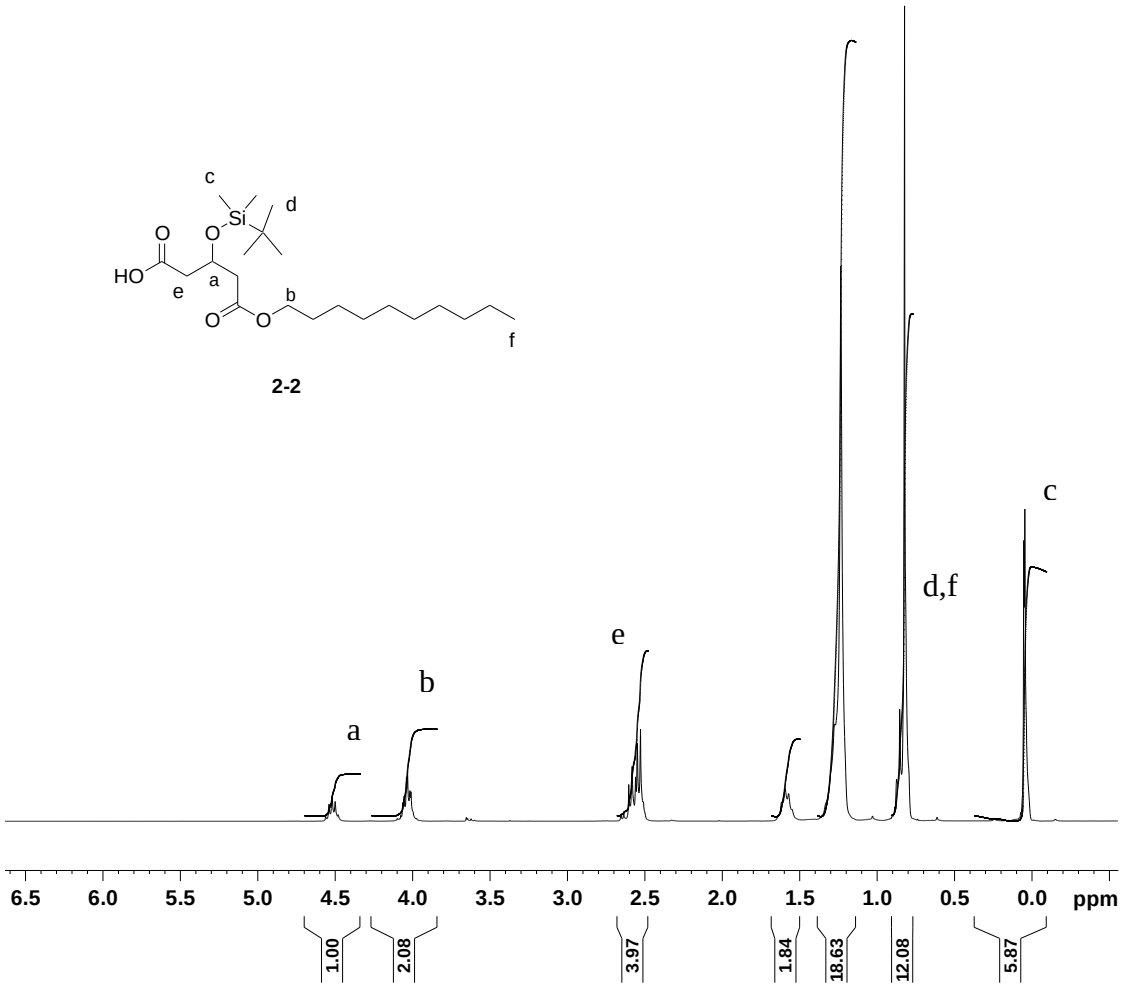

Figure 2-4. ^{1}H NMR spectrum of **2-2** in $CDCl_3$

At a later stage purity will be assessed by detailed examination of integrations. An example is illustrated here to show how this works in a trivial case. The purity of these compounds was analyzed based on the integrations of the ^{1}H NMR spectra (Table 2-1).

Table 2-1. ^{1}H NMR integrations for **2-2** to examine purity.

^{1}H signal	Expected Integration	Observed Integration	Error
a	1	1.00	0%
b	2	2.08	4%
c	6	5.87	2%
d,f	12	12.08	<1%
e	4	3.97	<1%

In Table 2-1 the errors in proton integration from what was expected were all under 5%. The errors are discussed if the integration difference between what was expected from what was observed by more than 5%. Otherwise it can be assumed that to the best of our knowledge the compound is "pure".

2.1.1.2 Amino Acid Derivatives

One method of achieving the three criteria set for the head group design was to use a starting material which has three functional groups for synthetic derivation. Since a Wang resin is used for coupling, by default a carboxylic acid functional group must be one of the components. A class of commonly found compounds with "tri-functionality" which has a carboxylic acid functionality are amino acids. All amino acids satisfy a di-functionality (possession of a carboxylic acid for coupling and an amino group for product extension) but there are some which do not meet the tri-functionality criteria such as glycine and alanine.

Keeping the same model as the glutaric acid derivatives (Figure 2-3), it would be convenient to have a lipophilic tail on the amino acid and an amino protecting group. Amongst the 20 amino acids with a range of functional groups, it would be easiest to functionalize glutamic or aspartic acid as both of these have a carboxylic acid side chain. A patent[72] was followed to selectively attach a dodecyl tail to a carboxylic acid side chain of glutamic acid to yield **2-6** (Scheme 2-2). The patent suggested using these alkylated compounds as surface active agents or further derivatized as N-carboxy anhydrides which possess interesting hydrocarbon solubility and physical properties. Compound **2-6** was made in 28% yield and the melting point of this product is 110-129 ºC while the reported

value is 177-177.4 ºC.[72] The discrepancy may be due to an impure, moist product with water from the filtration process.

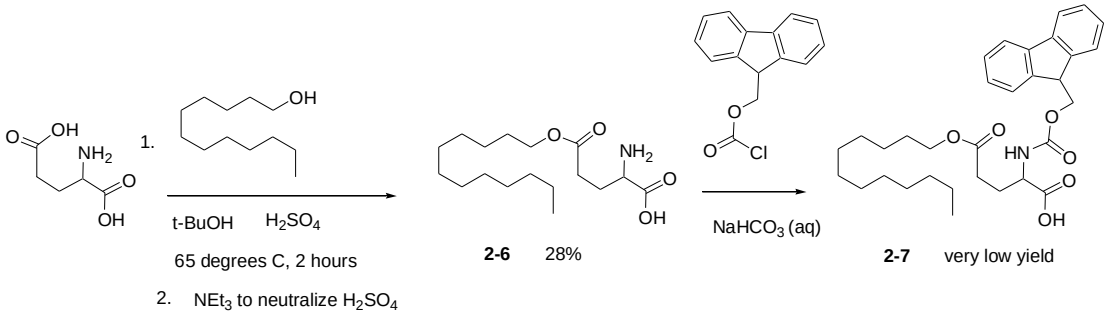

Scheme 2-2. Synthesis of alkyl ester amino acid **2-6** and Fmoc-protected **2-7**.

One of the advantages in using an amine group in SPOS is that when it is coupled to other building blocks, an amide is normally formed as the linker. Amides are a robust functional group and therefore it can probably withstand many types of chemical transformations. Prior to coupling amino acid derivatives to the solid-phase resin, the amino group must be protected, otherwise self-coupling would occur. Typical protecting groups used for amino groups of amino acids are 9-fluorenylmethyl carbamate (Fmoc) and di-*tert*-butyl dicarbonate (*t*-Boc). Fmoc was decided upon as the protecting group for its robustness to acidic reaction conditions compared with *t*-Boc and ease of amine deprotection. To deprotect the amine from the Fmoc group, a mild base solution is normally used; whereas to remove a *t*-Boc group, a strongly acidic solution is required. Unfortunately strongly acidic conditions may also release the product from the Wang resin. Conventional means of putting the Fmoc group on amino acids involve the reaction of the amino acid with 9-fluorenylmethyl chloroformate in a basic aqueous solution and this was followed to attempt to generate **2-7** (Scheme 2-2).[73]

The complication that occurred was that the ester-derivatized amino acid **2-6** is not water soluble under basic conditions. Other polar organic solvents were used but the

Fmoc just did not couple to the amino acid. Several methods were attempted to couple these components, such as grinding neat (all reagents excluding solvent were added to a mortar and pestle and then ground), but were unsuccessful. Finally, **2-7** was made, albeit in very low yield, by carefully controlling the pH conditions (acidifying the solution) so that **2-6** will dissolve in water but at the same time not be sufficiently acidic to risk ester cleavage.

The ^{1}H NMR spectrum of the crude **2-7** product is in Figure 2-5.

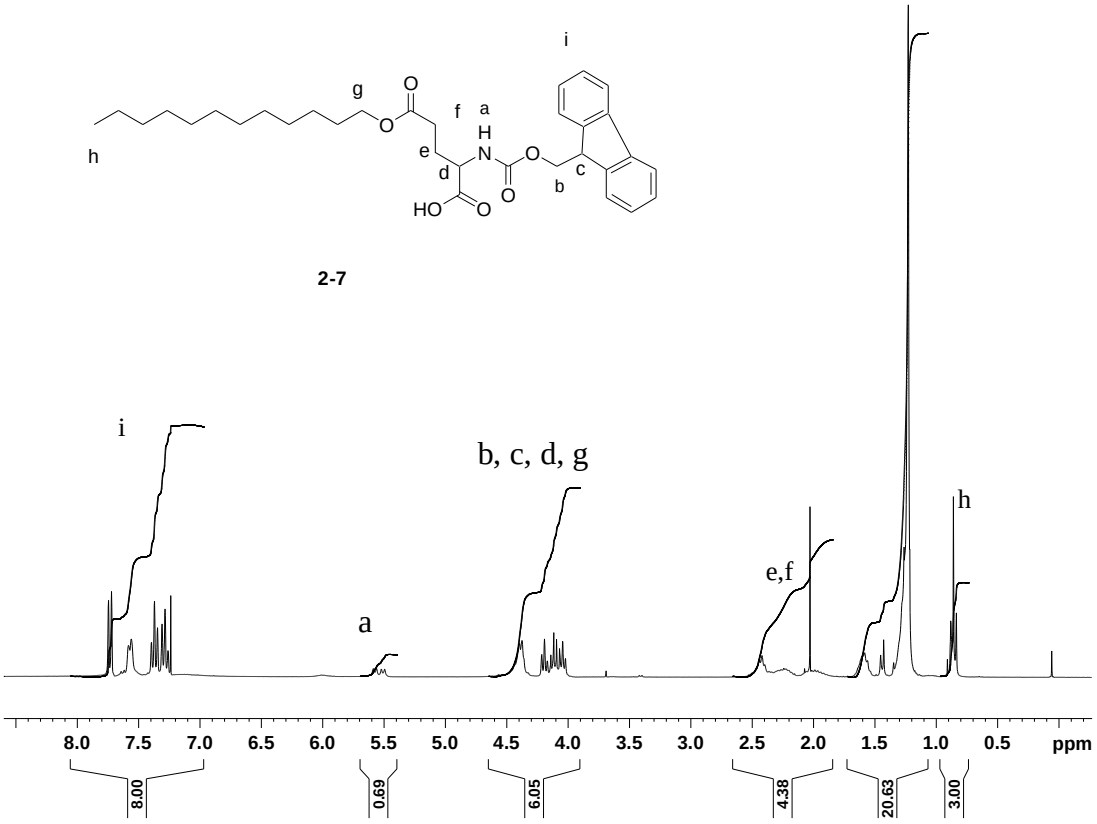

Figure 2-5. ^{1}H NMR spectrum of **2-7** (crude product only) in $CDCl_3$.

The Fmoc was attached as evident from the carbamate proton resonance (δ= 5.5 ppm, two broad doublets in Figure 2-5). The integration of H_a is under the expected 1 which is most likely due to incompetent integration of the H_a signal. Most of the other protons integrate to as expected.

The protecting group starting material 9-fluorenylmethyl chloroformate is expensive and therefore from an economical standpoint, this reaction is overly expensive to make a starting material which is used in three-fold excess for solid-phase purposes.

Trifluoroacetyl was another protecting group for the amino acid amine that could be used in SPOS. It was anticipated that this group would be a challenge to use because typically the trifluoroacetamide is cleaved under basic conditions. Since there are ester functional groups connecting the SPOS product to the resin, then the basic solution used to release the trifluoroacetyl group may be too harsh. Regardless, the trifluoroacetamide protecting group was still used to investigate the ease of deprotection. Trifluoroacetic anhydride was used to dehydrate aspartic acid and also form the trifluoroacetamide **2-8** (Scheme 2-3).[74]

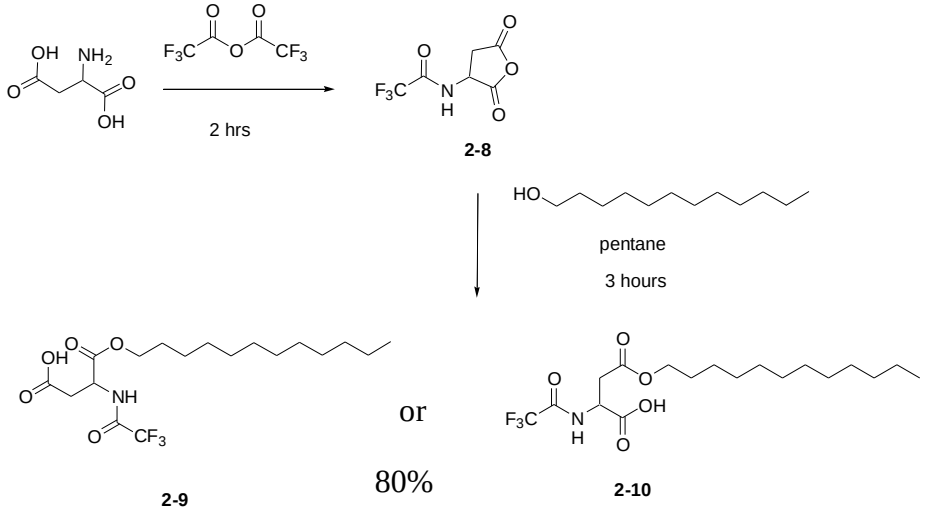

Scheme 2-3. Synthesis of **2-9** or **2-10**.

In the head group design, a lipophilic component was required. Therefore the anhydride (**2-8**) was treated with dodecanol for the alcoholysis according to a reference literature procedure[74] to yield one of two regioisomers (**2-9** or **2-10**) in 80.3% yield. It

would appear based on the relatively "clean" ^{1}H NMR spectrum (Figure 2-6) that there is regioselectivity for either **2-9** or **2-10** because the ^{1}H integration for H_b appears to be in two sets of doublet of doublets. No effort was made to determine which isomer was made. If there was an equal mixture of both **2-9** and **2-10** in the product, then it would have been anticipated that there would be distinct chemical shifts for the H_b of **2-9** and **2-10**. The small triplet at about 4.1 ppm is probably the H_c of the lesser of the two regioisomers while the small triplet at about 3.6 ppm is residual dodecanol.

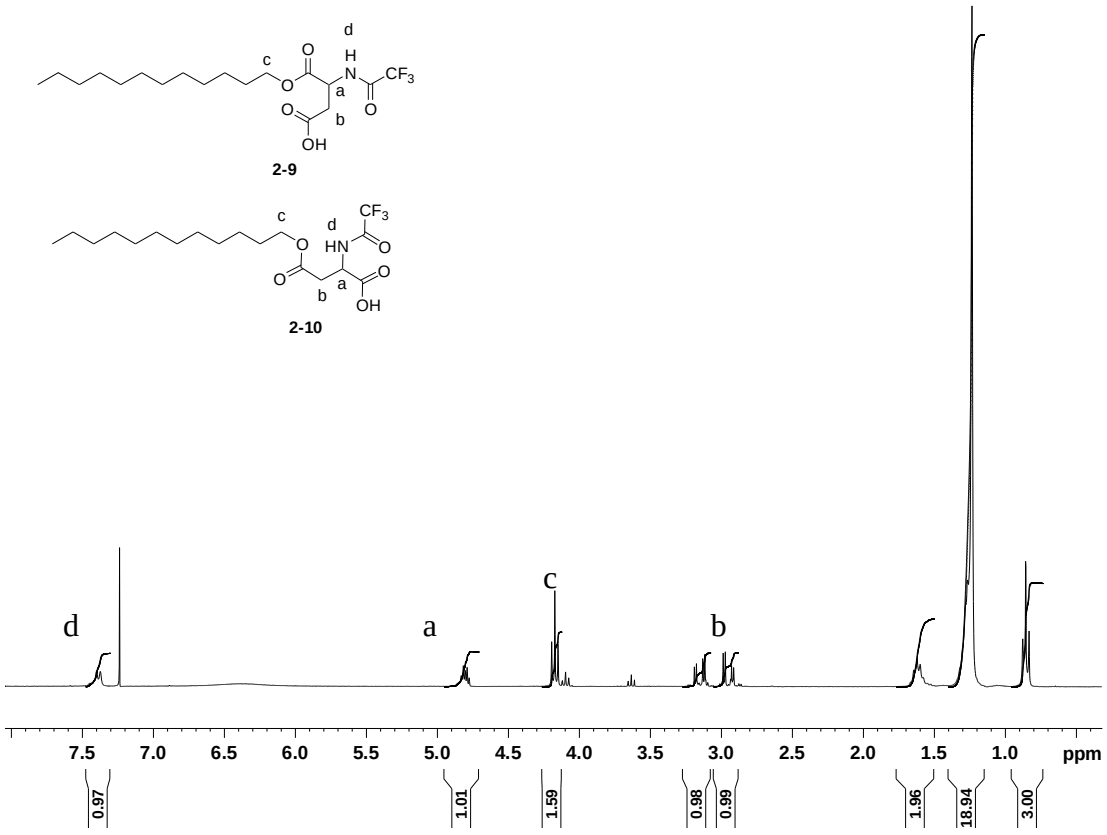

Figure 2-6. ^{1}H NMR spectrum of **2-9** or **2-10** in $CDCl_3$ synthesized according to Scheme 2-3.

The amino group of the glutamic acid derivative, **2-6**, can be protected with trifluoroacetic anhydride. As with **2-9** and **2-10**, evidence for the amide formation is the appearance of the amide doublet at about 8 ppm (Figure 2-7). This chemical shift is

downfield compared the amide N<u>H</u>-$COCF_3$ which may be caused by the sample concentration. This particular proton is acidic (due to the electron-withdrawing CF_3 group) and therefore similar to carboxylic acids where the proton resonances are concentration dependent.

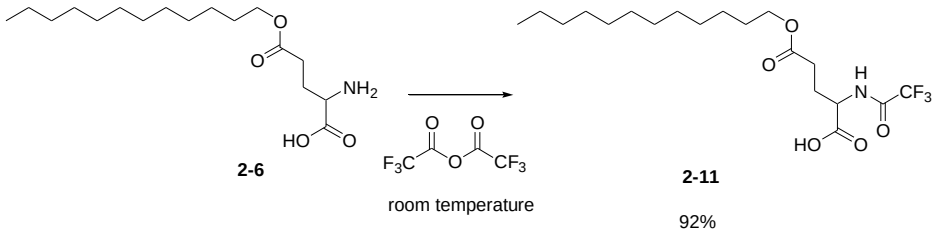

Scheme 2-4. Synthesis of **2-11**

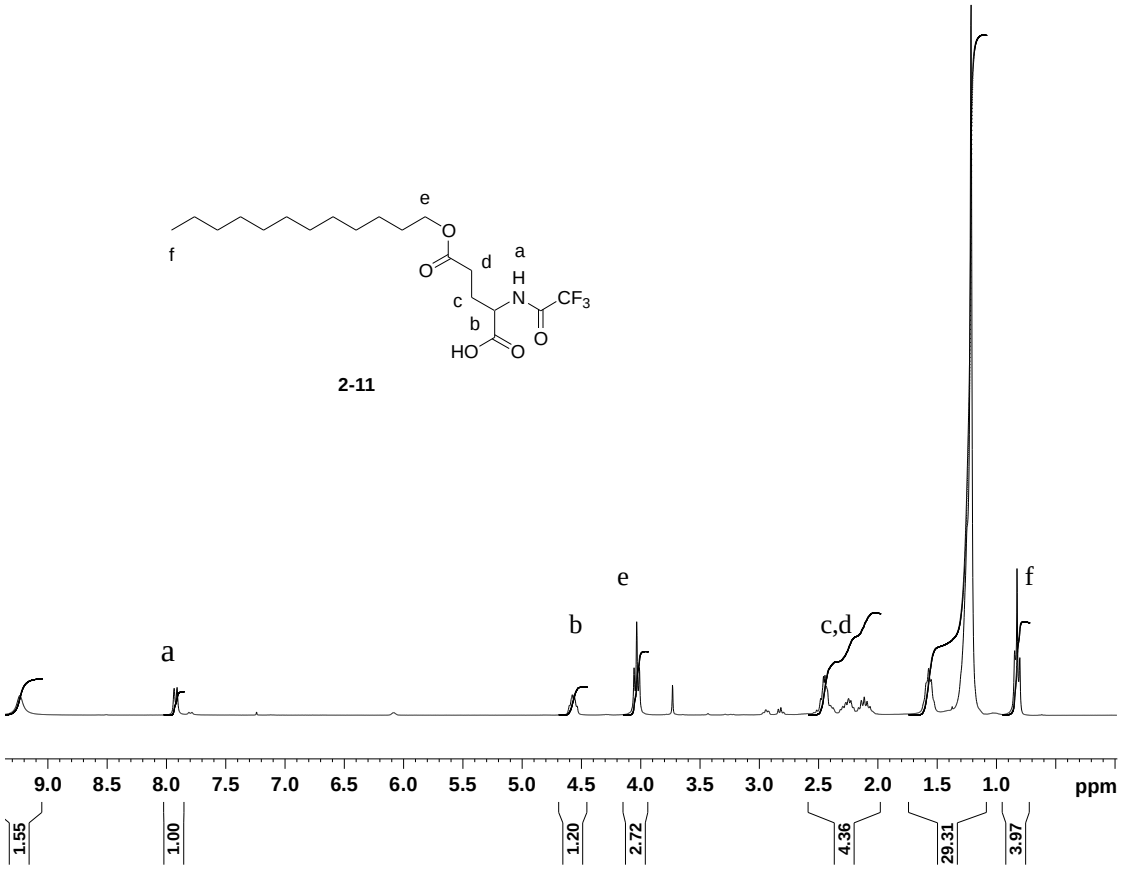

Figure 2-7. ^{1}H NMR spectrum of crude **2-11** in $CDCl_3$

There are several literature examples where trifluoroamides can be deprotected using conditions such as 10% K_2CO_3/MeOH-H_20[75], $NaBH_4$/MeOH[76], and NaOH/H_2O[76]. The latter condition is quite harsh for a compound that also contains esters. A more serious problem is that, the K_2CO_3/MeOH-H_2O condition is not strong enough to do the hydrolysis for **2-10** (recovered intact after reaction at room temperature). Reactions with stronger nucleophiles (such as NH_3) were avoided because of the risk that the esters, and not the trifluoroamide, may be cleaved. With this building block, the goal is to couple it to the SPOS resin. Once the building block is coupled onto growing product or the resin, it must be deprotected to allow for further building block coupling. In order to do the deprotection, it would be necessary to use these polar, protic solvents, which is not compatible with the normal Wang resin as the swelling of the polymer resin is greatly reduced; drying for subsequent coupling reactions would also have to be done.

Another common amine protecting group is trityl. The trityl group can be cleaved from the amino group by two general methods such as hydrogenation[77] and strong acid[78]. Hydrogenation on solid support using conventional heterogeneous catalysis can be a challenge to do because of poor contact between the catalyst and the substrate as well as the recovery of catalyst from the reaction mixture can be difficult because of the intimate mixing with the solid support. Although homogeneous catalysis might be used for the trityl deprotection, there are no current examples of this in the literature. The strongly acidic solutions necessary for cleavage of the trityl group may also release the product from the resin. As well, the trityl group is rather large and therefore it might attenuate the reactivity of the carboxylic acid by steric effects.

Therefore, with the difficulty of trying to deprotect the amine while preserving the ester and the bulkiness of the group, this protecting group was designated as inappropriate for our needs. Consequently, due to their difficult nature to functionalize, amino acids were eliminated from our list of head group building blocks.

2.1.1.3 Block 3: β-Hydroxy acid Derivatives

The link formed by the glutaric acid derivatives to the core building blocks is derived from a secondary alcohol. The stability of the ester of the secondary alcohol is discussed in Chapter 3 and it became of interest to generate head groups where the building block connection occurs at a primary alcohol. Recall that for a head group, three criteria should be met (carboxylic acid moiety, lipophilicity and connecting functional group), so in the design of this head group it would be necessary to satisfy as many of the criteria as possible. The synthesis of β-hydroxy acid derivatives was decided upon because the starting materials (lauric acid and oleic acid) possess a carboxylic acid functionality (for coupling onto the solid-phase resin or to the terminal primary alcohol of the core building block) and a long alkyl group is present for membrane partitioning. To append the primary alcohol, the acidic and α-protons of lauric and oleic acids were removed by LDA and then gaseous formaldehyde reacted with the dianion (first reactions in Scheme 2-5). This procedure was adapted from a literature preparation for the β-hydroxy acid of oleic acid.[79] The hydroxy acids are isolated by column chromatography at this point because the starting oleic and lauric acids are very difficult to separate at a later stage.

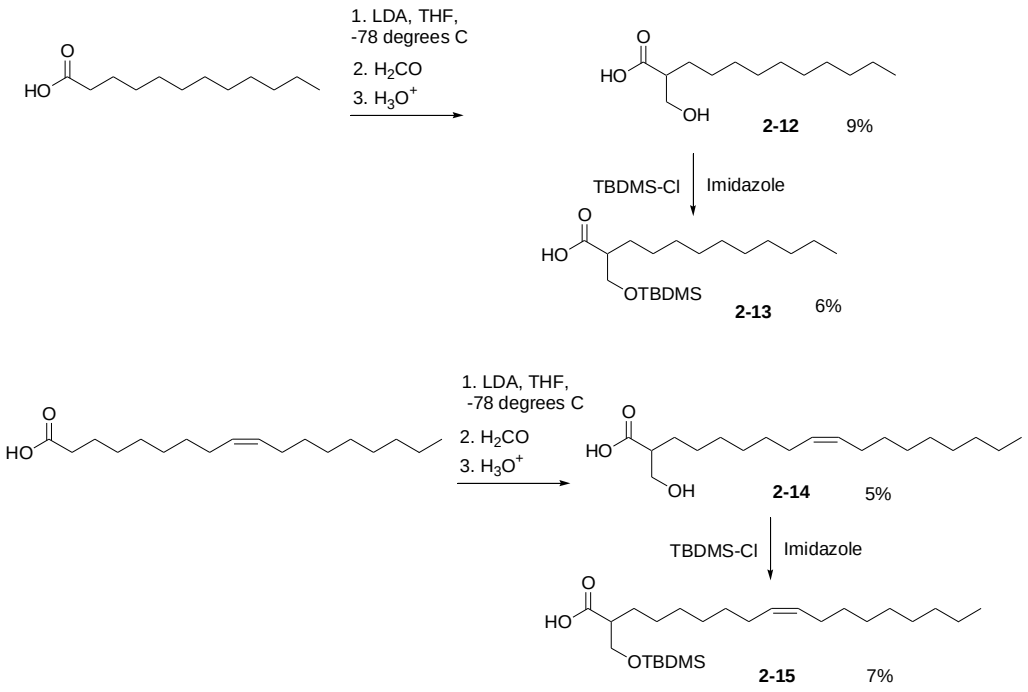

Scheme 2-5. Synthesis of **2-13** and **2-15.**

Evidence for the formation of **2-12** and **2-14** was the presence of a doublet at about 3.8 ppm in the ^{1}H NMR spectrum consistent with the expected C$\underline{H_2}$OH (H_b) group (Figure 2-8 and Figure 2-9).

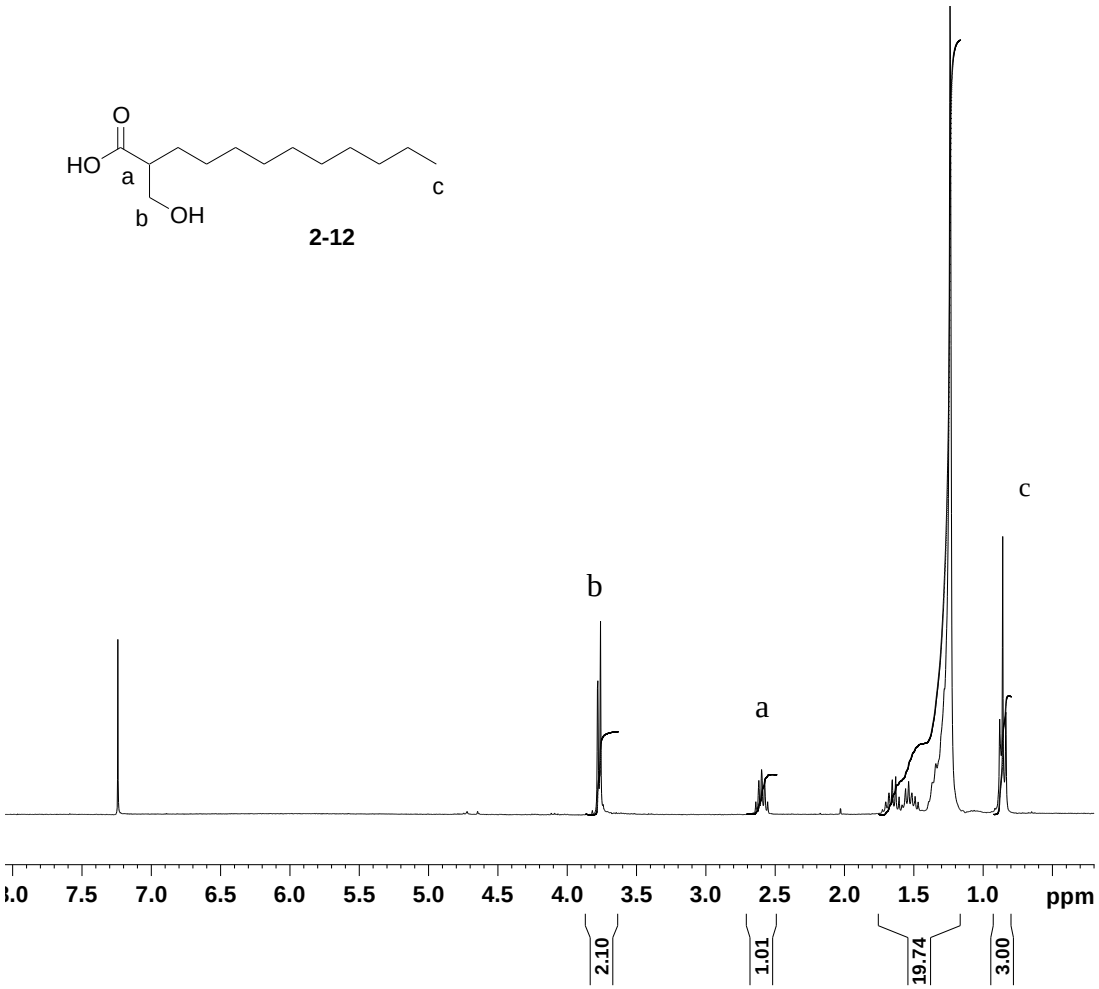

Figure 2-8. ^{1}H NMR spectrum of **2-12** in $CDCl_3$.

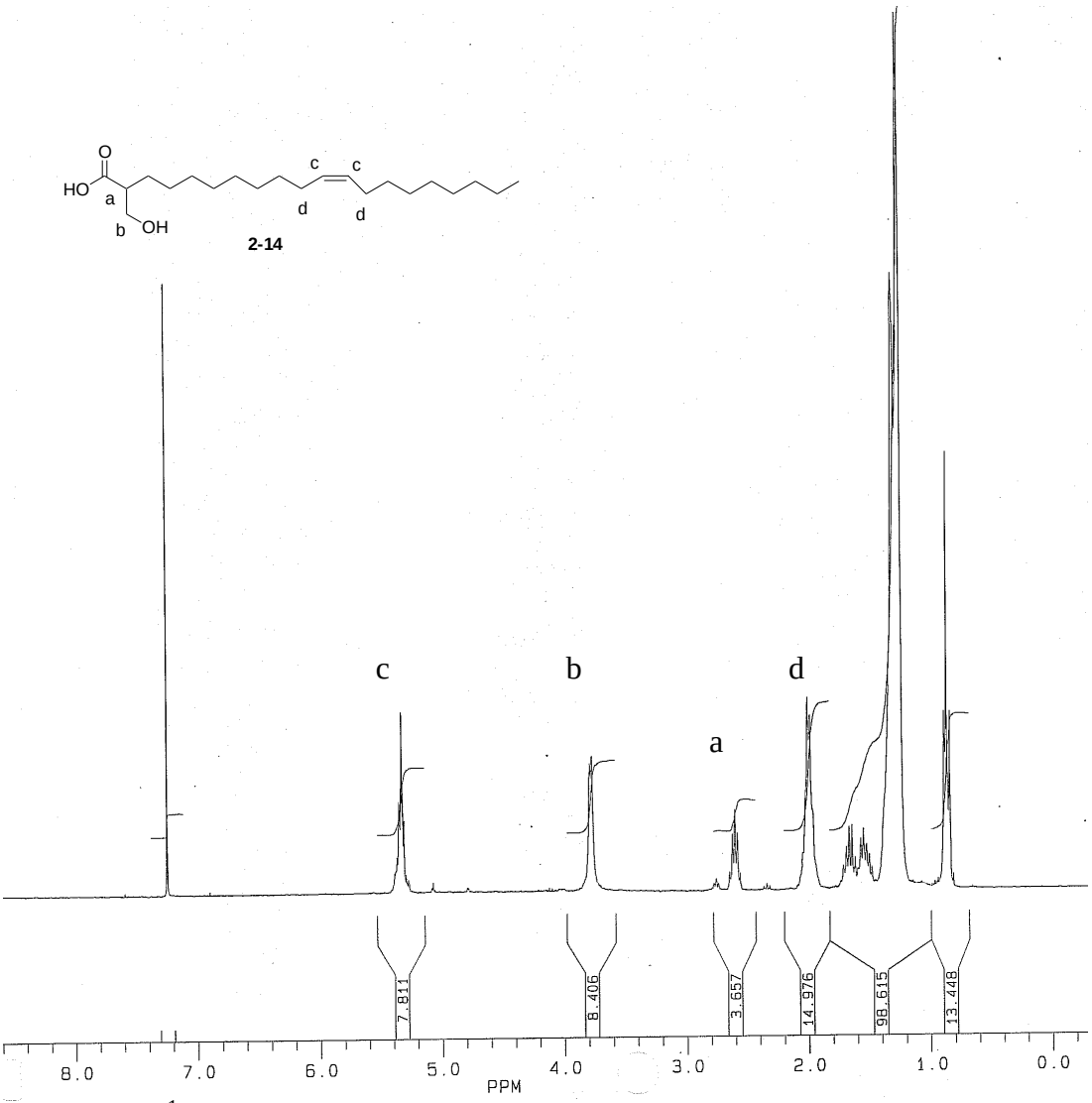

Figure 2-9. ^{1}H NMR spectrum (300 MHz) of crude **2-14** in $CDCl_3$.

A judicious choice of protecting groups must be made. Protecting groups such as THP contain a chiral center so with the chiral center already on the racemic hydroxy acid then further generation of another chirality center leads to diastereomers. The purification of diastereomers may be a challenge so it would be desirable to select protecting groups without chiral centers. A better protecting group choice is TBDMS because a racemic mixture of **2-13** or **2-15** would be generated. It was difficult to selectively protect only the alcohol over the carboxylic acid so consequently an excess of TBDMS-Cl was used to protect both functional groups followed by a mild acid workup

with ammonium chloride to cleave the TBDMS ester. The final (unoptimized reaction) yields after column chromatography from starting alkyl acids were 7% for **2-15** and 6% for **2-13** (Scheme 2-5).

The LSIMS of **2-13** showed both the $[M+Na]^+$ and $[M+H]^+$ ions at *m/z* 366.7 and 344.3, respectively. ^{1}H NMR spectroscopy once again was essential for determining when the TBDMS group has protected the alcohol moiety of **2-13** or **2-15**. Prior to the addition of the TBDMS, the protons of the hydroxymethyl (for **2-13** and **2-15**) can rotate freely so only an averaged doublet was observed. Since the TBDMS group is sterically demanding, it prevents the methylene next to the ether from freely rotating and the magnetic inequivalence of the two protons is then evident as multiplets in the ^{1}H NMR spectrum. The integrations in the ^{1}H NMR spectra also support the proposed structure of **2-13** (Figure 2-10). Based on the integrations of the ^{1}H NMR spectra, **2-13** was synthesized in high purity following column chromatography and no unprotected alcohol was observed.

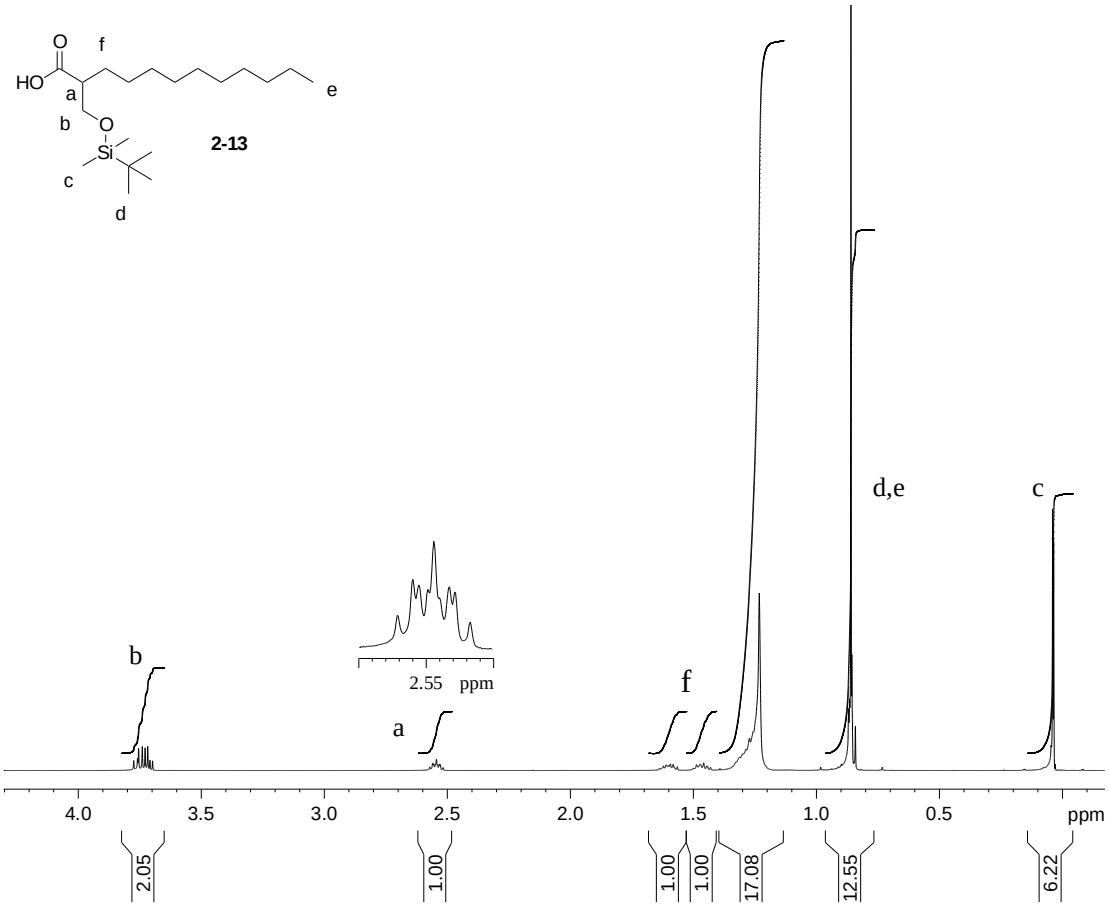

Figure 2-10. ^{1}H NMR spectrum of **2-13** in $CDCl_3$

For **2-15**, the mass spectrum showed the $[M+Na]^+$ ion at *m/z* 449.3. The ^{1}H NMR spectrum for **2-15** is shown in Figure 2-11. The spectrum is very clean and the ^{1}H integrations are as expected and no evidence of **2-14** was observed.

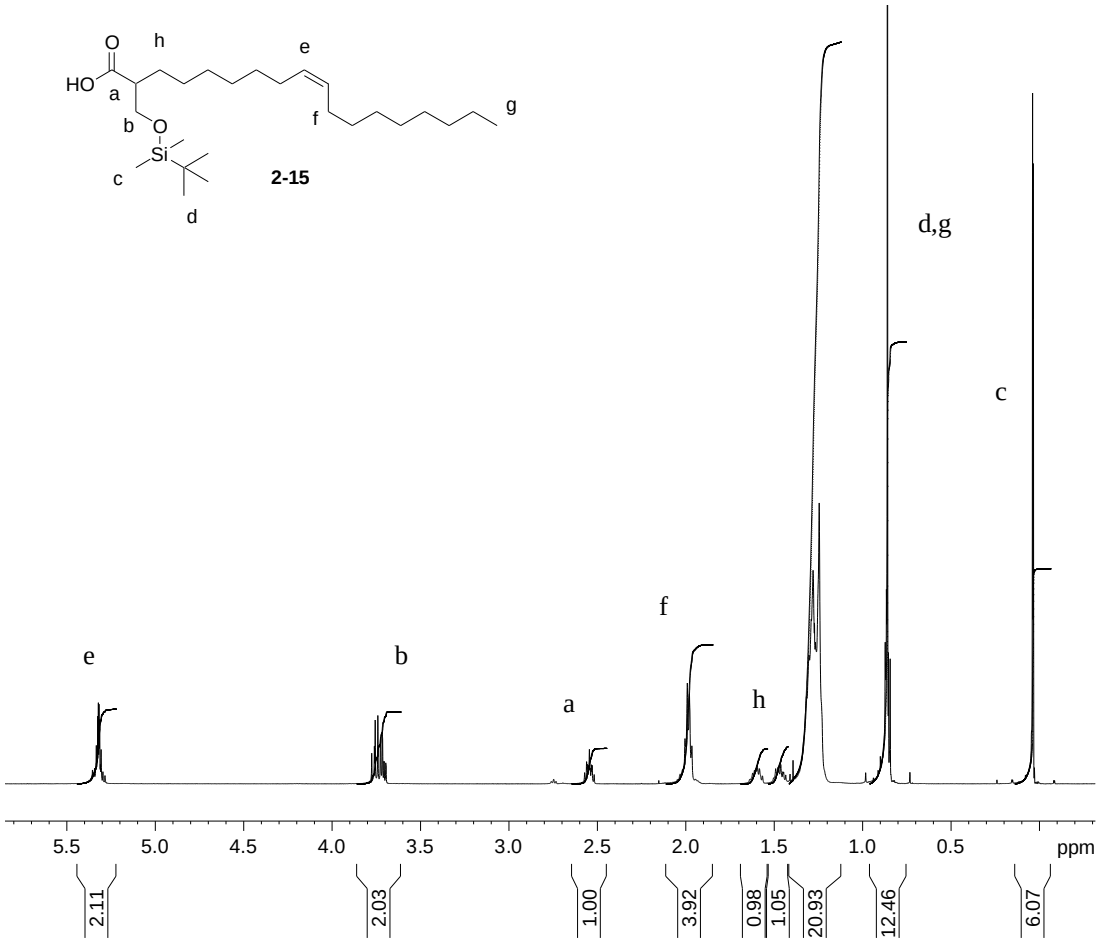

Figure 2-11. ^{1}H NMR spectrum of **2-15** in $CDCl_3$

2.1.2 Block 3: γ-Hydroxy Acids for Core Building Blocks

In the Riguera research[69] the building blocks were THP protected α-hydroxy acids. These α-hydroxy acids are too short for the length projected for the ion channels. In our research, we decided to adopt the strategy of using THP protected hydroxy acids. The carboxylic acid functionality is required for coupling to blocks on the resin and an alcohol functionality is required for further product extension. Since the core building blocks define the length of the ion channel core, then it is important that the core building blocks be of sufficient length such that the overall ion channel synthesis is efficient yet allow for easy variations in core length (Figure 2-12). If the core building blocks are too

short, then multiple steps are required to build the core which is inefficient and wastes material (Figure 2-12A). Whereas if the core building blocks were too long, then there would be limitations on how many core variations were possible (Figure 2-12B). Therefore hydroxy acids that contain a minimum of six carbons and can be easily synthesized from commercially available starting materials were selected.

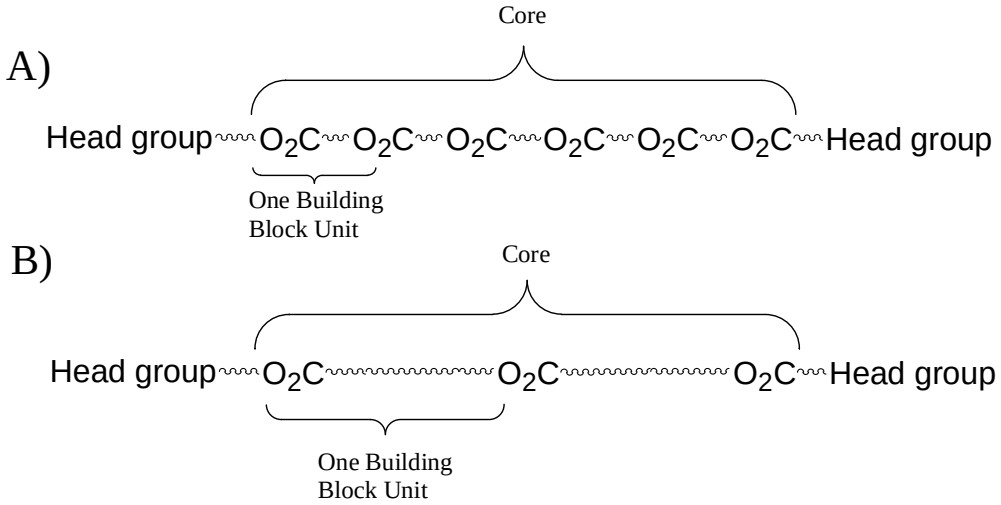

Figure 2-12. Core design considerations. A) The core is comprised of short building blocks. B) The core is comprised of very long building blocks.

2.1.2.1 6-Hydroxyhexanoic Acid Derivative

The simplest building block was prepared by hydrolyzing ε-caprolactone to yield the hydroxy acid (**2-16**) followed by alcohol protection using THP. The proton chemical shift of the methylene next to the oxygen of the lactone is around 4.1 ppm and upon hydrolysis, this resonance disappears and another resonance appears at 3.6 ppm which represents the methylene next to the open chain alcohol. The hydrolysis is best done under basic conditions over 2.5 hours followed by acidifying the aqueous solution and extraction to give a 37% yield of **2-16**. When the hydrolysis was conducted in acidic conditions, significant unidentifiable side products were observed in the ^{1}H NMR spectrum. The alcohol of **2-16** is then immediately protected with DHP (assuming that

the open form is not very stable relative to the lactone) and purified using column chromatography to yield **2-17** in 19% (Scheme 2-6).

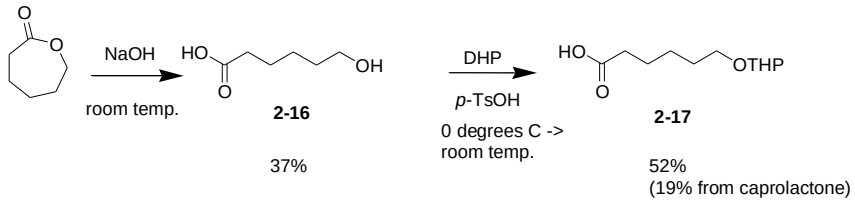

Scheme 2-6. Synthesis of **2-17.**

Compound **2-17** was characterized using ^{1}H and ^{13}C NMR spectroscopy and MS. The MS showed an ion at *m/z* of 215.1 for the $[M+H]^+$ ion of **2-17**. A peak observed at *m/z* 131 was consistent with the molecular ion of **2-16** $[M+H]^+$**.** It is unclear whether this peak is a fragment of **2-17** or if it is a component of product mixture.

In the ^{1}H NMR spectrum, when the protection with THP was sufficient, the triplet at about 3.6 ppm (from the $C\underline{H}_2OH$) between the proton resonances disappears (space is indicated with a circle in Figure 2-13). The ^{1}H NMR spectrum was very clean and showed no evidence of caprolactone. The typical shift for the $-C\underline{H}_2O_2C-$ of caprolactone is at 4.2 ppm (indicated by rectangle in Figure 2-13).

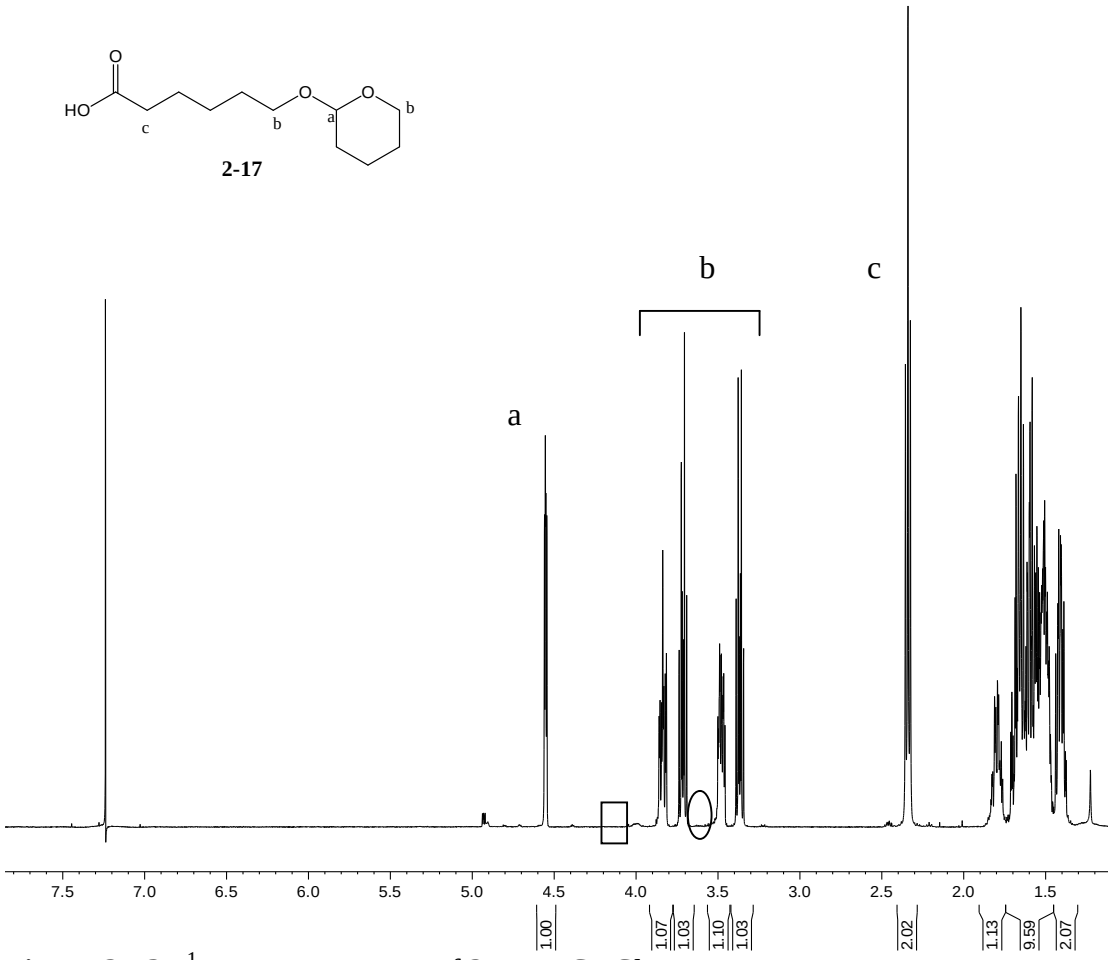

Figure 2-13. ^{1}H NMR spectrum of **2-17** in $CDCl_3$.

It was noted through taking ^{1}H NMR measurements of the same sample over a couple of months that **2-17** is not very stable with respect to the caprolactone and **2-18** (Scheme 2-7).

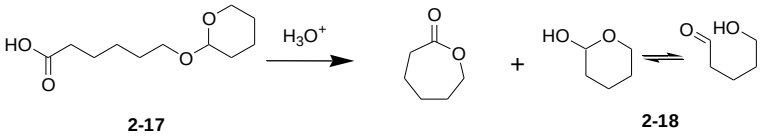

Scheme 2-7. Decomposition of **2-17**.

2.1.2.2 8-Hydroxyoctanoic Acid Derivative

Adopting the same strategy as **2-17** to make 8-hydroxyoctanoic acid (**2-19**), the eight carbon lactone was used. This ester is not commercially available at a reasonable

cost although it can be synthesized from cyclooctanone via a Baeyer-Villiger oxidation. The nine-membered lactone (**2-20**) is not an energetically favored ring size compared to a 5,6, or 7 membered ring[80] and the Baeyer-Villiger is very sluggish; extreme conditions (heating with *m*-CPBA for several days) were required. Similar to 6-hydroxyhexanoic acid, the lactone was hydrolyzed under basic conditions to give the sodium salt of **2-19**. Following the base hydrolysis, the aqueous solution was acidified and then extracted to yield **2-19** in 32%. Compound **2-19** was then hydroxy-protected as THP (**2-21**) and purified using column chromatography to yield **2-21** in 22% from cyclooctanone.

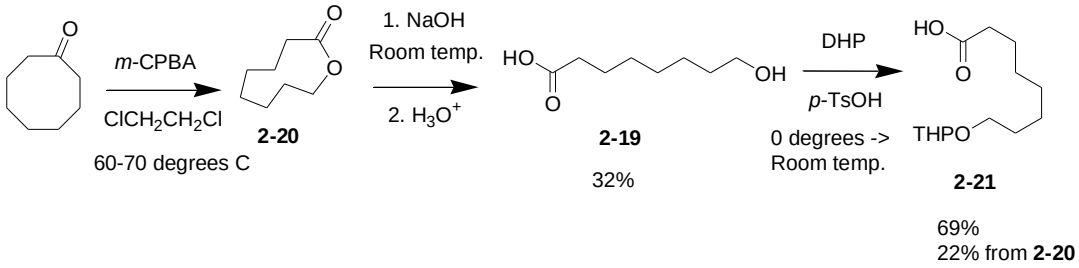

Scheme 2-8. Synthesis of **2-21.**

The $[M+H]^+$ signal in the MS for **2-21** is *m/z* 243.2. A peak at *m/z* 143 is the fragment dehydrated molecular ion for **2-19** ($[M+H-H_2O]^+$).

The ^1H and ^{13}C NMR spectra of **2-21** look very similar to those of **2-17** except for the alkyl proton integrations, which are slightly higher (by four protons) and there are two more carbon resonances in the latter spectrum. Similar to **2-17**, there was no evidence in the ^1H NMR spectrum of lactone (square in Figure 2-14) or **2-19** present.

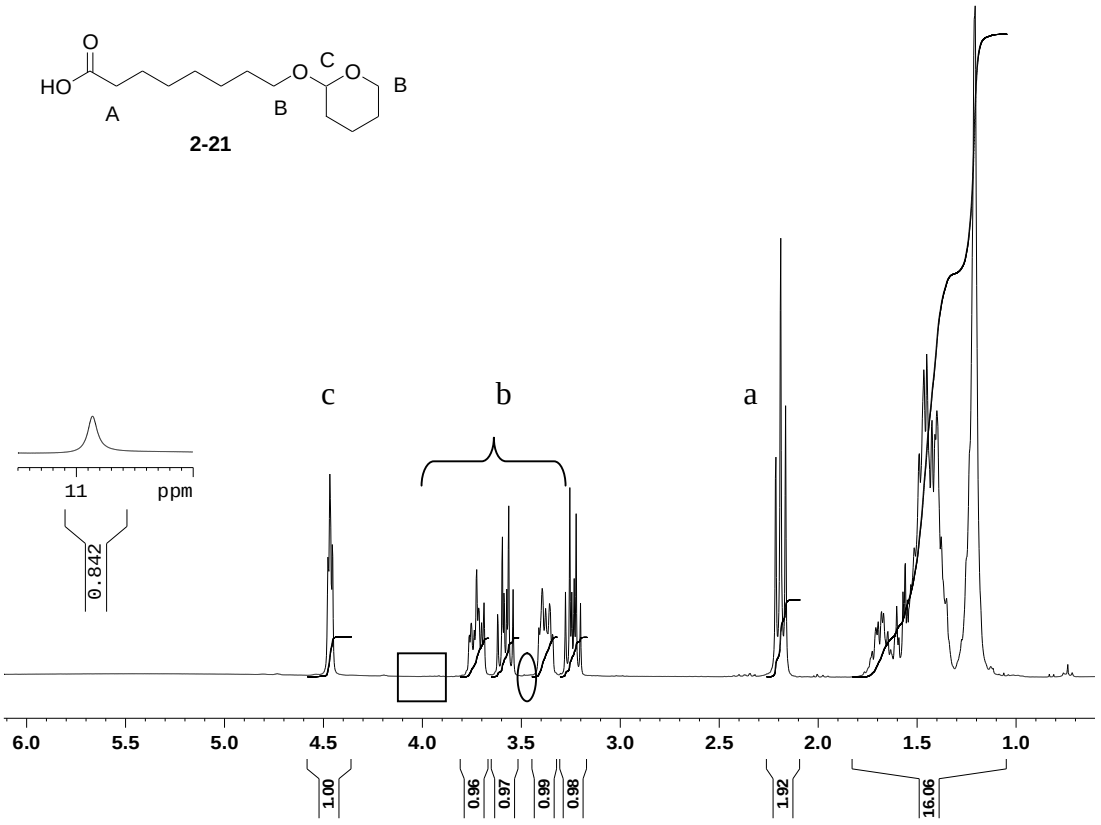

Figure 2-14. ^{1}H NMR spectrum of **2-21** in $CDCl_3$**.**

2.1.2.3 12-Hydroxydodecanoic Acid Derivative

The twelve carbon hydroxy acid is commercially available so it was just protected with DHP. Compound **2-22** was purified by column chromatography and the resulting yield was 95%. Hu has described the synthesis and characterization[25] of **2-22** although minor modifications were made in this thesis to give a higher yield (Scheme 2-9).

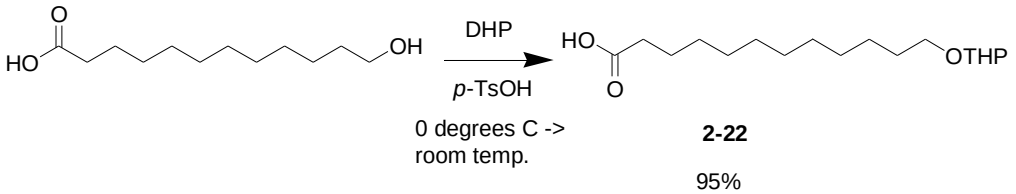

Scheme 2-9. Synthesis of **2-22**

The LSIMS showed that the $[M-H]^+$ ion was consistent with *m/z* 299. According to the ^1H NMR integrations, the **2-22** made was pure because there appeared to be no free hydroxy acid (lack of $C\underline{H_2}OH$ resonance in the ^1H NMR spectrum (oval)), and no lactone was observed (rectangle).

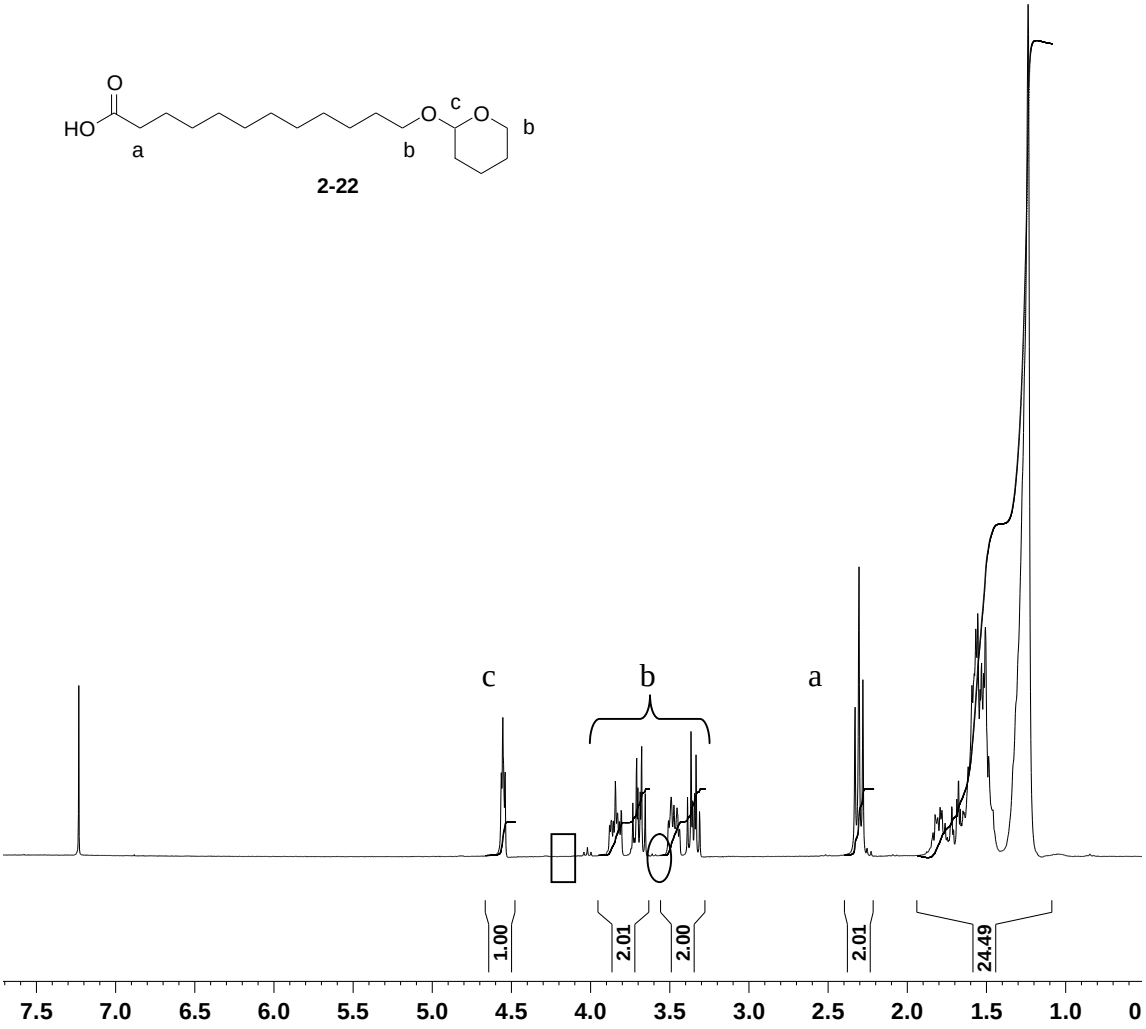

Figure 2-15. ^1H NMR spectrum of **2-22** in $CDCl_3$.

2.1.3 Summary of Building Block Synthesis

Addressing each building block as the compound name (e.g. **2-2**) would be uninformative. Hence the collection of the nine building blocks is listed in Table 2-2 along with their "alternative names" which will help in quickly identifying the building

block. As well, the yields from the syntheses are listed in Table 2-2. The "G" of G10, G12, etc. represents a glutaric acid derivative which is the product from alcoholysis of glutaric anhydride.

Table 2-2. Available building blocks and their yields.

Building block	Alternative Name	Building block yields (%)
2-2	G10	93
2-3	G12	Quantitative yield
2-4	G14	71
2-5	G16	33
2-13	Lau	6
2-15	Ole	7
2-17	Hex	22
2-21	Oct	22
2-22	Dod	95

In Table 2-3 a list of building blocks and an abbreviation to their structure when used in a SPOS product is presented. The subscripts have meanings of: T = tail (the carboxylic acid is coupled while the alcohol is either protected or free), H = head (the carboxylic acid is attached to the resin or free and the alcohol is used to couple), C = core (both the alcohol and carboxylic acid ends are coupled), and P = the alcohol end is protected.

Table 2-3. Available building blocks and their SPOS abbreviations.

Building block	SPOS abbreviation	n	Structure (= on resin)
2-2	$G10_T$	8	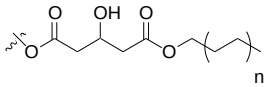
2-3	$G12_T$	10	
2-4	$G14_T$	12	
2-5	$G16_T$	14	
2-3	$G12_H$	5	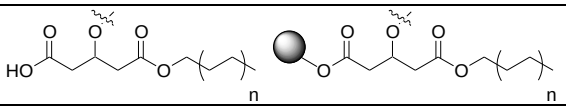
2-3	$G12_C$	5	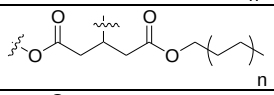
2-13	Lau_T		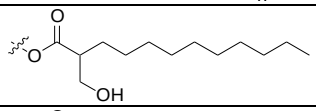
2-13	Lau_C		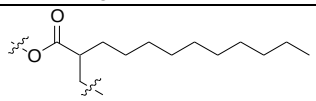
2-13	Lau_H		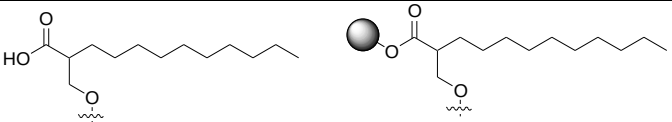
2-15	Ole_H		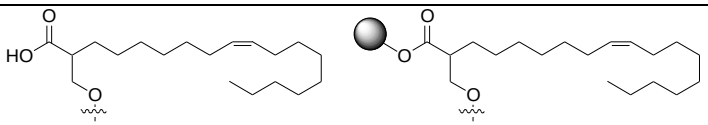
2-17	Hex_c	1	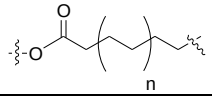
2-21	Oct_c	2	
2-22	Dod_c	5	
2-17	Hex_H	1	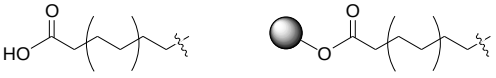
2-21	Oct_H	2	
2-22	Dod_H	5	
2-21	Oct_T	2	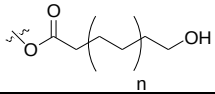
2-22	Dod_T	5	
2-3	$G12_{TP}$	5	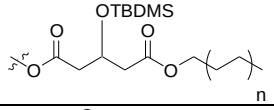
2-21	Oct_{HP}	2	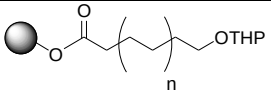

2.2 Solid-Phase Reactions

When the SPOS method was first adapted for synthesizing oligoester ion channels by Hu[25], the conditions with which the coupling or deprotection occurred were not optimized. Similarly the characterization of intermediates and products was quite limited. The goal of this section is to describe the extensive optimization that was done to generate reliable SPOS conditions for oligoester ion channel candidates. The ultimate goal in the syntheses is to generate an ion channel using only one attempt for each compound. Thus, synthesis of each compound is not individually optimized and therefore the compounds synthesized should require rapid and easy purification, in order to be useful for rapid evaluation of ion transport activity. This process mimics a true combinatorial library synthesis.

The solid support used for the solid phase reactions in this thesis is Wang resin. The loading capacity that controls the amount of material that can be coupled onto the resin varies from lot to lot from the commercial suppliers from 0.5 mmole to 4 mmole per gram of resin.[70] The loading capacity of the resin affects the scale of the reactions. Typically we aimed for about 0.1-0.2 mmole of product which required about 200 mg of resin at 0.75 mmole/g. If possible, a loading capacity of about 0.75 mmole/g was used because any lower loading capacity would require large solvent volumes. Higher loading capacities are reported to lead to cross-linking and multiple couplings.[71]

Industrially, solid phase synthesizers are machines used to perform SPOS reactions. In our case, all SPOS reactions were performed manually in a fritted peptide synthesizer vessel of 25 mL maximum volume. In order to drive the reactions forward, excess reagents are always used relative to the loading capacity of the resin and the

reactions are usually done multiple times. The resin cannot be stirred to achieve adequate mixing with the solutions because of mechanical degradation of the polymer; instead a wrist-action shaker was used. The polymer resin is porous to enhance solvent diffusion so after each reaction cycle it is necessary to remove all excess reagents from these crevices. The polymer backbone of the Wang resin responds physically to different solvents. By using alternate solvents which swell and shrink the resin (three cycles of THF, ether, and dichloromethane), it is assumed that any residual excess reagents and byproducts are squeezed out from the resin. For convenience, all SPOS reactions were performed at room temperature.

Like Riguera[69], N,N'-diisopropylcarbodiimide (DIC) was used as the acylating agent in our synthesis to couple the building blocks together with a catalytic amount of 4-dimethylaminopyridine (DMAP). The reaction times were individually optimized in our system.

Every type of reaction that can be performed on the resin needed to be optimized. Building blocks with similar structures such as G10 and G16 were assumed to have the same reactivity as G12, so the optimized reactions for G12 were applied to similar structural building blocks. A schematic of the reactions studied are shown in Figure 2-16 . The two types of reactions are Reaction 1: loading of the resin with G12 or Oct and Reaction 2: the coupling of another building block to that previously loaded.

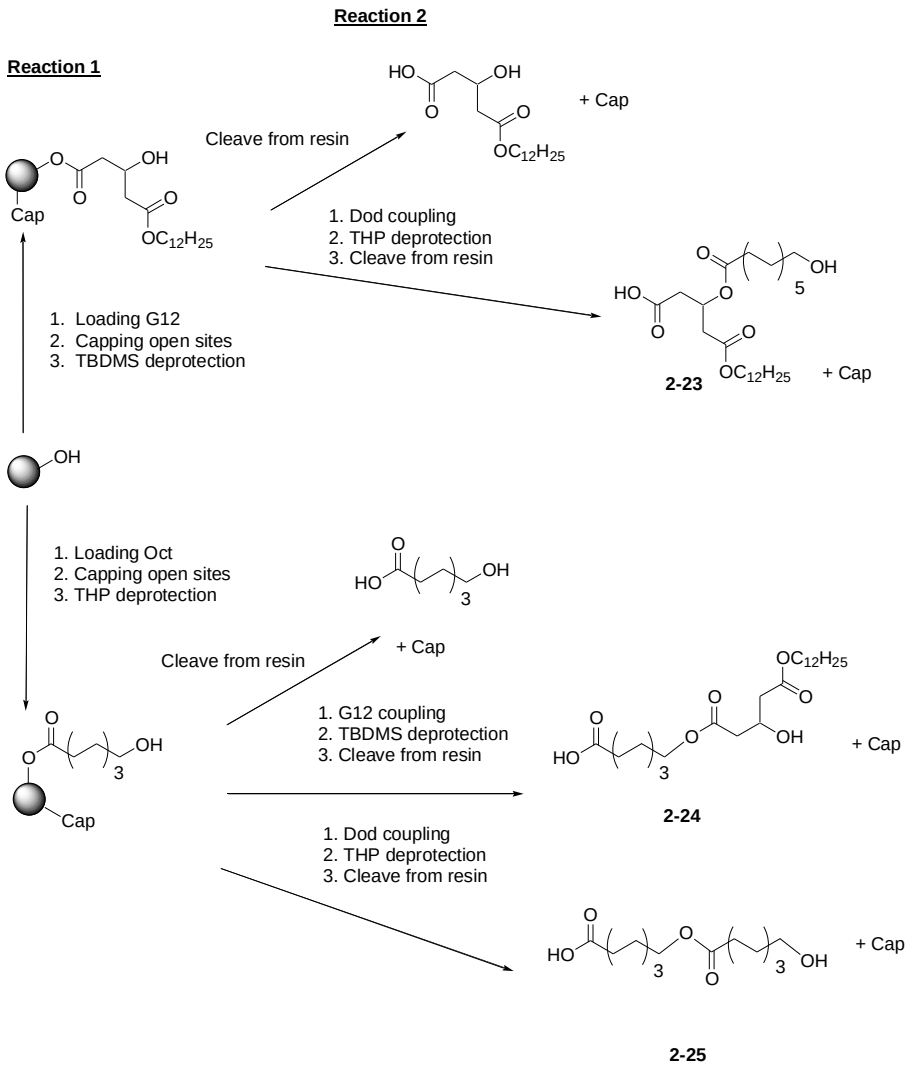

Figure 2-16. Schematic of possible reaction sequence studied on resin.

FT-IR spectroscopy is a useful tool for observing the progress of SPOS reactions because most reactions involve either the appearance or disappearance of an OH band. When the building block syntheses were discussed, ^{1}H NMR proved to be very important in the determination of impurities. A later section in this chapter will develop a detailed approach to the analysis of sample purity.

Since many of the SPOS compounds possess similar structures because of where the linkages are located (Figure 2-17), then the proton resonances would appear at about the same chemical shifts. The only major difference would be in the integrations of the

signals. There are some protons that repeat through the channel candidate structure that are different (i.e. C<u>H</u>$_2$(CO)OR and C<u>H</u>$_2$(CO)OH) but in the ^{1}H NMR spectrum they are labeled the same for the purposes of simplification.

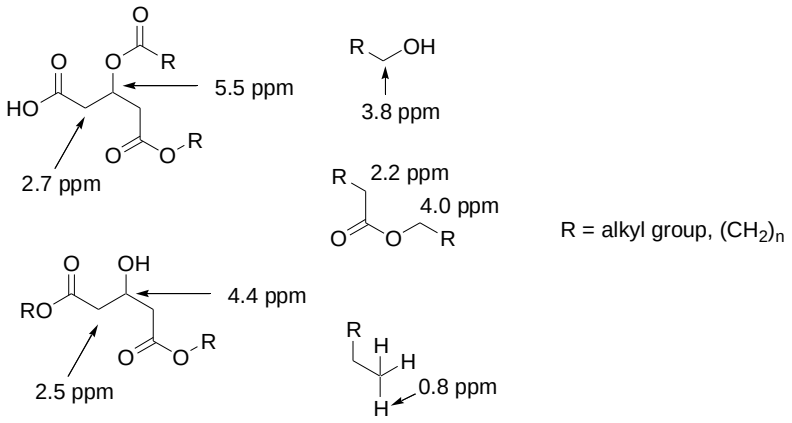

Figure 2-17. Common structural elements correlated with ^{1}H NMR chemical shifts.

Further support was needed for determining that the resin loading was sufficient to cover all the free hydroxyl sites. Phenylacetic acid and biphenylacetic acid (BPAA) are reagents that can be coupled efficiently onto Wang resin. The efficiency was determined from first loading of BPAA or phenylacetic acid onto the resin with three equivalents of each BPAA/phenylacetic acid and DIC with 0.3 equivalents of DMAP and coupling time of four hours. Then after one cycle of loading, a quantitative recovery of these acids was attained from the cleavage step.

Phenylacetic acid and BPAA do not have functionality which can further react under the SPOS reaction conditions. These two acids are known as ``cappers`` because after the loading of the first building block, these acids are added to ``cap`` any free hydroxyl sites.

When the products on the Wang resin were cleaved and analyzed by ^{1}H NMR spectroscopy, it was very obvious if the capper was present because of the distinct

aromatic chemical shifts. For phenylacetic acid there is also a methylene signal at 3.7 ppm. Since there are many aromatic protons for each acid, then even a small percentage of the cappers present is evident. As well, some of the building blocks were made in low yield or only a small quantity was available so it was important to cap the Wang resin after these building blocks have been loaded to prevent the direct coupling of the second building block onto the resin. The molecular weight difference between the cappers and some of the SPOS products was also an advantage for their removal using gel filtration.

Normally the cleavage of a product from Wang resin is done with a trifluoroacetic acid (TFA) in dichloromethane solution. This is quite an effective cleaving agent and easy to prepare, although one of the shortcomings is that if primary alcohols are present, they can likely form trifluoroacetates with the TFA. The presence of these esters is supported by the downfield shift of the methylene (next to the primary alcohol, 3.6 ppm) to about 4.3 ppm. In situations where primary alcohols are exposed in the desired product, the best method is to use a dry solution of dioxane and HCl (5-7 M). The HCl/dioxane solution is prepared by bubbling HCl through dry dioxane and then determining the concentration of HCl by titrating a sample with 1.0 M NaOH. The optimizing of the TFA cleavage solution for our oligoesters started with three TFA:CH_2Cl_2 solutions in ratios of 1:4, 2:3, and 0.5:4.5 on three resins coupled with $G12_T$. All of the solutions were shaken with the product on the resin for one hour. The results showed that the 1:4 mixture was not concentrated enough to cleave the entire product off the resin whereas 2:3 was too strong (the benzyl group of the resin was also cleaved). Therefore a TFA:CH_2Cl_2 (1:3) solution was used to cleave the SPOS products which did not have a primary alcohol.

2.2.1 Reaction 1: Loading of G12

The steps for loading of the hydroxy acids to Wang resin and ester coupling with building blocks were optimized by monitoring the resin after a coupling step and a washing cycle. A small sample of loaded resin was incorporated into a KBr pellet and monitored with FT-IR spectroscopy for the presence of free OH as detected by the OH stretching band at about 3200-3700 cm^{-1}. After a five hour coupling of G12 onto Wang resin it appeared that the OH of the Wang resin (about 3450 cm^{-1}) had disappeared (Figure 2-18). The band at about 3700 cm^{-1} may be the OH stretch of water from the hygroscopic KBr. The band at about 1730 cm^{-1} is also good evidence (C=O stretch) that the ester between Wang resin and $G12_{TP}$ is formed.

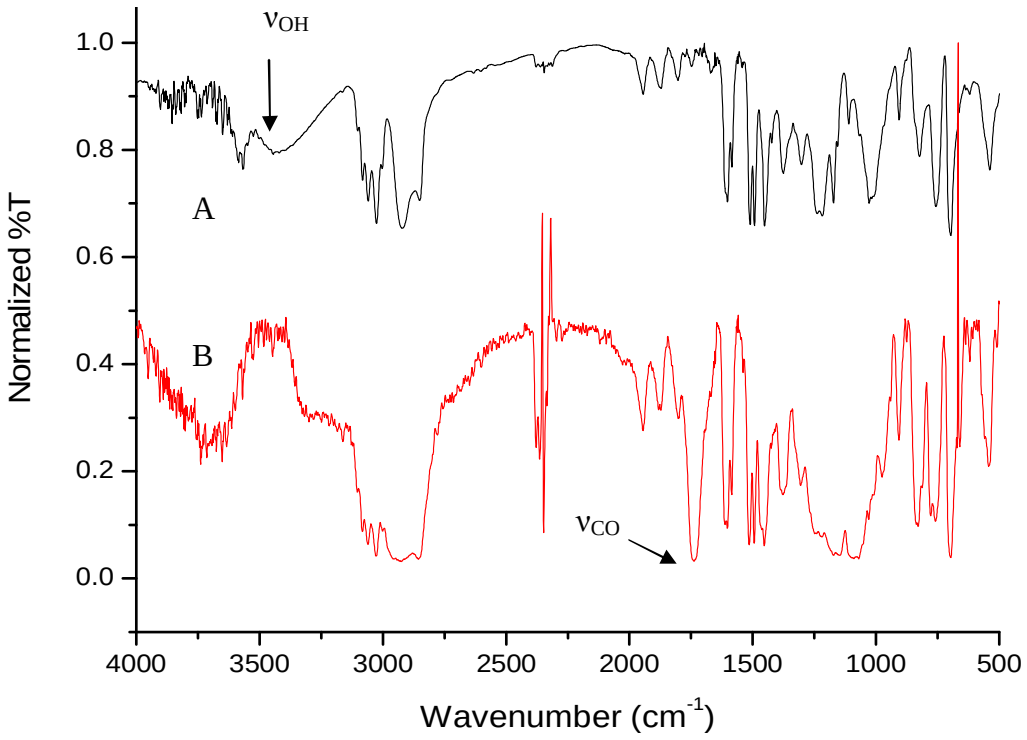

Figure 2-18. FT-IR spectrum of Wang resin A) before and B) after one cycle of G12 loading (KBr pellet, air background).

To determine the coupling efficiency of two cycles, G12 was loaded onto the resin using one five hour and one overnight cycle followed by capping the resin with BPAA. The coupling solution was comprised of three equivalents of the acid (G12 or BPAA) and DIC, and DMAP in a THF solution. The TBDMS group was deprotected using fluoride from a THF solution of tetrabutylammonium fluoride (TBAF) and acetic acid. Following the TBDMS deprotection, the $G12_T$ was cleaved off of the resin by exposure to a TFA:CH_2Cl_2 (1:3) solution for one hour. Figure 2-19 is the ^{1}H NMR spectrum of the crude product from the cleavage of the loaded resin. The methine of $G12_H$-OH (H_a) was calibrated to 1 and the biphenyl protons (H_b) accounted for 1.79/9 H x 100% = 20% which implied that following two cycles only 80% loading was achieved.

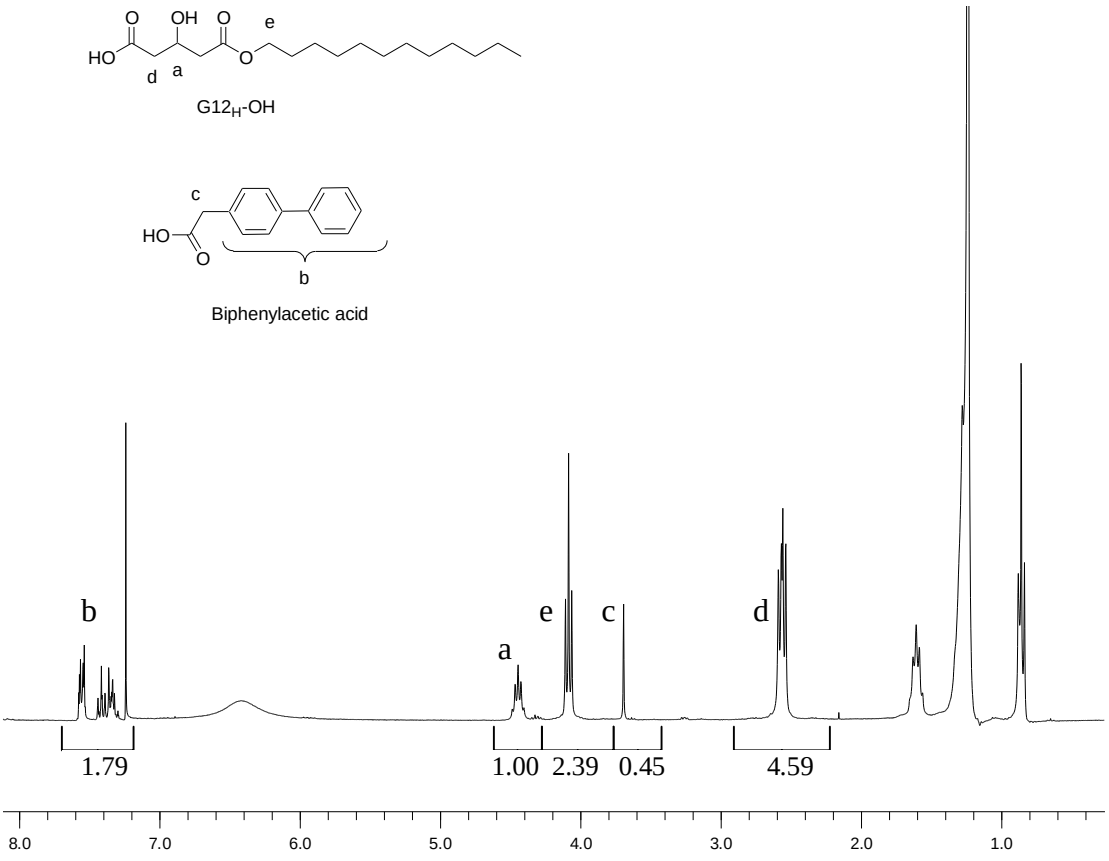

Figure 2-19. ^{1}H NMR spectrum of crude $G12_H$-OH product after two cycles of coupling.

Since the coupling time of one five hour and one over-night cycle did not provide for total G12 loading, then in consideration of time and starting material, another five hour cycle was added to the G12 loading. Therefore the coupling times required for loading G12 onto the resin were two five-hour cycles and one overnight cycle. The final efficiency of these three cycles will be evaluated later in a dimeric product. These coupling times can be applied to any of the other glutaric acid derivatives (G10, G14, and G16).

With $G12_{TP}$ loaded onto the resin, it was important to deprotect the TBDMS group. A couple of conditions were initially tried such as CsF in DMF/THF and $CuNO_3$ in CH_2Cl_2/acetonitrile[81] to deprotect the TBDMS group. These conditions did not work well and the solvents that were required in order to solvate the salts resulted in the solid support shrinking. An alternative condition was sought which provided efficient TBDMS-cleavage in a solvent that swelled the polymer; tetrabutylammonium fluoride (TBAF) in THF appeared to fulfill these requirements. In Figure 2-20 it is apparent that after one deprotection step (two hours), the OH stretching band is observed at about 3500 cm^{-1}.

Normally after the fluoride treatment, residual tetrabutylammonium remains entrapped within the resin so a wash with NaI in aqueous acetone is necessary followed by dry THF and ether to remove the water from the resin. Alternatively, washing the final cleaved product with dilute aqueous sodium citrate can also remove the TBAF residue. In the SPOS reactions where there was a successive coupling step, the resin was washed with dry THF to remove any remaining water from the sodium iodide wash. Two cycles of about two hours were necessary to ensure that total TBDMS-deprotection

occurred as judged by IR band intensity changes, and coupling/cleavage results for subsequent reactions.

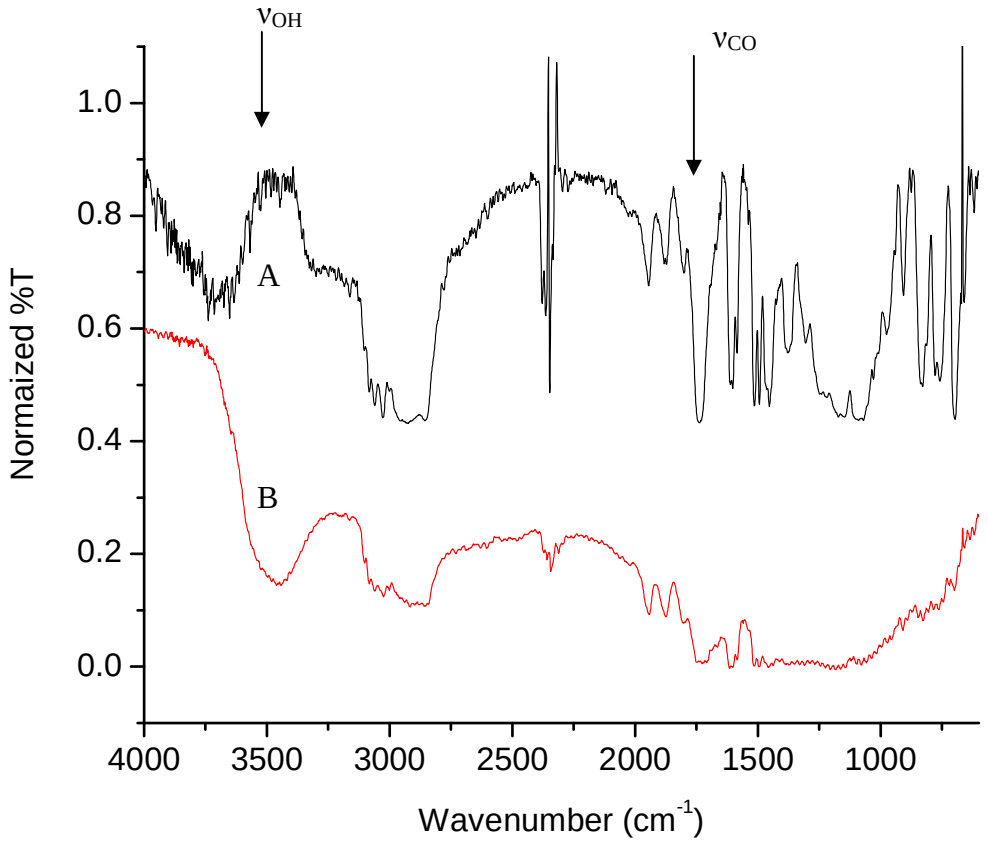

Figure 2-20. FT-IR spectrum of Wang resin loaded with A) $G12_{TP}$ and B) after one cycle of TBDMS-deprotection to yield on resin $G12_{TP}$ and $G12_T$ (KBr pellet, air background).

In Figure 2-20B the CO stretch (~1730 cm^{-1}) appears to be weak which may imply that the ester has also degraded during the TBDMS deprotection. It was assumed that this particular spectrum is poor (lack of sample in the KBr press) for observing the CO stretch, but the more interesting OH stretch was evident. If the methodology for deprotecting TBDMS was damaging the $G12_{TP}/G12_T$ fragment, then the result of coupling the next building block would show this as the product would be released without the terminal $G12_T$ unit. This was not found in any sequence, so the deprotection

must behave appropriately. Therefore the optimal time for TBDMS deprotection was chosen as two cycles of 2 and 2.5 hours followed by a NaI/acetone wash.

2.2.2 Reaction 1: Loading of Oct

Building block Oct was used to optimize the loading of ϖ-hydroxy acids onto the resin. Oct was coupled onto the resin using a THF solution of three equivalents of the acid and DIC and a catalytic amount of DMAP. In Figure 2-21 two five-hour cycles are compared and it showed the reduction of the Wang resin OH peak at about 3500 cm^{-1}.

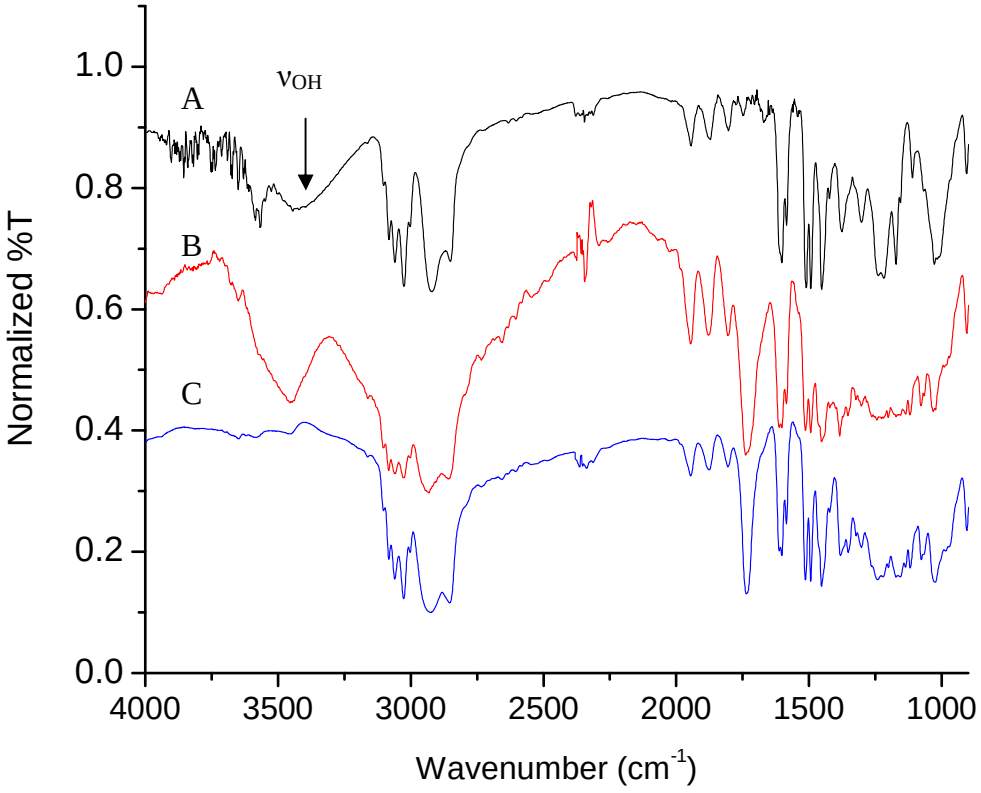

Figure 2-21. FT-IR spectrum monitoring of the Oct coupling to resin. (A) Unloaded resin, B) loaded resin after first cycle (5 hours) of coupling, and C) loaded resin after second cycle (5 hours) of coupling (KBr pellet, air background).

By the end of the second cycle the IR spectrum showed that most of OH sites have been consumed as the ester Oct_{HP}. After two five hour cycles, there is still a

possibility of the incomplete coupling. Therefore it would make sense to end the coupling cycle with a third overnight cycle to optimize the use of time in a day. Therefore the loading of Oct required two five hour cycles and one overnight cycle. These conditions should also apply to Dod and Hex.

Each building block has a protecting group to ensure that the compounds do not self-couple instead of coupling to the solid support. The THP protecting group is deprotected using a dilute acid solution (*p*-TsOH in CH_2Cl_2). The deprotection of the THP protecting group was monitored with FT-IR. After three cycles of two hours each, it was noted that the OH stretch (about 3500 cm^{-1}) has made an appearance (Figure 2-22). One difficulty with this method of observing for the "optimal" condition for the THP and TBDMS deprotection is that it is hard to identify when the OH signal reaches a maximum. A way to indirectly observe for any delinquent protecting groups which survived the deprotection is in subsequent coupling and cleavage steps. The resulting oligomeric products would have some units missing if the deprotection/coupling did not occur. For the reason that it is difficult to monitor the optimal time and conditions, three two-hour cycles were used for the deprotection of the THP group.

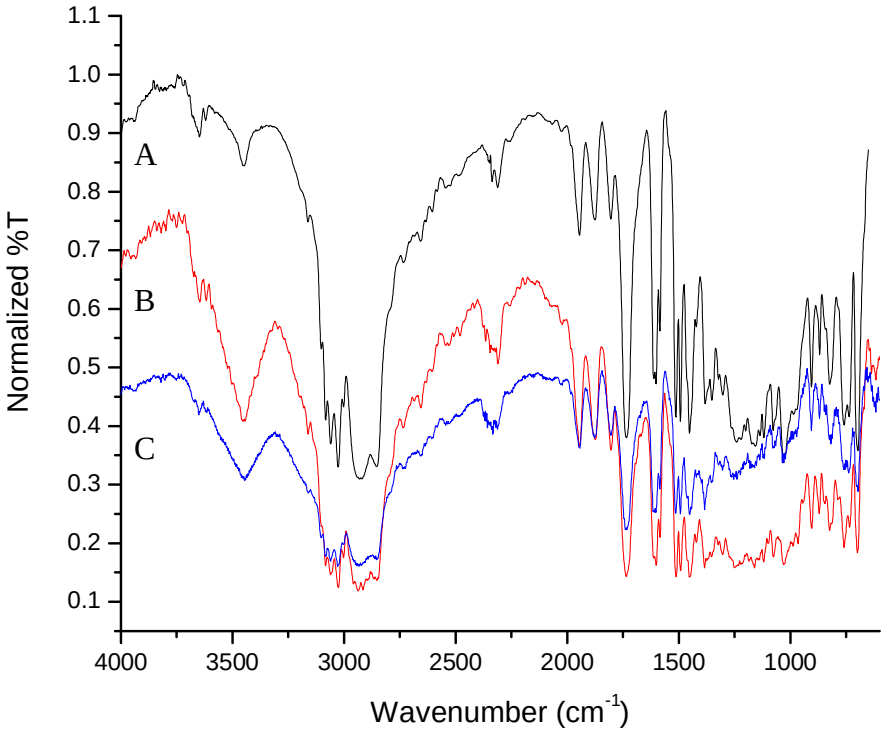

Figure 2-22. FT-IR monitoring of the THP deprotection of Oct_{HP} after A) first cycle (2 hours total), B) second cycle (4 hours total), and C) third cycle (6 hours total) (KBr pellet, air background).

2.2.3 Reaction 2: Coupling of G12 onto Oct_T

The coupling of one building block to another is important for chain extension. One of the shortcomings of solid-phase synthesis is the possibility of generating shorter analogues, known as "deletion sequences" of the desired product due to incomplete coupling/deprotecting steps. Consider a hypothetical example in which the coupling of Building Block 1 onto Wang resin is only 98% efficient but the coupling of Building Block 2 is quantitative (Figure 2-23). Then upon cleavage from the Wang support, there is expected to be a mixture of 2% of Building Block 2 (deletion sequence) and 98% of the dimeric product (Building Block 1-Building Block 2).

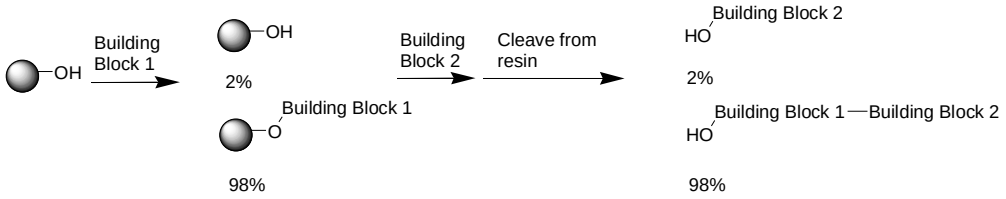

Figure 2-23. Details of how deletion sequences arise.

From resin loaded with Oct_H and any remaining open sites capped with BPAA, G12 was coupled onto the Oct_T. Three coupling reaction cycles were performed which comprised of two five-hour cycles and one overnight (Scheme 2-10).

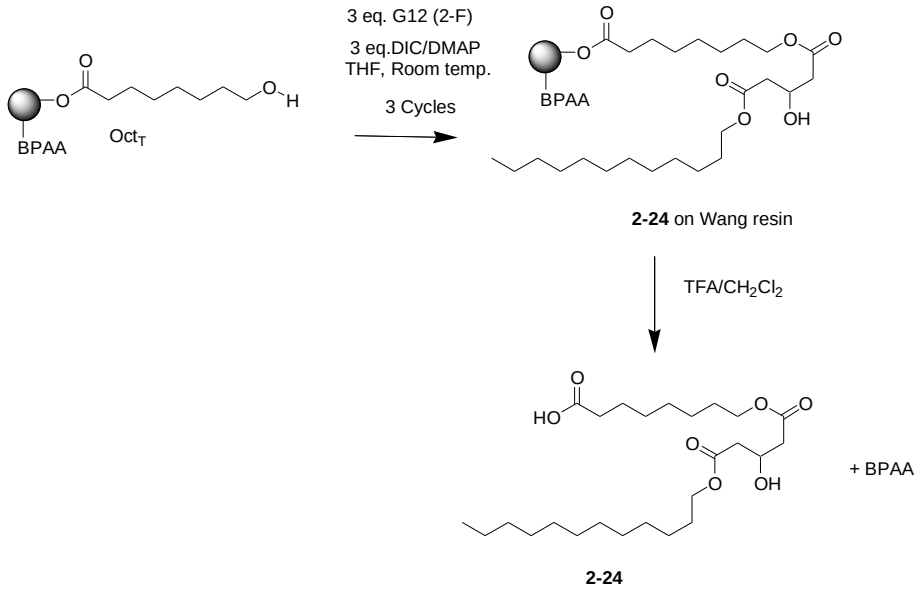

Scheme 2-10. Coupling of G12 onto Oct_H on Wang resin.

This coupling reaction was not monitored with FT-IR spectroscopy. The growing product had the TBDMS deprotected using the standard conditions and then the resulting product **2-24** was cleaved from the solid support using a TFA:CH_2Cl_2 solution. The ^1H NMR spectrum of the crude product is Figure 2-24.

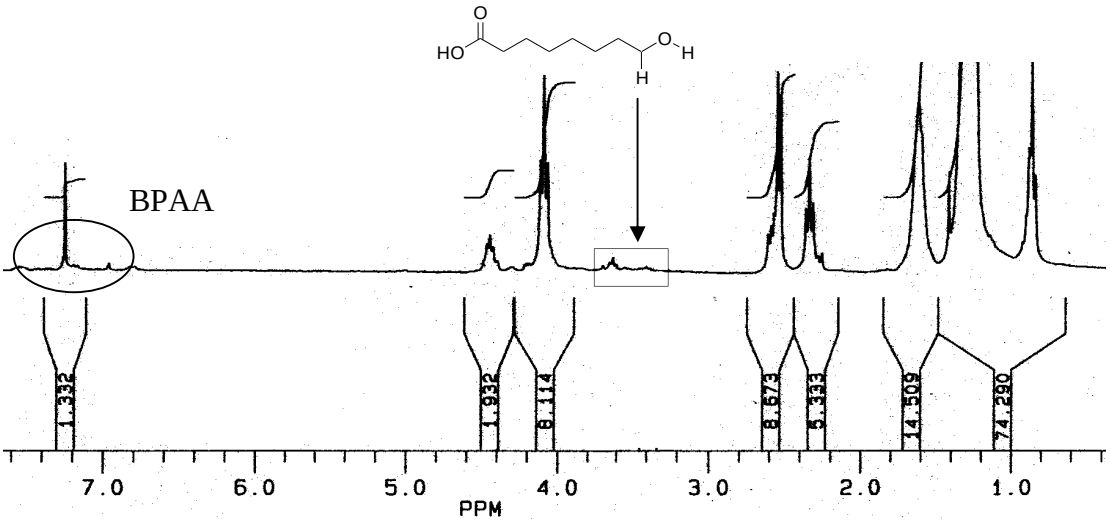

Figure 2-24. ^{1}H NMR spectrum (300 MHz) of crude product **2-24** in $CDCl_3$.

The ^{1}H NMR spectrum showed a couple of interesting points. Firstly, cleavage confirmed that Oct_H was present and the lack of any significant biphenylacetic acid aromatic protons (circled) in the ^{1}H NMR spectrum confirmed that a majority of the resin OH sites were initially occupied by Oct_{HP}. Secondly, there is a very small signal at about 3.8 ppm which may represent the C$\underline{H_2}$OH of 8-hydroxyoctanoic acid as well as some other smaller resonances within the rectangle which are residual THP signals (rectangle in Figure 2-24). The presence of the resonances within the rectangle indicated that there are some impurities but it was not obvious that they must belong to the free or protected primary alcohol. Either way, a majority of the product is the coupled G12 onto Oct_T.

2.2.4 Reaction 2: Coupling of Dod onto Oct_T

For product extension in the SPOS products the core pieces such as Hex, Oct and Dod are coupled onto other core pieces. As a trial of this type of reaction, Oct was first loaded onto the resin using the standard DIC/DMAP coupling conditions followed by capping any vacant sites with BPAA. Following the deprotection of the THP using the

dilute acid solution in CH_2Cl_2, Dod was coupled onto Oct_T using the standard coupling conditions (Scheme 2-11).

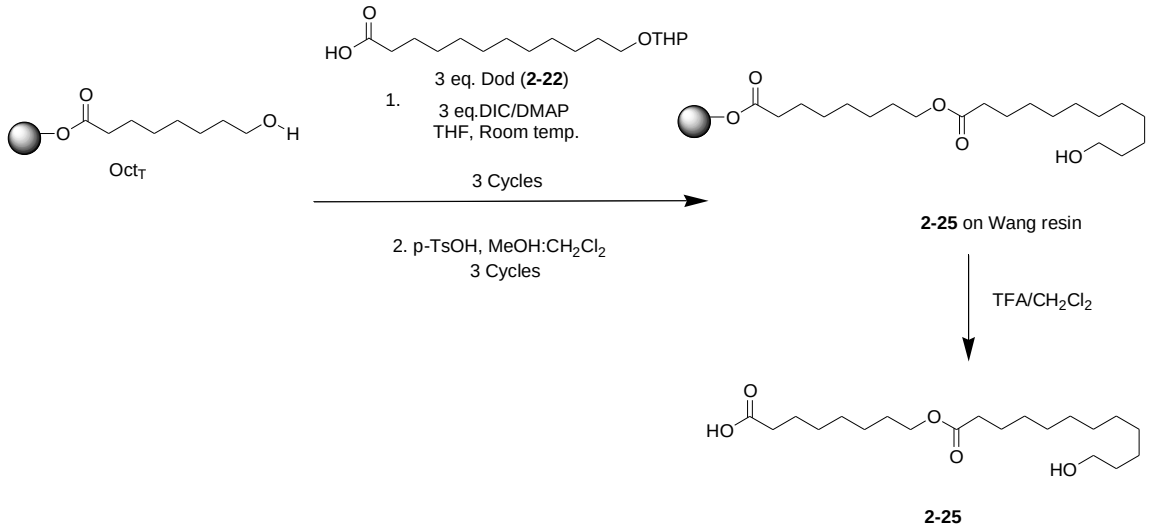

Scheme 2-11. Coupling of Dod onto Oct_T on Wang resin.

In Figure 2-25 the FT-IR spectra are shown after all three cycles of coupling Dod onto an Oct_T on Wang resin.

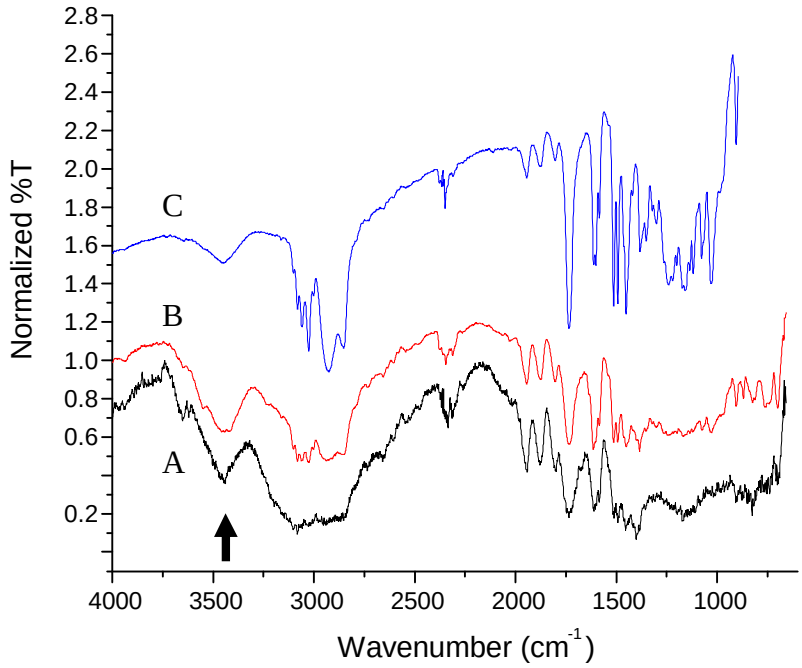

Figure 2-25. FT-IR monitoring the coupling of Dod to Oct_T (KBr pellet, air background).

The OH stretch of the Oct_T connected to the solid support diminished after the first coupling (A), then the second coupling (B) and finally after an overnight cycle (C). There was still a small OH stretch after the overnight cycle but it was relatively small. When the product **2-25** was cleaved from the resin using a solution of TFA:CH_2Cl_2, the ^{1}H NMR spectrum (Figure 2-26) showed that there were quite a few impurities. The boxed areas are the proton resonances consistent with residual THP from unsuccessful THP deprotection. The triangle highlights the resonance which corresponds to the $C\underline{H}_2$-O_2CCF_3 when the primary alcohol of Dod_T esterifies with trifluoroacetic acid. Finally the circled region showed some evidence of biphenylacetic acid present.

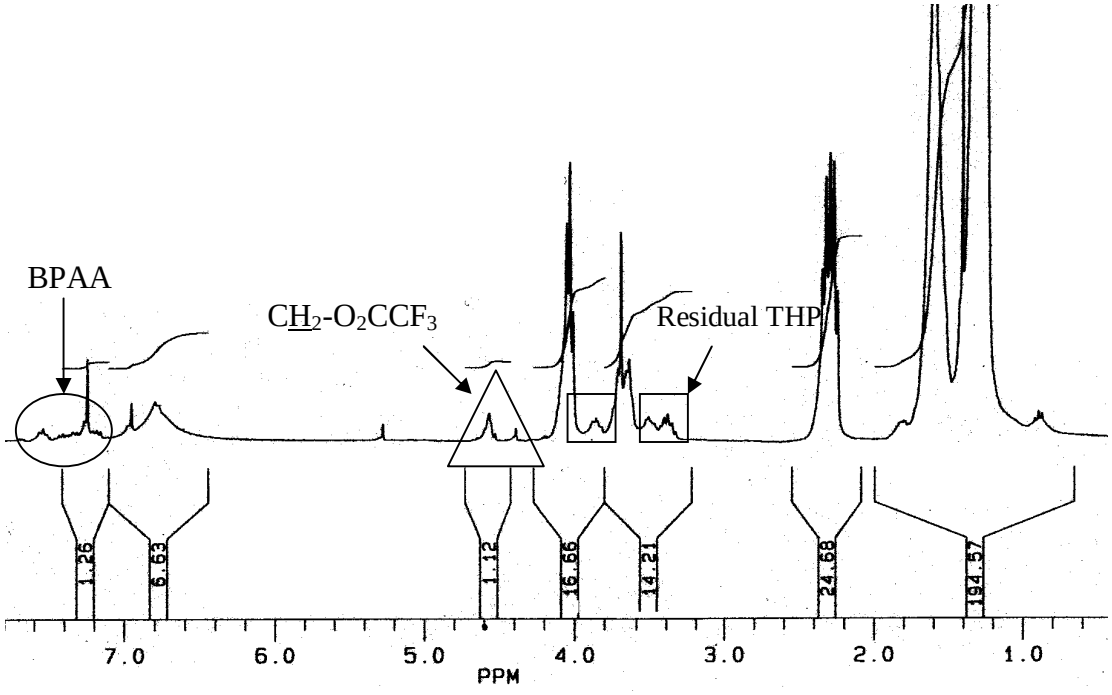

Figure 2-26. ^{1}H NMR spectrum (300 MHz) of crude **2-25** in $CDCl_3$.

Overall, this particular experiment illustrated that careful attention must be paid to the THP deprotection step. A very small amount of *p*-TsOH (about 5 mg) was used for the THP deprotection. *p*-TsOH is a hygroscopic acid and it was likely that the correct

weight was measured but water may have accounted for most of the weight and not the pure acid. Therefore, it is imperative that relatively dry *p*-TsOH be used for the THP deprotection. The coupling though was a success as shown by the large resonance at about 4 ppm corresponding to the $C\underline{H_2}$-O_2C (ester formed). In later sections, compounds will be shown where the THP deprotection is successful (no residual THP group after product cleavage from resin) by using drier p-TsOH.

2.2.5 Reaction 2: Coupling of Dod onto $G12_T$

After the loading and deprotection to yield $G12_T$ onto the resin, the next step was to couple either an Oct or Dod block to optimize the reaction conditions for extending the product. Similar to the method of monitoring the coupling of Dod to Oct_H, the IR spectrum after the second coupling step (five hours for each coupling cycle) was recorded (Figure 2-27). The OH stretching band at about 3300 cm^{-1} disappears after the second coupling.

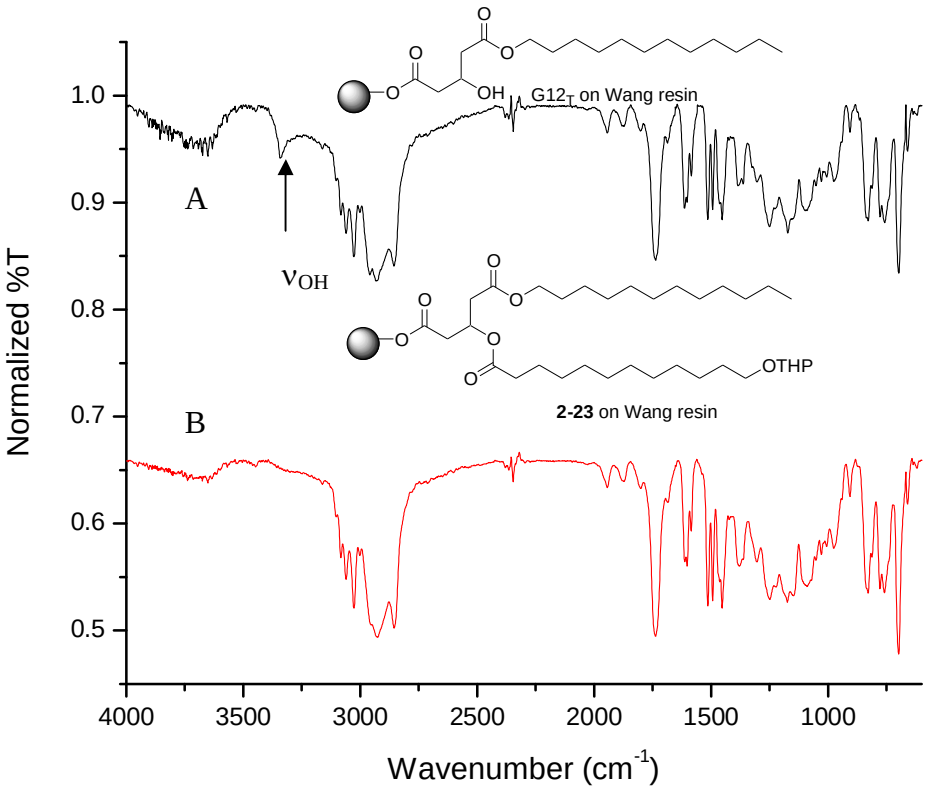

Figure 2-27. FT-IR monitoring the coupling of Oct to $G12_T$ on Wang resin. A) Before the coupling of Oct on $G12_T$ on resin. B) After two cycles of coupling Oct. (KBr pellet, air background).

The THP on **2-23** on resin was removed using the standard THP deprotection conditions and then the product was released from the resin using TFA:CH_2Cl_2 conditions. The ^{1}H NMR spectrum (Figure 2-28) of the crude product showed that $G12_T$ was not coupled efficiently because about 16% of the resin sites were occupied by BPAA (singlet at about 3.7 ppm, 0.31 /2 H x 100% = 16%). However, all of the exposed secondary alcohol from $G12_T$ has been converted to the ester because of the lack of a proton resonance at 4.5 ppm (circle). As well, the THP deprotection was successful because there are no THP resonances between 3.5 and 4.0 ppm (the triplet at 3.8 ppm and 1.9 ppm belong to residual THF).

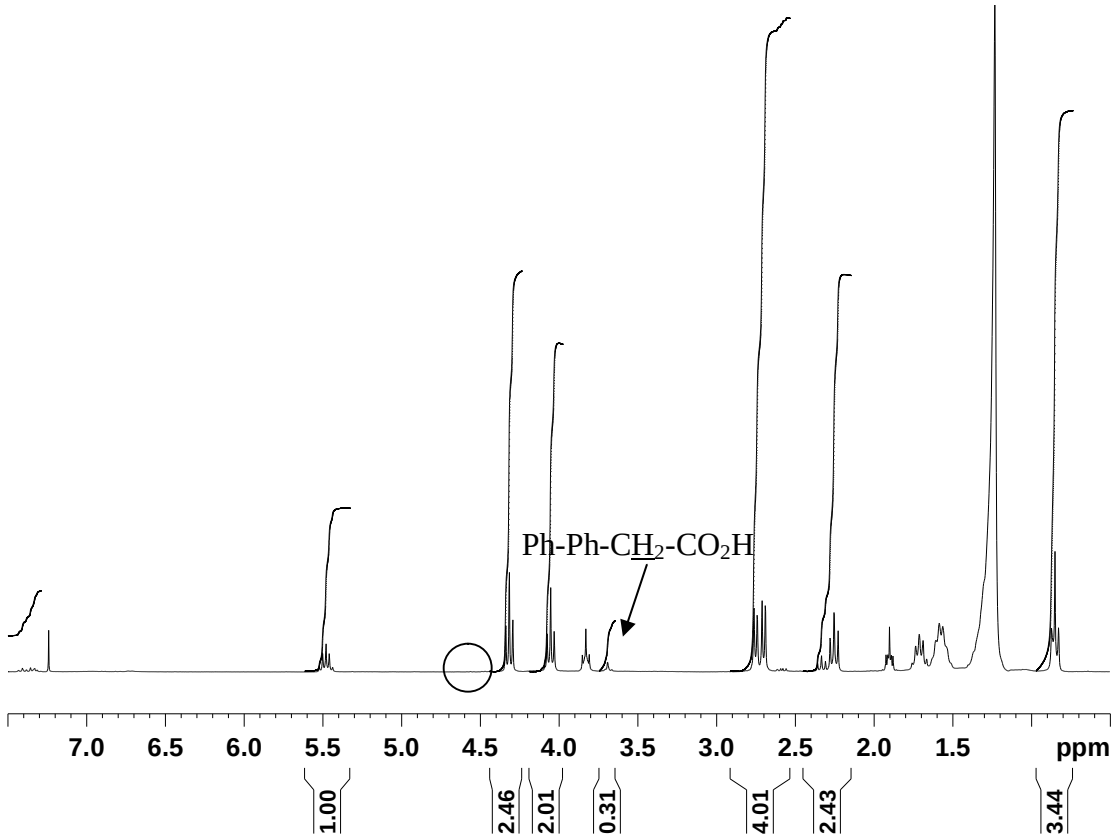

Figure 2-28. ^{1}H NMR spectrum of crude **2-23** in $CDCl_3$.

The crude **2-23** product was purified by gel filtration using an LH-20 column with MeOH:$CHCl_3$ (4:3). The ^{1}H NMR spectrum of the purified product is in Figure 2-29.

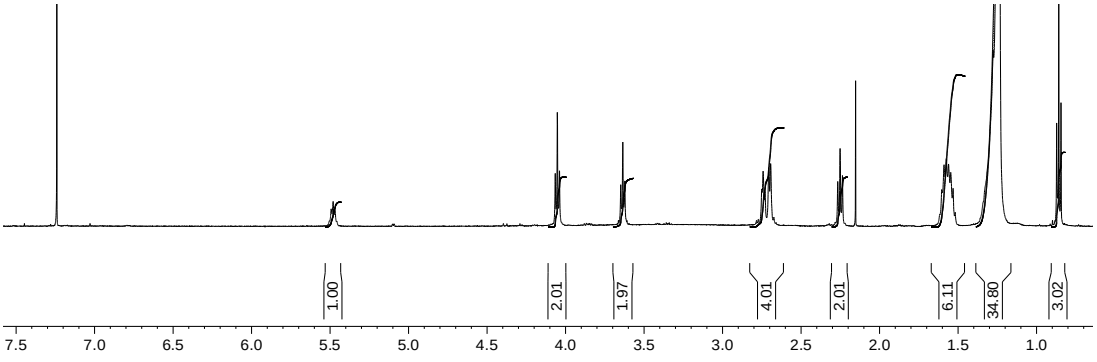

Figure 2-29. ^{1}H NMR spectrum of purified **2-23** in $CDCl_3$.

From the ^{1}H NMR spectrum it is evident that the gel filtration of **2-23** removed all of the BPAA and further exposure to methanol cleaved the trifluoroacetate esters.

The final conditions for the coupling of Oct or Dod to $G12_T$ were two five-hour cycles and an overnight cycle for time efficiency.

2.2.6 Summary of SPOS Reaction Methodology

A summary of the reaction conditions is seen in Table 2-4. The building blocks are grouped into one of three "block" type based on whether they are head groups (Block 1 and 2) or core components (Block 3) and then further into groups based on structural similarities.

Table 2-4. Standard solid-phase protocols.

Block 1	Block 2	Block 3
G10, G12	Lau	Hex, Oct
G14, G16	Ole	Dod

Reaction Type	Equation	Reagents (/cycle)	Reaction times (hours)
Resin Loading	Wang resin + Block 1	DIC (3 eq), THF (5 mL) DMAP (0.3 equiv), Block 1 (3 eq)	5 + 5 + overnight
Resin Loading	Wang resin + Block 3	DIC (3 eq), THF (5 mL) DMAP (0.3 equiv), Block 1 (3 eq)	5 + 5 + overnight
Resin Loading	Wang resin + Block 2	DIC (3 eq), THF (5 mL) DMAP (0.3 equiv), Block 2 (3 eq)	8 + 16 + overnight
Resin Capping	Wang Resin (loaded) + BPAA	DIC (3 eq), THF (5 mL) DMAP (0.3 equiv), BPAA (3 eq)	4
Coupling	Block 1 + 3	DIC (3 eq), THF (5 mL) DMAP (0.3 equiv), Block 3 (3 eq)	5 + 5 + overnight
Coupling	Block 3 + 1	DIC (3 eq), THF (5 mL) DMAP (0.3 equiv), Block 1 (3 eq)	5 + 5 + overnight
Coupling	Block 3 + 3	DIC (3 eq), THF (5 mL) DMAP (0.3 equiv), Block 3 (3 eq)	5 + 5 + overnight
Coupling	Block 2 + 3	DIC (3 eq), THF (5 mL) DMAP (0.3 equiv), Block 3 (3 eq)	5.5 + overnight
THP Deprotection	Block 3	*p*-TsOH (5 mg) CH_2Cl_2:MeOH (97:3, 10 mL)	2 + 2
TBDMS Deprotection	Block 1 Block 2	Acetic acid (100 uL) TBAF (1 M in THF, 10 mL)	2 + 2.5
Resin Cleavage		HCl (5-7 M in dioxane)	1
Resin Cleavage		TFA:CH_2Cl_2 (1:3)	1

2.2.7 Scope of Methodology

The preceding sections described the optimization of coupling and deprotection conditions for individual reactions and short sequences. The purpose of this section is to explore the scope of this SPOS method. The overall goal is to develop an effective characterization of the types of products the set of building blocks can make. Previously the method for generating deletion sequences was discussed. If the building blocks are impure with small amounts of free hydroxy acid then additional building blocks may appear in the final sample leading to "addition sequences". In this section the identification of addition and deletion sequences are discussed.

2.2.7.1 Spectroscopic Methods Used for Compound Characterization

In conventional syntheses, compounds are usually characterized by methods such as NMR and IR spectroscopy and mass spectrometry. The confirmation of purity usually comes from elemental analyses or high performance liquid chromatography (HPLC).

With any synthesis the generation of a pure compound is desired, and that is true for the oligoester compounds as well. Given the methodology it is reasonable to assume that there may be a small percentage of some of the shorter and/or longer analogues for any oligoester compound synthesized by the SPOS methods discussed above. Small molecule impurities can be detected by ^{1}H NMR spectroscopy, but more of interest is the detection of the shorter and/or longer analogues. Generally the integrity is reported in percent (%) which represents the mole percentage of the compound of interest in the overall product mixture (analogues and desired product) after gel filtration.

In a hypothetical example to demonstrate the effects of analogue impurities to typical purity quantification methods, the synthesis of pentamer **2-26** could well be

contaminated with tetramer **2-27** and dimer **2-28**. These compounds have very similar elemental analyses (EA) (Figure 2-30). Using the standard acceptable precision of ±0.4% for EA, a mixture comprised of **2-26** and **2-27** does not reveal the possibility of contamination because the EA for both compounds are the same. In order to observe the 0.4% difference in the %C, a contaminant such as **2-28** must need to be present in at least 24% of the **2-26** mixture composition. Therefore elemental analysis will always provide a result for purity which is inconclusive.

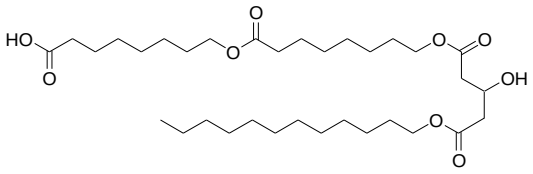

2-28

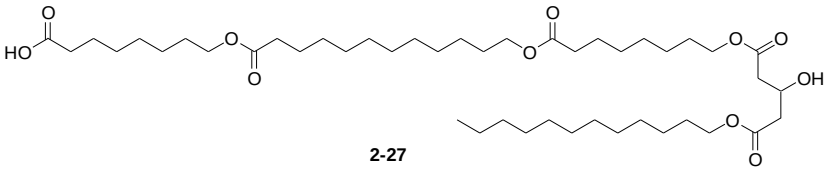

2-27

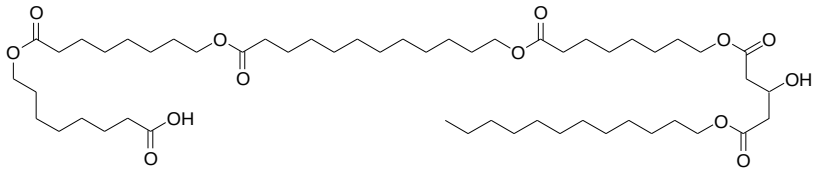

2-26

	Molecular Formula	Calculated %C	Calculated %H
2-28	$C_{33}H_{60}O_9$	65.97	10.07
2-27	$C_{45}H_{82}O_{11}$	67.63	10.34
2-26	$C_{53}H_{96}O_{13}$	67.62	10.28

Figure 2-30. Elemental analyses calculations for SPOS products.

^{1}H and ^{13}C NMR spectra were collected for all oligoester compounds. Carbon-13 NMR spectra were collected for all the SPOS generated compounds but the amount of

useful information that was given by the spectra is very limited because from one structure to the next, there are many things in common – ester carbonyl, methylene carbons next to oxygens, and finally alkyl carbons. In small molecules "peak counting" can give the appropriate information on the constituents, however in these linear structures the ^{13}C signals overlap so the total carbon count is not evident from the spectra. Therefore ^{13}C NMR spectroscopy did not provide very much useful information for determining compound integrity; addition and deletion sequences have different carbon numbers but the carbon environments are very similar, if not the same. ^{1}H NMR spectroscopy on the other hand, was very useful for determining compound integrity because even though the addition and deletion sequences have the same proton environments, the proton integrations differ.

To determine the consistency of the compound molecular weights, LSIMS was used. As well, the mass spectrum also revealed if the molecular ions of addition or deletion sequences were present because of their differences in mass.

Hu's thesis[25] used a method where HPLC (using a size exclusion column) with a UV-Vis detector was used to determine the purity of the compounds synthesized by SPOS. Unfortunately the carboxylic acid/ester chromophore absorbs (190 nm) in the same region as many common HPLC solvents. Hu's samples showed addition and deletion sequences in the MS while the ^{1}H NMR integrations had all the expected values. Therefore, it is believed that Hu may have synthesized some shorter and longer oligoesters along with some of **1-20** which all happened to have been in the appropriate proportions to generate the ^{1}H NMR spectrum obtained (integrations and chemical shifts).

The use of HPLC for determining compound purity is not appropriate for our oligoester compounds because of the lack of any useful UV-chromophore. Therefore most of the integrity discussions utilized ^{1}H NMR spectra and MS for the identification of impurities. The process of impurity analysis involved examining the MS for possible contaminants such as the presence of addition and deletion sequences. Then the ^{1}H NMR spectrum revealed the approximate quantities of these contaminants through the integration values. For some of the spectra, the signal-to-noise was poor so as a consequence the integrations may not be very precise, especially for those resonances which come from single protons. If the $G12_T$ or similar unit was present, the methine proton (H_a at about 4.5 ppm) to methylene proton (H_b at about 2.5 ppm) should be in a ratio of 1:4 (Figure 2-31). Any deviation from this ratio would be the percent difference from the expected integration (% difference) and is calculated using equation (2-1).

(2-1) $$\% \text{ difference} = \frac{(\text{expected integration} - \text{observed integration})}{\text{expected integration}} \times 100\%$$

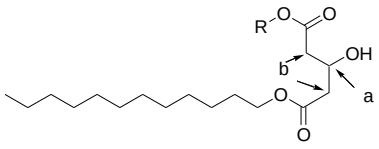

Figure 2-31. Protons on the $G12_T$ unit for determining precision in the ^{1}H NMR integrations.

The expected proton integrations for the unique sections of the molecule were then compared to what was found and an example is shown in Figure 2-17. The numbers calculated from the differences in the integrations established the integrity of the compound analyzed. The general equation used to calculate the amount of contaminant (Y) in product (X) is equation (2-2):

(2-2) $$\text{Ratio of Y/X} = \frac{(\#\ H_X)}{1\ \text{mol X}} \times (\%\ \text{difference in peak z}) \times \frac{(1\ \text{mol Y})}{\#\ H_Y}$$

In equation (2-2), the peak z was first selected which has contributions from both the contaminant (Y) and desired product (X). The percent difference of this peak from the expected was calculated using the % difference calculation in (2-1). Then the number of protons for X (# H_x) and number of protons for Y and which contribute to peak Z are inserted into the equation.

To demonstrate the application of equation (2-2), the ^{1}H NMR spectrum for compound **2-25** is used (Figure 2-32).

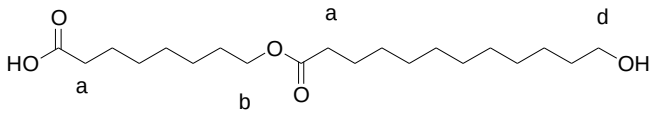

2-25

label	δ (ppm)	Expected Integration	Found Integration
a	2.27-2.33	4	4.46
d	3.62	2	2.00
b	4.04	2	2.36

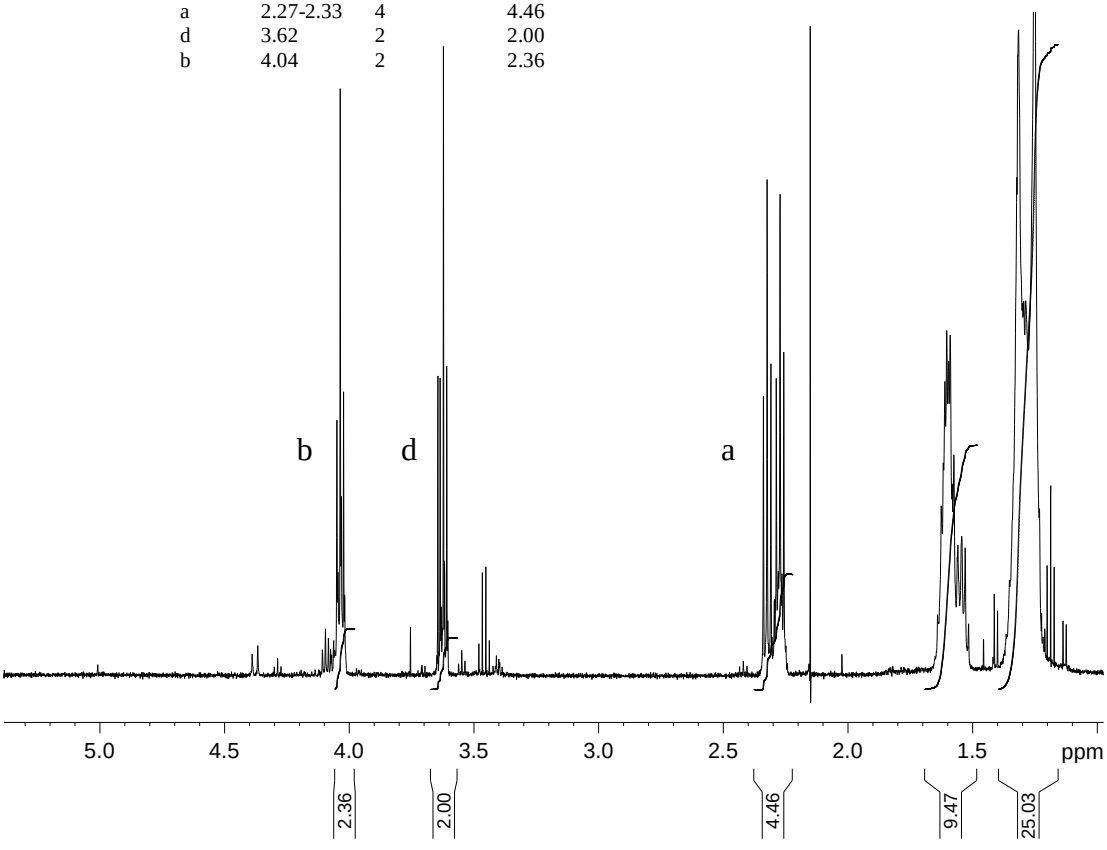

Figure 2-32. ^{1}H NMR spectrum of **2-25** in $CDCl_3$.

For simplicity, contamination by 8-hydroxyoctanoic acid (**2-19**) was considered in the sample of **2-25** (Figure 2-33). The integral of the resonances between 2.2 and 2.4 ppm is "peak z". Normally for a sample of only **2-25** the integration should be 4.0 but since the integration is 4.46, then the % difference is 11.5%. The contaminant Y has two protons (H_y) while the X product **2-25** has four protons (H_y).

Y:

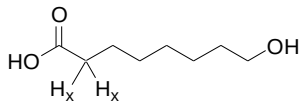

2-19

X:

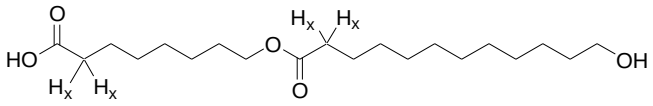

2-25

$$\%\ difference\ = \frac{(4.00 - 4.46) \times 100\%}{4.00} = 11.5\%$$

$$Ratio\ of\ Y / X\ = \frac{4H_x}{1mol\ X} \times 11.5\% \times \frac{1mol\ Y}{2H_y} = 23\%$$

Figure 2-33. Calculation of **2-19** contamination in **2-25.**

Applying equation (2-2) to **2-25** revealed a contamination of **2-19** of about 23%. In the synthesis of a compound library, the characterization of each compound should be efficient because there are many compounds to analyze. The goal of generating a library was for structure-activity surveying. Therefore focus was placed on rapidly generating compounds of relatively high integrity so that preliminary differences in structure-activity can be deduced.

2.2.7.2 Synthesis of Dimers

Dimers are the simplest oligoesters that can be synthesized by SPOS. The generation of dimers can give insight and feedback into our SPOS synthesis and characterization process.

In the optimization of the coupling and deprotecting conditions, dimers **2-25** and **2-23** were made on Wang resin. A dimeric product **2-23** was made by first coupling G12 onto Wang resin, followed by a TBDMS-deprotection, followed by coupling Dod to the $G12_T$ using conditions in Table 2-4. Finally the THP was removed with the THP deprotection conditions in Table 2-4 prior to releasing **2-23** from the resin using a HCl:dioxane solution.

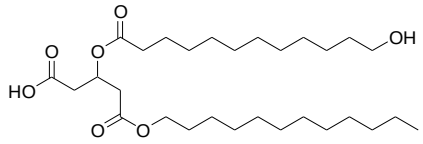

2-23

The dimer **2-23** was recovered after a gel filtration column in 15% yield from Wang resin. All SPOS products made in this thesis are reported in percent recovery calculated according to the theoretical loading capacity reported by the manufacturer on the Wang resin (about 0.75 mmole/g). Dimer **2-23** was characterized by ^{1}H and ^{13}C NMR spectroscopy and LSIMS. The MS showed a peak at *m/z* of 537.4 consistent with $[M+Na]^+$ (Figure 2-34). The peaks at *m/z* 559.3 and 515.3 are consistent with $[M+2Na-H]^+$ and $[M+H]^+$, respectively. The $[M+2Na-H]^+$ was interpreted as the sodium adduct of the sodium salt of the target. The peak at *m/z* 607.4 cannot be identified. A deletion of the Dod_T fragment may have been observed as the $[M+H]^+$ ion at the *m/z* 317, but this is most likely a fragmentation in the MS as opposed to the product mixture containing this

deletion sequence (supported by the ^{1}H NMR spectrum analysis below) since there are no peaks at *m/z* 316+22=338 or at *m/z* 316+2x22-1=349 which would be consistent with the ions $[M+Na]^+$ and $[M-H+2Na]^+$.

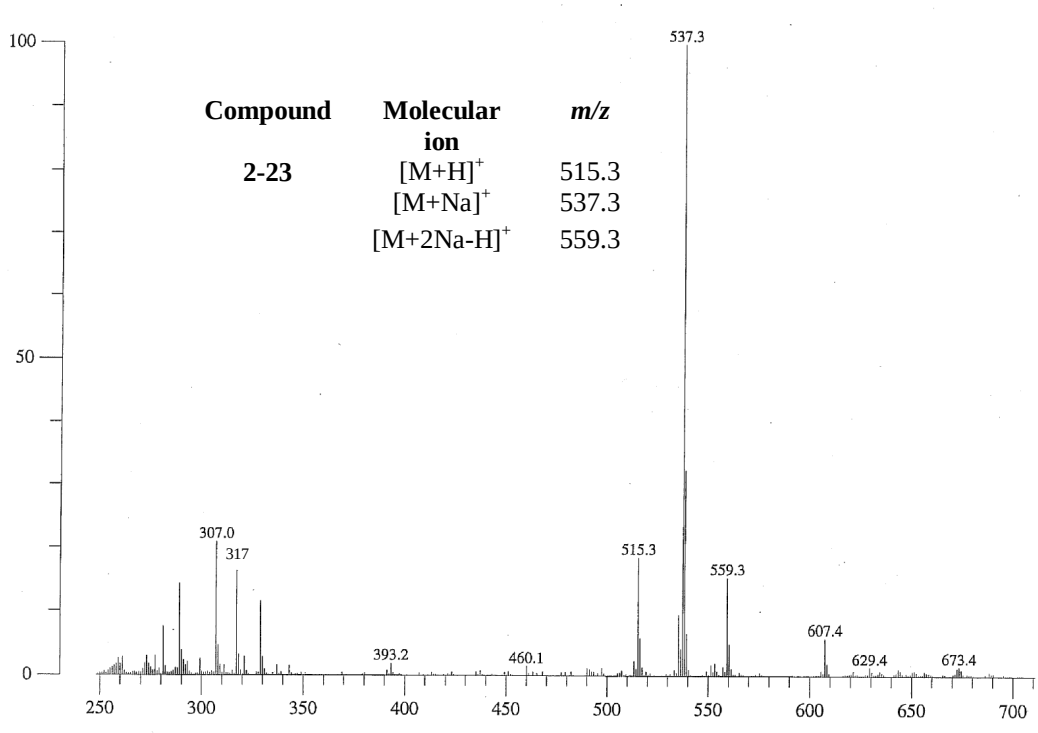

Figure 2-34. LSIMS of **2-23**. 100% = 27606 mV.

The ^{1}H NMR spectrum (Figure 2-35) supported the structure of **2-23**. The integrations are correct and the multiplet at 5.5 ppm belonged to the methine proton (H_a) which suggested the presence of the ester linking Dod_T and $G12_H$. If this ester was cleaved, then the methine resonance of the $G12_T$ group would appear upfield of 4.5 ppm. The integrity of **2-23** was greater than 95%.

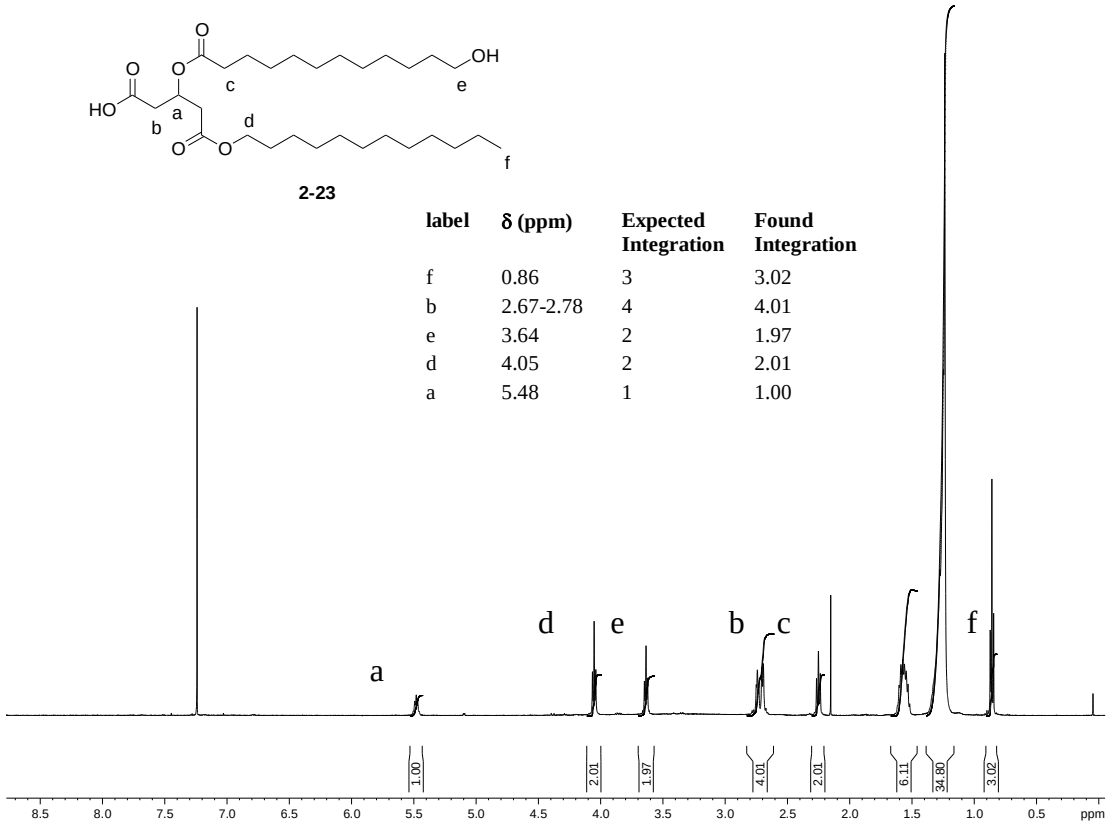

Figure 2-35. ^{1}H NMR spectrum of **2-23** in $CDCl_3$.

Dimer **2-24** was also made to demonstrate the coupling of the G12 building block onto a core block (Oct_H) as part of the reaction optimization by SPOS. From Wang resin, **2-24** was recovered in 15% yield.

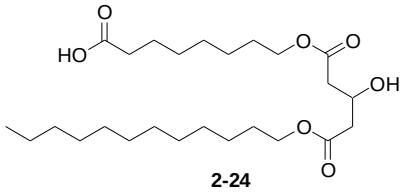

Dimer **2-24** showed a peak at *m/z* 481.3 in the MS consistent with the $[M+Na]^+$ ion (Figure 2-36). In the MS of **2-24** there was a peak at *m/z* 921.6 which is consistent with the $[M+Na-H]^+$ ion of self-esterified dimer of **2-24**, **2-29**. In this sample, there is no peak observed at *m/z* 943.6 which would be the $[M+2Na-H]^+$ ion for **2-29**. The dimer of **2-24** was thought to have been observed in the MS at *m/z* 921.6. It was probable that this

compound would have formed only in the MS because the secondary proton resonance for H_a would be expected at about 5 ppm; this would have been simple to observe had it been present.

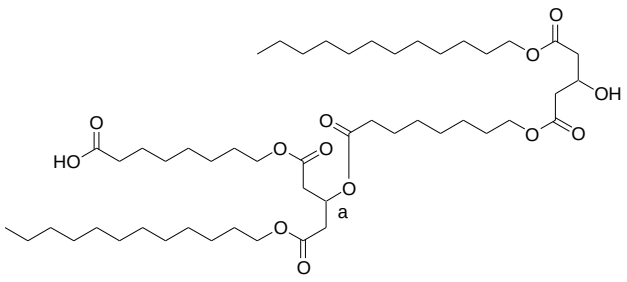

2-29

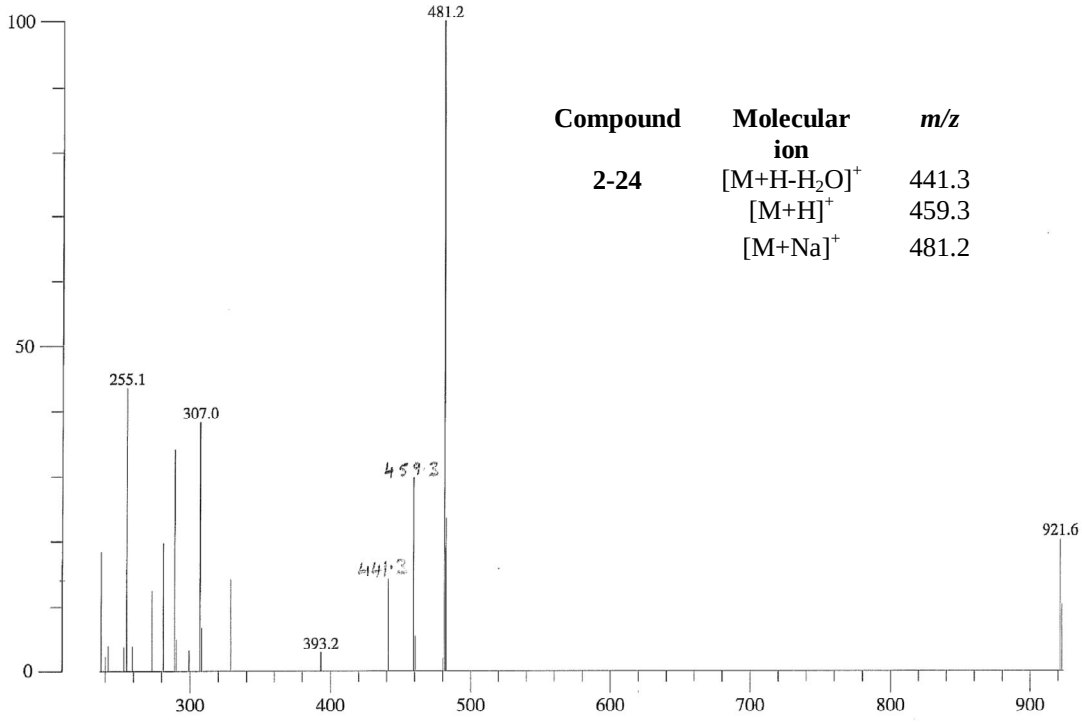

Compound	Molecular ion	*m/z*
2-24	$[M+H-H_2O]^+$	441.3
	$[M+H]^+$	459.3
	$[M+Na]^+$	481.2

Figure 2-36. LSIMS for **2-24**. 100% = 1066 mV.

The ^{1}H NMR spectrum of purified **2-24** is given as Figure 2-37. The ^{1}H NMR spectrum is generally consistent with the anticipated spectrum of pure **2-24**. However, there were obvious minor impurities in the ^{1}H NMR spectrum.

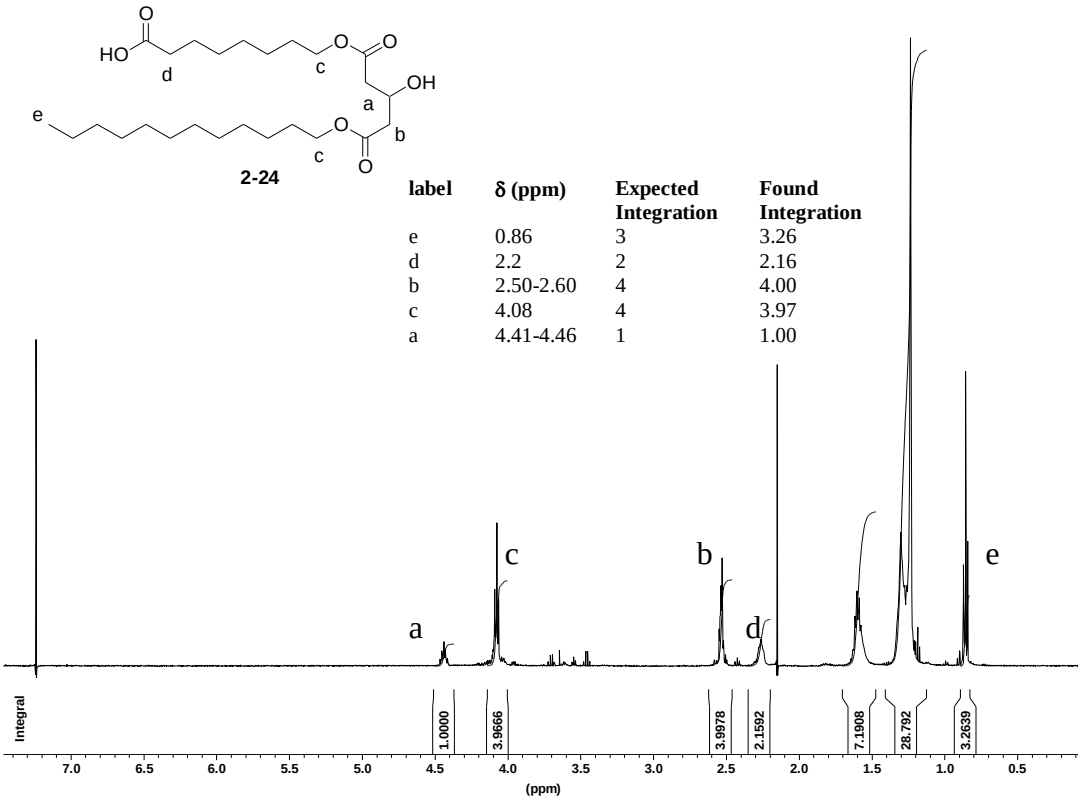

Figure 2-37. ^{1}H NMR spectrum of **2-24** in $CDCl_3$

In this particular ^{1}H NMR spectrum, the methyl H_e integration was about 10% greater than theory. For most of the SPOS products, this type of difference was observed for the methyl protons and would be consistent to have been the result of some grease contamination. The integration for H_d was over integrated by about 8%; however the other protons (H_c and H_b) were integrated correctly. Sometimes the peak for the alcohol proton would appear in the H_d region and therefore be a minor contribution to the integration.

Given the close correspondence of H_c and H_b integrations, this sample is assumed to contain **2-24** as the dominant (>95%) component.

The last type of dimer combination explored with blocks 1 and 3 was by coupling of two core units (Oct and Dod) to generate dimer **2-25** using the standard protocols. This product was recovered after gel filtration in 12% yield.

The LSIMS of simple dimer **2-25** showed a peaks at *m/z* 381.3 and 359.2 for the $[M+Na]^+$ and $[M+H]^+$ ion of **2-25** (Figure 2-38).

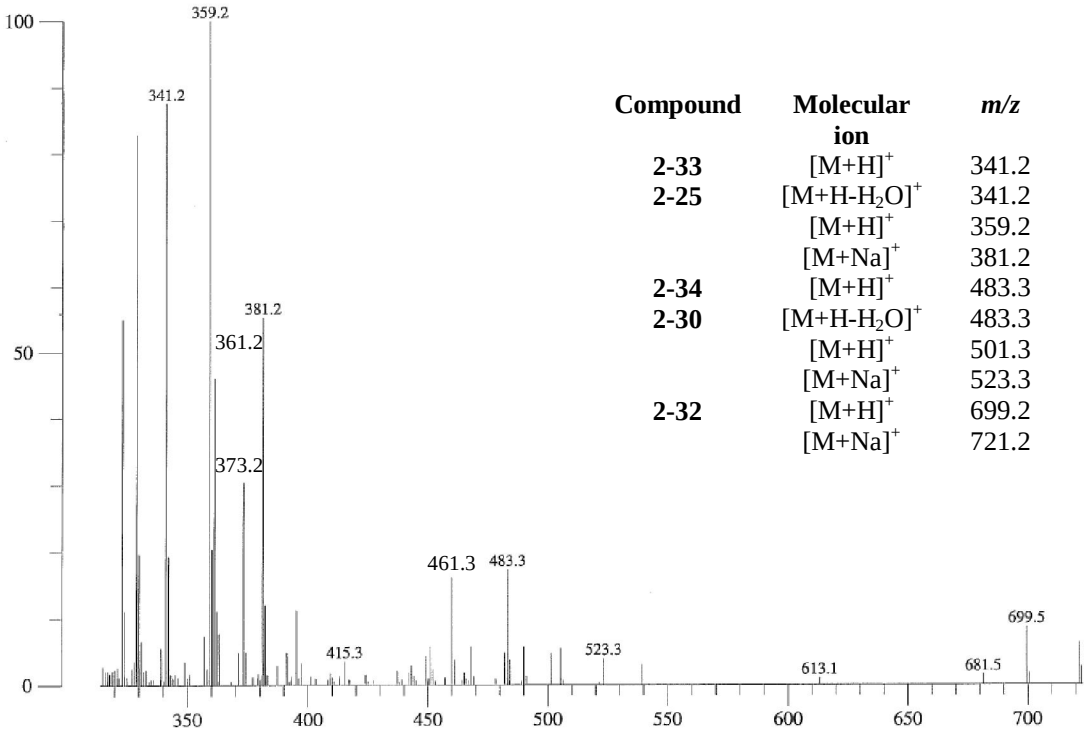

Compound	Molecular ion	*m/z*
2-33	$[M+H]^+$	341.2
2-25	$[M+H-H_2O]^+$	341.2
	$[M+H]^+$	359.2
	$[M+Na]^+$	381.2
2-34	$[M+H]^+$	483.3
2-30	$[M+H-H_2O]^+$	483.3
	$[M+H]^+$	501.3
	$[M+Na]^+$	523.3
2-32	$[M+H]^+$	699.2
	$[M+Na]^+$	721.2

Figure 2-38. LSIMS of **2-25**. 100% = 1589 mV.

Although there are many intense peaks in the MS, some can be accounted for by a decomposition pathway such as the peak at *m/z* 341.2 consistent with the $[M-H_2O+H]^+$ ion. There are some higher molecular weight peaks as well which are consistent with trimeric (**2-30:** $[M+H]^+$=501.3, $[M+Na]^+$=523.3 and **2-31:** $[M+H]^+$=415.3) and tetrameric (**2-32:** $[M+H]^+$=699.2, $[M+Na]^+$=721.2) products.

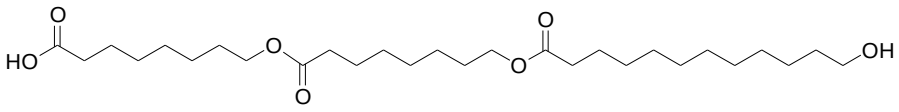

2-30

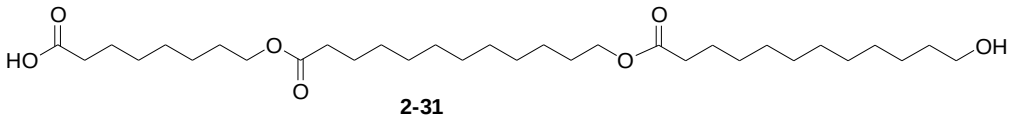

2-31

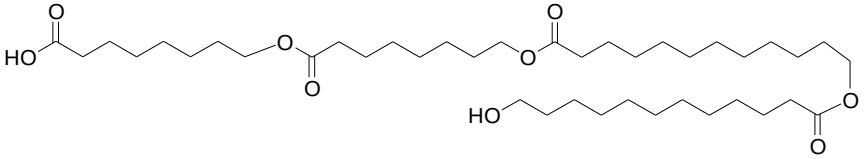

2-32

To understand how the compounds of higher molecular weight (addition sequences) arise, the ^{1}H NMR spectra of the building blocks **2-22** and **2-21** were first examined which showed no evidence of any free alcohol (lack of the resonances from the C<u>H$_2$</u>OH). Nevertheless, an ion for the hydroxy acid was observed for some of the MS collected, but it was inconclusive as to whether these were fragments in the MS or molecular ions. However, suppose there was a 5% impurity of the hydroxy acid (HO-Oct$_T$) in the sample of protected building block. This would probably be above the maximum level that would be "undetected" by ^{1}H NMR spectroscopy. Even so, if this were the case, the addition sequences could arise assuming that the coupling is the same for the protected and unprotected hydroxy acids (Figure 2-39).

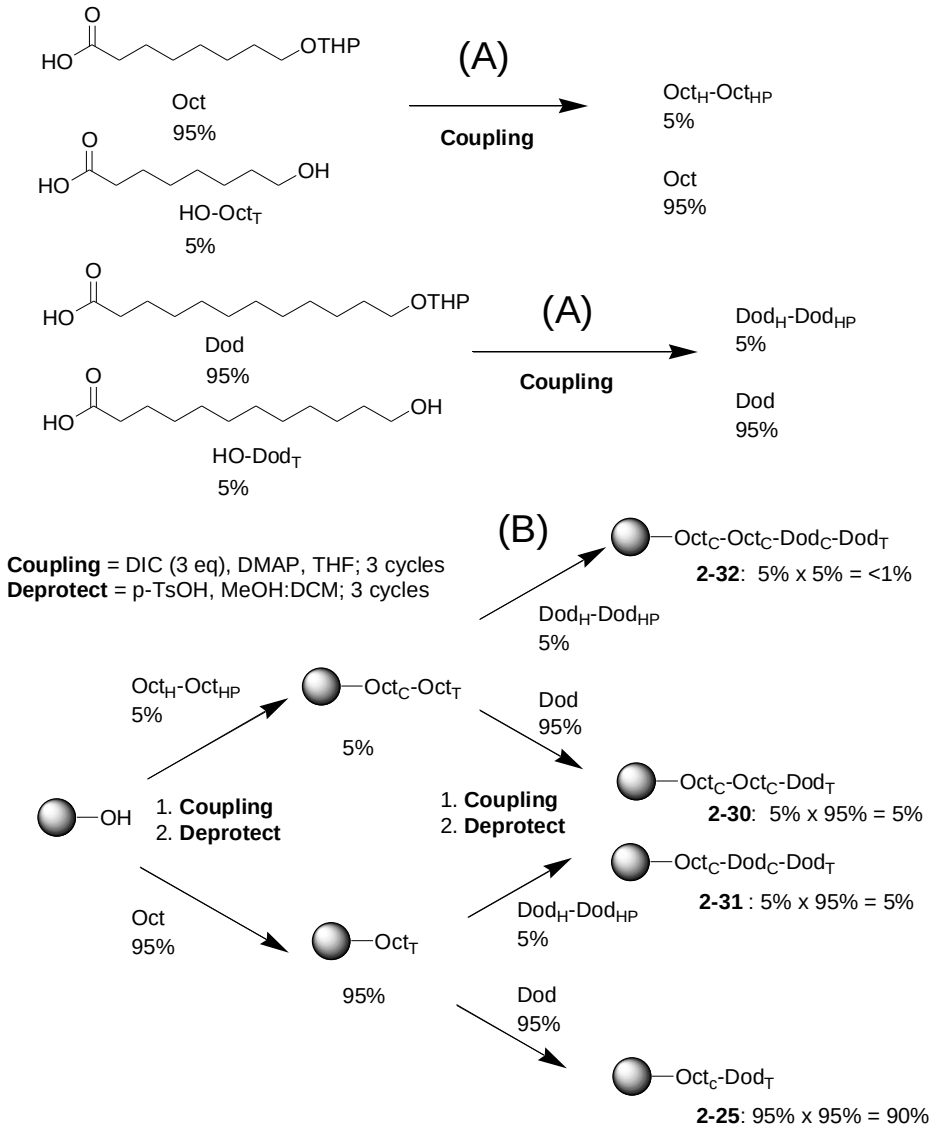

Figure 2-39. Details of how addition sequences could arise.

In Figure 2-39A the propagation of a small amount of free hydroxy acid is shown to couple to the protected hydroxy acid leading to a 5% formation of the Oct and Dod self-dimers, Oct_H-Oct_{HP} and Dod_H-Dod_{HP}, respectively. If this occurred, using the Oct mixture as a loading solution for the resin, followed by deprotection of the alcohol then 95% of the alcohol sites on the resin were the monomer while 5% were the dimer. From another coupling via a 95:5 mixture of Dod:Dod_H-Dod_{HP} was added to yield a mixture of

2-32, **2-30**, **2-31**, and **2-25** (Figure 2-39B). According to this model, it is expected that there are three major products **2-25**:**2-31**:**2-30** (90:5:5) and very little of **2-32**.

In the LSIMS of **2-25**, Figure 2-38, the molecular ion $[M+H]^+$ and $[M+Na]^+$ were observed at *m/z* 359.2 and 381.2, respectively. The peak observed at *m/z* 341.2 is consistent with a dehydration of the molecular ion **2-25** ($[M+H-H_2O]^+$) or alternatively it could also be the cyclic dimer **2-33**. The cyclic dimer **2-33** can form by an intramolecular cyclization under the cleavage conditions (Figure 2-40).

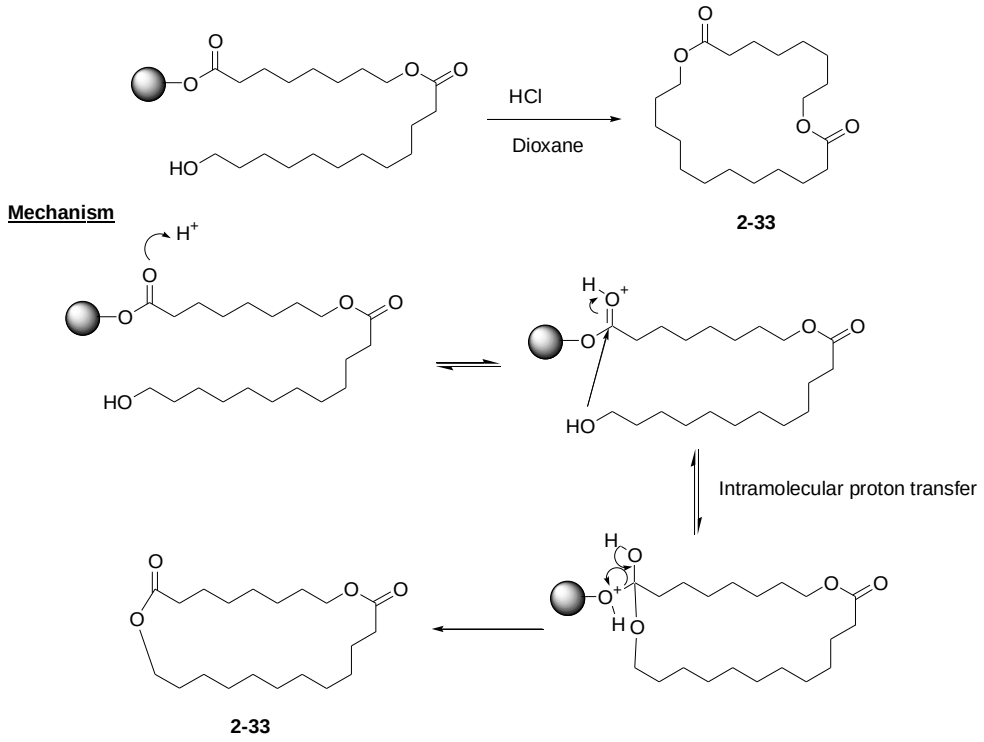

Figure 2-40. Intramolecular cyclization of **2-25** on resin to yield **2-33**.

Trimer **2-31** ($[M+H]^+$= 557.2, $[M+Na]^+$ = 579.2) was not observed in Figure 2-38 whereas trimer **2-30** was. This is not consistent with the model discussed in Figure 2-23 and the outcome of forming trimer **2-30** but not **2-31** could have been related to the purity of the Dod and Oct building blocks. If the free hydroxy acid component in the particular sample of Dod used was lower compared to the composition of the Oct sample, then the

observed result could be anticipated. As well, a peak at *m/z* 483.3 was consistent with either a cyclic trimer **2-34** ($[M+H]^+$ ion) or a dehydration of **2-30**.

The cyclization process can be envisioned to occur as an intramolecular reaction of **2-30** on resin during the cleavage step (similar to the formation of **2-33**). However, there was a peak at *m/z* 461.3 which could be the loss of a sodium (*m/z* -22) implying that **2-34** may not be a likely product.

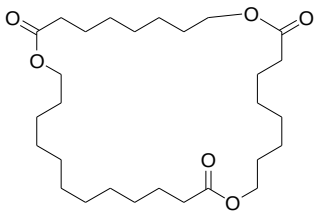

2-34

In the proposed model of how the addition sequences arise, **2-32** was not expected to form in detectable quantities, however the peaks observed at *m/z* 699.5 and 721.2 in the MS were consistent with **2-32**. Alternatively, these two peaks are also consistent with the dimerization of **2-25** to yield an isomer of **2-32**: Oct_H-Dod_C-Oct_C-Dod_T. The dimerization could either happen in the matrix (acidic mNBA) or in the cleavage process from the resin as a transesterification (primary alcohol of one **2-25** attacks the ester linking another **2-25** to the Wang support) (Figure 2-41).

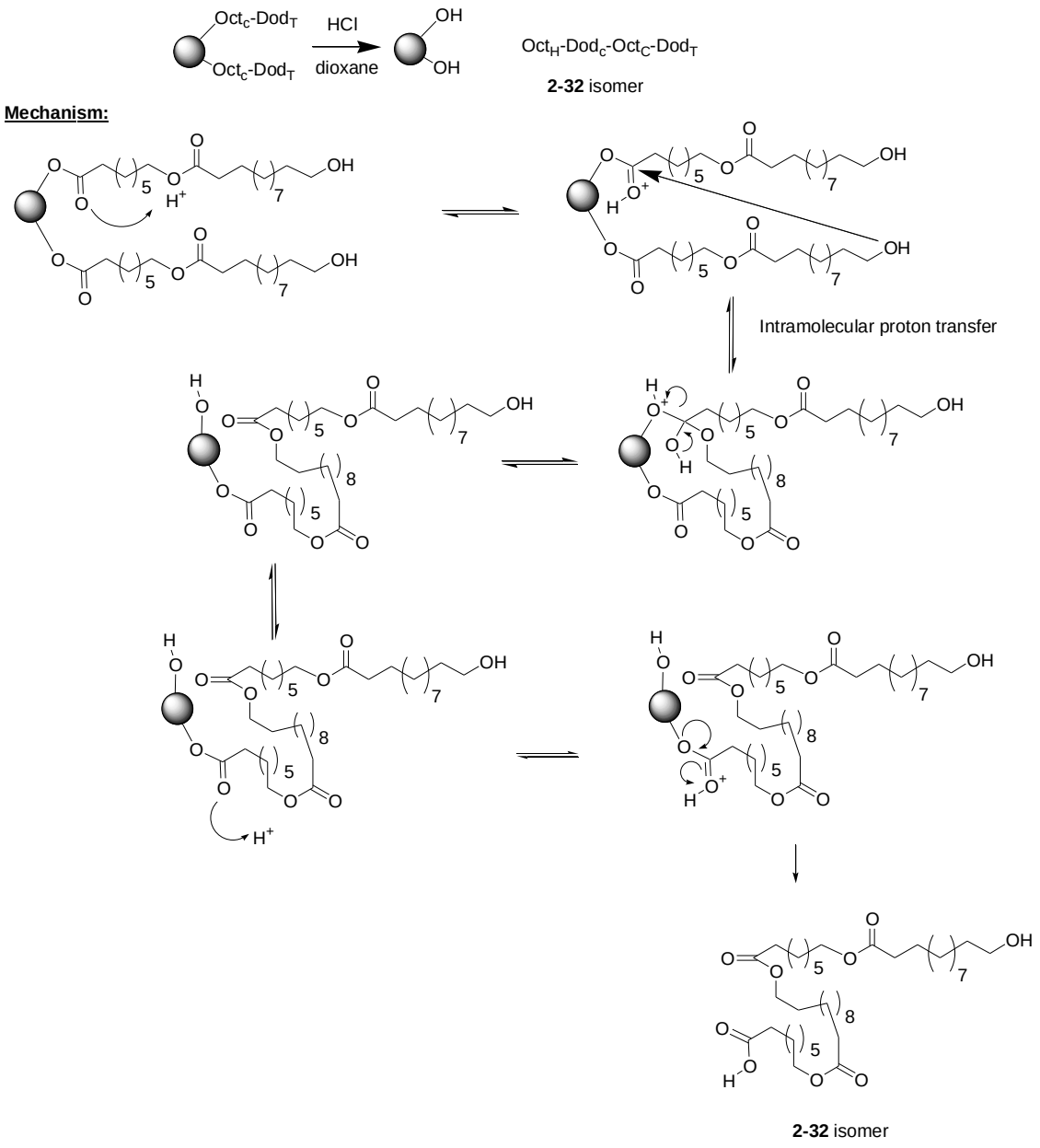

Figure 2-41. Proposed dimerization mechanism to yield an isomer of **2-32**.

The MS provided much information on the impurities in the **2-25** sample. Within the MS, the expected peaks consistent for the product are observed. There is evidence of impurities from addition sequences which could arise from starting materials containing free hydroxy acids. Finally there are also peaks which are consistent with inter- and intramolecular decomposition during cleavage. The decomposition was evident in this

sample where there is a terminal primary alcohol. In earlier dimeric products with terminal secondary alcohols, this method of decomposition was not observed.

The ^{1}H NMR spectrum of **2-25** was shown previously in Figure 2-32. The expected ^{1}H NMR integration for the proposed products in the **2-25** synthesis is given in Table 2-5. Regardless of product there are only three types of proton signal: HOC$\underline{H}_2$,C$\underline{H}_2$CO_2, and C$\underline{H}_2O_2$C.

Table 2-5. Expected proton integrations for **2-25**, **2-33, 2-30**, and **2-32**.

Compound	HOC$\underline{H}_2$	C$\underline{H}_2$CO_2	C$\underline{H}_2O_2$C
2-25	2	4	2
2-30	2	6	4
2-32	2	8	6
2-33	0	4	4

In the ^{1}H NMR spectrum for **2-25**, the H_a and H_b signals are over-integrated by about 20% each when H_d was used as the calibration peak (Figure 2-32). In the LSIMS, the addition sequences were observed and therefore may be one of the components which contribute to the 20% increase in the integration. Alternatively the cyclic products could contribute in an increase in the integration as well.

To calculate the amount of addition sequences observed, an assumption was made that **2-30** was the dominant contaminant. In the **2-25** example, the calculated **2-30** contaminant is about 9% based on the C$\underline{H}_2O_2$C signal at ~4.0 ppm or 8% based on the C$\underline{H}_2$CO_2 signal at ~2.3 ppm.

Alternatively if **2-33** was the dominant contaminant in **2-25,** then there would be about a 9% or 12% contamination based on the C$\underline{H}_2O_2$C and C$\underline{H}_2$CO_2 signal, respectively.

Recall that in order to generate **2-30** the model in Figure 2-39 would have to be correct. Relating to Figure 2-39 an assumption that there was a 5% contamination of the free hydroxy acid in the Oct building block should give only a 5% contamination product. In order to generate a >10% contamination, the contamination in building block must also be >10%. This substantial amount would have easily been observed in the ^{1}H NMR spectrum of the Oct building block. Therefore between the two types of possible contaminants **2-33** or **2-30**, the more likely type in this example is **2-33**.

Clearly this example of synthesizing **2-25** showed that gel filtration as a method for separating the product from the contaminating sequences was not very effective. This type of problem can be expected with products terminated with a primary alcohol. Even with these small impurities present it is expected that they cannot participate in ion transport activity because of their small size and structure.

2.2.7.3 Synthesis of Trimers

From the establishment that dimers can be made (with the production of some impurities), the next step in the methodology development was to build a trimer where building blocks Dod, Oct and G12 were used together to make **2-35**. This product, **2-35**, was made on Wang resin in 45% yield using the standard protocols in Table 2-4.

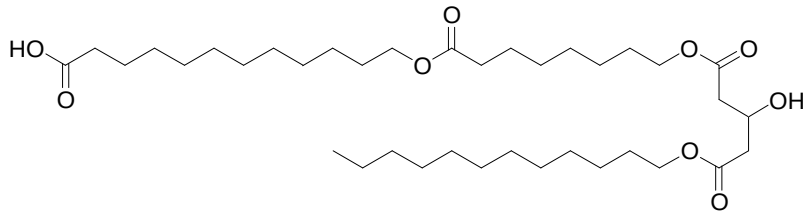

2-35

The expected peaks for $[M+H]^+$, $[M+H-H_2O]^+$, and $[M+Na]^+$ for **2-35** were observed at *m/z* 657.5, 639.4, and 679.5, respectively (Figure 2-42). In the MS of **2-35**, a

peak was observed at *m/z* 821.6 which is consistent with the $[M+Na]^+$ ion of **2-36** (an additional Oct_c unit on **2-35**).

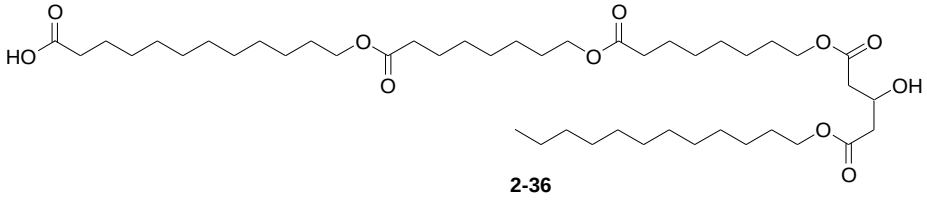

2-36

It should be noted that there was no product in any of the SPOS reactions to be discussed where there was an addition of a second G12 unit. The rationale relates to the synthesis of the starting material. The starting material for G12 was protected prior to esterification while for any of the hydroxy acids (Dod, Oct, and Hex), the hydroxy acid had to be protected as one of the synthetic steps.

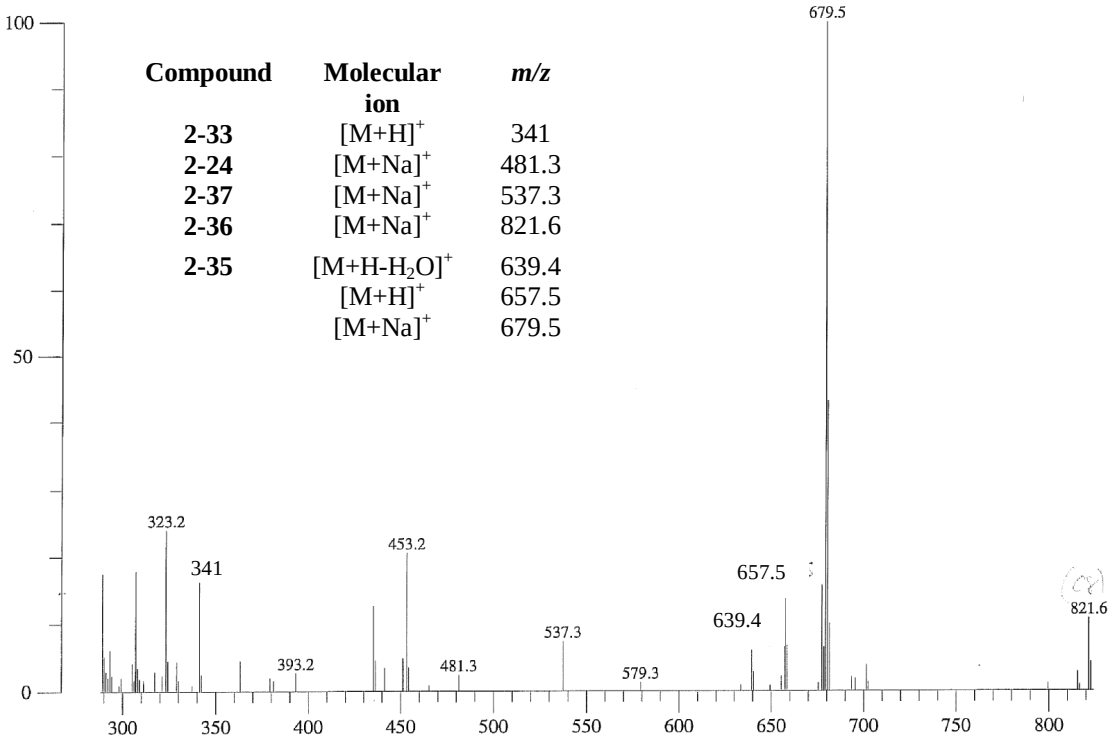

Figure 2-42. LSIMS of **2-35**. 100% = 2837 mV.

In the MS of **2-35** (Figure 2-42), there was evidence of some **2-24** ($[M+Na]^+$ ion at *m/z* 481.3) in the mixture. It was probable that **2-24** was an actual component in the mixture as opposed to a fragmentation because the peak at *m/z* 537.3 was consistent with the $[M+Na]^+$ ion for **2-37**. These two components would be the result of inefficient loading of Dod (for **2-24**) or coupling of Oct (for **2-37**).

Similar to the dimer **2-25**, a peak at *m/z* 341 is observed in the MS of **2-35** which is proposed to be the $[M+H]^+$ of the lactone **2-33**. Compound **2-33** would be the result of inefficient G12 coupling onto the Oct_T unit on the solid support and then upon product cleavage from the support, cyclization occurs.

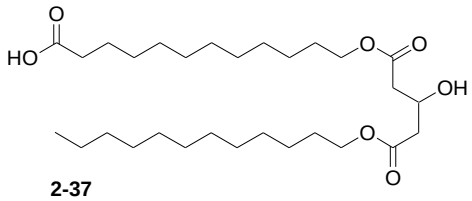

2-37

The ^1H NMR spectrum for **2-35** is Figure 2-43. In comparison to the other SPOS products made, the ^1H NMR spectrum for **2-35** (Figure 2-43) was interesting because of unique contribution by the contaminant **2-36**. Tetramer **2-36** is expected to contribute two additional protons to each of the H_c and H_d resonances.

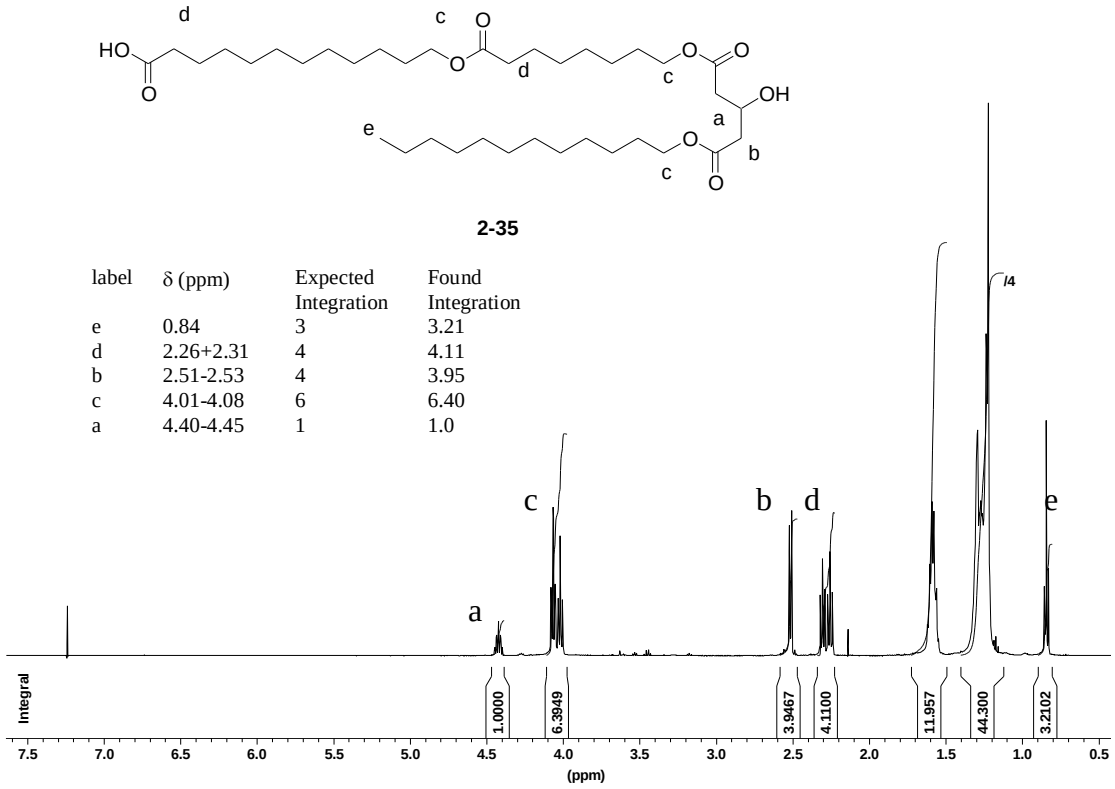

Figure 2-43. ^{1}H NMR spectrum of **2-35** in $CDCl_3$.

According to Figure 2-43 the error in integration is 1.3% using the H_b integration as a standard. From the MS, the deletion sequences of **2-37** and **2-24** may be present and these could affect the proton integration by increasing the H_a:H_d ratio. Since in the ^{1}H NMR spectrum the inverse is true (decrease of the H_a:H_d) then it can be assumed that the percentages of the deletion sequences **2-37** and **2-24** were not very significant. The dominant contaminant was the addition sequence **2-36** or some lactone such as **2-33**. Using the method of quantifying the amount of contamination in equation (2-2), then the percentage of **2-36** in the product mixture was an average of 4% and **2-35** was about 96% integrity.

The first trimer product discussed (**2-35)** was analyzed by LSIMS and ^{1}H NMR spectroscopy. The MS showed that there are many potential impurities such as addition sequences and lactones. The ^{1}H NMR spectrum confirmed the presence of impurities with some increased proton integration values. However, the amount of contamination was minute.

Trimer **2-39** was made on resin using standard protocols (Table 2-4) to couple the sequence of Oct, Dod and Oct. The product was cleaved from resin using HCl:dioxane and recovered in 23% yield. This trimer product demonstrated the ability to couple three core components together.

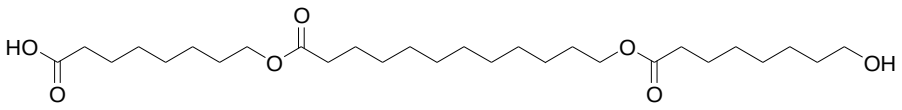

2-39

The observed peaks at *m/z* 523.4, 501.3, and 483.3 were consistent with the $[M+Na]^{+}$, $[M+H]^{+}$, and $[M+H-H_2O]^{+}$ ions of **2-39**, respectively (Figure 2-44).

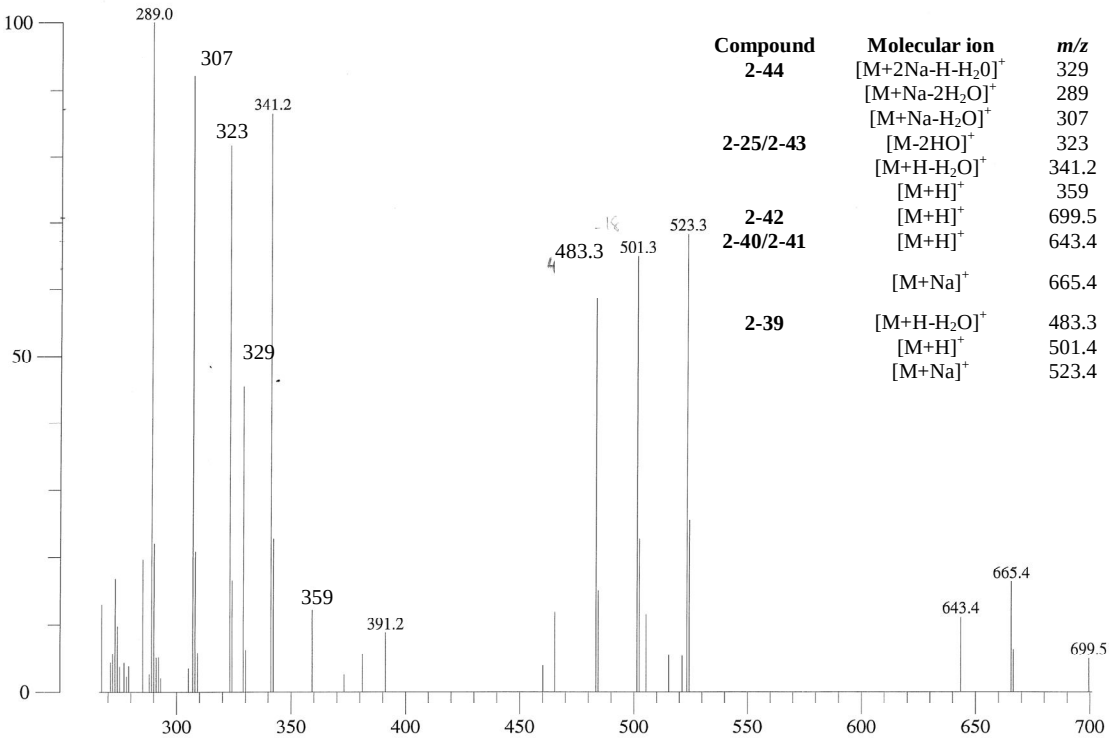

Figure 2-44. LSIMS of **2-39**. 100% = 811 mV.

It is plausible that the $[M+H-H_2O]^+$ ion for **2-39** may instead be the $[M+H]^+$ for **2-34** which formed under the intramolecular reaction proposed previously. There are some higher molecular weight ions which are consistent with tetramers containing an extra Oct_T or Oct_H block (**2-40** or **2-41**) with a $[M+H]^+$ ion at *m/z* 643.4 or $[M+Na]^+$ ion at *m/z* 665.4 or an extra Dod_c block (**2-42**) with a $[M+H]^+$ ion at *m/z* 699.5.

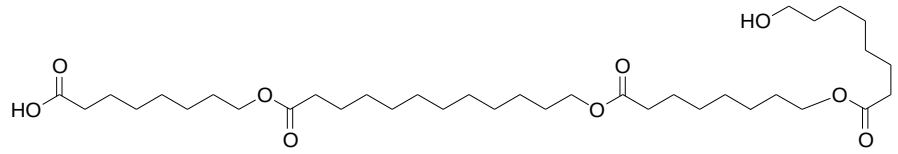

2-40

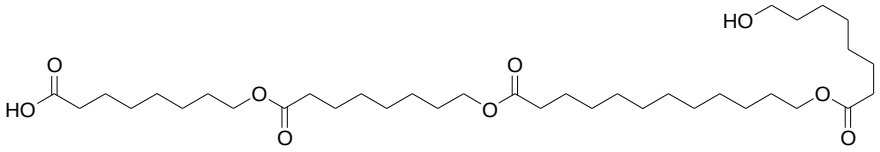

2-41

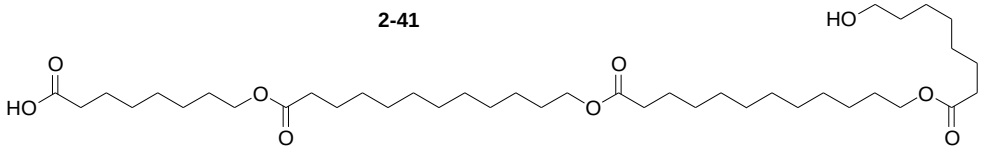

2-42

The peak at *m/z* 359 ($[M+H]^+$) was consistent with the dimer **2-25** or **2-43**. The peak at *m/z* 341 was consistent with the dehydration of this compound ($[M+H-H_2O]^+$) and a further dehydration ($[M-2OH]^+$) lead to *m/z* 323. Since there are no sodium adducts or salts observed for **2-25** or **2-43** then it was quite probable that these observed $[M+H]^+$ peaks are a fragmentation of **2-39**. Dimer **2-44** was either the result of improper Dod coupling or a fragment of **2-41** where the Dod_c-Oct_T unit breaks off. The expected $[M+H]^+$ and $[M+Na]^+$ ions for **2-44** were not observed, but the $[M+Na-H_2O]^+$ was observed at *m/z* 307. Therefore the lack of molecular ions for proposed **2-44** strongly suggested that the deletion sequence was not as likely as a fragment from **2-41**. A further dehydration yielded the peak $[M+Na-2H_2O]^+$ *m/z* 289 while an addition of another Na^+ ($[M+2Na-H-H_2O]^+$) gave the peak at *m/z* 329.

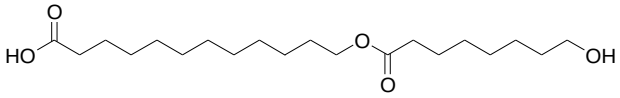

2-43

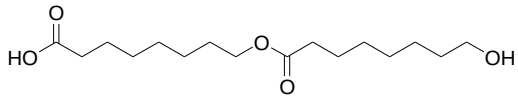

2-44

The MS suggested the presence of addition sequences (**2-40, 2-41** and **2-42**) while the deletion sequences were not as likely. These are the same issues that were discussed for **2-25**. The ^{1}H NMR spectrum was used for quantifying the impurities (Figure 2-45).

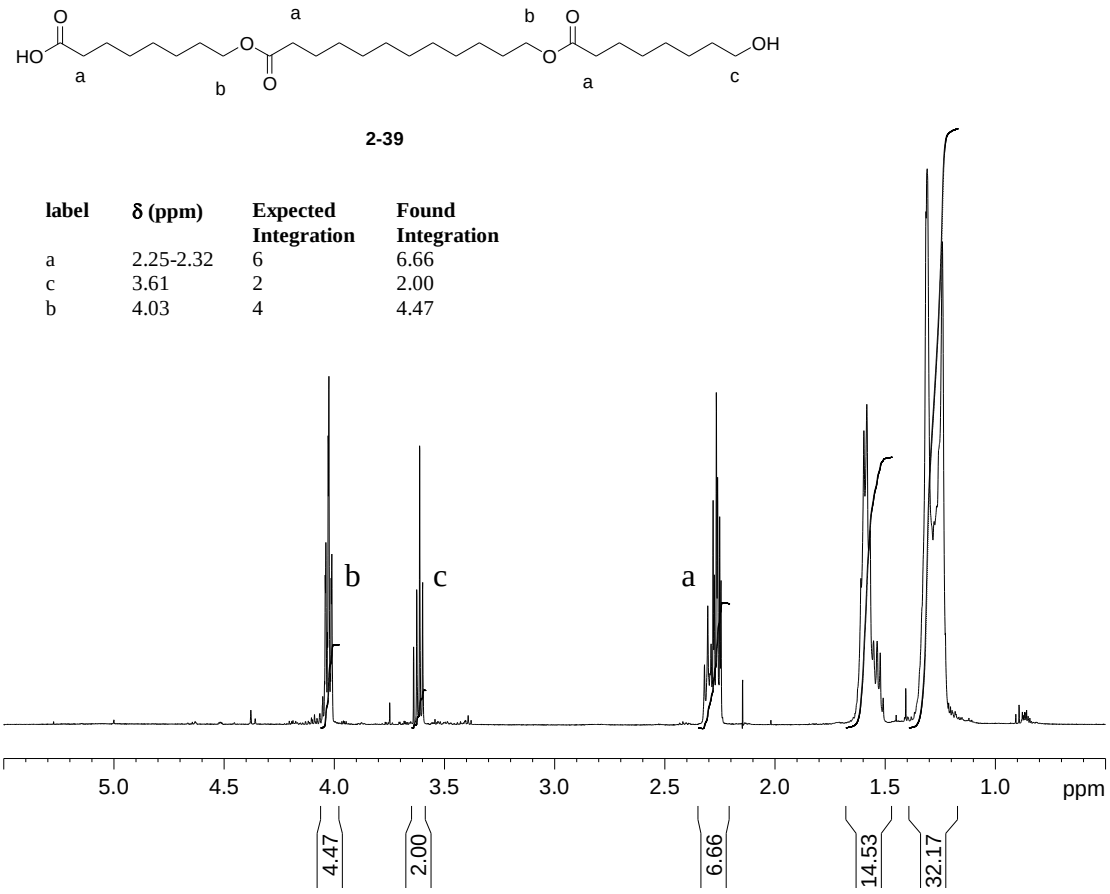

Figure 2-45. ^{1}H NMR spectrum of **2-39** in $CDCl_3$

All of these products have the same "distinct" proton types: C$\underline{H_2}$OH, C$\underline{H_2}O_2$C, and C$\underline{H_2}CO_2$. By setting the C$\underline{H_2}$OH protons to a reference value of 2 protons, then the H_a and H_b resonances are over-integrated by about 10%. Assuming that the contaminants were the additions of Oct_C or Dod_C to the **2-39** structure then the integrity of **2-39** was an average of 93%. If the lactone were present, then the integrity of **2-39** is 90 % and 85% if the H_b and H_a were used.

In the ^{1}H NMR spectrum for **2-39** there are some resonances between 0.8 and 0.95 ppm. This is hydrocarbon grease as the typical resonances for grease are 0.86 and 1.26 ppm.[82] Unfortunately the resonance at 1.26 ppm is under the alkyl resonances of **2-39**.

2.2.7.4 Synthesis of Tetramers

The coupling of building blocks to make dimers and trimers were shown to be effective. Tetrameric products are expected to be long enough to span a bilayer membrane. Using the standard coupling and deprotection conditions (Table 2-4), **2-27** was cleaved from Wang resin in a 49% yield using a TFA:CH_2Cl_2 solution. Tetramer **2-27** was characterized by ^{1}H, ^{13}C NMR spectroscopy and MS.

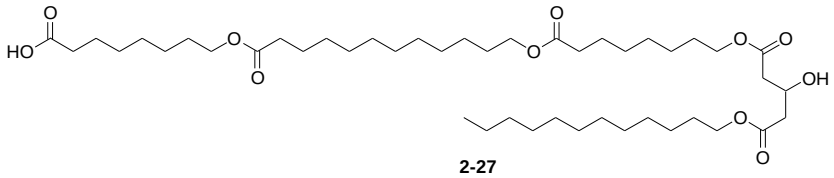

2-27

The peaks in the MS for **2-27** at *m/z* 821.6 and 799.6 are consistent with the $[M+Na]^+$ and $[M+H]^+$ ions (Figure 2-46). The peak at *m/z* 963.6 is consistent with the $[M+Na]^+$ ion of an additional Oct unit to **2-27, 2-45** or **2-46** (there is no way to tell the difference between these two structures in the MS). The peak at *m/z* 1019.7 is consistent with the $[M+Na]^+$ ion for **2-47**.

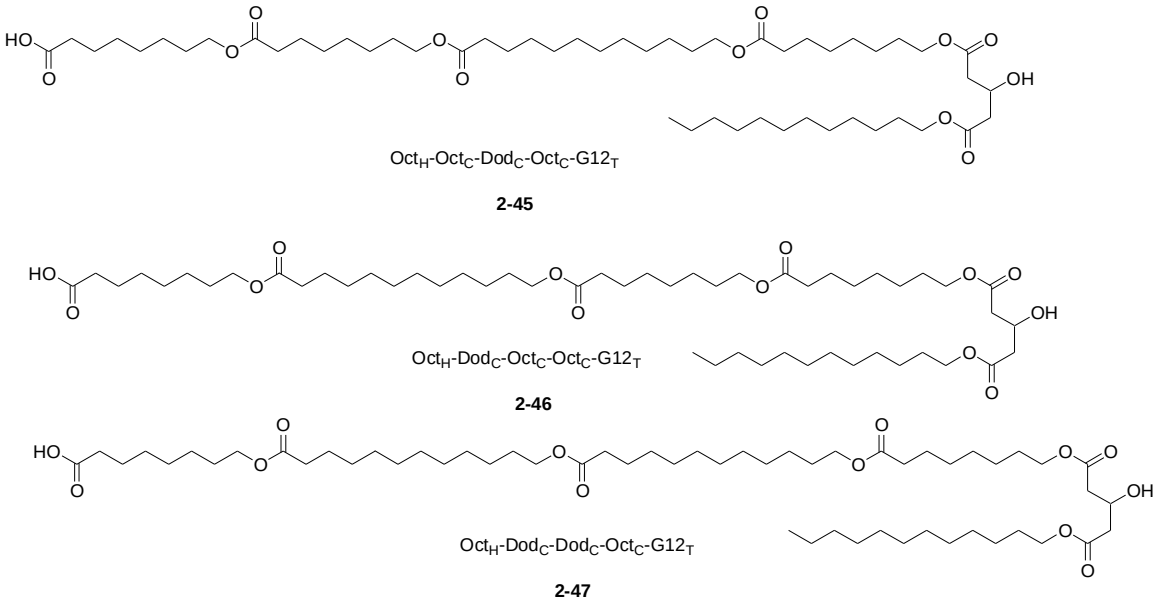

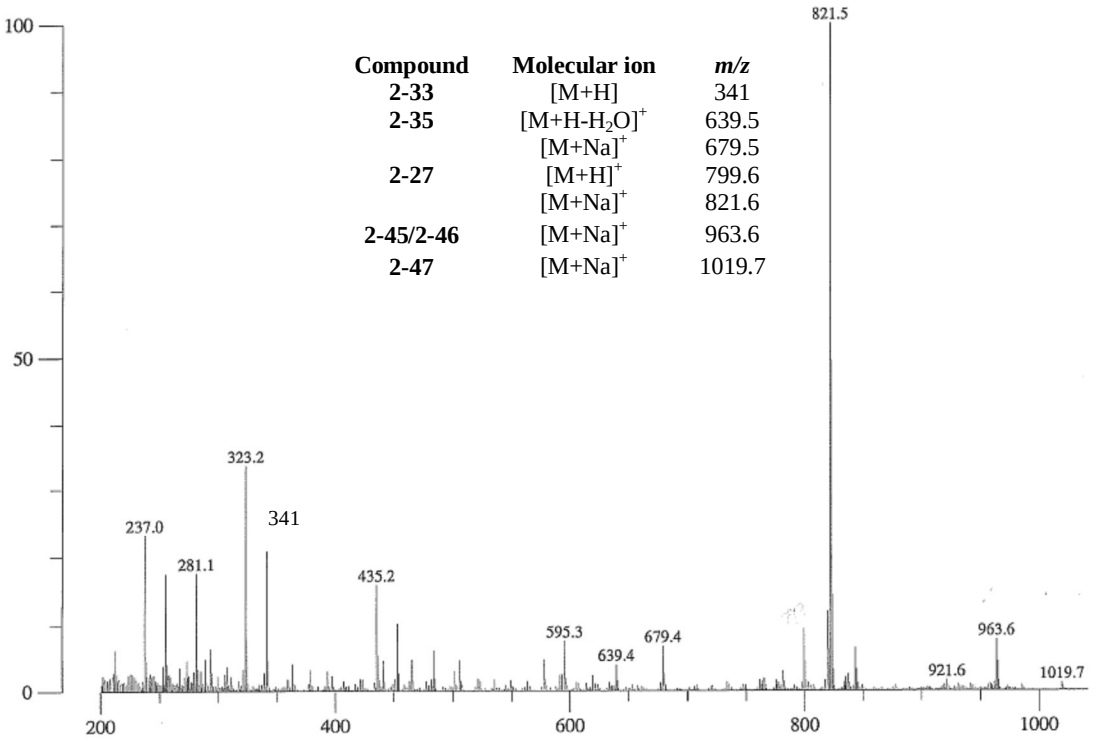

Compound	Molecular ion	*m/z*
2-33	$[M+H]$	341
2-35	$[M+H-H_2O]^+$	639.5
	$[M+Na]^+$	679.5
2-27	$[M+H]^+$	799.6
	$[M+Na]^+$	821.6
2-45/2-46	$[M+Na]^+$	963.6
2-47	$[M+Na]^+$	1019.7

Figure 2-46. LSIMS of **2-27**. 100% = 26642 mV.

In the MS of **2-27**, there is a peak at *m/z* 341 which is consistent with the lactone **2-33** observed in many of the previously discussed dimers and trimers. In order to generate the lactone **2-33** the product on the resin would have had to miss two coupling

cycles – the Oct and G12 couplings. Such a situation is highly improbable. In this sample, the peaks at *m/z* 639.5 and 679.5 are consistent with the $[M\text{-}H_2O+H]^+$, and $[M+Na]^+$ of **2-35**. Since there is a Na^+ peak then this is probably a deletion sequence and not a fragment of **2-27**.

The ^1H NMR spectrum of **2-27** is shown in Figure 2-47. The precision of the instrument and method can be quantified by examining the proton resonances which belong to one unit of the product. It is assumed that the methine proton at about 4.5 ppm vs. methylene protons at about 2.5 ppm from the glutaric structure of the G12 fragment is in a 1:4 ratio. Therefore under high precision, the integrations that correspond to these two types of protons should be 1:4. In the event that there is low instrument precision, then there can be error in the integration (calculated by using equation (2-1)). In Figure 2-47, the error in the integration was only about 0.5%.

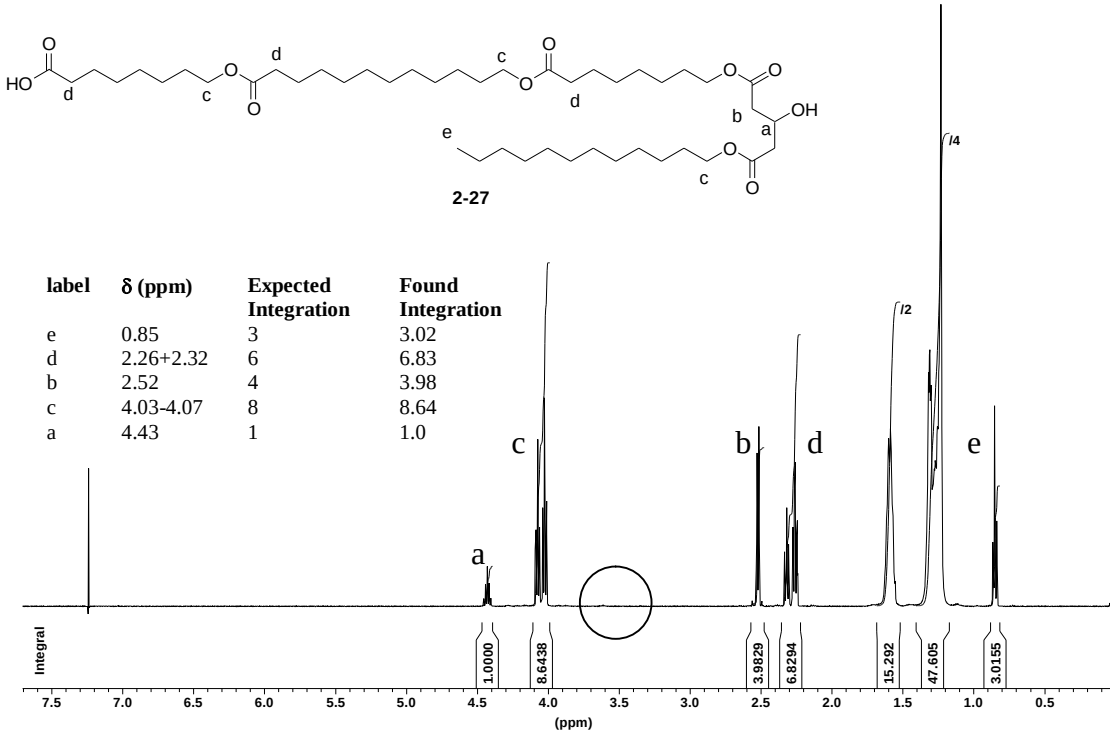

Figure 2-47. ^1H NMR spectrum of **2-27** in $CDCl_3$.

The ^{1}H NMR spectrum (Figure 2-47) fully supports that the compound was made because all of the expected proton resonances are present. The C$\underline{H_2}O_2$C and C$\underline{H_2}CO_2$ resonances were higher than anticipated (they were expected to be 8 and 6 respectively but they are observed as 8.64 and 6.83) which suggested that there was a minor contribution of some **2-45** or **2-46** and **2-47**. Since those particular integrations were higher than expected, we conclude that the amount of addition dominates the deletion sequences. If deletion sequences were present, then the anticipated C$\underline{H_2}O_2$C and C$\underline{H_2}CO_2$ resonances would be lower than expected (under 8 and 6, respectively). According to the ^{1}H NMR spectrum for **2-27**, there was no resonance for C$\underline{H_2}$OH (circled area), which implied that the coupling of G12 was efficient in the products isolated.

Applying the same treatment to the ^{1}H NMR data for **2-27** as for **2-35**, the percentage of **2-27** in the product mixture was 84% if the C$\underline{H_2}O_2$C signal (H_c) was used, while the C$\underline{H_2}CO_2$ signal (H_d) yielded 80%. These numbers were calculated assuming that the cyclic dimer **2-33** was present in the mixture. The cyclization would form during the cleavage step by the trimer (not the dimer) on the resin which lacks the $G12_T$ unit (**2-39** on resin). The cyclization was proposed to have originated from the trimer and not the dimer because in order for the dimer to have existed, it would have had to miss two coupling steps, which is highly unlikely.

The tetramer **2-48** was made using the standard protocol (Table 2-4) using the G12, Oct, and Dod building blocks in 37% recovery from Wang resin and characterized by ^{1}H, ^{13}C NMR spectroscopy and MS. Product **2-48** is a demonstration that it was possible to make a tetrameric product with the $G12_H$ as the carboxylic acid end of the oligoester.

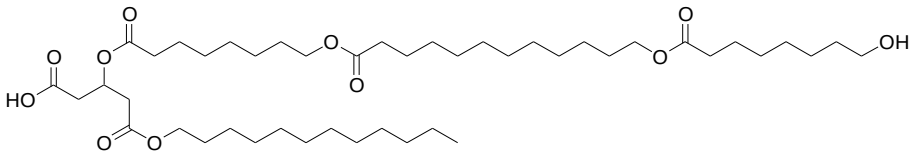

$G12_H$-Oct_C-Dod_C-Oct_T

2-48

The expected $[M+Na^+]$ ion for **2-48** was observed in the MS at *m/z* 821.5 (Figure 2-48). No addition sequences were observed in this sample, but that may be the result of the relative intensities being low; the maximum intensity of this spectrum was only 634 mV.

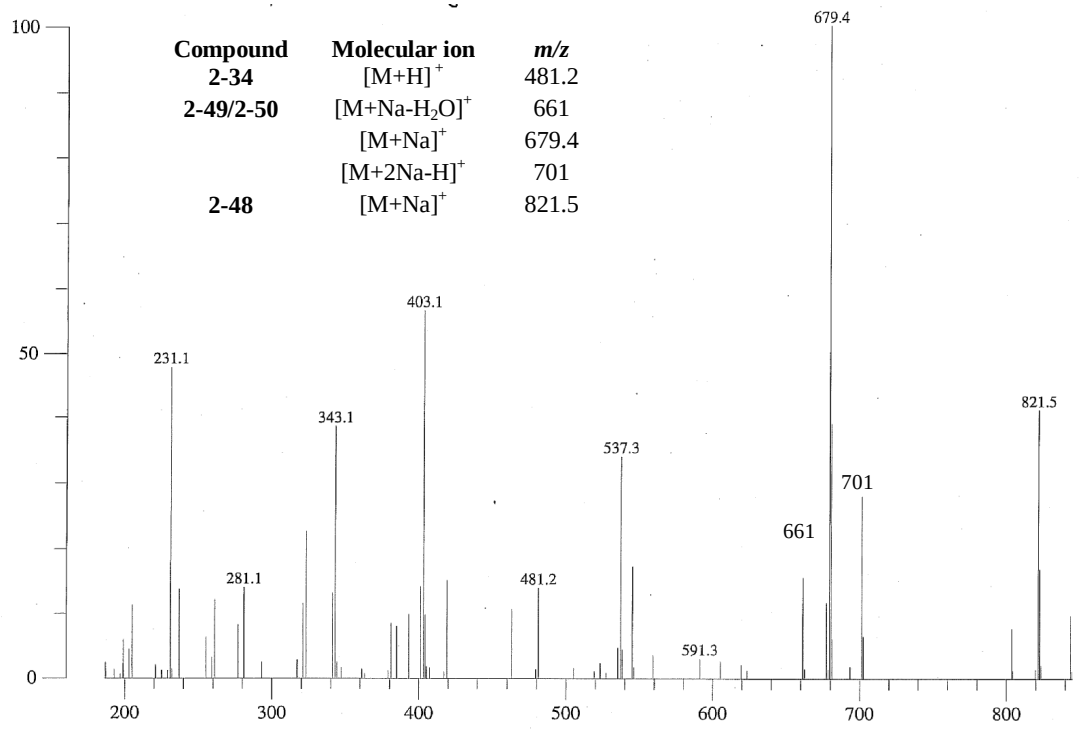

Figure 2-48. LSIMS of **2-48**. 100% = 634 mV.

In the MS, there is a peak at *m/z* 481.2 which is consistent with the $[M+H]^+$ ion of **2-34**. The formation of this lactone would be from the product on the Wang resin which lacks the $G12_H$ unit. However, it is believed that the free alcohol sites have been capped

with BPAA so this theory is not possible. Alternatively, the ester linking the Oct_C and $G12_H$ may have cleaved in solution during the resin cleavage step and then the cyclization occurred *in situ*.

The base peak at *m/z* 679.4 was most likely not a fragment of **2-48** with a loss of a Oct_C or Oct_T block, but instead the $[M+Na]^+$ of either **2-49** or **2-50**. The sodium salt, sodium adduct molecular ion ($[M+2Na-H]^+$) for **2-49** or **2-50** may have been observed at *m/z* 701 and a dehydration $[M+Na-H_2O]^+$ was consistent with the peak at *m/z* 661.

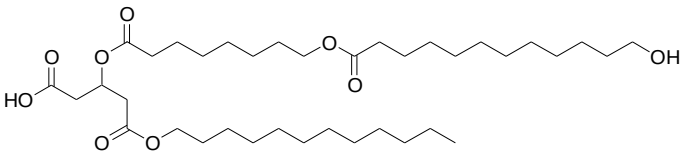

$G12_H$-Oct_C-Dod_T

2-49

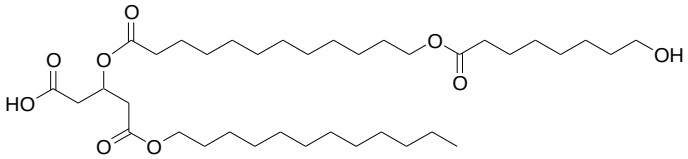

$G12_H$-Dod_C-Oct_T

2-50

In the MS, there appeared to be no evidence of the deletion sequence where a Dod_c or Oct_T/Oct_C unit was missing ($[M+Na]^+$ ion at *m/z* 623 and 567, respectively). Therefore, based on these two absences, the coupling of the Dod and Oct building block to $G12_T$ appeared to be efficient.

The multiplet at about 5.5 ppm in the ^{1}H NMR spectrum of **2-48** (Figure 2-49) signifies that the ester derived from the secondary alcohol survived the acidic-cleavage from the resin. If the bond is cleaved during the acid-cleavage stage, then this resonance shifts upfield to about 4.5 ppm. With the ^{1}H NMR spectrum for this sample, unfortunately the acid proton resonance occurred in the same region as the methine and

therefore the area was integrated to 2.00. This may be a slight overestimate because normally the exchanging acid proton does not always have an exact integration of one due to water.

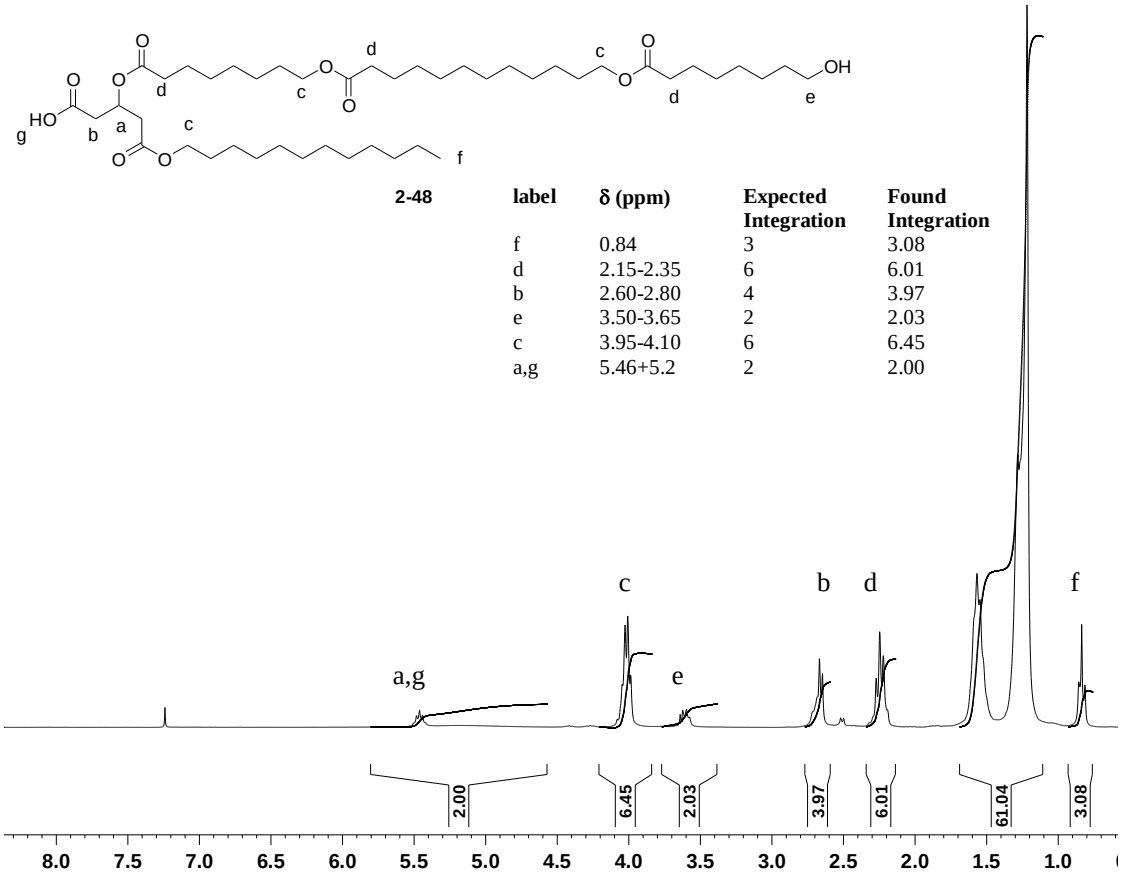

Figure 2-49. ^{1}H NMR spectrum of **2-48** in $CDCl_3$

Almost all the proton integrations are as expected except for H_c. Since the integration for H_d was at the expected value (6.0), then the increase in the H_c integration cannot be a contribution from deletion sequence (otherwise H_d would also decrease) nor can it be from an addition sequence. Addition sequences were not observed in the MS, but deletion sequences were (e.g. **2-49** or **2-50**). Although the contribution by the deletion sequences were minute because the H_d resonance was not greatly affected.

Therefore to account for the increase in the H_c signal, perhaps the alcohol H resonance may be in this region. The integrity of **2-48** was therefore assumed to be >95%

2.3 Summary of SPOS Methodology

SPOS is a promising method for quickly generating a large library of ion channel-forming compounds. The data demonstrated that the building blocks can be coupled fairly efficiently to generate dimer, trimers and tetramers. The crude products from the cleavage of the resin were purified by a gel filtration column (LH-20).

The crude products cleaved from the solid support would have two types of contaminants that should be removed. First, there could be small molecules such as residual TBAF, DIC byproducts, and solvents. The second type of contaminant are molecules which are shorter (known as deletion sequences) and/or longer (known as addition sequences) than the target molecule. Generally, the deletion sequence contaminants for dimeric and trimeric products had molecular weights which are about half the molecular weights for these products. For example, dimer contaminants can exist in a trimeric product if inadequate coupling/deprotection occurs. The contaminants have a mass of roughly 60% of the trimer. For larger compounds such as tetramers and pentamers, the difference in molecular weights of the contaminants of each of these compounds is much less. Tetrameric contaminants can be present in a pentameric product and the difference in molecular weight can only be about 25% so good separation by gel filtration is not be expected. Following purification, the ^{1}H NMR spectrum of the purified product showed that small molecule contaminants such as residual TBAF, BPAA and THP were not present.

Addition sequences tended to be more abundant than deletion sequences. It was suspected that the addition sequences developed because of a very small percentage of the hydroxy acid in the building block starting material.

The method to characterize SPOS compounds used mass spectrometry to determine if addition and deletion sequences were present. Deletion sequences are rarely observed directly in the MS but most products tend to have dimeric and trimeric lactones which contaminate the product. The lactones are the result of deletion sequences which are missing a unit to block off a primary alcohol. ^{1}H NMR spectroscopy for quantifying the approximate amount of these impurities.

Whether deletions or additions are present, the efficiency of coupling in all SPOS product cases are less than 100%. The primary alcohol is proposed to lactonize under the product resin-cleavage conditions. The calculated proportions of contaminants can be up to 10% for a dimer or 14% for a tetramer (assuming $G12_T$ is one of the units) if the building block was comprised of 5% hydroxy acid.

The interest is in the generation of ion channel candidates using SPOS methodologies. The presence of the addition and deletion sequences should not mask the potential transport activity of a compound.

Chapter 3 Directed-Library Synthesis of Ion Channels

In Chapter 2, the methodology for making the dimeric, trimeric and tetrameric oligoester compounds was developed. The building blocks used to make these oligoester compounds were classified into two types: head group and core. Within each type of building block the alkyl length varied and by incorporating different combinations of these building blocks, it is possible to generate structures which have different lengths and therefore lipophilicities. The advantage of SPOS is that once these building blocks are defined, various combinations of the building blocks can be used to generate a library of compounds. The purpose in generating a selection of compounds with permutations in the structure is to explore the relationship of structure to activity of these ion channel-forming compounds.

In order to span the membrane bilayer for ion channel activity with the set of building blocks described, a tetrameric or pentameric product is needed. Using a combinatorial approach, with nine building blocks in hand there are 9^4 = 6561 possibilities for tetrameric products. Therefore, SPOS products must be tailored to address certain issues. The goal of this chapter is to generate tetrameric and pentameric oligoester compounds to address structure-activity questions. Therefore a "directed-library" approach is used to decide on tetrameric and pentameric targets rather than randomly generating a large number of possible permutations. These oligoester compounds are only made once to resemble a true library synthesis. The particular structural questions that need to be addressed in the relationship to transport activities are: 1) What effects are observed if the lipophilic tail on the head group is varied? 2) What

effect does the number of esters have on the activity? 3) Does varying the core length affect the activity? 4) What happens if lipophilic groups are placed on both sides of a core? Hence, in this chapter, these questions are addressed through SPOS of specifically selected tetrameric and pentameric compounds; in Chapter 4, the ion transport activity of these compounds are described.

3.1 Synthesis of Tetramers – Variation in Lipophilic Tail Length

The extent of lipophilicity will affect the ability of a compound to partition into a membrane. To examine the optimum lipophilic tail length on the head-group (i.e. $G12_T$), the core length may be kept constant with units of Oct_H-Dod_C-Oct_T (**2-39**) and appending one of the four lipophilic head groups G10 (**2-2**), G12 (**2-3**), G14 (**2-4**), or G16 (**2-5**). The tetramers generated are **3-1**, **2-27**, **3-2**, and **3-3**. Tetramer **2-27** was discussed in the previous chapter. The additional tetramers were characterized by ^{1}H, ^{13}C NMR spectroscopy and MS.

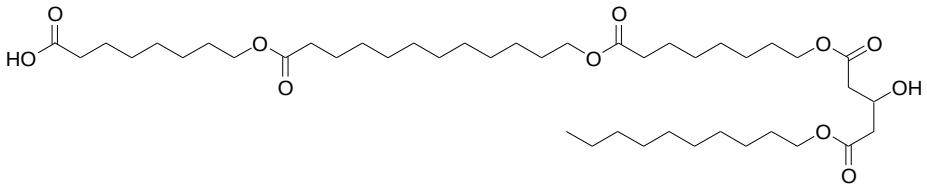

3-1

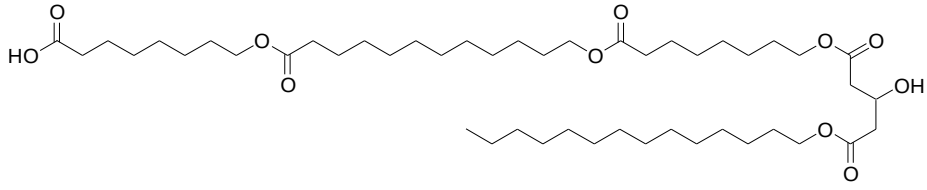

3-2

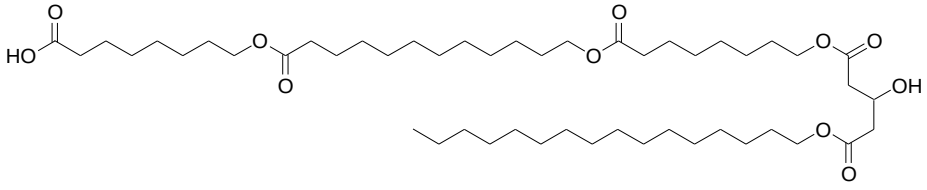

3-3

The $[M+Na]^+$ ion for **3-1** was at *m/z* 793.5 (Figure 3-1). Also observed in the MS were some of the higher mass contaminants such as the *m/z* 991.6 and 935 which were consistent with the $[M+Dod_C+Na]^+$ and $[M+Oct_C+Na]^+$ of **3-1** (an additional Dod_C and Oct_C block, respectively). Henceforth structures of these addition sequences will not be drawn (to conserve space) and they will be represented as "$[M+Na+Oct_C]^+$" for the sodium salt of the molecular ion with the additional Oct_C unit and "$[M+Na+Dod_C]^+$" for the sodium salt of the molecular ion with the additional Dod_C unit. There was no evidence of the deletion sequences lacking a Dod_C or Oct_C block ($[M-Dod_C+Na]^+$ = 608.5, $[M-Oct_C+Na]^+$ = 664.5) in the MS of **3-1**.

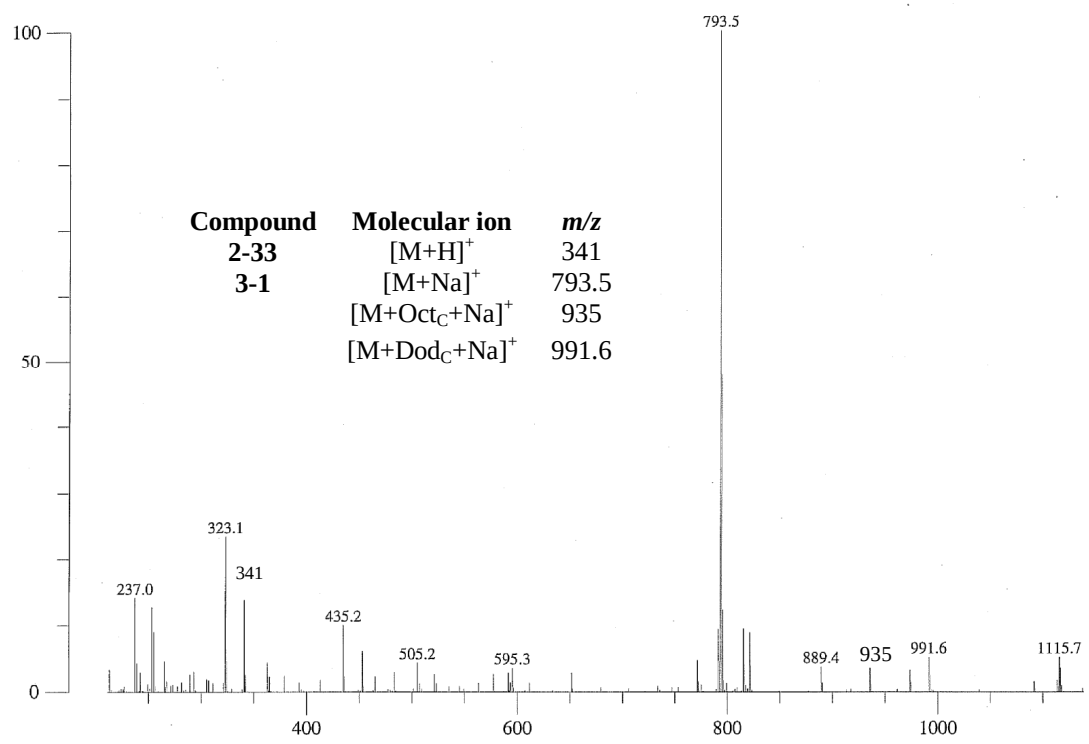

Figure 3-1. LSIMS of **3-1**. 100% = 7566 mV.

The ^1H NMR spectrum of **3-1** (Figure 3-2) does show a few impurities are present (little peaks between 2.5 and 3). Using the integration check from H_a and H_b, it was

found that there was at least 2% error in the integrations. The integral of the expected H_c and H_d resonances are on average ~7% higher than expected from theory. Assuming the impurities are solely additions of either Oct_C or Dod_C, then at 7% difference the integrity of **3-1** can be at least 94% pure. There is evidence in the MS that the lactone **2-33** is present in the product, so assuming this **2-33** is the major contaminant, then the integrity of **3-1** can be at least 88% pure.

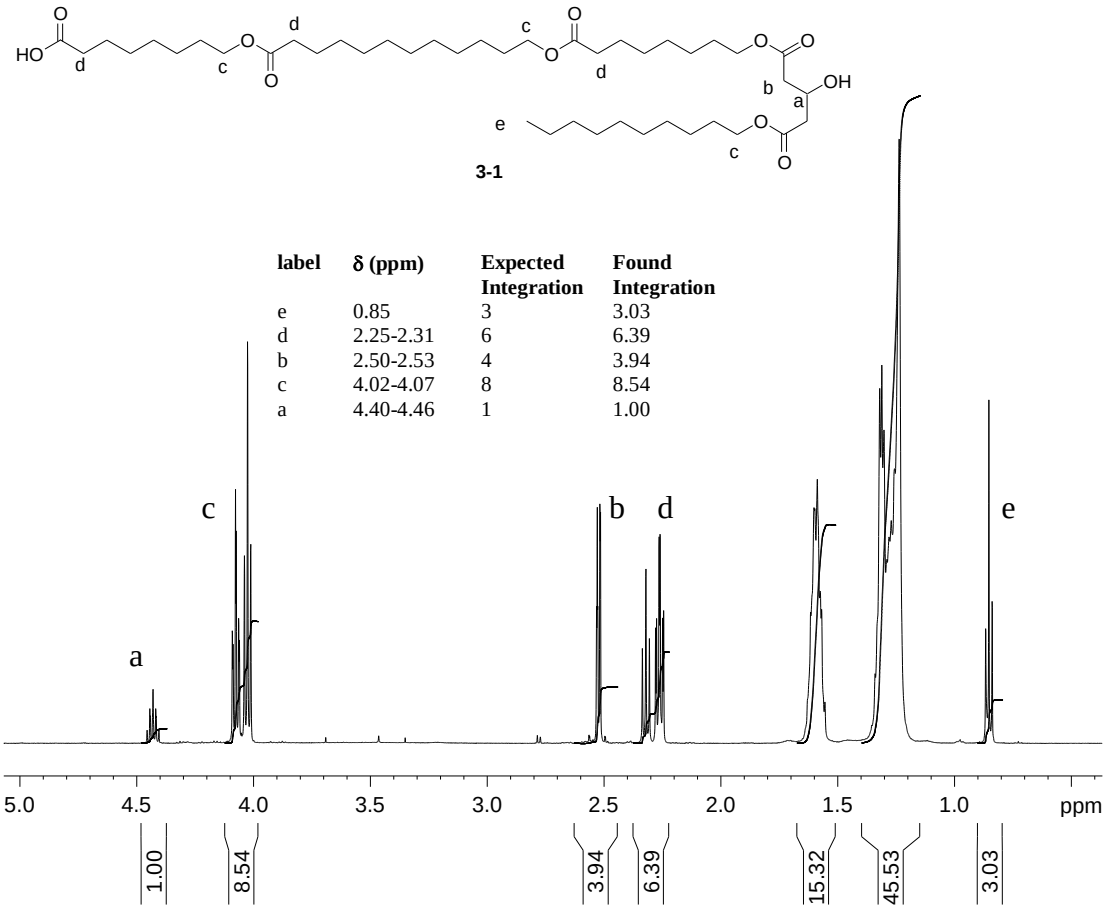

Figure 3-2. ^1H NMR spectrum of **3-1** in $CDCl_3$

For **3-2,** the $[M+Na]^+$ and $[M+2Na-H]^+$ ions were observed at *m/z* 849.6 and 871.6 (Figure 3-3). The other major peaks can be attributed to the sodium adduct of the

sodium salt of **3-2** observed at *m/z* 871.6. The peak at *m/z* 707.5 could be a loss of Oct_C ($[M\text{-}Oct_C+Na]^+$) while *m/z* 651.4 could be a loss of Dod_C ($[M\text{-}Dod_C+Na]^+$).

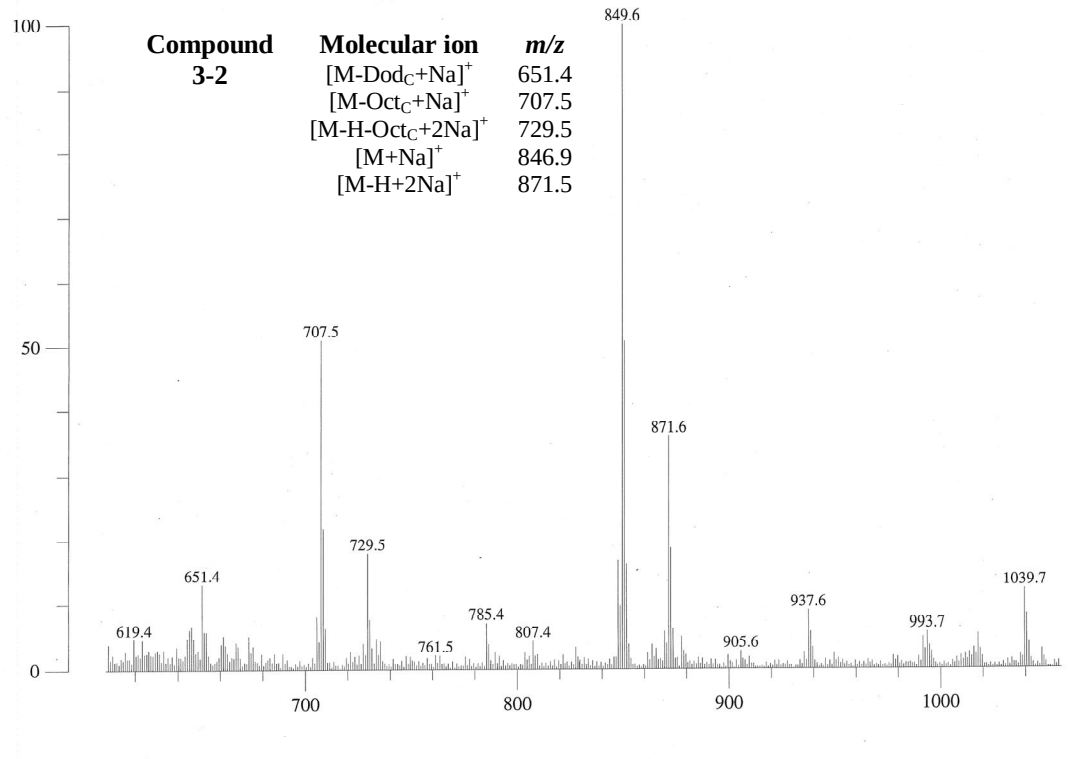

Figure 3-3. LSIMS of **3-2**. 100% = 12511 mV.

The ^1H NMR spectrum of **3-2** (Figure 3-4) showed an under-integration of the H_c and H_d when the usual H_a was set to 1 which may be a sign that the acid proton resonance may be under the H_a signal as well. If the integrations were recalculated and H_b was set to 4, then the H_c and H_d are over-integrated just like in all the other tetramer cases. The excess integration of H_c and H_d are 3% each and assuming this came from addition sequences because of the over integration, that would imply that **3-2** had only about 2% impurity of the addition sequences.

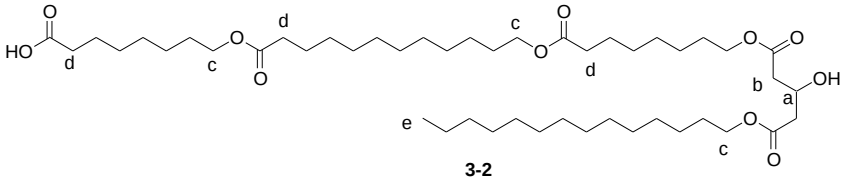

3-2

label	δ (ppm)	Expected Integration	Found Integration	Recalculated Integration
e	0.85	3	2.91	3.06
d	2.25-2.31	6	5.89	6.18
b	2.50-2.53	4	3.81	4.00
c	4.02-4.07	8	7.87	8.26
a	4.40-4.46	1	1.00	-

Figure 3-4. ^{1}H NMR spectrum of **3-2** in $CDCl_3$

The MS of **3-3** showed a peak at *m/z* 877.6 consistent with the $[M+Na]^+$ ion (Figure 3-5). The fragment of **3-3** without an Oct_C unit has a $[M-Oct_C+Na]^+$ ion consistent with the peak at *m/z* 735.5 in the MS. The peak at *m/z* 1019.6 is consistent with the expected $[M+Oct_C+Na]^+$ ion of the **3-3** containing an extra Oct_C unit. The peak at *m/z* 679.5 is consistent with the deletion sequence $[M-Dod_C+Na]^+$ ion. The addition sequence with Dod $[M+Dod_C+Na]^+$ was not observed (most likely due to low relative intensity).

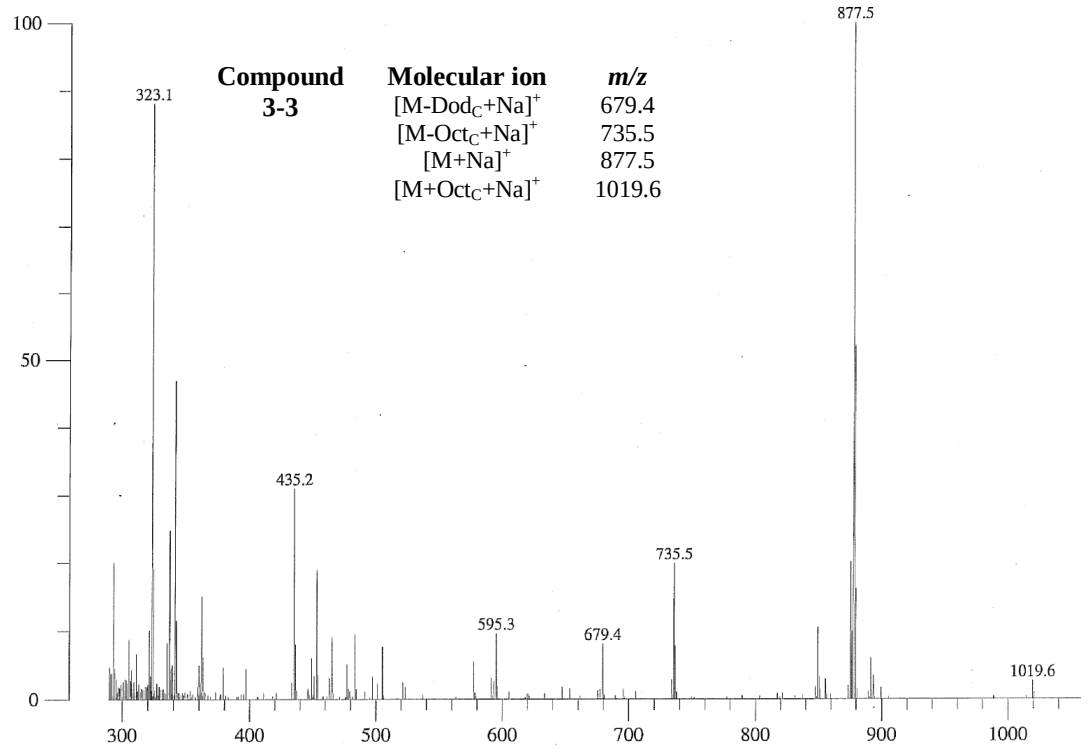

Figure 3-5. LSIMS of **3-3**. 100% = 2471 mV.

Integration of the ^{1}H NMR spectrum of **3-3** (Figure 3-6) showed the expected H_a:H_b proton ratio (H_a:H_b, 1.00:4.00) while the H_c and H_d are over integrated by about 11% and 16% each. Deletion sequences are apparent (at least the sequences missing the Dod_C unit) but in minute contribution because the proton integrations are greater than expected. The deletion sequence of missing a Dod_C would be the result of incomplete coupling of Dod which could either be due to inefficient THP deprotection or inefficient coupling with DIC/DMAP. From the MS, there is an unlabelled peak at *m/z* 483, which has previously been proposed as the cyclic trimer **2-34** in other oligoester tetramers. The over-integration of H_c and H_d can either be from the addition sequence of one Oct_C unit or the presence of **2-34**. If the addition sequence was the dominant contaminant then the integrity of **3-3** was about 89% whereas if **2-34** was the contaminant then the integrity dropped to about 84%.

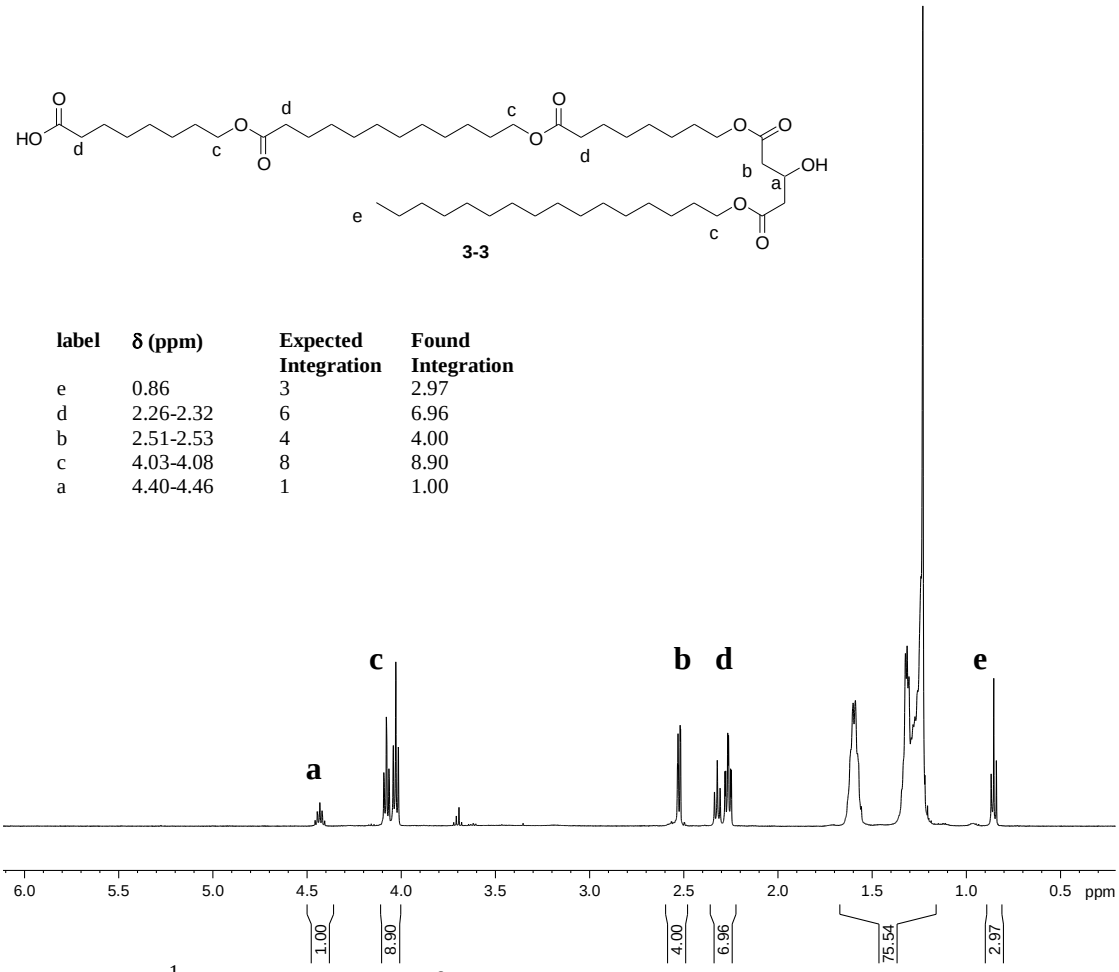

label	δ (ppm)	Expected Integration	Found Integration
e	0.86	3	2.97
d	2.26-2.32	6	6.96
b	2.51-2.53	4	4.00
c	4.03-4.08	8	8.90
a	4.40-4.46	1	1.00

Figure 3-6. ^{1}H NMR spectrum of **3-3** in $CDCl_3$.

The consequence of a contamination of 11% by the addition sequence (additional Oct to **3-3**) would imply that there is about a 5% contamination by the hydroxy acid in the Oct sample, assuming that the Dod sample is pure. This is an appropriate assumption and model because 5% is about the NMR instrumental precision so the hydroxy acid may not be detected in the ^{1}H NMR spectrum of the Oct building block. In contrast, if the lactone **2-34** were present, then the large amount contamination of 16% would imply that the overall coupling efficiency of G16 is only 84%. An overall coupling efficiency of 84% is unusually low considering the similarity of the G12 and G16 building blocks. The G12 building block was optimized to couple fairly efficiently so it was believed that

the conditions would have also applied to the other glutaric acid derivatives. The inconsistent ability to couple the G12 building block will be discussed in the next section. Therefore it is believed that the G16 building block was not coupled efficiently and therefore the major contaminant is **2-34**.

3.2 Synthesis of Tetramers – Variation in Location of Dod_C Unit

Considering the structure of **2-27**, it is possible to move the core Dod_C unit to two other positions to generate a total of three isomeric compounds (**2-27**, **2-36,** and **3-4**). The testing of these compounds in a transport assay determines whether there are significant differences in activity by modifying the core lipophilic component/ester location. As a unit, the Dod block is expected to be more lipophilic than an Oct block. However, these three isomers have the same core length and therefore it is expect that there may not be a difference in transport activity between these compounds. The consequences of these structural changes are probed by isomers **2-27**, **2-36** and **3-4**.

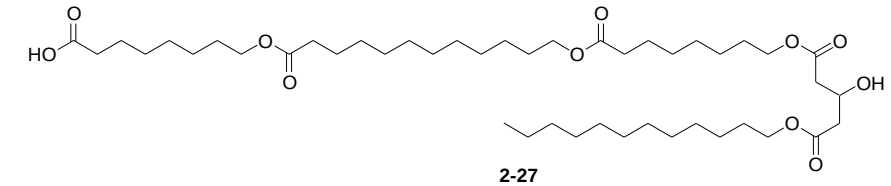

2-27

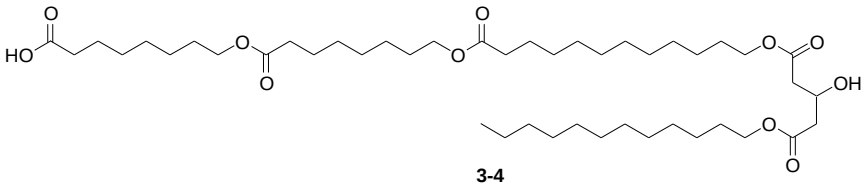

3-4

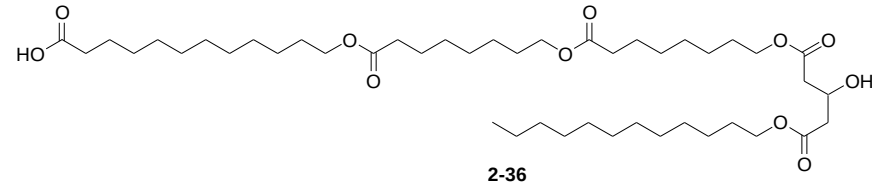

2-36

Both **3-4** and **2-36** were characterized by ^{1}H and ^{13}C NMR spectroscopy and MS. Compounds **3-4** and **2-36** were made in 1% and 3% recovery. These yields were unusually low relative to the amount of resin that was used. The standard SPOS protocol used for the synthesis of **2-36** and **3-4** suggested that the desired SPOS products were collected from fraction 8-10 from the gel filtration. Perhaps in these samples, the product was not recovered in high yield because it was either in an earlier or later fraction.

The MS for **3-4** (Figure 3-7) showed peak at *m/z* 821.6 which is consistent with the $[M+Na]^+$ ion. The MS showed products of higher mass (probably a combination of addition sequences $[M+Oct_C+Na]^+$ and $[M+Dod_C+Na]^+$ but because the observed ion intensities were low, these higher molecular weights may also be from the background. It was interesting to note the peak at *m/z* 877.5 in the MS of **3-4** because this was consistent with the product when there are two Dod_C (or one each of Dod_C and Dod_H) and an Oct_C or Oct_H in the structure. A peak at *m/z* 679.4 was consistent with the $[M-Oct_C+Na]^+$ ion of **3-4**.

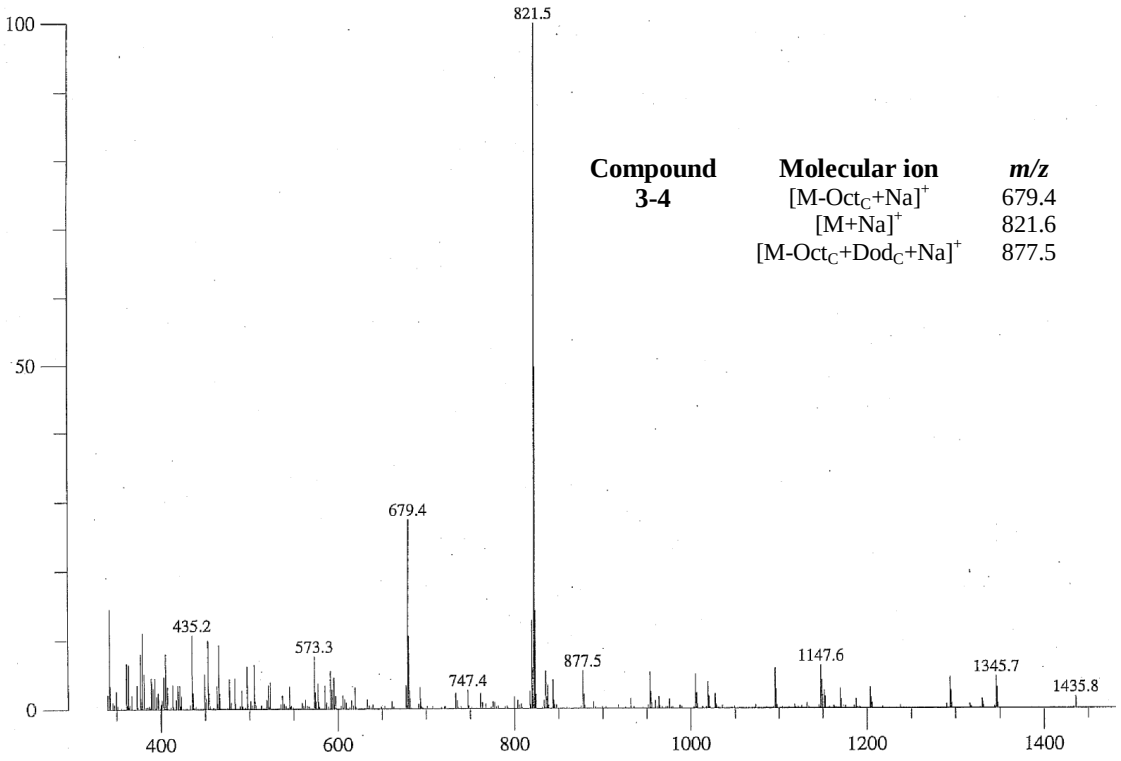

Figure 3-7. LSIMS **3-4.** 100% = 3842 mV.

The ^{1}H NMR spectrum for **3-4** showed an unusual resonance at about 4.3 ppm (Figure 3-8). This peak was assumed to be the $C\underline{H}_2O_2CF_3$ and was thought to have been the result of the cleavage of one of the core components (Oct_C or Dod_C) or $G12_T$ from the product which would expose a primary alcohol. Alternatively if the G12 coupling did not work efficiently the primary alcohols would remain exposed. In preliminary studies, the TFA cleavage of products terminated in primary alcohols produced TFA-esters; secondary alcohols do not readily do so. Upon treatment of the products on resin with TFA any exposed primary alcohol may esterify. This reaction was common for several oligoester products and the evidence was the triplet at about 4.3 ppm. The proton integrations show a large overestimate for H_c and H_d while the integration check showed only a 1% error. The excess integration implied that the contaminant would be either **3-5** or **3-6.**

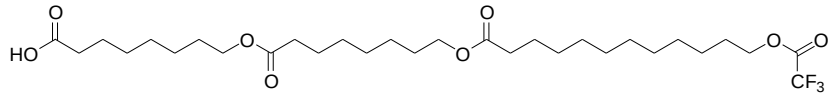

3-5

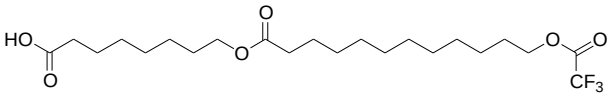

3-6

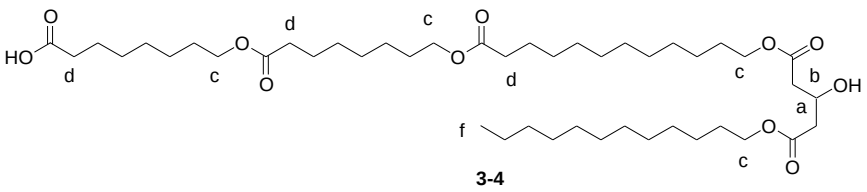

3-4

label	δ (ppm)	Expected Integration	Found Integration
f	0.86	3	4.06
d	2.26-2.33	6	7.76
b	2.50-2.57	4	3.96
c	4.03-4.08	8	9.46
a	4.40-4.46	1	1.00

Figure 3-8. ^{1}H NMR spectrum of **3-4** in $CDCl_3$.

The MS did not confirm the presence of these two proposed contaminants because of the poor signal-to-noise and no usable data was collected below *m/z* 350 (**3-4**). A calculation using the triplet at 4.3 ppm (integration = 0.58, 2H) to the quintet at 4.4 ppm

(integration of 1, 1H) showed that there was at least 29% contamination by the TFA-ester. Assuming that the contaminant was **3-5**, then the over-integrations of H_c and H_d showed that the contamination was about 36% and 29% according to the H_c and H_d signal, respectively.

The MS for **2-36** (Figure 3-9) showed a peak at *m/z* 821.6 which is consistent with the $[M+Na]^+$ ion. Higher mass fragments were observed which may have been the $[M+Dod+Na]^+$ and $[M+Oct+Na]^+$ ions but similar to the MS of **3-4** the observed ion intensities were low so these higher molecular weights may also be from the background. The peak at *m/z* 877.5 in the MS of **2-36** was also in the **3-4** MS and it was consistent with the product when there are two Dod_C (or one each of Dod_C and Dod_H) and an Oct_C or Oct_H in the structure. A loss of Oct_C in the **2-36** structure would lead to a $[M-Oct_C+Na]^+$ ion as evident with the peak at *m/z* 679.4. For **2-36**, the missing Oct_C unit was most likely a deletion sequence rather than a product fragmentation during the collection of MS data because the Oct_C unit is in the building block B or C core position of the product structure.

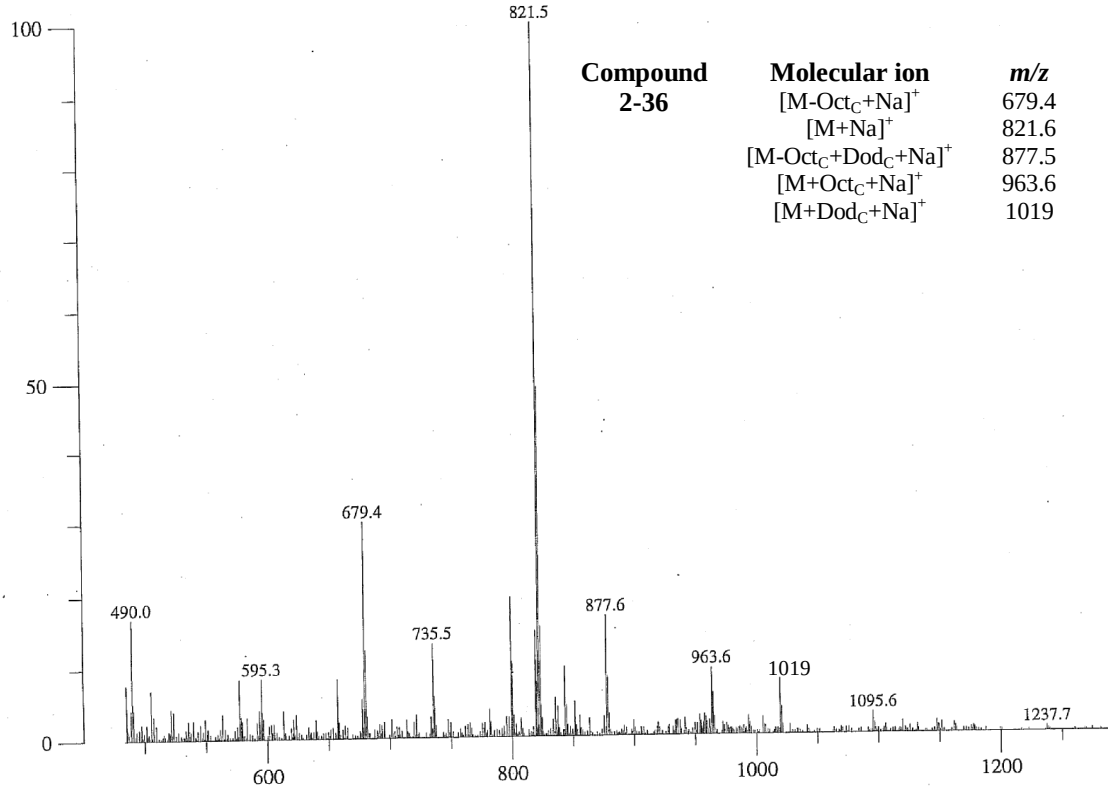

Figure 3-9. LSIMS for **2-36**. 100% = 3244 mV.

Similar to **3-4**, the ^{1}H NMR spectrum of **2-36** (Figure 3-10) showed the same TFA-ester contaminant and like **3-4**, this was not confirmed by the MS. But in this particular sample, the TFA-ester contaminant accounted for over 40% of the sample (using the TFA-ester triplet and the G12$_T$ methine integrations and not accounting for the errors in the integration – 4%). The broad peak under the H$_d$ resonances could be the rapid exchange of the alcohol proton.

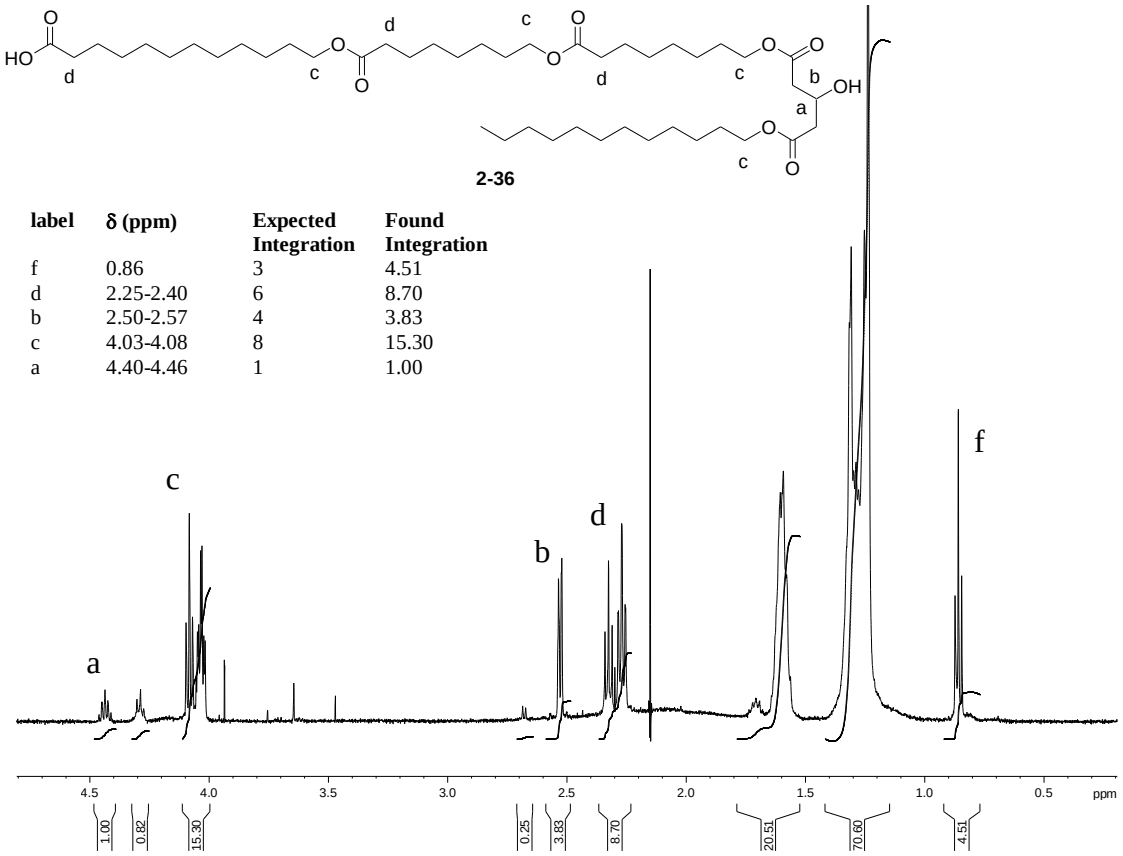

Figure 3-10. ^{1}H NMR spectrum of **2-36** in $CDCl_3$.

Many of the synthesized compounds discussed in this section show a range of integrities. Evidence of an additional Oct_C unit to the target molecules is apparent in many of the MS of the compounds. There is not enough evidence to support the presence of dimeric and/or trimeric lactones. Many of the deletions which are missing a $G12_T$ unit showed that the remaining primary alcohol of Oct_T was converted to the trifluoroacetate. In these examples, where there is a lower number of $G12_T$, units it is difficult to tell whether it was incomplete G12 coupling or if the $G12_T$ unit was cleaved during product cleavage from resin. Examining the crude ^{1}H NMR spectrum does not reveal if there is free $G12_H$ in solution because the chemical shifts for all the protons are about the same as the $G12_T$ on the tetrameric product. Since in other samples the missing $G12_T$ unit is not a

prominent issue, then it might be assumed that in the synthesis of **2-36** and **3-4**, the inefficient G12 coupling was to blame (perhaps from water quenching the activated carboxylic acids). In Chapter 4, the effects of the $G12_T$ unit are discussed and its importance for creating an active structure. It was assumed that structures without this unit were not very active ion channels.

3.3 Synthesis of Tetramers – Variation in Core Length

The length difference between the Dod and Oct building block is four methylene groups. Therefore, in keeping the core comprised of three building blocks, a combination of Dod and Oct can be used to generate structures which have from 21 methylene units in the core (**2-38**) and up to 33 methylene units (**3-7**). This series includes compounds **3-8** and **3-9** which both have an intermediate core length of 29 internal methylenes and are constitutional isomers of each other. This series of compounds is interesting because the core length was varied, which may affect how the compounds partition into the bilayer as well as their ability to span a bilayer.

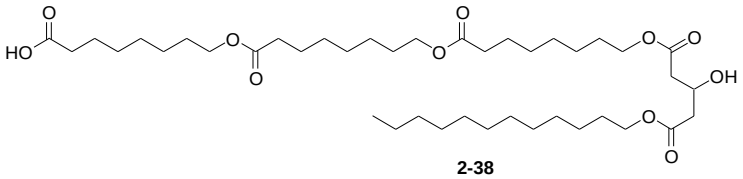

2-38

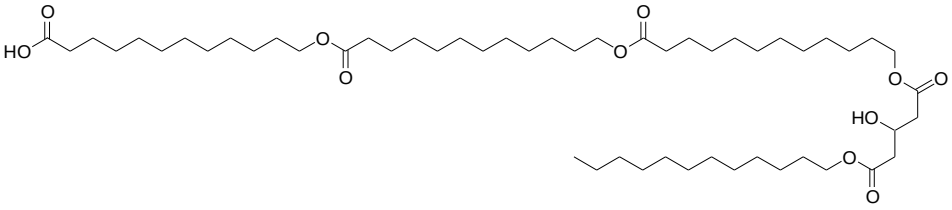

3-7

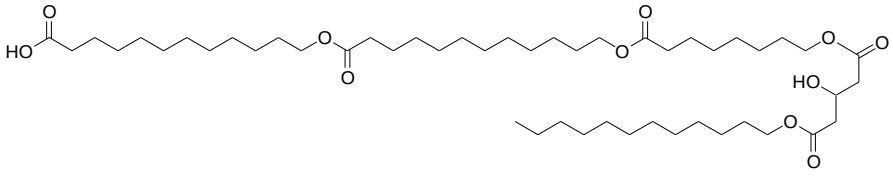

3-8

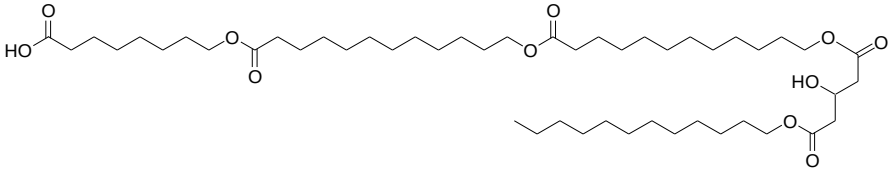

3-9

The ^{1}H and ^{13}C NMR spectra were recorded for all these compounds as well as the MS. The yields for these compounds were rather low: **2-38** (8%), **3-7** (24%), **3-8** (18%), and **3-9** (9%).

From the MS of **2-38**, the peak at *m/z* 765.5 is consistent with the $[M+Na]^+$ ion. (Figure 3-11). In Figure 3-11, the *m/z* 907.7 was consistent with the $[M+Oct_C+Na]^+$ ion of **2-38** while the *m/z* 634.4 may be the $[M-Oct_C+Na]^+$ ion. The MS showed a peaks at *m/z* 539.3 which was consistent with $[M-H]^+$ ion for **3-10**.

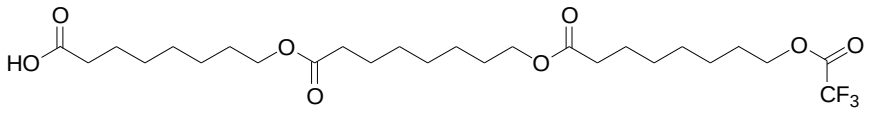

3-10

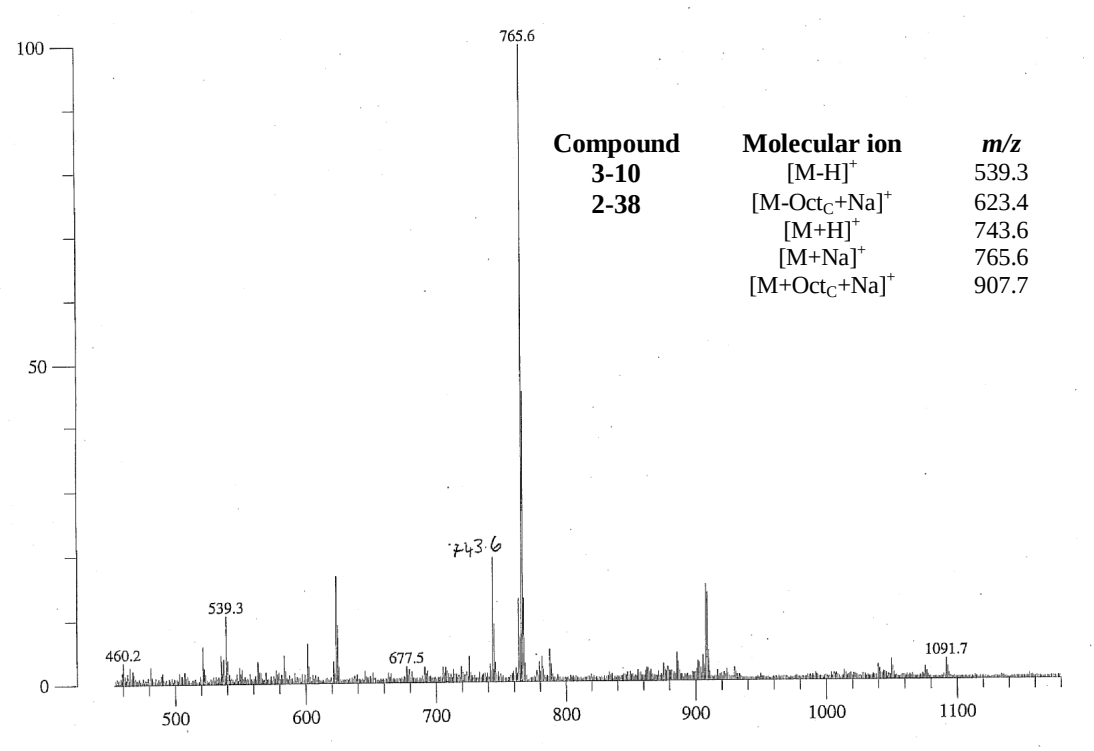

Figure 3-11. LSIMS for **2-38**. 100% = 30196 mV.

Based on the ^{1}H NMR spectrum of **2-38** (Figure 3-12) there was some minor impurity of the TFA-ester in the product (evident by the triplet at 4.3 ppm). The anticipated peak for this TFA-ester ($[M-H]^+$ ion) at *m/z* 539.3 was observed in the MS. The set of doublets at about 2.7 ppm are the methylenes on the $G12_T$ after the esters have cleaved to leave glutaric acid.

Based on the integration of the TFA-ester, there appeared to be a 60% contribution of the product mixture by this component. The H_c and H_d are also over their expected integrations by 35% and 64% but these numbers are the result of having an addition sequence and the **3-10** present. The 64% of H_d may also be affected by the broad peak under the H_d resonance. The TFA-ester contaminant is an unusually high 60% relative to the $G12_T$ unit. If **3-10** was the contaminant at 60%, then 30% in the 35% over-integration of H_c and 60% in the 64% over-integration of H_d can be accounted for.

The remaining 5% and 4% for H_c and H_d might come from the addition sequence of one Oct_C or more likely from the integration precision

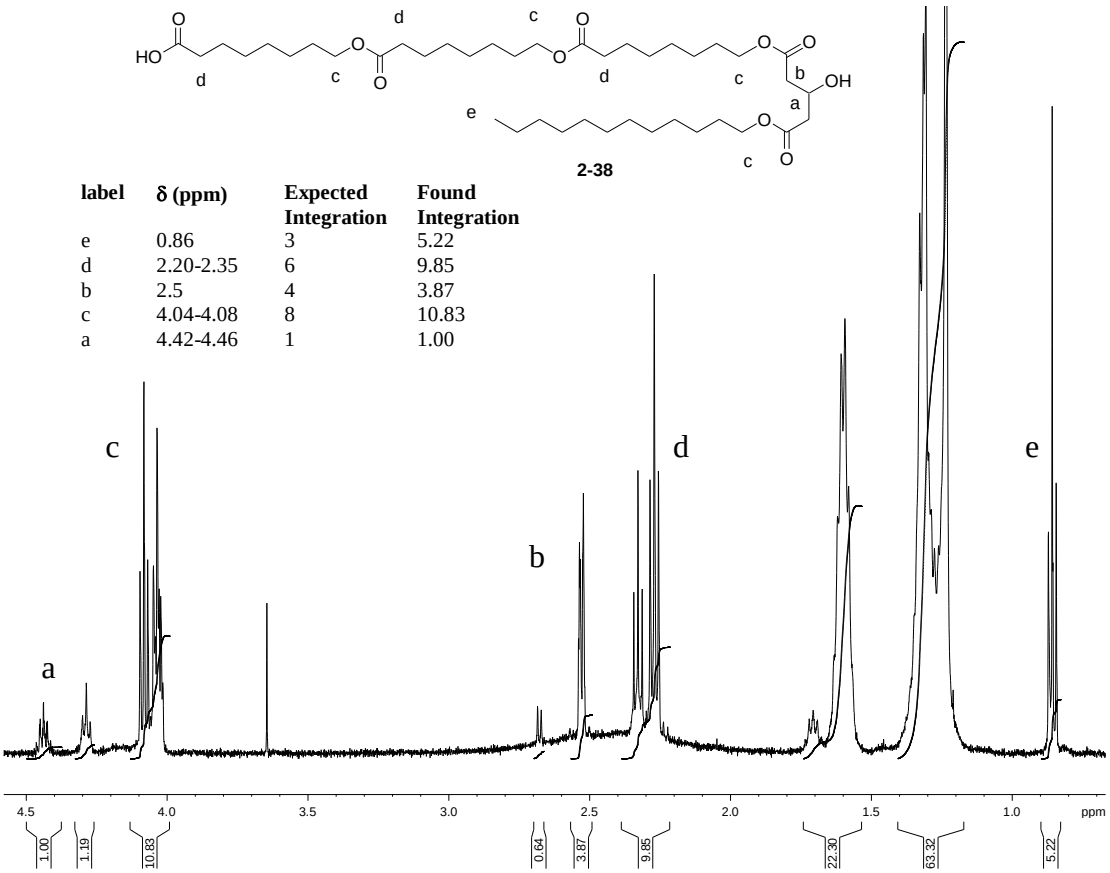

Figure 3-12. ^{1}H NMR spectrum of **2-38** in $CDCl_3$.

From previous syntheses, the addition sequences of an extra Oct_C was believed to be from impure starting material with the free hydroxy acid. There are three couplings of Oct in the synthesis of **2-38**, so it is expected that the percentage of Oct_C contamination would be more than the compounds with a core of Oct_H-Dod_C-Oct_C. Assuming that there was 5% contamination by the hydroxy acid, then in a **2-38** product mixture 86% of the composition is the anticipated product while 13.5% is the product with an additional Oct_C unit. The other 0.5% would come from **2-38** with two Oct_C units. As the contaminant with the tetrameric core was built, it is probable that the SPOS

limitation of how long the product can be before coupling becomes inefficient has been reached. In such a case, the final $G12_T$ cannot be appended efficiently and there can be Oct_H-Oct_C-Oct_C-Oct_T/Oct_H-Oct_C-Oct_C-Oct_C-O_2CF_3 as major product contaminants. Under the acidic cleavage conditions the Oct_T of Oct_H-Oct_C-Oct_C-Oct_T may lactonize and yield Oct_H-Oct_C-Oct_T which further reacts with TFA to yield **3-10**.

The longest core of this series of compounds containing a Dod_H and two Dod_C units is **3-7**. From the MS, the peak at *m/z* 933.7 is consistent with the $[M+Na]^+$ ion for **3-7** (Figure 3-13). The extra Dod_C may be observed at *m/*z 1131.8 while the peak at *m/z* 735.5 is consistent with the product missing a Dod_C.

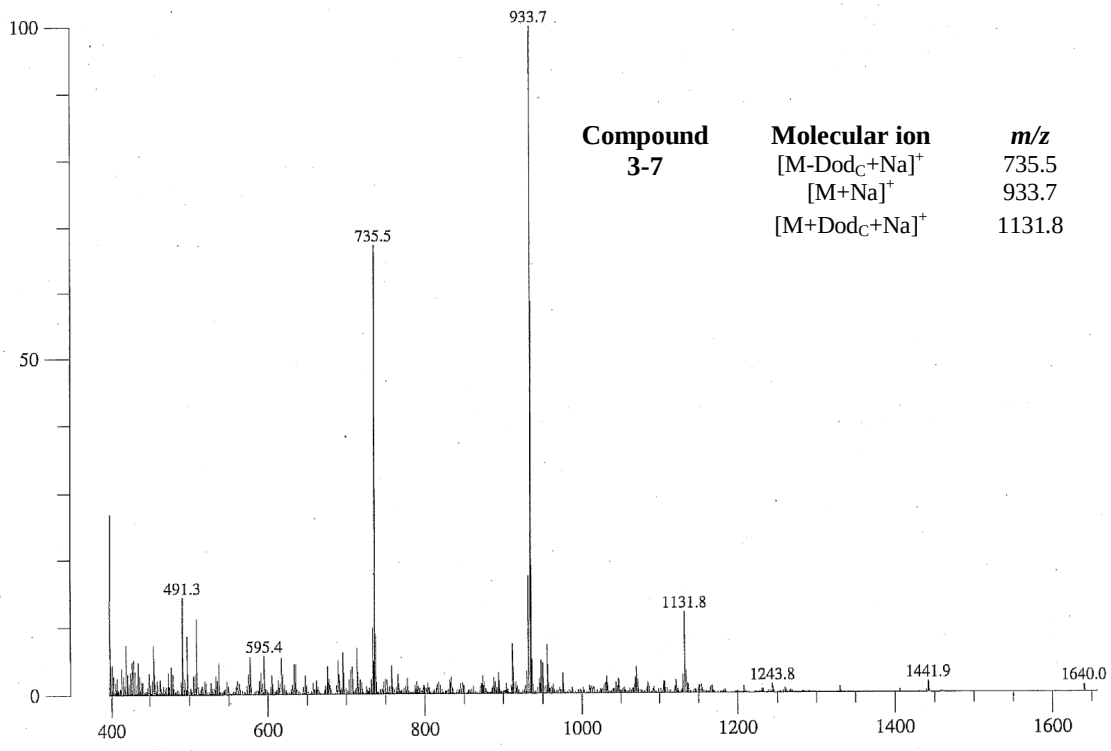

Figure 3-13. LSIMS of **3-7**. 100% = 8343 mV.

The ^1H NMR for **3-7** (Figure 3-14) integrations for H_c and H_d were under-integrated (8% and 10%, respectively) to what were expected. The under-integrations

were a sign that the deletion sequences dominate the product mixture relative to the addition sequences. Although when calculated assuming that the deletion sequence of one missing Dod_C unit, then there was a mol % contamination of about 13% and therefore the integrity was 87%.

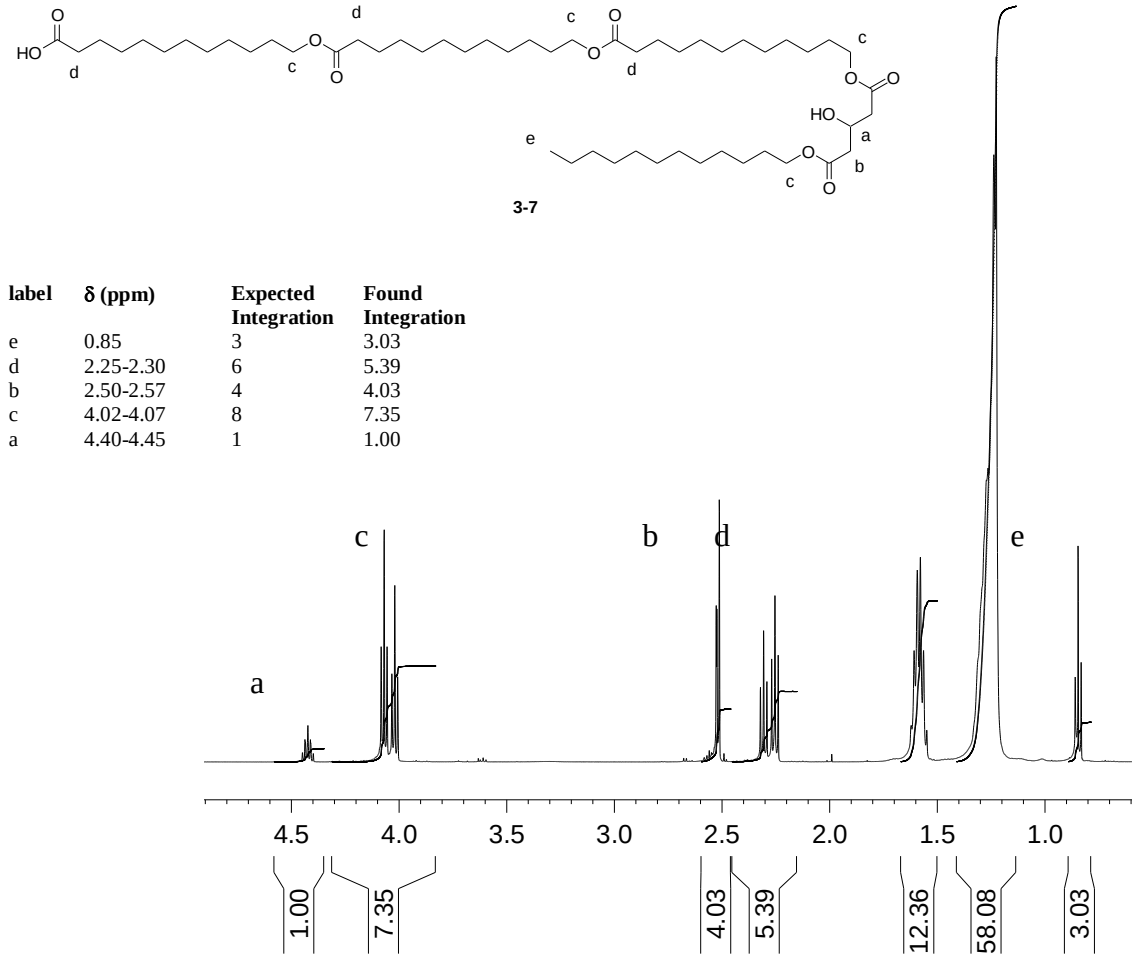

Figure 3-14. ^1H NMR spectrum of **3-7** in $CDCl_3$

Previously an isomeric series was generated where the core is kept constant in length but the location of the Dod_C/Dod_H changed. Similar to that study, in this section one Oct_C unit was replaced by a Dod_C and then the location of the remaining Oct_H was varied to generate **3-8** and **3-9**. From the MS, $[M+Na]^+$ for **3-8** is consistent with the

peak at *m/z* 877.6 (Figure 3-15). The base peak was consistent with $[M\text{-}Oct+Na]^+$ which was most likely a deletion sequence rather than a MS fragmentation because the Oct fragment is sandwiched between a Dod_C and $G12_T$ unit. The peak at *m/z* 679.4 was consistent with the $[M\text{-}Dod+Na]^+$.

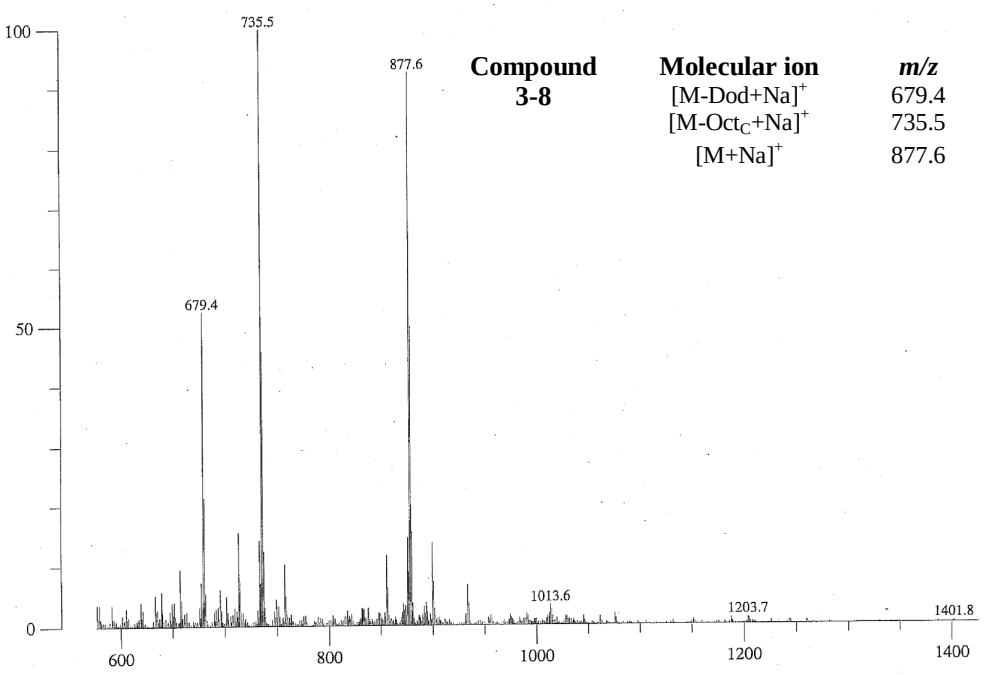

Figure 3-15. LSIMS for **3-8**. 100% = 7684 mV.

Similar to **3-7**, the proton signals (Figure 3-16) for H_c and H_d in **3-8** were under-integrated (6% and 7%, respectively) which also implied the domination of the deletion sequences. From the under-integrations of H_c and H_d, a calculated percentage of the deletion sequence of one Dod unit gave 8% and 11%, respectively.

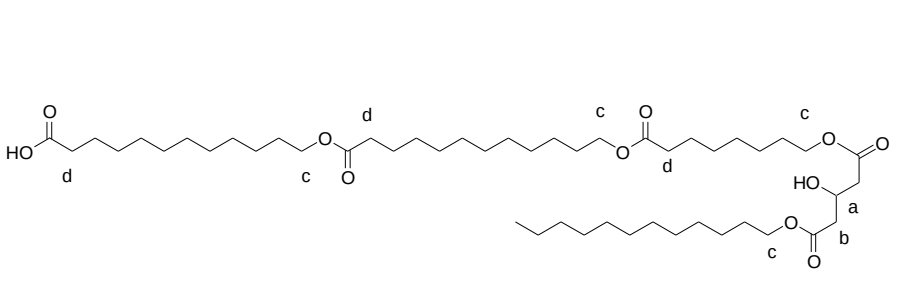

3-8

label	δ (ppm)	Expected Integration	Found Integration
e	0.85	3	3.64
d	2.26-2.32	6	5.58
b	2.51- 2.58	4	3.92
c	4.03-4.08	8	7.49
a	4.40-4.46	1	1.00

Figure 3-16. ^{1}H NMR spectrum of **3-8** in $CDCl_3$

The Oct block in **3-9** is in the Oct_H position compared with **3-8** where the Oct_C was between Dod_C and $G12_T$. From the MS, the peak at *m/z* 877.6 and 855.5 are consistent with $[M+Na]^+$ and $[M+H]^+$ ions for **3-9**, respectively (Figure 3-17). The peak at *m/z* 899.4 was consistent with the sodium adduct of the sodium salt ($[M-H+2Na]^+$ ion). The base peak at *m/z* 735.4 was consistent with the $[M-Oct_H+Na]^+$ ion. Similar to **3-8**, the peak at *m/z* 679.4 was consistent with the deletion sequence $[M-Dod_C+Na]^+$ ion. The

higher molecular weight of *m/z* 933.5 was consistent with the incomplete coupling of Oct_H and the addition of a Dod_C (**3-7**), $[M+Dod_H-Oct_H+Na]^+$).

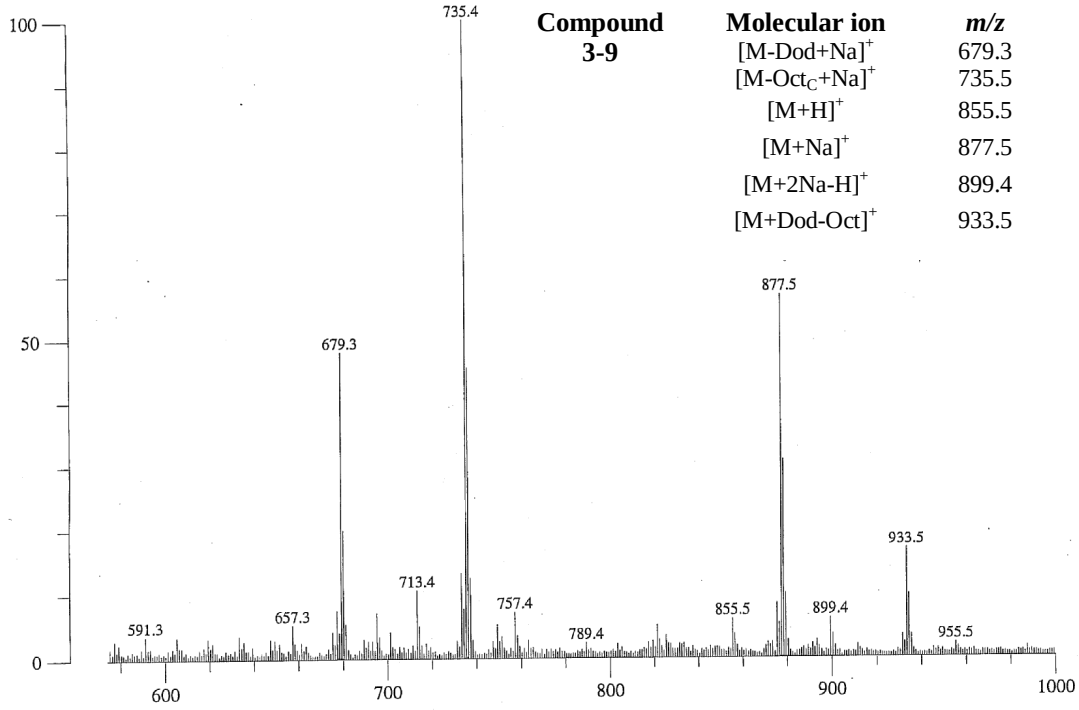

Figure 3-17. LSIMS of **3-9**. 100% = 34216 mV.

The ^1H NMR spectrum (Figure 3-18) for **3-9** showed that the H_c and H_d are integrated to below what was expected (18 and 23%, respectively). Similar to **3-8** and **3-7**, the integration suggested that deletion sequences were dominant. In the case of **3-9**, the mixture was contaminated, containing about 29% deletion sequences. The deletion sequences missing a Dod_C unit suggested inefficient and incompetent coupling of Dod. Such a result could be the effect of this particular synthesis having solvent (THF) with traces of water since the deletions are not as dominant in other compounds. Water will quench the DIC-activated carboxylic acid.

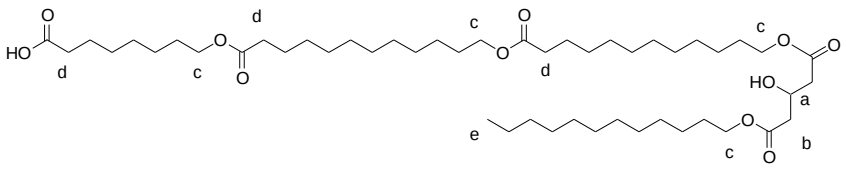

3-9

label	δ (ppm)	Expected Integration	Found Integration
e	0.85	3	3.20
d	2.26- 2.31	6	4.61
b	2.49-2.56	4	3.93
c	4.02-4.07	8	6.56
a	4.40-4.46	1	1.00

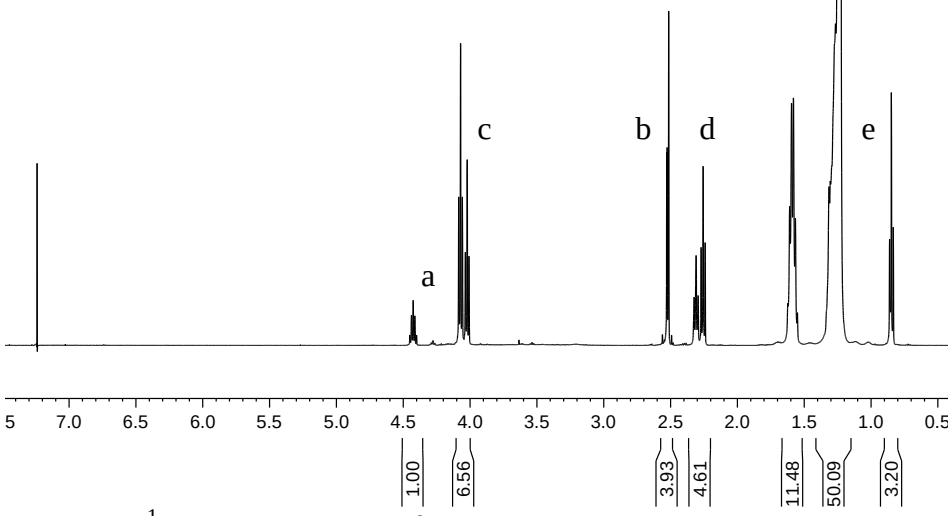

Figure 3-18. ^{1}H NMR spectrum of **3-9** in $CDCl_3$.

3.4 Synthesis of Tetramers – Variation in the Number of Esters

One of the questions that should be faced for the structure-activity analysis is: What effect the number of esters would have on the transport? Building block Hex (**2-17)** could be used to address this issue. When Hex is incorporated into a channel candidate (**3-11)**, it is possible to combine it with Oct such that the resulting product is about the

same length as **2-27** but gives a difference in the number of esters, four versus three relative to **2-27**.

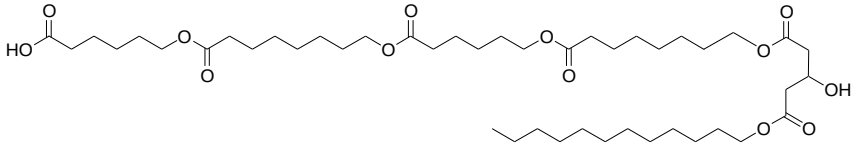

3-11

Pentamer **3-11** was made in 8% yield. Despite the instability of the **2-17** building block, when Hex was incorporated into the channel structure, it was stable to product decomposition (a ^{1}H NMR spectrum of the product was collected after months of dry storage and no change was observed).

From the MS, the *m/z* 851.3 was consistent with the $[M+Na]^+$ ion for **3-11** (Figure 3-19). Addition sequences of another Hex_C or Oct_C unit were consistent with the peaks at *m/z* 965.3 and 993.3, respectively. The peak at *m/z* 823.3 could be the Oct_C deletion sequence of the addition sequence with an extra Hex ($[M+Hex_C-Oct_C+Na]^+$ ion). The peaks at *m/z* 709.2 and 737.2 are consistent with the $[M-Oct_C+Na]^+$ and $[M-Hex_{C/H}+Na]^+$ ions of the deletion sequences of missing a $Oct_{C/H}$ and $Hex_{C/H}$ unit, respectively. The base peak of *m/z* 595.0 was consistent with the structure containing only one Hex_H, Oct_C and $G12_T$ fragment ($[M-Oct_C-Hex_C+Na]^+$ ion).

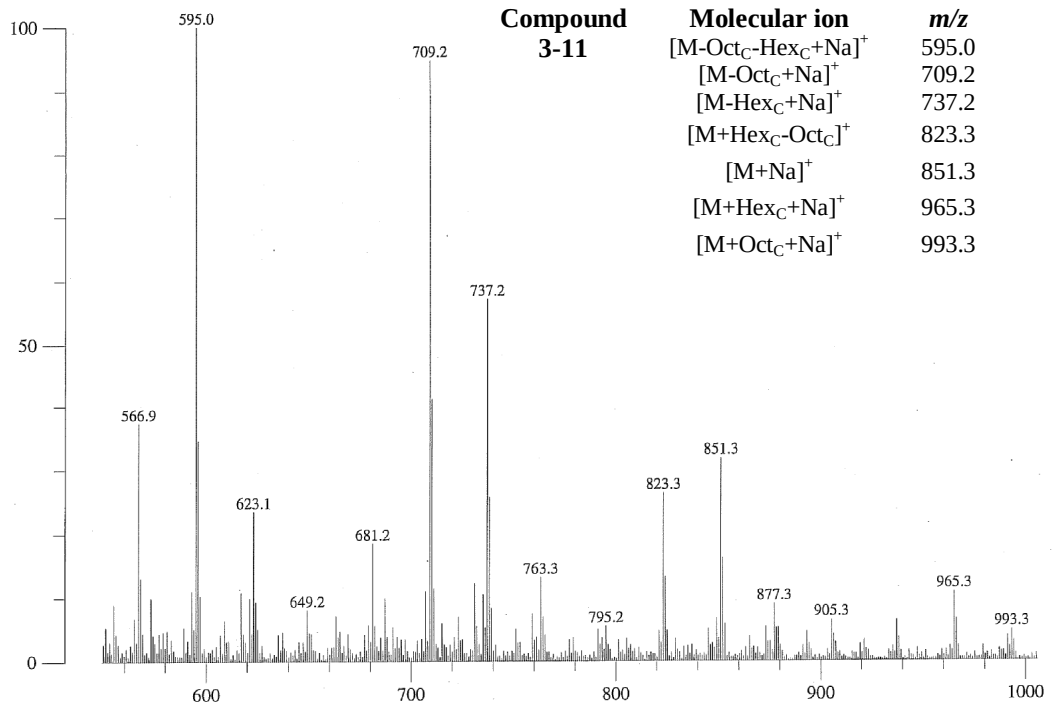

Figure 3-19. LSIMS of **3-11**. 100% = 7242 mV.

The ^{1}H (Figure 3-20) and ^{13}C NMR spectra were recorded for **3-11**. The check for ^{1}H NMR integrations revealed an error of about 4%. The proton resonances between 3.6-3.8 are the primary alcohol protons from the cleavage at some point in the core. There was no evidence in the MS of Hex$_H$-Oct$_C$-Hex$_C$-Oct$_T$ or any fragment thereof; however, if products missing the G12$_T$ component were present, then the expected integrations for H_c and H_d would increase.

The proton integration for H_d was over-integrated by 11%. If the integration of the resonances between 3.6-3.8 were added to the H_c integration, then H_c was over-integrated by 9%. Some of the resonances between 3.6 and 3.8 belong to the C$\underline{H_2}$O of THF while the rest belong to the free primary alcohol of the deletion sequence missing the G12$_T$. The contamination therefore by the deletion sequences without the G12$_T$ or a core building block can account for on average 11% according to H_c and H_d.

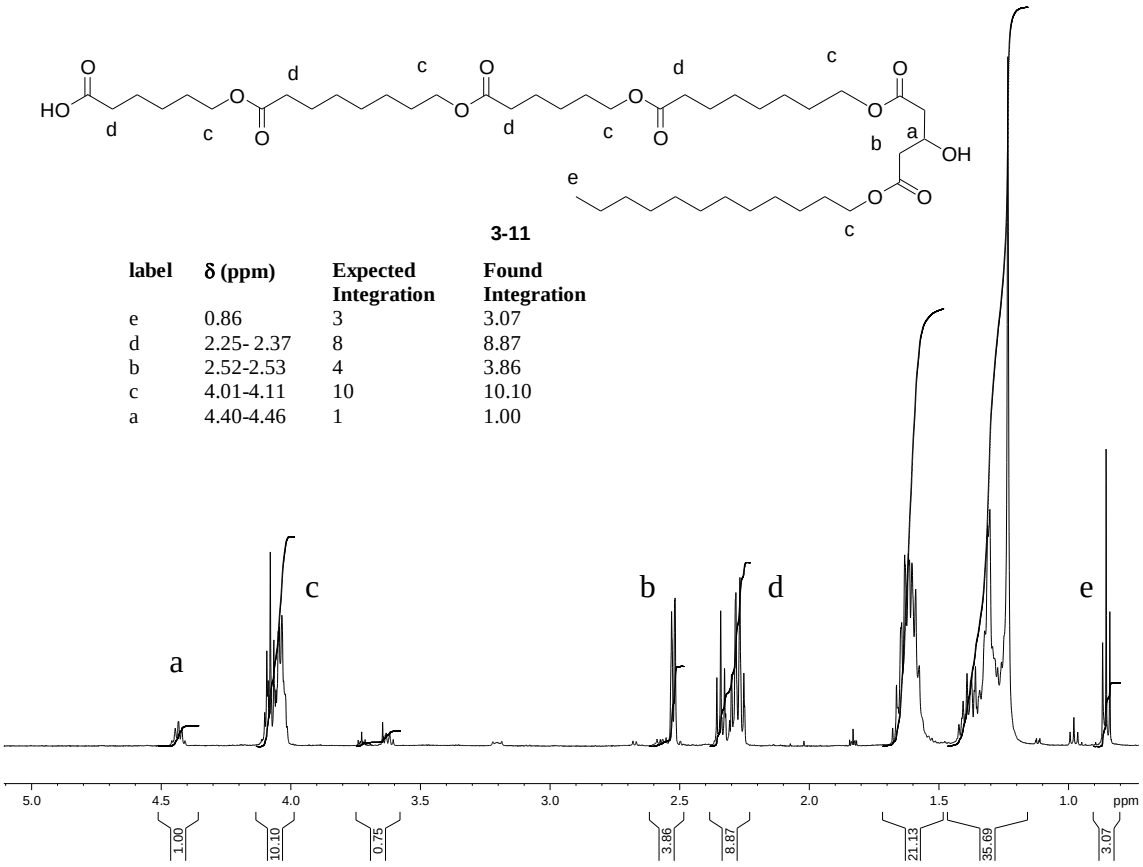

Figure 3-20. ^{1}H NMR of **3-11** in $CDCl_3$

Building blocks such as Lau (**2-13)** and Ole (**2-15)** could be used to replace the glutaric acid building block (G12). Each of the Lau and Ole blocks have one fewer ester functionality than G12, so in keeping the same core as **2-27**, probing the effects of a missing ester in the head group region is possible by using a Lau_T instead of $G12_T$. The building block Ole also lacks an ester relative to G12 but it also has more lipophilic character than the Lau block, making it is more comparable to G16.

The coupling of Lau to an Oct_T unit or loading Ole or Lau to resin took much longer than any of the glutaric acid head groups. Ole was coupled onto Wang resin using the standard coupling conditions, after which the vacant resin sites were capped with

BPAA and the TBDMS deprotection with a TBAF solution. Then the resin was subjected to cleavage conditions to release everything loaded. The ^{1}H NMR spectrum of the crude product is shown in Figure 3-21.

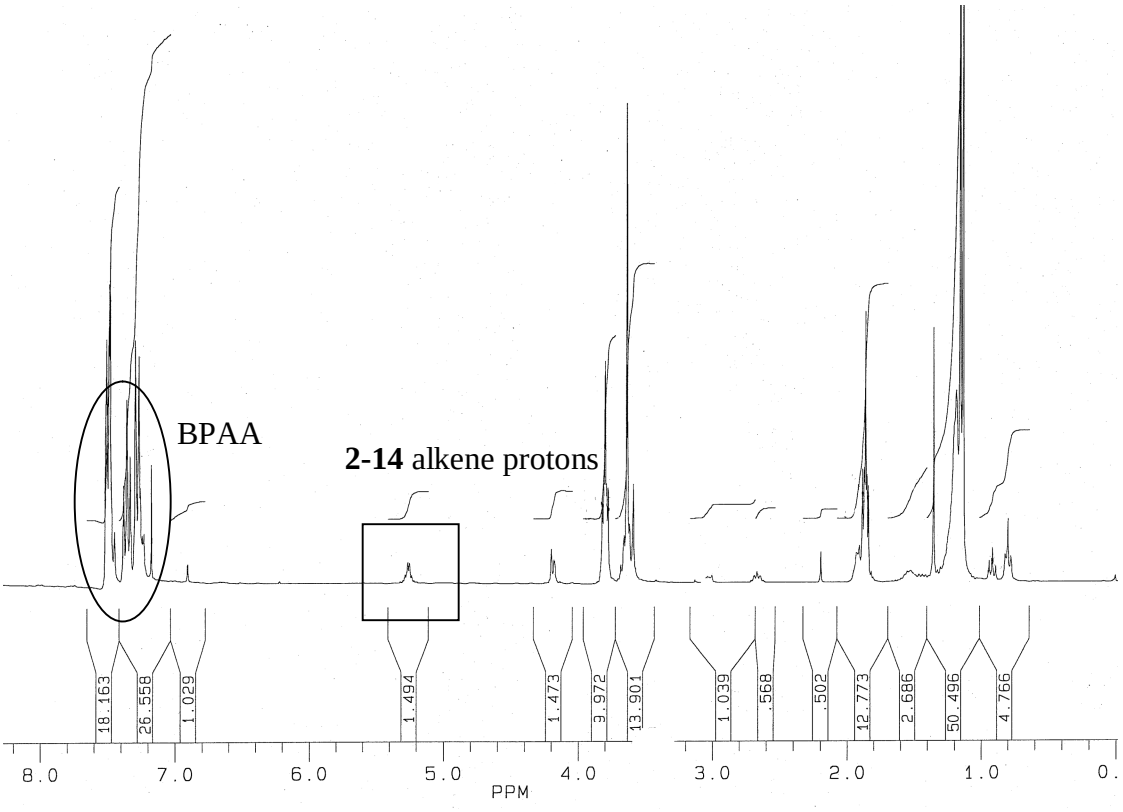

Figure 3-21. ^{1}H NMR spectrum (300 MHz) of crude **2-14** in $CDCl_3$.

In Figure 3-21, the important point is the large, or significant proton integration contributed by BPAA. Using the integrations of the aromatic BPAA protons (circled in Figure 3-21) and the alkene protons on **2-14** (boxed area)**,** there is almost a seven-fold excess of BPAA relative to **2-14**. This suggested that most of the resin sites were occupied by BPAA and not Ole_H. It was speculated that the bulky TBDMS protecting group was to blame. Therefore very long, yet unoptimized, coupling times of 8 hours, 16 hours, and overnight reaction times were used to couple the Lau and Ole groups.

Tetramer **3-12** is structurally similar to **2-27** with the exception of a missing ester unit to link the alkyl tail (missing four carbons total).

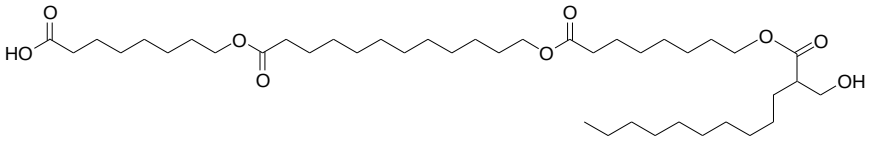

3-12

Tetramer **3-12** was made in 81% yield and characterized by ^{1}H and ^{13}C NMR spectroscopy and MS. The peak at *m/z* 735.5 was consistent with the $[M+Na]^+$ ion in the MS (Figure 3-22). There was a higher mass product at *m/z* 877.6 which was consistent with the $[M+Oct_C+Na]^+$ ion.

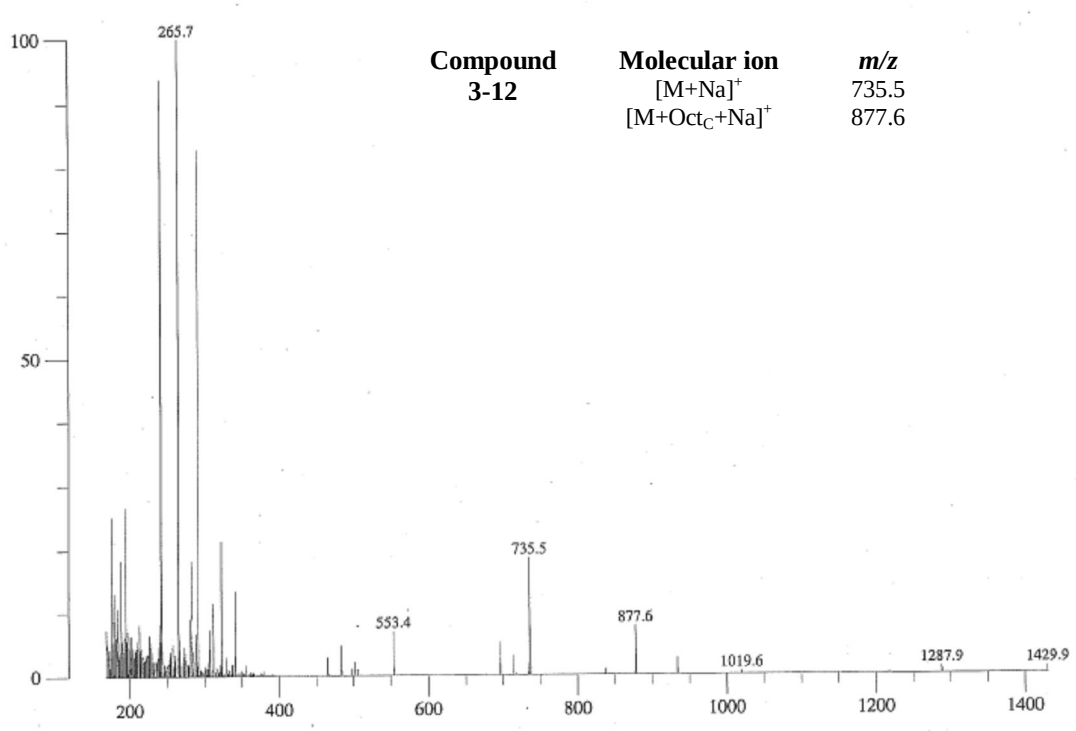

Figure 3-22. LSIMS of **3-12.** 100% = 3713 mV.

The ^{1}H NMR spectrum for **3-12** is Figure 3-23. The ^{1}H NMR spectrum looks a bit different from previously synthesized tetramers with glutaric acid tails. The characteristic $C\underline{H_2}OH$ of the Lau_T appears at about 3.7 ppm.

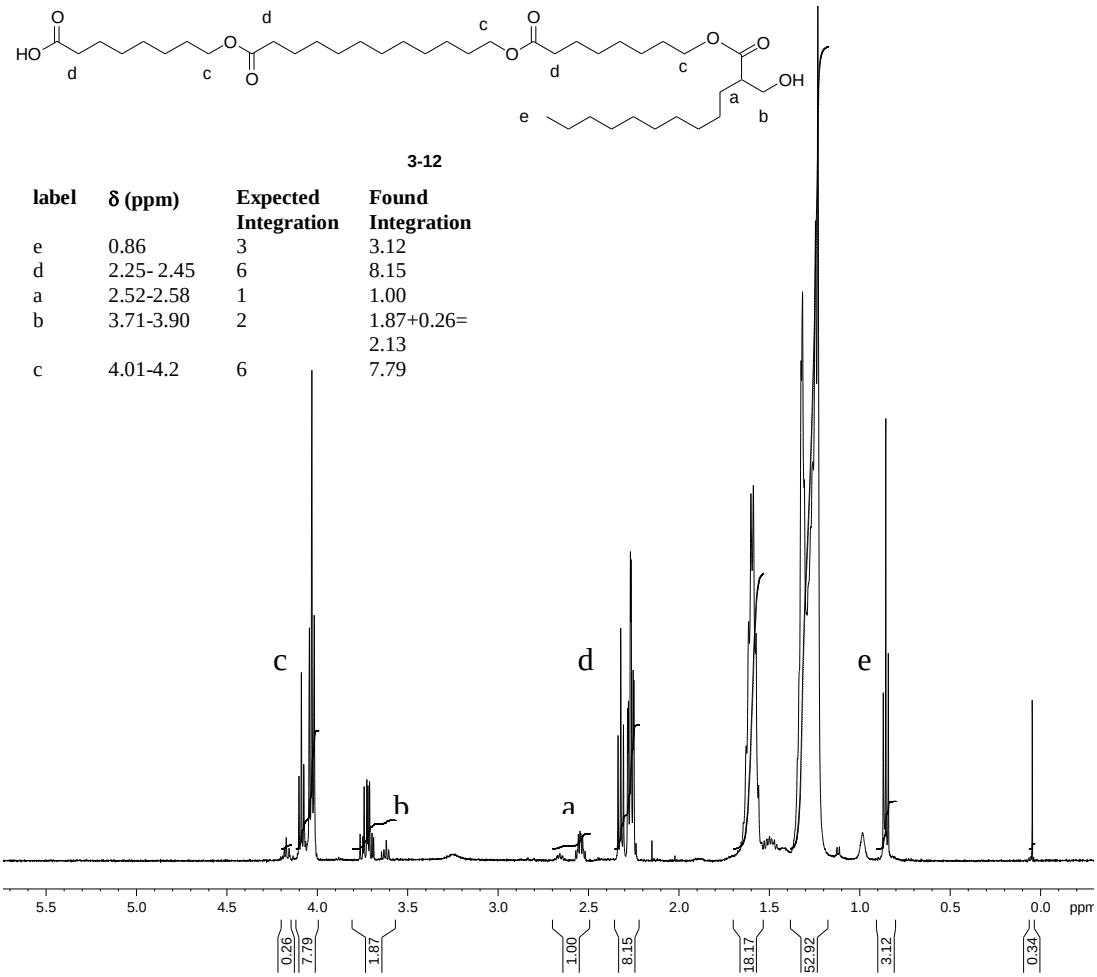

Figure 3-23. ^{1}H NMR spectrum of **3-12** in $CDCl_3$

According to the integrations of the C<u>H</u>$_2$OH:C<u>H</u> signal about 0.13 protons from the Lau$_T$ CH_2OH are missing. Trifluoroacetic acid was used to cleave the product from the resin and therefore some of the exposed primary alcohol may have converted to the TFA-ester. As well there is evidence that the TBDMS has not been fully cleaved (singlet at about 0 ppm comes from the C<u>H</u>$_3$-Si and the Lau C<u>H</u>$_2$O-TBDMS has a chemical shift at 3.6 ppm). Therefore when the integrations were calculated, the integrations for resonances due to the TFA-ester (4.2 ppm) and C<u>H</u>$_2$O-TBDMS (3.6 ppm) were combined to yield a total integration of 2.13 for the Lau$_T$ C<u>H</u>$_2$-O. The error in integrating was about

7% using the methine on the Lau_T and the total Lau_T methylene ($C\underline{H}_2O$). However the 7% may be an overestimate because any **3-13** present from the incomplete coupling of Lau may leave a primary alcohol on Oct_T which can then be derivatized to the TFA-ester. The $C\underline{H}_2$-O_2CF_3 of **3-13** has approximately the same chemical shift as the $C\underline{H}_2$-O_2CF_3 of the TFA-ester of **3-12**.

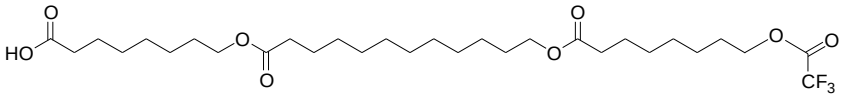

3-13

The integrations for H_c and H_d in the ^1H NMR spectrum for **3-12** were higher than expected, which was supportive of the presence of addition sequences (with an additional Oct_C). Using the H_c and H_d proton integrations, the percentage of the addition sequence was about 23% and 27%, respectively.

A tetrameric product, **3-14**, was made where oleic acid was coupled as the head group so that no alcohol group was available at the other end.

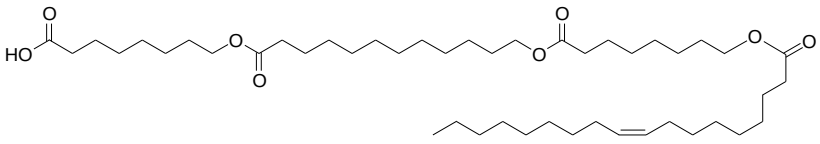

3-14

Synthetically, this molecule is of little future use because the structure lacks the terminal hydroxyl group which potentially could be used for further functionalization. This tetramer can be compared with **3-12** to see what the transport effects are by lengthening the lipophilic tail and removal of the terminal alcohol functionality.

The yield for the production of **3-14** was 0.2% and the compound was characterized by ^1H and ^{13}C NMR spectroscopy and MS. The yield was exceptionally low for this compound and it may have been due to losses in manipulation (e.g. gel

filtration). Alternatively, while following the gel filtration protocol, an inappropriate fraction may have been collected. The MS showed a peak at *m/z* 787.5 which is consistent with the $[M+Na]^+$ ion (Figure 3-24).

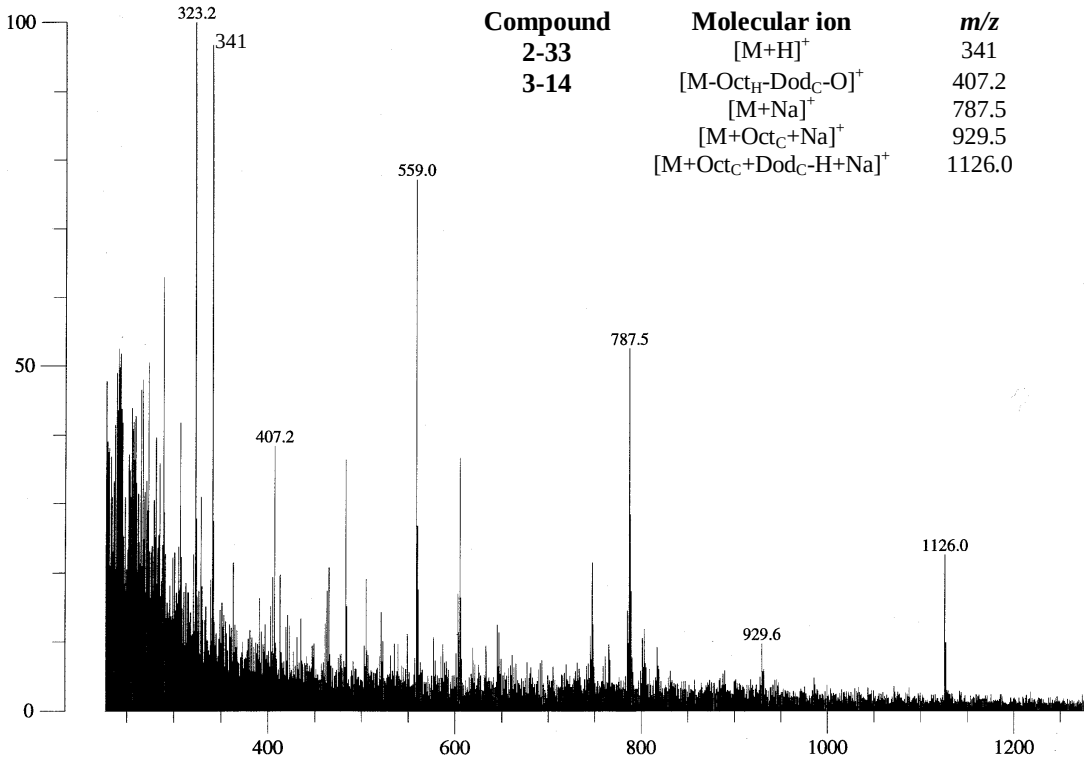

Figure 3-24. LSIMS of **3-14**. 100% = 7738 mV.

The MS of **3-14** showed several peaks of interest. The peak at *m/z* 341 has been seen in many other samples and this is consistent with the $[M+H]^+$ ion of the dimeric lactone, **2-33**. The peak at *m/z* 407.2 is consistent with the $[M-Oct_H-Dod_C-O]^+$ ion of the **3-14** fragment with the cleavage of Oct_H, Dod_C, and O. The peak at *m/z* 1126.0 is consistent with the $[M+Oct_C+Dod_C-H+Na]^+$ ion of **3-14**. This is the first occurrence of an oligoester compound with two addition units. Using our previously proposed model on how additions arise this sort of contamination is highly improbable. An even more peculiar observation is that no addition of Dod_C on **3-14** was observed, which is expected

to have an $[M+Dod_C+Na]^+$ ion at *m/z* 985.5. Therefore the peak at *m/z* 1126.0 must be a product formed within the MS.

The alkene protons on the oleic acid block were used as the reference integration in the ^1H NMR spectrum (Figure 3-25). The coupling of the oleic acid was efficient because there was no evidence of free primary alcohol resonances at about 3.8 ppm.

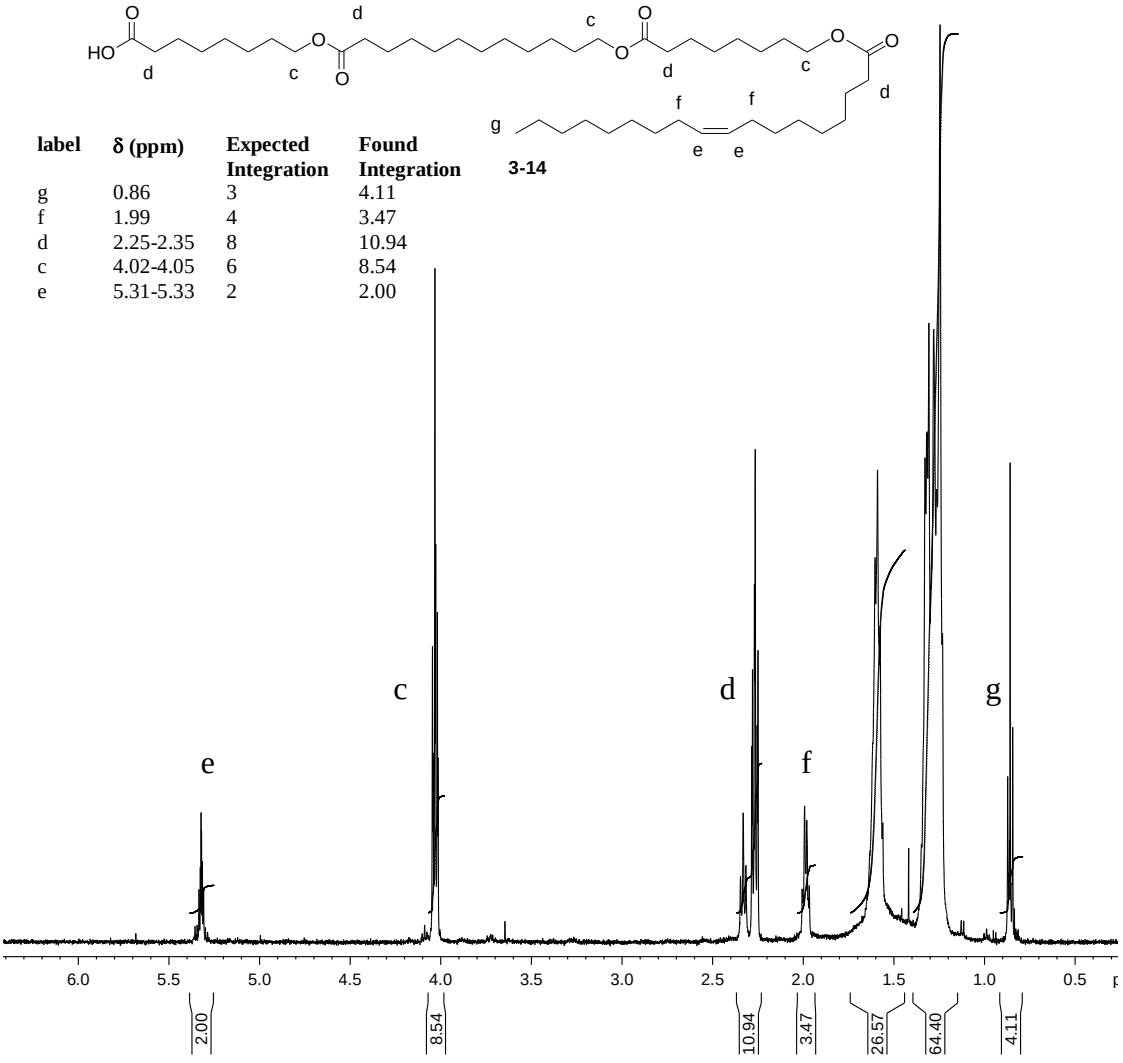

label	δ (ppm)	Expected Integration	Found Integration
g	0.86	3	4.11
f	1.99	4	3.47
d	2.25-2.35	8	10.94
c	4.02-4.05	6	8.54
e	5.31-5.33	2	2.00

Figure 3-25. ^1H NMR spectrum of **3-14** in $CDCl_3$

The check for the ^1H NMR integration in Figure 3-25 showed an error of 13% using H_f and H_e which should have appeared in a 2:1 ratio. The ^1H NMR spectrum for **3-**

14 was one of those examples where the signal-to-noise ratio was poor and therefore the integrations are assumed to be inaccurate. The H_c and H_d proton integrations are over-integrated by 42% and 37%, respectively. The MS showed that there were no deletion sequences missing a core unit but there was some evidence for an addition sequence with an additional Oct_C unit as well as a speculative addition of two core units. Therefore the combination of analyzing the ^{1}H NMR spectrum and MS, the over-integration of H_c and H_d would translate to contamination of 32% and 30% assuming that the contaminant is an addition sequence.

The synthesis of various tetramers have been shown which are expected to address issues related to the structure-activity questions posed. Yields for these tetramers ranged dramatically as well as their composition integrity.

3.5 Attempts to Synthesize Pentamer 1-20

In Chapter 2, the synthesis of tetramer **2-48** was discussed. From that product on Wang resin, a $G12_T$ could be appended to the end to yield **1-20**. This was attempted followed by cleaving with the acid solution. The product was analyzed using ^{1}H NMR spectroscopy (Figure 3-26).

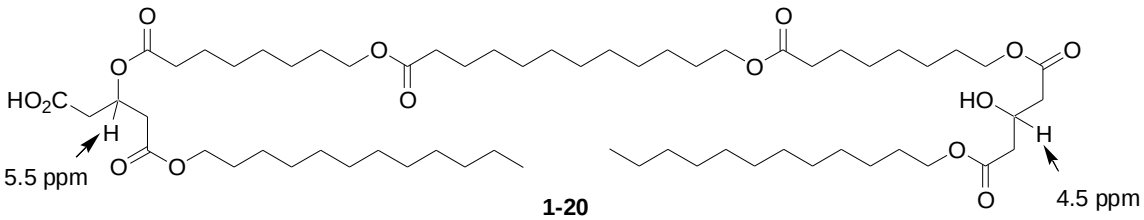

1-20

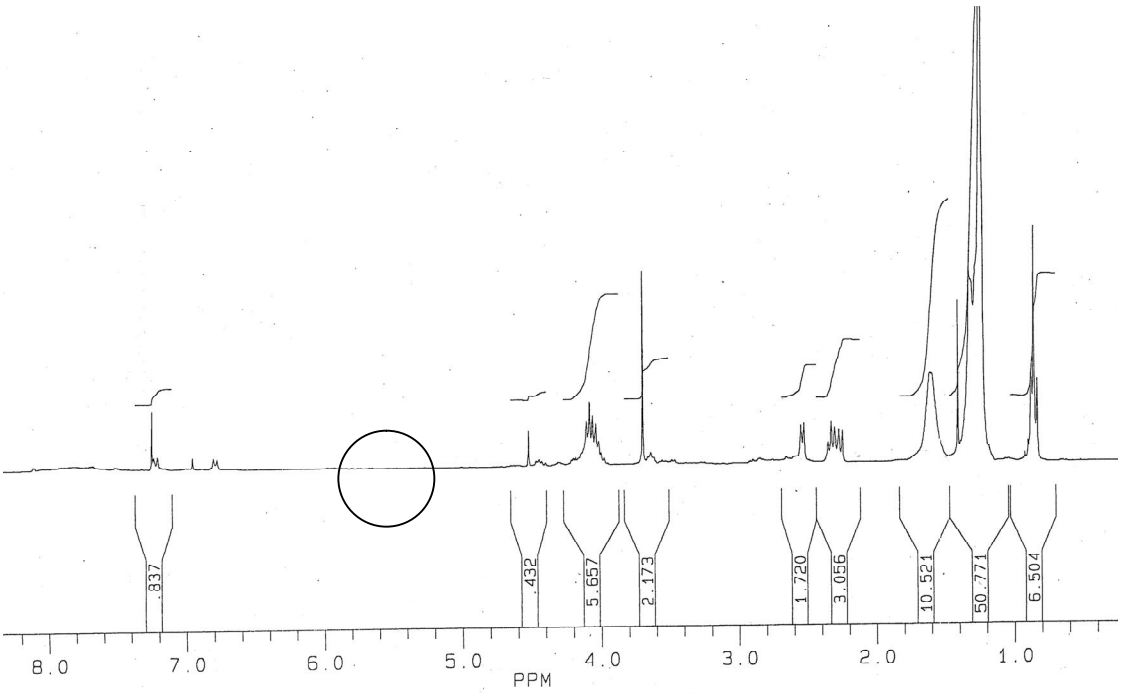

Figure 3-26. ^{1}H NMR spectrum (performed in $CDCl_3$) of the crude product from the cleavage of **1-20** from Wang resin.

For product **1-20**, the presence of two methine environments (one at chemical shift 4.5 ppm while the other at about 5.5 ppm) would be expected. However, the ^{1}H NMR spectrum (Figure 3-26) of the crude product released did not contain the resonance at 5.5 ppm (circled area). Instead the ^{1}H NMR spectrum was more consistent with **2-27** or some analogue thereof than **1-20**. No MS data was collected to determine the identity of the major product from this synthesis.

Once the resin linked to **1-20** has been treated with acid (HCl/dioxane) a product that resembled **2-27** was released (Scheme 3-1).

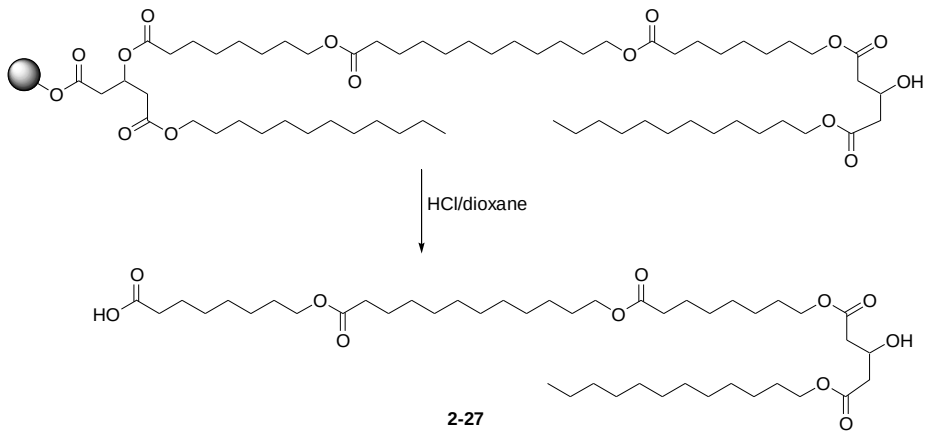

2-27

Scheme 3-1. Releasing **1-20** from resin yielded possibly **2-27.**

After washing cycles, further treatment of the resin did not release any additional material. Since **2-27** was released, then the $G12_T$ unit should still be on the resin but under the acidic conditions attempted, this unit could not be cleaved. IR spectra were collected of the bare resin, the resin loaded with the various **1-20** components in order, and the resin following acid treatment. The IR spectra (Figure 3-27) clearly showed a carbonyl stretch at about 1735 cm^{-1} which is consistent with some acid stable ester.

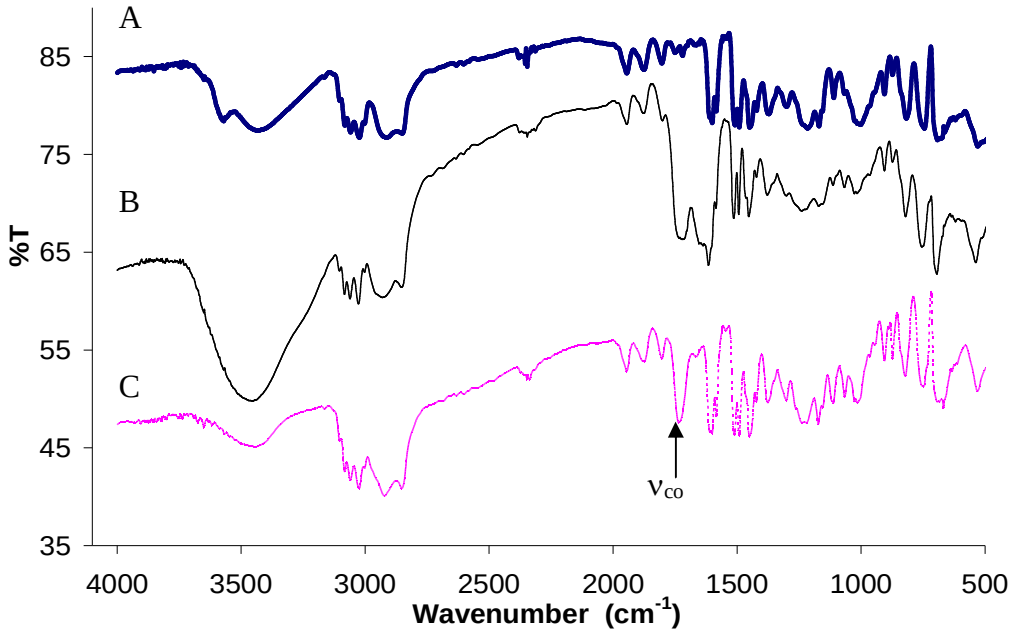

Figure 3-27. IR spectral evidence for the unsuccessful cleavage of **1-20** from Wang resin (KBr pellet, air background). (A) Wang resin prior to any loading. (B) Wang resin with the necessary building blocks to form **1-20**; just prior to acid treatment. (C) Wang resin after acid treatment and resin washes.

One possible explanation is that the secondary alcohol in the glutaric acid building block is unstable under the resin cleavage conditions. The secondary alcohol may be too close to the aromatic ring of the solid support, so upon acid cleavage conditions a Friedel-Crafts type reaction could occur forming a carbon-carbon bond (Scheme 3-2).

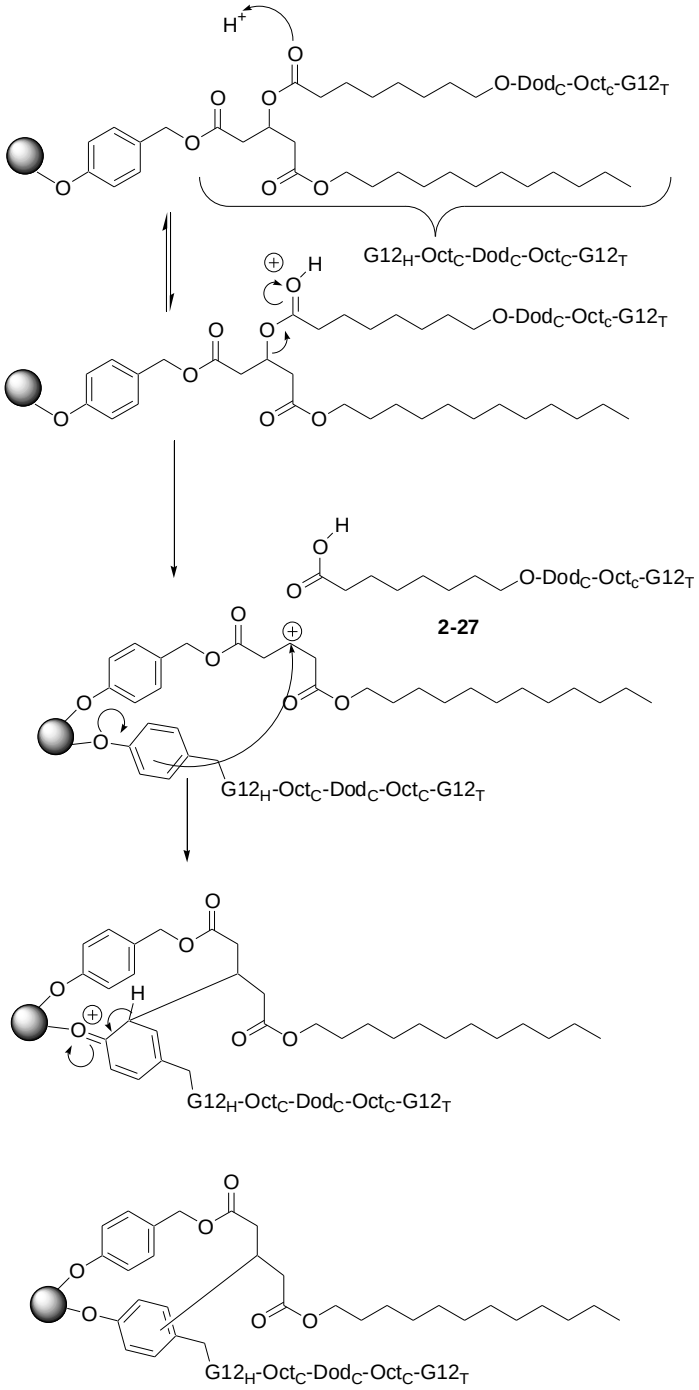

Scheme 3-2. Proposed cleavage of $G12_H$ from **1-20**.

If the product was further away from the support, then it may be possible to isolate the desired **1-20**. One way to extend the product out was with the addition of another building block (such as **2-21**). It was possible to synthesize the pentameric

product **3-15** in a 40% yield. The product was characterized by ^{1}H and ^{13}C NMR spectroscopy and MS. The MS showed peaks at *m/z* 963.7 and 986 consistent with the $[M+Na]^+$ and $[M+2Na-H]^+$ ions. The deletion of an Oct_C or Oct_T from **3-15** would give a $[M-Oct_C+Na]^+$ ion at *m/z* 821.5 (Figure 3-28). The peak at *m/z* 483.3 was observed in several other earlier tetrameric products and was proposed to be the $[M+H]^+$ ion of the cyclic trimer **2-34**.

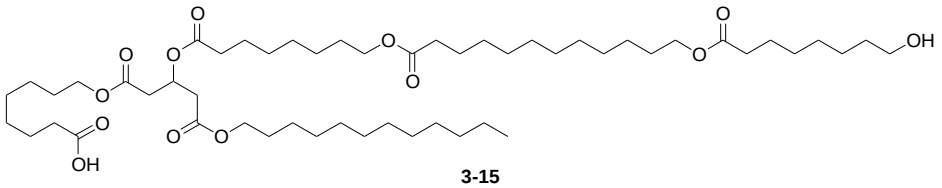

3-15

Compound	Molecular ion	*m/z*
2-34	$[M+H]^+$	483.3
3-15	$[M-Oct]^+$	821.5
	$[M+Na]^+$	963.6
	$[M-H+2Na]^+$	986

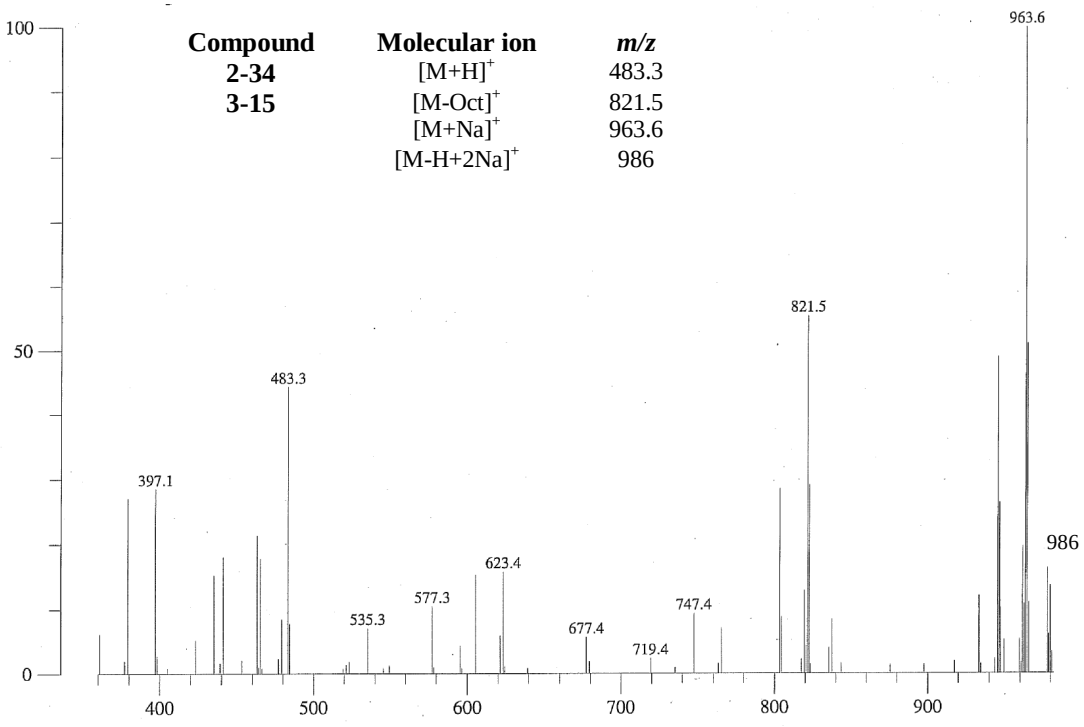

Figure 3-28. LSIMS of **3-15**. 100% = 556 mV.

Normally the methine proton (H_a) on the $G12_T$ unit in most of the tetramers was used as the reference proton, but in this case since the acid proton (H_g) has an overlapping proton with the methine of $G12_C$, then the methylenes (H_b) on $G12_C$ were

used as the reference (Figure 3-29). Importantly, the ester of the secondary alcohol has been formed which is evident by the downfield signal at about 5.5 ppm. Using the methylene H_b as the reference protons, the H_c and H_d are over-integrated by 6% each suggesting that either there are addition sequences or that there are products which do not contain $G12_C$ such as **2-34**. The MS did not show any addition sequences, so the presence of **2-34** was more appropriate for explaining the increase in integrations. The singlet seen at about 2.1 ppm was the residual signal from the CH_3 on acetone used to clean the NMR tubes. Using H_c and H_d the percentage of contamination by **2-34** was only 8%.

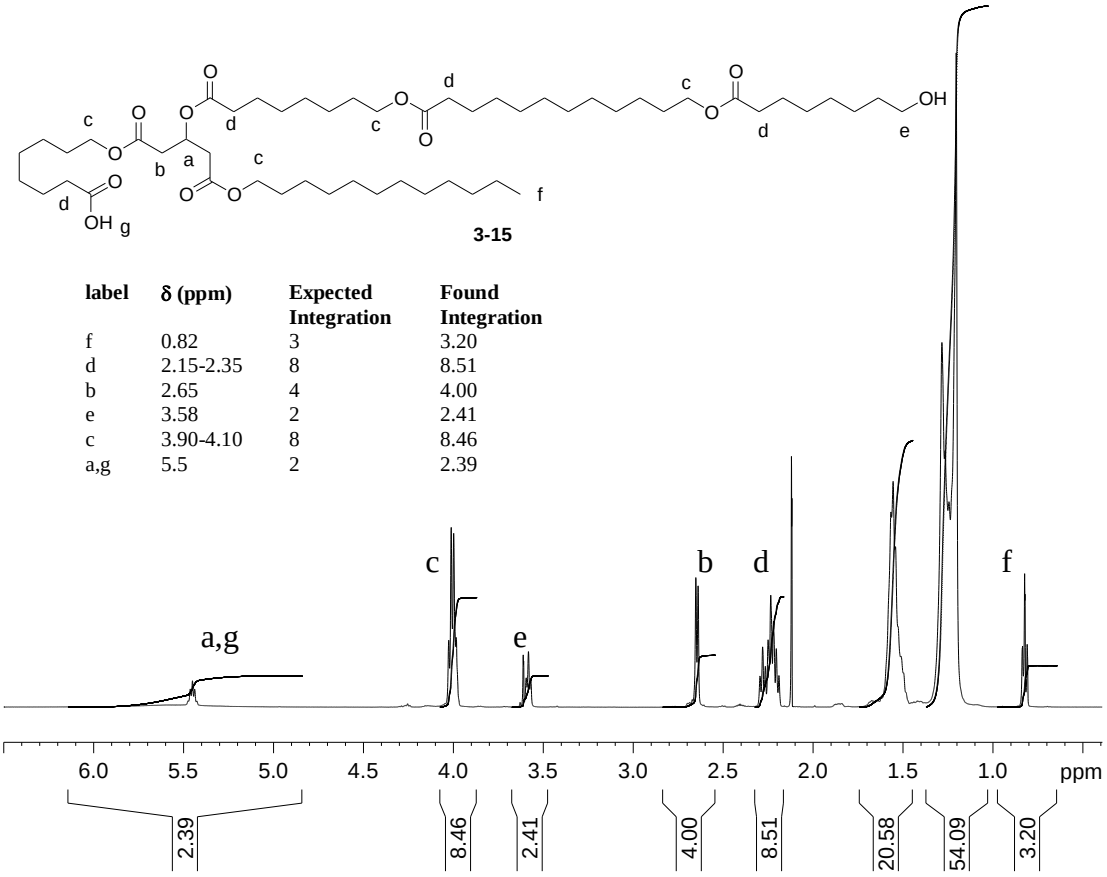

Figure 3-29. ^{1}H NMR spectrum of **3-15** in $CDCl_3$

The synthesis of **3-15** was applied towards **1-20** by appending a $G12_T$ at the terminal Oct_T of **3-15** on resin (Scheme 3-3)**.**

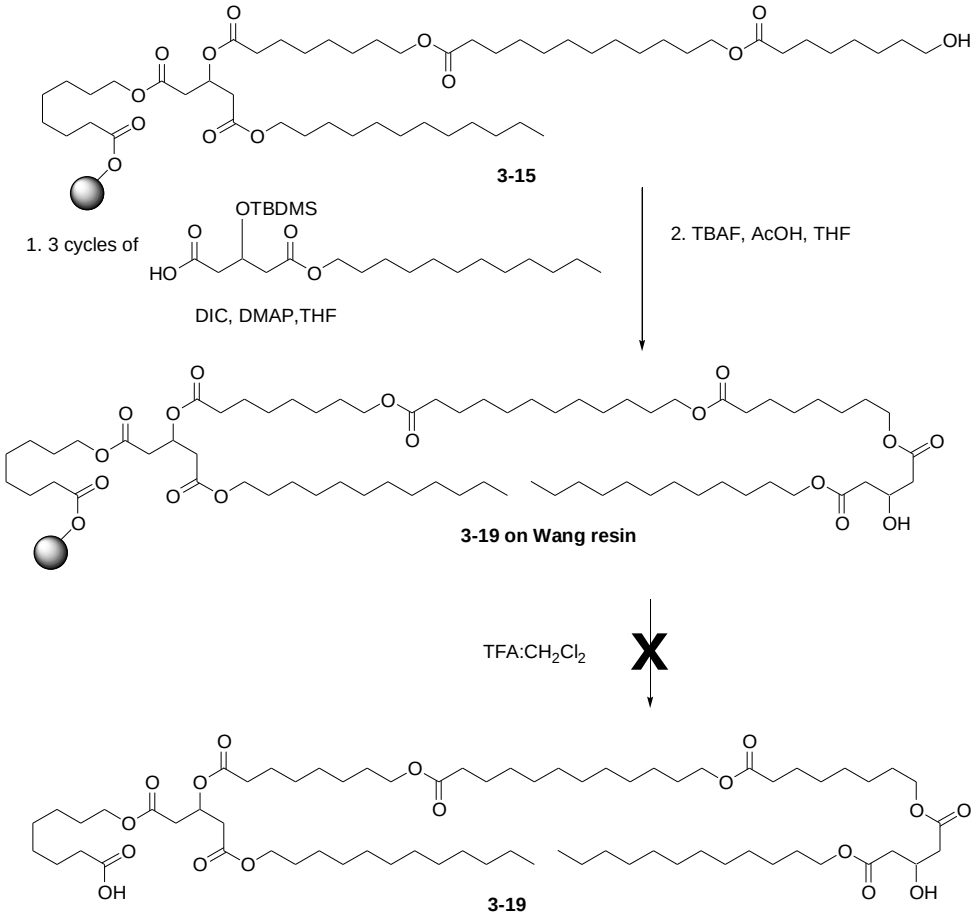

Scheme 3-3. Towards the synthesis of **1-20** by extending from Wang resin by one Oct_H unit.

The ^{1}H NMR spectrum for this crude product (**3-19**) did not show a resonance at 5.5 ppm (circled area) which was expected to be the resonance of the H_a methine for $G12_C$ (Figure 3-30).

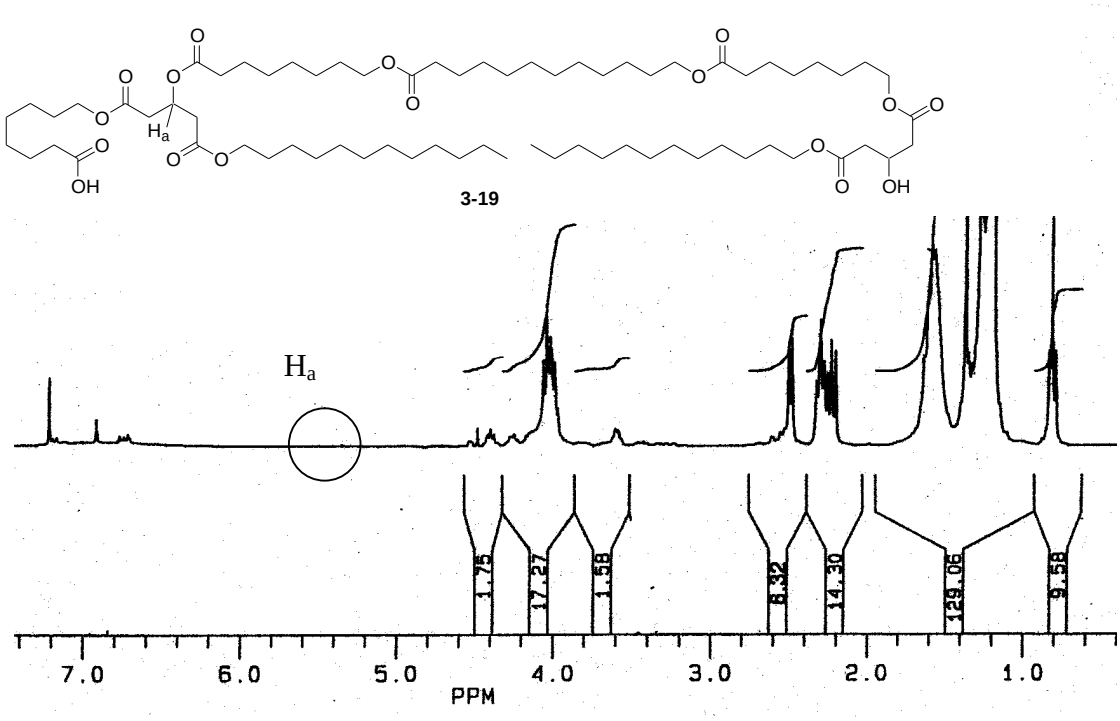

Figure 3-30. ^{1}H NMR spectrum for the expected crude product **3-19** in $CDCl_3$.

Unfortunately, the $G12_T$ was appended onto **3-15** and then the product was cleaved from the resin, the product cleaved did not contain the $G12_C$ fragment. This crude product from resin was not further analyzed to identify what the major compound is.

Analogous to **3-19**, **3-20** was made on Wang resin using the same reaction conditions and the only difference in structure is that a Hex_H replaced the Oct_H in **3-19**.

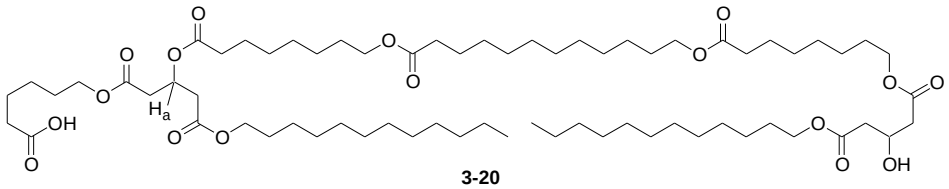

When the **3-20** product was cleaved from Wang resin, the ^{1}H NMR spectrum was very similar to the ^{1}H NMR spectrum of **3-19** in that there was no methine H_a signal at the expected 5.5 ppm. A MS was collected for the crude product (Figure 3-31). The

$[M+Na]^+$ and $[M+H]^+$ ions for **3-20** are expected to be at *m/z* 1231.9 and 1210.9, respectively. Neither of these molecular ions were observed in the MS. The peak at *m/z* 877.7 cannot be identified as any possible fragmentation of **3-20**.

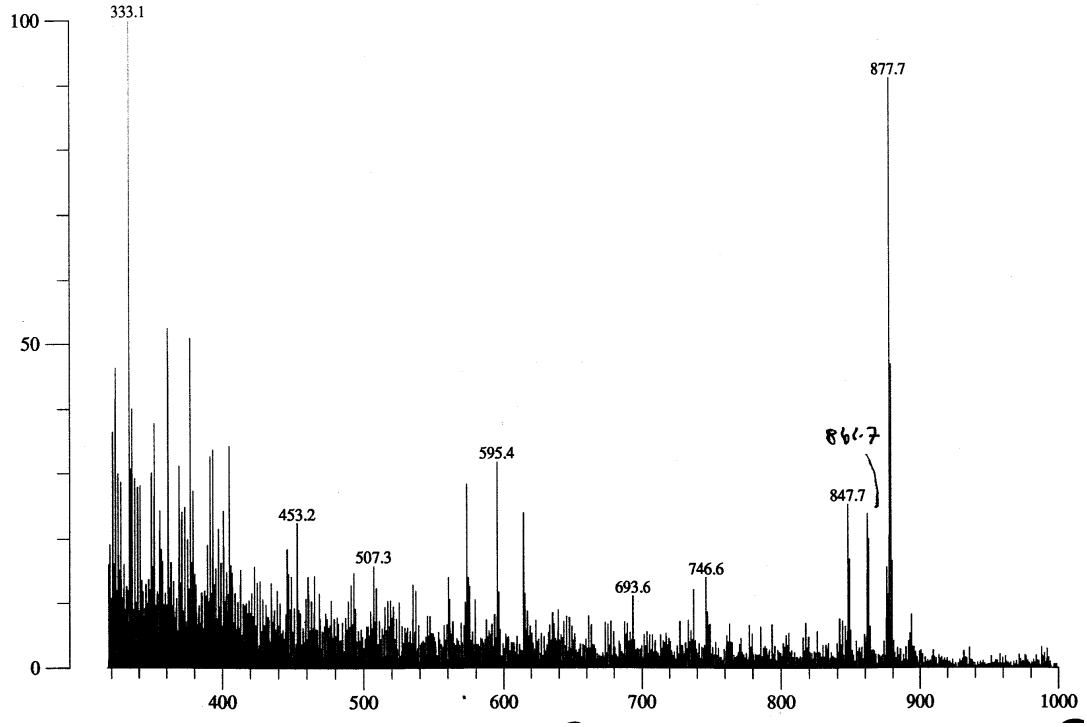

Figure 3-31. LSIMS of product synthesized from **3-20** synthesis. 100% = 3442 mV.

From the attempted synthesis of **3-20** and **3-19** it was concluded that the extension of a building block was not sufficient to reduce the risk of losing a G12 head group during resin cleavage.

A second way to distance the molecule from the aromatic linker was to use a resin where there is a lengthy tether between the resin and molecule. Trying to produce **1-20** by using Wang Tentagel resin (a special SPOS resin where a lengthy ethylene glycol chain connects the molecules to the resin) also failed using the same method of analysis (it was noted that there was no evidence of the ^{1}H NMR signal at 5.5 ppm). The added complication with using Wang TentaGel resin is that it is hygroscopic so it can readily

pick up water from washing steps or even the atmosphere which can reduce the coupling efficiency.

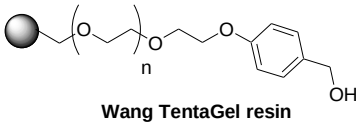

Wang TentaGel resin

Therefore with the failed attempts at synthesizing **1-20**, limitations were identified with the SPOS methodology. The length of the oligoester product formed on SPOS should not be more than tetramers when the $G12_H$ unit is used. Secondly, the functionality used for coupling, secondary alcohols, are prone to elimination under acidic conditions and therefore should not be used structurally close to the resin because of the likelihood of reaction with the polymer resin.

After extensive investigation and optimization of the synthetic steps, the unambiguous synthesis of **1-20** proved to be impossible using the developed SPOS methods. In my view the sample reported previously by Hu was a mixture of related compounds that fortunately combined to give the appropriate ^{1}H NMR spectrum.

3.6 Synthesis of Pentamers – Increasing the Lipophilicity

Since it was not possible to generate a pentameric product using the $G12_H$ unit, then alternative building blocks to put that head group on, Lau_H (from **2-13)** and Ole_H (from **2-15)** were used because they have a primary alcohol for the linkages. Using the Lau and Ole blocks, pentameric products (**3-16** and **3-17**) were made.

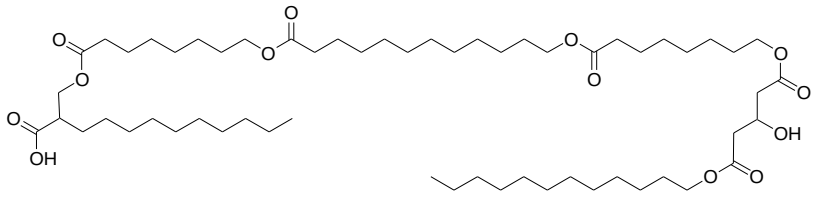

3-16

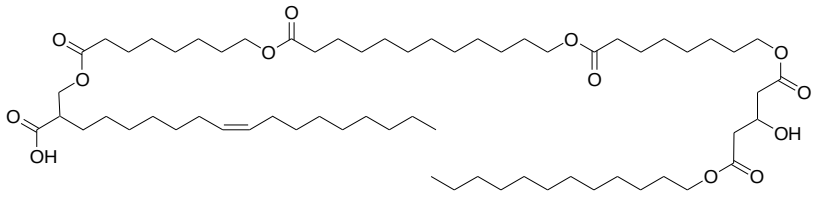

3-17

Pentamer **3-16** was made in 4% yield. The $[M+Na]^+$ ion for **3-16** appeared at *m/z* 1033.7 in the MS (Figure 3-32). It should be stated at this point that there are two chiral centers in the molecule which means that diastereomers are generated; no effort was made to separate the diastereomers. In the mass spectrum of **3-16**, the higher mass fragments of *m/z* 1245.5 was likely the $[M+Na^+]$ ion of **3-16** containing an additional Lau_C, **3-18** (Figure 3-32). The dimer of the Lau building blocks would have occurred similarly as the dimerization of the building blocks. With the Lau building block part of the synthesis entailed of protecting the alcohol with TBDMS and from the ^1H NMR resonances it is hard to tell if there is sufficient coupling.

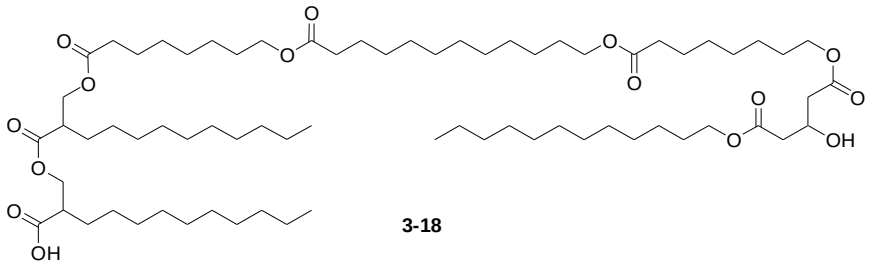

3-18

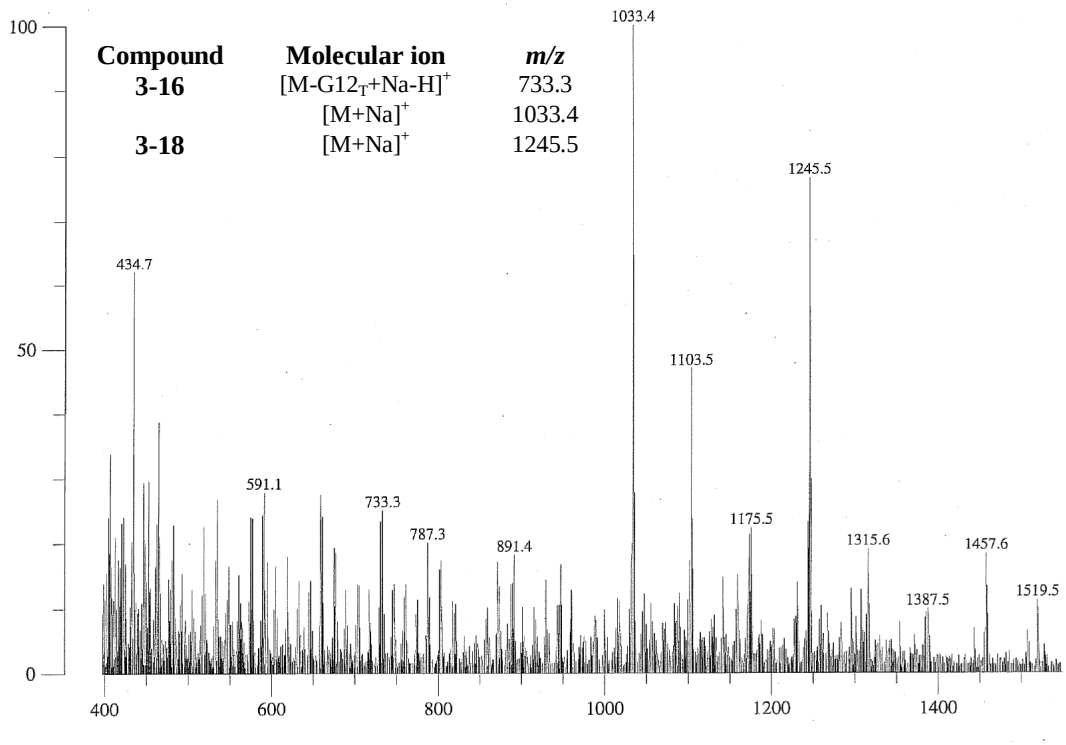

Figure 3-32. LSIMS of **3-16.** 100% = 1191 mV.

The ^{1}H NMR spectrum for pentamer **3-16** showed that when the methine on the $G12_T$ was referenced as 1H, then the integrations from the Lau_H unit are greater than predicted by theory (Figure 3-33). If the Lau_H and $G12_T$ were present in equal proportions, then the expected ratio of methines H_a:H_f would be 1:1. The integrations for the Lau_H unit are over-integrated, suggesting that there are more Lau_H units than $G12_T$. Based on the MS, a product **3-18** was proposed which is composed of one Lau_H and one Lau_C unit, and this would account for why more Lau_H/Lau_C units were present according to the ^{1}H NMR integrations.

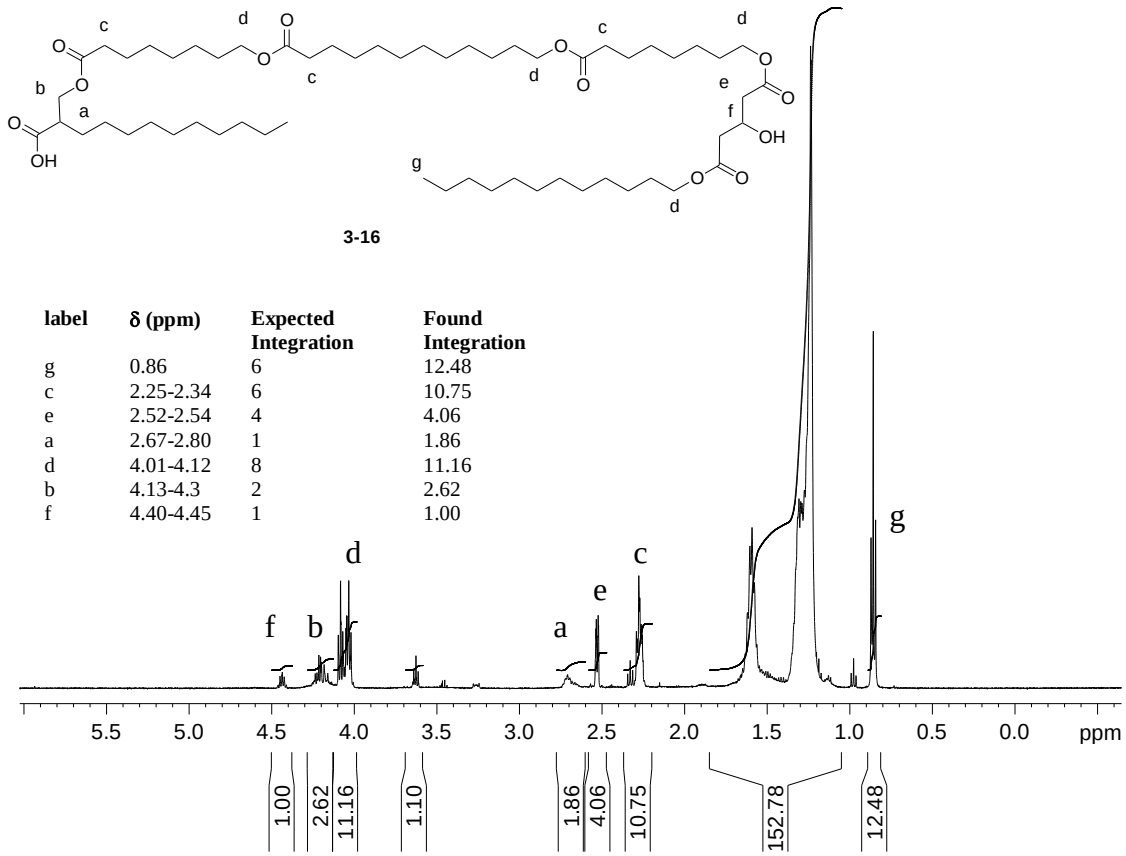

Figure 3-33. ^{1}H NMR spectrum of **3-16** in $CDCl_3$.

The integration for H_a was over-integrated by about 86%, but the alcohol proton may also be under this signal. By taking H_b as the indication of how much excess was present, 30% was calculated. Therefore there was at most 30% of **3-18** present in the product. The triplet at about 3.65 ppm was the free primary alcohol when the $G12_T$ unit was missing (also suggested by the MS for the peak at *m/z* 733.3). If $G12_T$ was missing and the $G12_T$ methine was referenced as 1, then most of the integrations should be over-integrated because the sample would contain more Lau_H, Oct_C, and Dod_C relative to $G12_T$.

Pentamer **3-17** was made in 7% yield. In the MS, the observed peak at *m/z* 1115.8 was consistent with the $[M+Na]^+$ ion for **3-17** (Figure 3-34). There were no addition sequences observed in the MS. The masses at *m/z* 973.6, 917.6, 821.5, and

679.4 were consistent with $[M\text{-}Oct_C+Na]^+$, $[M\text{-}Dod_C+Na]^+$, $[M\text{-}Ole_H+Na]^+$, and $[M\text{-}Ole_H\text{-}Oct_C+Na]^+$ ions.

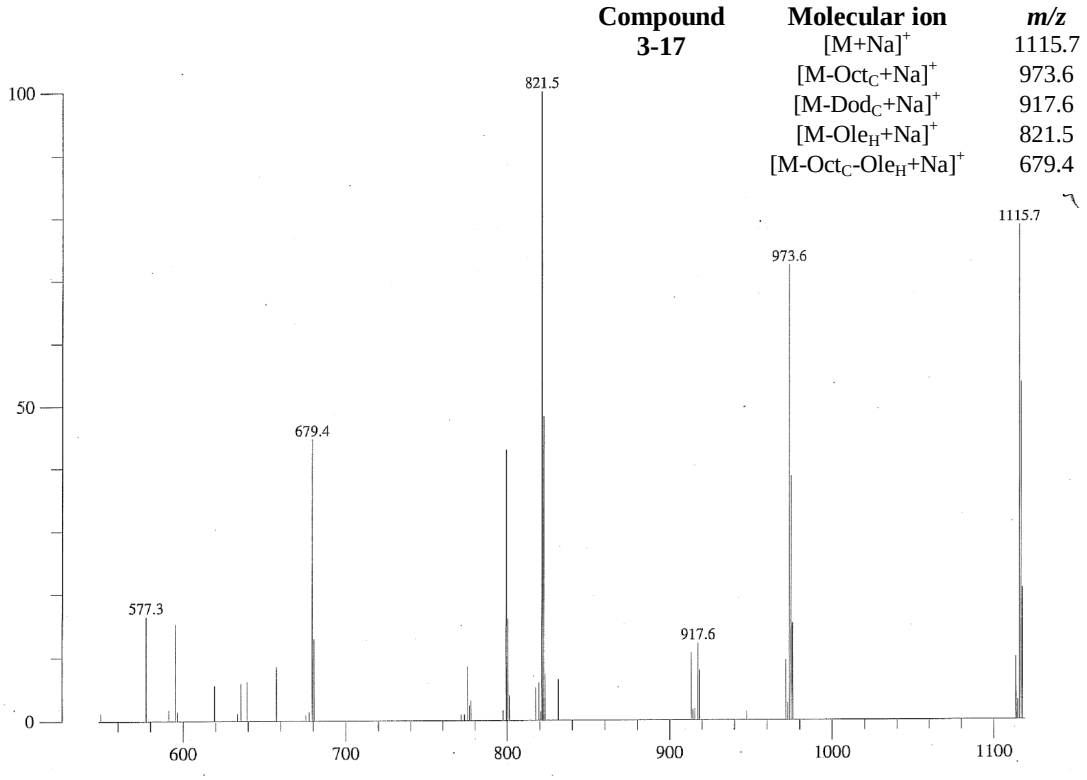

Figure 3-34. LSIMS of **3-17.** 100% = 1140 mV.

In the ^1H NMR spectrum of **3-17** (Figure 3-35), the methine on the $G12_T$ was set to 1H (H_g), and the signals which belonged to Ole_H (H_a, H_c, H_i) were under-integrated which meant that there were more products with the $G12_T$ unit compared to those which contained both a $G12_T$ and Ole_H. However, the error between H_g and H_f was about 10% which was also the error observed between H_a and H_g. Therefore the fraction of compounds which were missing the Ole_H must be very minute. The compounds which were missing either an Oct_C or Dod_C would contribute to H_e and H_d by diluting the integrations, which was not observed. Therefore, the sample of **3-17** was of relatively high integrity.

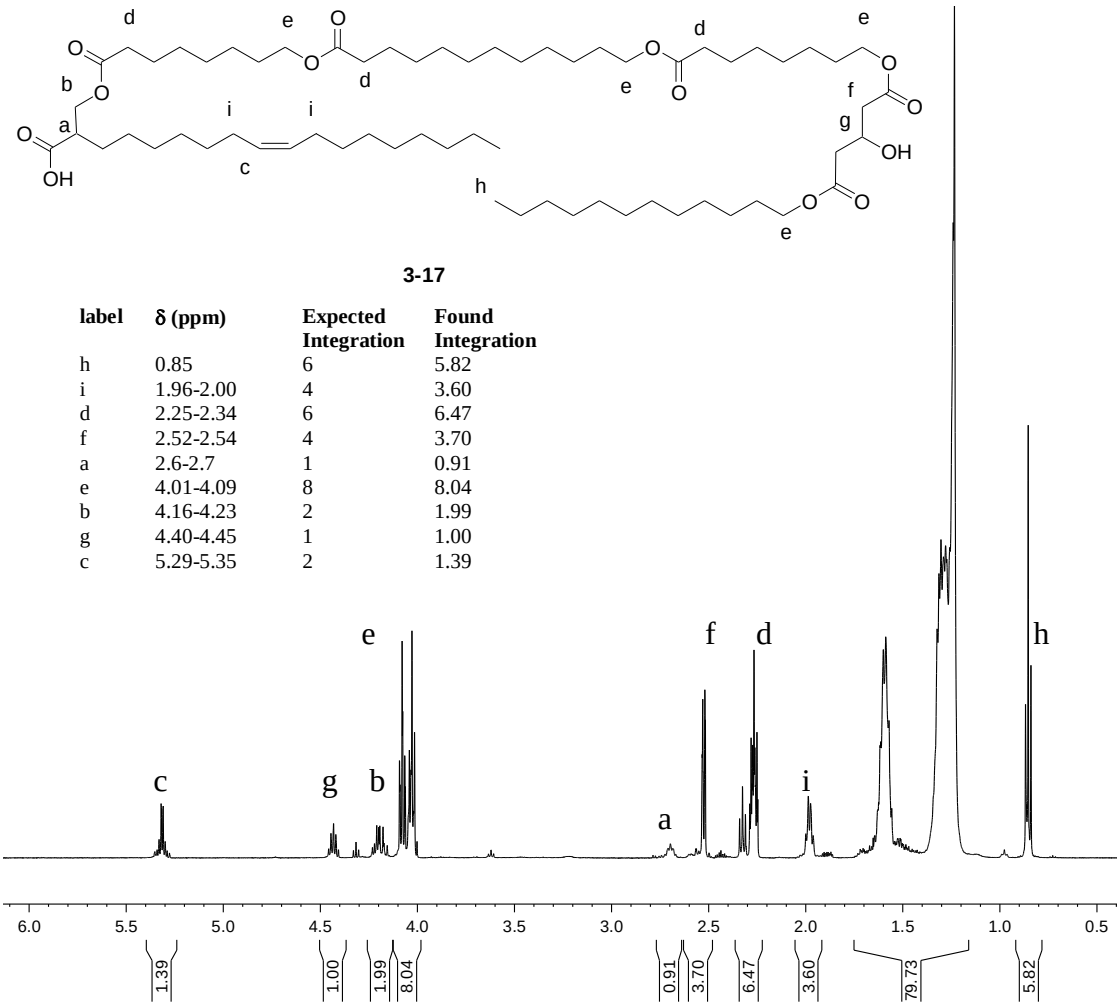

Figure 3-35. ^{1}H NMR spectrum of **3-17** in $CDCl_3$.

3.7 Overview of SPOS Products

All the products from the SPOS reactions have been summarized below in Table 3-1. These compounds were characterized by ^{1}H and ^{13}C NMR spectroscopy and MS. The integrities were calculated based on integrations in the ^{1}H NMR spectra and in particular it was usually the integration of H_c (-C$\underline{H}_2O_2C$-) and H_d (-C$\underline{H}_2CO_2$-).

Table 3-1. Reaction sequences to yield the products made by SPOS.

Compound	Sequence[a]	Recovery (%)	Integrity (%)	Impurity used to calculate integrity[b]
2-23	G12 + Dod	15	>95	-
2-24	Oct + G12	15	>95	-
2-25	Oct + Dod	12	89	**2-33**
2-27	Oct + Dod + Oct + G12	49	82	**2-33**
2-35	Dod + Oct + G12	45	>95	**2-36**
2-36	Dod + Oct + Oct + G12	3	60	TFA
2-38	Oct + Oct + Oct + G12	8	40	TFA
2-39	Oct + Dod + Oct	23	93	$+Oct_C$,$+Dod_C$
2-48	G12 + Oct + Dod + Oct	37	>95	-
3-1	Oct + Dod + Oct + G10	13	94	$+Oct_C$,$+Dod_C$
3-2	Oct + Dod + Oct + G14	38	>95	-
3-3	Oct + Dod + Oct + G16	34	87	$+Oct_C$, **2-34**
3-4	Oct + Oct + Dod + G12	1	67	**3-5**, **3-6**, TFA
3-7	Dod + Dod + Dod + G12	24	87	$-Dod_C$
3-8	Dod + Dod + Oct + G12	18	91	$-Dod_C$,$-Oct_C$
3-9	Oct + Dod + Dod + G12	9	71	$-Dod_C$
3-11	Hex +Oct +Hex + Oct + G12	8	89	$-Oct_C$,$-Hex_C$,$-G12_T$
3-12	Oct + Dod + Oct + Lau	81	75	$+Oct_C$
3-14	Oct + Dod + Oct + Oleic acid	0.2	69	$+Oct_C$,$+Dod_C$
3-15	Oct + G12 +Oct + Dod + Oct	40	92	**2-34**
3-16	Lau + Oct+ Dod + Oct + G12	4	70	**3-18**
3-17	Ole +Oct + Dod + Oct + G12	7	>95	-

[a] Appropriate deprotection steps are used after every loading/coupling sequence.
[b] For the symbol TFA, this implies the TFA ester of the primary alcohol as the dominant contaminant.

The purity of the building blocks is very important otherwise addition sequences arise. This assumption can explain many of the tetrameric compounds with high integrity >85% because the building blocks could have a hydroxy acid impurity of about 5% which was within the precision of the NMR instrument. This model becomes unrealistic

for compounds of much lower integrity (<75%) because the impurity in the building blocks would definitely be seen. There are several possibilities for why all of the compounds do not exhibit the addition sequences. Firstly the MS was used to look for the molecular ion of the target molecule; any addition sequences observed at higher molecular weights are periphery to the target molecule. That is, no particular attention was made to look for the addition sequence ions during the MS data collection. Therefore the addition sequences may be present in all of the samples but data was not collected when they flew in the MS. Alternatively, some of the building block samples were purer than others. Since in SPOS a lot of building block material is used up then there is frequent synthesis of building blocks and there may be variation in the quality from batch to batch.

There are several examples of the integrity compromised by sequences which are missing the terminal $G12_{T.}$ These deletion sequences have been found as lactones or trifluoroacetates (when TFA was used as the cleavage solution). Any of the deletion sequences would reflect inefficient coupling or deprotection of the alcohol to allow for further coupling. The inefficiencies may arise due to traces of water in the solvent which can quench the activated carboxylic acid.

The length of the product built on SPOS was an important consideration because there are limitations. Pentameric and tetrameric products are probably the longest oligoesters that can be efficiently made. Purification may become an issue for longer oligoesters. The functionalities are also important in the design consideration. A secondary alcohol cannot be used to link the core to the head group whereas a primary alcohol can have better success.

The target samples made by SPOS do show contamination by addition sequences, some deletion sequences, as well as lactones. The ion transport ability of the SPOS targets were still surveyed despite the presence of these contaminants.

Chapter 4 Survey of Activities of Ion Channel Candidates

The activities of synthetic ion channels are surveyed using either a bilayer clamp technique or a vesicle technique and the advantages and disadvantages of such techniques were discussed in Chapter 1. A vesicle assay was used to characterize the transport activity of the oligoester compounds because of the need to survey the large number of compounds prepared in preceding chapters. For the measurement of ion transport, a fluorescence analysis of the pH-sensitive dye 8-hydroxy-1,3,6-pyrene trisulfonate (HPTS) within unilamellar vesicles of diameter between 200-400 nm was used.

This chapter discusses the methodology in depth and then turns to the structure-activity questions that guided the synthetic choices made in earlier chapters. This data provides a starting point for discussion of ion transport mechanism.

4.1 Vesicle Assay Protocol

The preparation of the vesicles for the HPTS assay were reported by Sidorov et al.[83] Their methods were used with minor adjustments to the procedure.[84] The unilamellar vesicles were made by hydrating a thin film of lipid containing a 8:1:1 mol ratio of phosphatidylcholine:phosphatidic acid:cholesterol with the internal buffer solution. Any multilamellar aggregates are assumed to be destroyed through three freeze-thaw cycles in liquid nitrogen. Vesicles were then formed by probe sonication and the resulting mixture was allowed to anneal overnight. To size the vesicles so that the diameters are less than 400 nm, the mixture was extruded though a 400 nm polycarbonate Nucleopore filter using a membrane extrusion apparatus. Any excess dye that was not encapsulated was removed in a PD-10 Sephadex G-25 column and the vesicles were

diluted with external buffer. Dynamic light scattering measurements were taken of the vesicle mixture to find the average vesicle diameters. The concentration of lipid in the vesicle solution was determined from using a Bartlett assay[2]. To find evidence for the dye being entrapped, a pH gradient was induced between the external buffer and internal buffer which did not change the dye fluorescence very much; upon vesicle lysis using a 5% Triton® X-100 solution (known by the name "Triton"), a dramatic response in the fluorescence was observed.

In the preparation of vesicles, it is important to keep the internal and external buffer at about the same concentration and content to relieve any osmotic pressure differences. The vesicles used for the HPTS fluorescence assay had the same intravesicular and extravesicular phosphate buffer concentrations (10.1 mM Na_3PO_4, 74.7 mM Na_2SO_4 and adjusted the pH to 6.4 using H_3PO_4) with the only exception that the internal buffer contained 9.9 μM HPTS.

In the procedure for the HPTS fluorescence vesicle assay, the ion channel candidates were first introduced into an external buffer solution containing the HPTS-entrapped vesicles; this mixture was equilibrated for about 30 seconds. Fluorescence emission and excitation data of the HPTS dye was collected as a function of time. A pH pulse was achieved by injection of a NaOH solution into the external buffer solution to create a pH gradient between the internal and external buffer. After sufficient data has been collected, the vesicles were lysed with a solution of Triton.

4.2 HPTS Fluorescence Assay

As shown in Figure 4-1 the dye exists in deprotonated and protonated forms. Each form has an independent excitation wavelength but the two forms share a common emission at 510 nm.

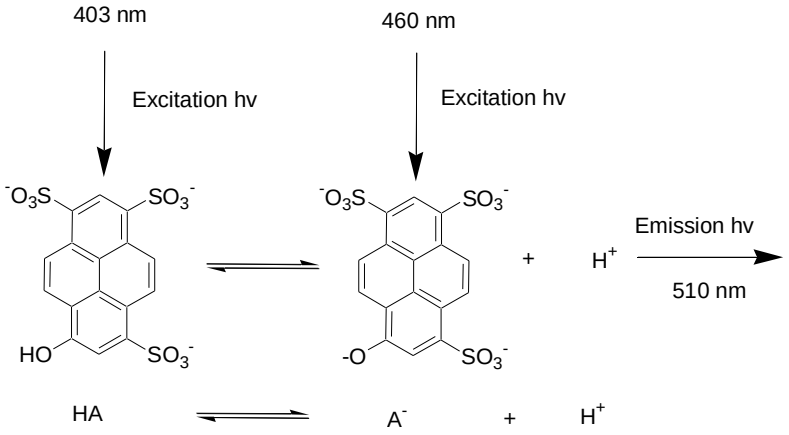

Figure 4-1. HPTS dye fluorescence schematic.

The HPTS dye in the buffer shifted between the acid (HA) and base (A^-) form depending on the pH of the buffer environment. The Henderson-Hasselbach equation (4-1) can be applied to the system:

(4-1) $$pH = pK_a - \log\left(\frac{[HA]}{[A^-]}\right)$$

The concentration of A^- can be related to the intensity of emission at 510 nm when the solution is excited at 460 nm (E_{460}); likewise the concentration of HA can be related to the intensity of the emission at 510 nm when the solution is excited at 403 nm (E_{403}). Substituting the relationship of the ratio of the emission intensities into equation (4-1), equation (4-2) is created with an additional m_s term. By plotting pH versus $\log(E_{403}/E_{460})$, the slope of the line will be m_s.

(4-2) $$pH = pK_a - m_s \log\left(\frac{E_{403}}{E_{460}}\right)$$

To get a calibration plot, a sodium hydroxide solution was added to the buffer solution containing the HPTS dye and the pH was measured with a pH electrode. The emission at 510 nm was recorded for excitation at 403 and 460 nm, (E_{403} and E_{460}, respectively). The logarithmic ratio of E_{403}/E_{460} is plotted versus pH to give Figure 4-2. According to the equation of the line in Figure 4-2, the pK_a found for HPTS was 7.25 which is comparable to the literature value[85] of 7.3. Therefore the conversion of the ratio E_{403}/E_{460} can be converted to pH in the range 6.4 to 7.2 according to equation (4-3).

(4-3) $pH = 7.25\text{-}1.13 \log(E_{403}/E_{460})$

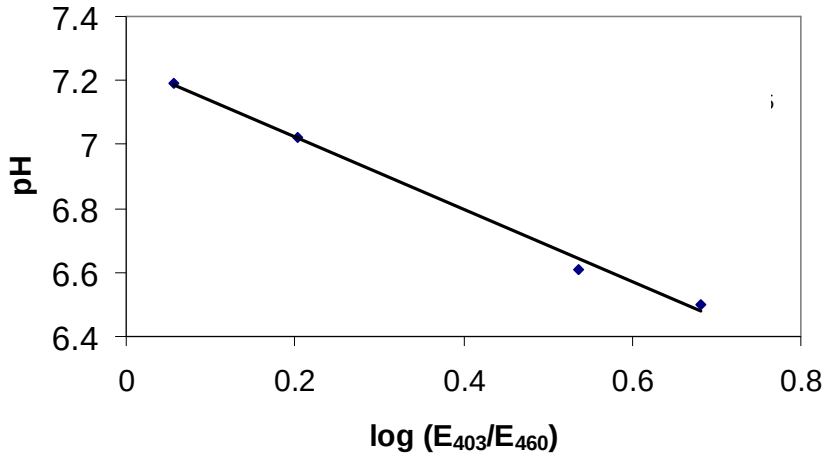

Figure 4-2. Calibration plot of pH as a function of log (E_{403}/E_{460}).

When the HPTS dye is encapsulated in a vesicle, it is assumed that the fluorescence response is the same as when the dye is in a buffer solution outside a vesicle. The use of the fluorescence ratio is particularly important for the vesicle assay because the absolute emission intensities and light scattering vary from vesicle experiment to vesicle experiment and therefore the sample to sample variance can be minimized.

In the early stages of the fluorescence assay development this pulse was achieved by opening the top of the fluorimeter and injecting the aliquot of base into the cuvette. The cuvette was inverted several times for about five seconds to achieve adequate mixing. This whole procedure took about 20-30 seconds and therefore the problem with this method of inducing the pH gradient was that approximately the first 20 seconds of data were lost. At a later point, an injector port was built into the fluorimeter to resolve the problem of missing data. The injector port consisted of a piece of tubing from a syringe containing the base solution going into the fluorescence cuvette and contacting the vesicle solution. The solution in the cuvette was stirred using a small stir bead by a magnetic stirrer in the fluorimeter. Therefore, it was possible to use data within a few seconds following injection of base.

A typical fluorescence trace is shown in Figure 4-3. There are two lines which represent the data collected from the two excitation wavelengths (403 and 460 nm). Three positions have been labeled as A, B, and C. In position A, this is the equilibration of the channel candidate with the vesicles. Once the baseline was stable a 1-unit pH jump was induced by adding NaOH (position B). The pH gradient caused an exchange of either the cations or anions by the transporter and was represented by the decrease in the emission at 510 nm due to excitation at 403 nm and increase in the emission at 510 nm due to excitation at 460 nm. When the transport activity plateaus (or when sufficient data points have been collected), Triton was injected (position C) to lyse the vesicles. The jump in the emission from the basic form and corresponding drop in the emission for the acid form establishes that the vesicles had largely maintained the pH gradient to this point in the experiment. The area boxed between 100-120 seconds is expanded in the offset

graph and it is important to note that the data points collected for the two excitations are staggered over time.

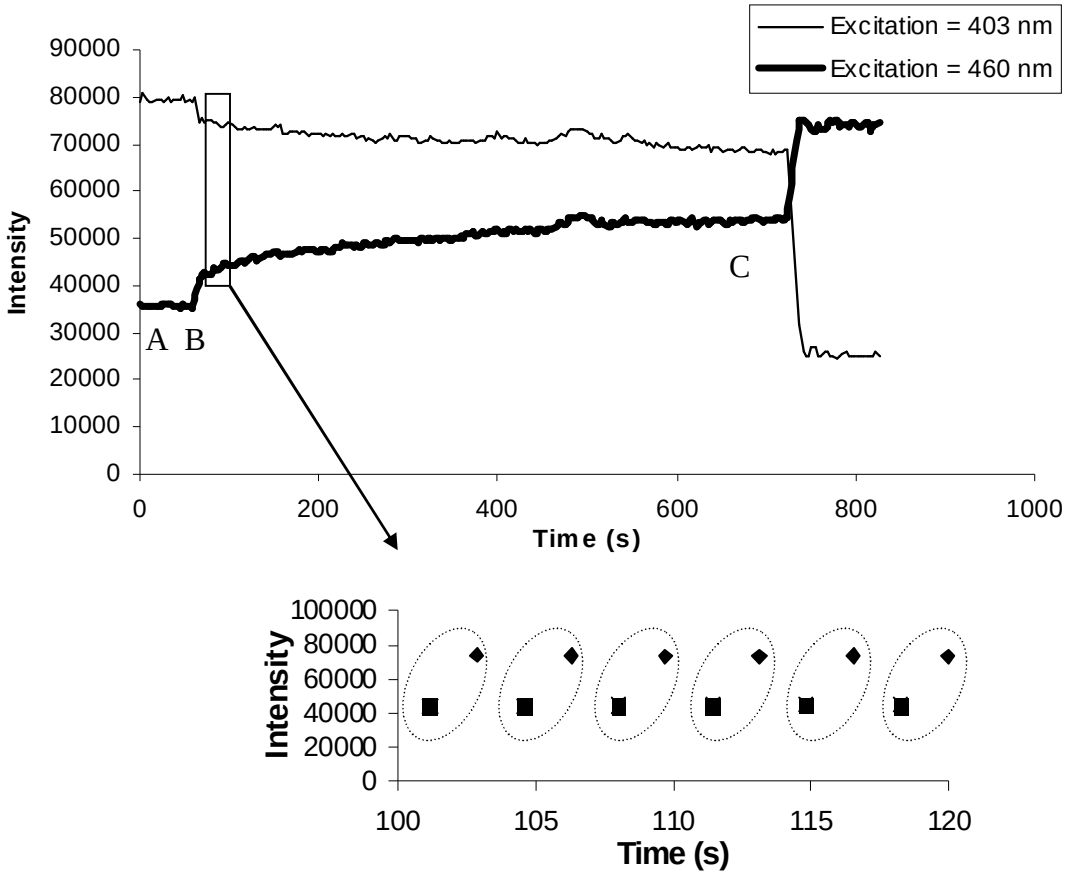

Figure 4-3. Typical HPTS fluorescence data collected from HPTS/vesicle experiments.

The two sets of data for each wavelength can be combined using the relationship of E_{403}/E_{460} and plotted as a function of time (Figure 4-4). Since the data between the excitation wavelengths were not collected at the same instant in time, the average time for each set of consecutive E_{403} and E_{460} measurements was used to represent the time for each E_{403}/E_{460} data point (the offset of data points are circled in the magnified graph in Figure 4-3).

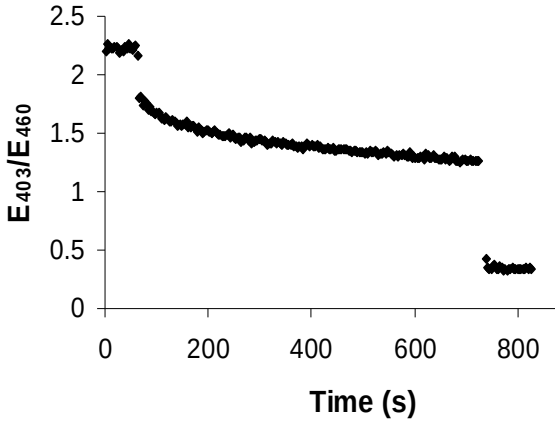

Figure 4-4. Ratio plot of E_{403}/E_{460} versus time for the data collected in Figure 4-3.

The conversion of the ratio plot of E_{403}/E_{460} to internal pH (pH_{in}) was done by applying the data to equation (4-3). When done using the data from Figure 4-4, a graph is constructed as in Figure 4-5.

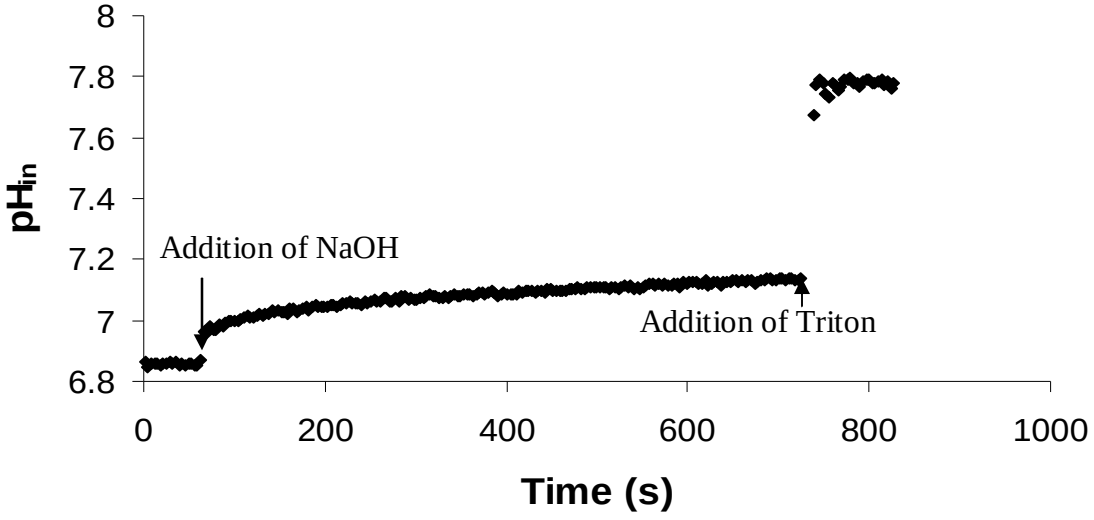

Figure 4-5. A plot of the internal pH (pH_{in}) versus time.

In Figure 4-5 there is a steep jump of about 0.1 pH units from the addition of an aliquot of NaOH. Within the first 100 seconds following the base addition a much slower increase pH followed a curved line, afterwhich the pH appeared to increase linearly until

the point that Triton was added. A bigger pH jump (about 0.7 units) was induced when Triton was added because of vesicle lysis. Since there is a linear section in the pH curve over time, then the transport can be assumed to follow some first order process.

4.2.1 Processing Data using pH Relationship

In principle, the ratio of emission intensities can be related to the internal buffer pH of the vesicle. This approach has been previously described in the above section and in the literature[83]. At present, most of the literature uses the pH_{in} vs. time graph (Figure 4-5) to compare the activities between channel compounds. Rarely is it possible to find cases where rate constants have been calculated. In this thesis, deriving the actual rate constant was of interest because the activity between channels needed to be compared. Each transport experiment for a compound tested takes about 20 minutes to run and with many compounds, this is a significant amount of time. As well, experimentally the vesicles vary from batch to batch, making it difficult to compare the data between batches. There are just too many compounds to deal with qualitatively and therefore the more simple qualitative approach (plotting pH_{in} vs. time) is not sufficient.

From the internal pH graph (Figure 4-5), the rate of proton efflux or hydroxide influx can be determined. To measure the transport rate constant for such a process, the data in the region of time from the end of the addition of the pH pulse to just before the addition of Triton was examined. The external pH was determined using equation (4-3) and applied to the fluorescence data attained after vesicle lysis. It was assumed that the external pH remained constant even with the transport of proton or hydroxide because of the large base excess. From the pH_{in} calculations (and any pH in general), the

concentration of protons can be calculated at any instant in time using the general equation (4-4).

(4-4) $pH = - \log[H^+]$

The transport process was linear in pH_{in} versus time which indicated a pseudo first order decay process. If this is the case then equation (4-5) should apply. This is similar to other vesicles assays, such as those using pH-stat measurements.[25]

(4-5) $$\ln\left(\frac{[H^+]_{in} - [H^+]_\infty}{[H^+]_o - [H^+]_\infty}\right) = -kt$$

In equation (4-5), $[H^+]_{in}$ is the proton concentration in the internal buffer as calculated using equation (4-4) at time (t) taken as the average between two data points. For the transport processes which followed a pseudo-first order process, following the addition of NaOH, the ion transport process (pH) plateaus after about 500 seconds. After the plateau process has been reached then the vesicles were lysed with Triton. The point just before the addition of Triton is termed $[H^+]_o$. For zero order reactions where no plateau occurs, then vesicles are arbitrarily lysed by about 750 seconds and the point just before vesicle lysis is labelled $[H^+]_o$ (about 720 seconds in Figure 4-5). $[H^+]_\infty$ is the proton concentration after vesicle lysis which is calculated from the resultant pH after the vesicles have been lysed; k is the transport rate constant.

The Triton used for these experiments was delivered as a solution of 5% in water neutralized to the same pH as the buffer solution after equilibration with the aliquot of NaOH (pH of 7.4). The 5% Triton solution made from the commercial reagent and water is slightly acidic and induces a pH drop of about 0.2 units if not neutralized. Since the extent of transport was measured, then a drop in pH was due to the release of protons from the vesicles when the neutralized Triton was used. The unneutralized Triton caused

a drop in the pH which overlapped with the protons released by the unreacted vesicles and therefore be a poor representation of what was entrapped in the remaining vesicles.

If the transport follows a pseudo-first order process, then plotting ln $(([H^+]_{in}-[H^+]_\infty)/([H^+]_o-[H^+]_\infty))$ versus time will be a linear function and the slope should be k. Using the pH data from Figure 4-5 during the transport process between approximately 200-650 seconds and applying equation (4-5) results in Figure 4-6. The data prior to 200 seconds includes mixing time and equilibration time. The found rate constant (k) for this particular example was $5.7 \times 10^{-4}\ s^{-1}$.

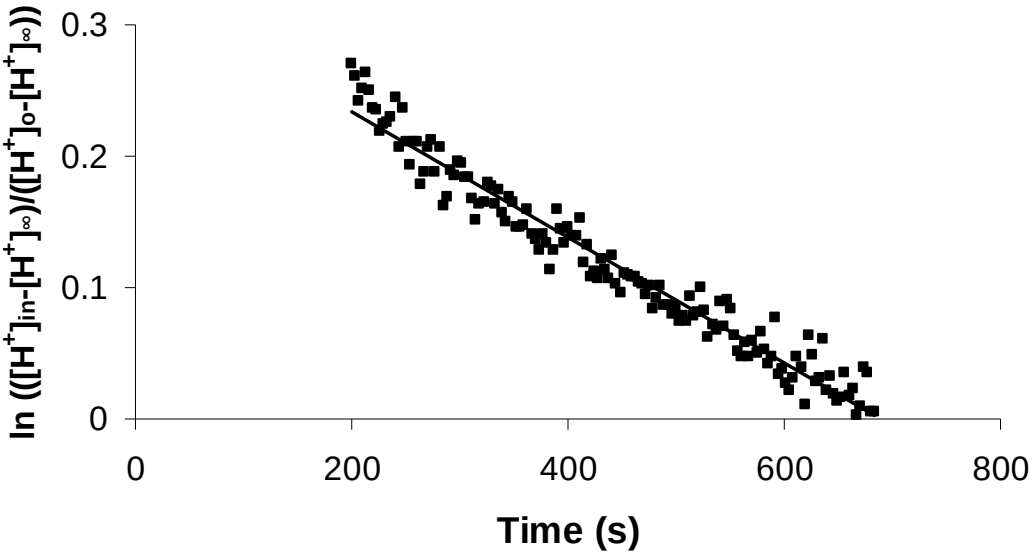

Figure 4-6. Typical first order analysis of data from Figure 4-5.

Applying the method of using the pH to some sample data is shown here. To a vesicle mixture, a solution of **2-27** was added such that the bulk concentration (compound concentration in the external buffer solution) of **2-27** was 5.6 μM (1.3 mol % in lipid). The conversion of the fluorescence emission intensities to pH was achieved by using equation (4-3). The pH was plotted against time from the pH jump and the equilibration of the vesicles, which was normally about 100 seconds (Figure 4-7 A). From the pH

values the internal and external proton concentrations were calculated and the natural logarithm of the difference was calculated and plotted versus time (Figure 4-7 B). The value for the slope (rate constant) is 4.7 x 10^{-4} s^{-1}.

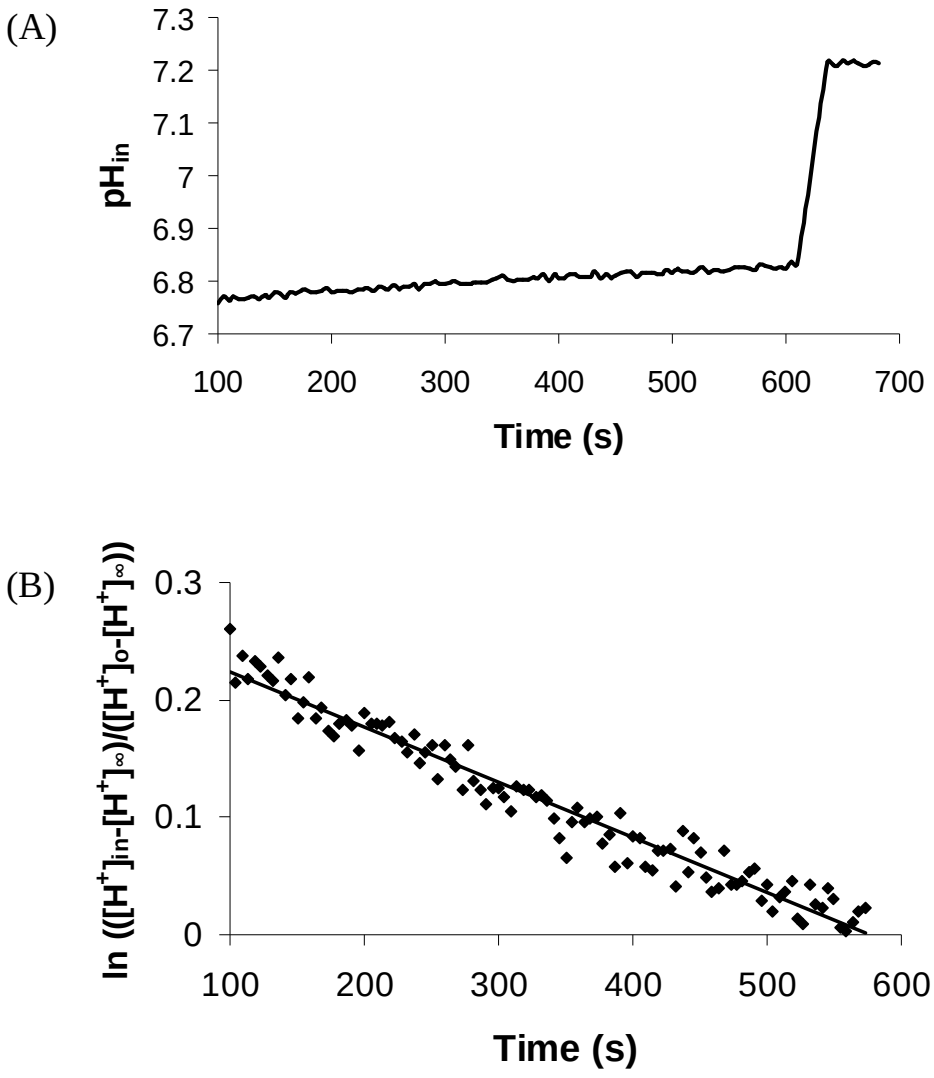

Figure 4-7. Derivation of rate constant for **2-27** (5.6 μM,1.3 mol %) (A) Plot of pH_{in} versus time. (B) Analysis of the pseudo first order rate constant.

Several compounds were treated with the pH method and the results have been tabulated in Table 4-1.

Table 4-1. Summary of data using pH method analysis to attain rate constants.

Compound	Bulk Concentration (μM)	Concentration Relative to Lipid (mol %)	k (x 10^4 s^{-1})
2-27	5.6	1.3	4.7 ± 0.9
2-35	4.1	1.0	9.2 ± 2.5
2-39	29.6	7.1	3.4 ± 0.7
2-25	34.4	8.3	2.1 ± 0.5

4.2.2 Processing Data using Normalized Concentration

Transformation of data from the ratio of emission intensities to the transport rate constant requires using the pH relationships. The pH method takes the E_{403}/E_{460} ratio and via a linear transformation gives the pH_{in}. From the pH_{in}, an antilog relationship can be applied to give the concentration of internal protons. The internal protons at various stages of the transport process are used in a logarithmic relationship to give a normalized value. The various normalized values are linearly related to k. Since some of these mathematical transformations can offset each other then it is possible to bypass the first three transformations and leave only a linear transformation of the emission intensity data to get to a transport rate constant. However, there is the normalization condition incorporated in (4-5) that must be considered. In Figure 4-8 the E_{403}/E_{460} is plotted versus averaged time for several concentrations of **2-27** using the same batch of vesicles but different experiments.

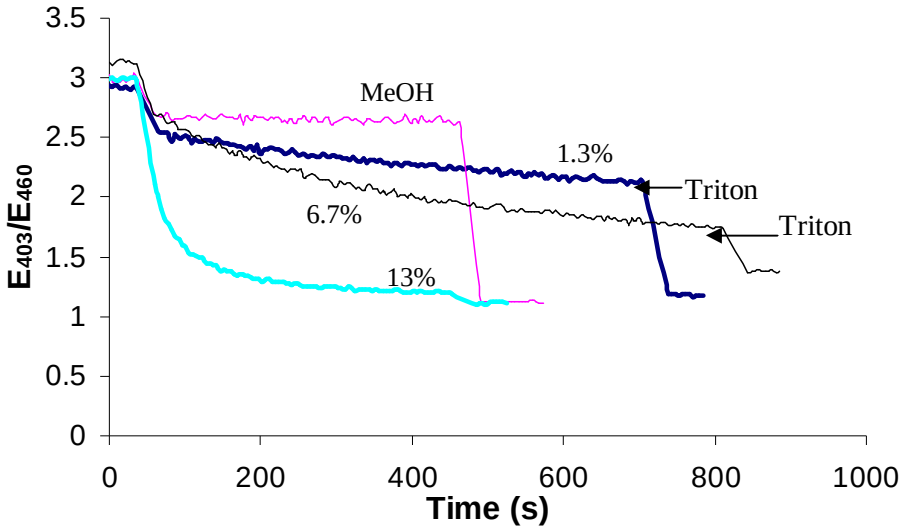

Figure 4-8. Plot of E_{403}/E_{460} versus time for various concentrations of **2-27**.

The traces in Figure 4-8 start and end at different levels on the E_{403}/E_{460} axis. The slopes for these traces are also negative. Therefore, treatment of the data to normalize the curves gave a better representation of the data and also satisfied the normalization condition in the pH data treatment. The normalization process can be accomplished using equation (4-6) to give the "normalized extent of transport" from the E_{403}/E_{460} ratio.

(4-6) $$\text{Normalized Extent of Transport} = \frac{\left(\frac{E_{403}}{E_{460}}\right)_t - \left(\frac{E_{403}}{E_{460}}\right)_o}{\left(\frac{E_{403}}{E_{460}}\right)_\infty - \left(\frac{E_{403}}{E_{460}}\right)_o}$$

The term $(E_{403}/E_{460})_t$ is the ratio of the pair of points at an instant in time t; $(E_{403}/E_{460})_o$ is the average of the emission intensity ratio prior to the addition of base and $(E_{403}/E_{460})_\infty$ is the emission intensity ratio after the vesicles have been lysed (100% transport). Experiments can be compared by setting the initial and final E_{403}/E_{460} ratio equal to 100% transport.

Applying the data in Figure 4-8 to get a normalized extent of transport versus time graph gave traces with positive slopes and the shape of the curves resembled closely to the pH_{in} versus time graphs (Figure 4-9).

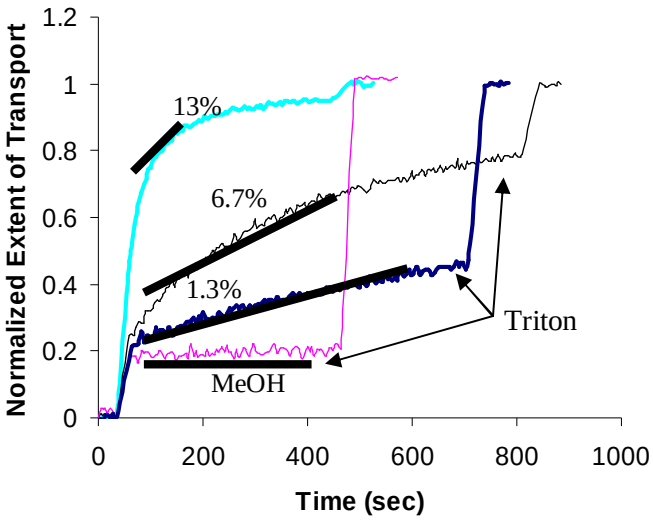

Figure 4-9. Plot of normalized extent of transport versus time for **2-27** at concentrations of 1.3, 6.7, and 13 mole % to lipid.

The rate constant was calculated from the slope of the transport period using a plot of normalized extent of transport versus time (typically 100-800 seconds). The extent of transport is capable of determining the rate constants at relatively low transporter concentrations. For slower transport processes, generally a trend line is inserted between 100-800 seconds to yield the k. Overall, the method of deriving k using the normalized extent of transport can be useful only with relatively slow rates where the pH gradient is relatively constant. For example, in Figure 4-9 at 13 mol%, **2-27** would finish the transport process in about 250 seconds from the time of base injection. Therefore the rate constant for such a concentration would have to be measured within a very short time frame (between 100-180 seconds). This very fast rate was usually a sign that the pH gradient collapsed so the first order approach would not work effectively. For

some concentrations of transporter such as 6.7% of **2-27** in Figure 4-9 the line would not be strictly linear between 100-800 seconds. At this concentration, the ion transport was still considered first order but in such a situation, the rate constant was calculated by using the data between 100-400 seconds.

Generally the slope of the transport process increases with increasing concentration and therefore can be plotted in a linear relationship Figure 4-10.

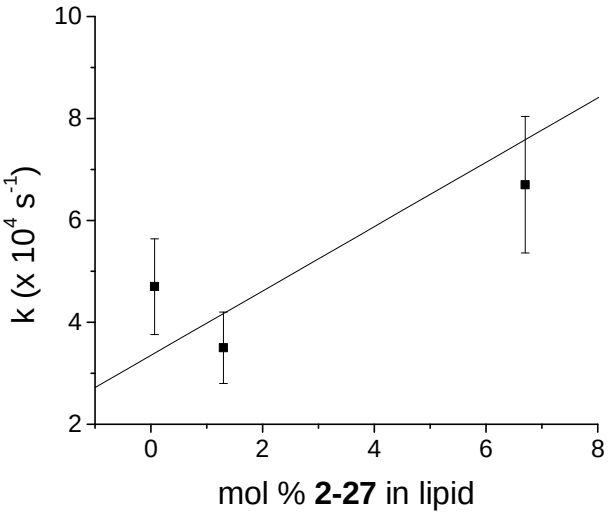

Figure 4-10. Rate constants as a function of mol % of **2-27** in lipid using the emission intensity ratio method for determining k.

The k was found for compound **2-27** in the same dataset using the pH and emission intensities ratio method. A summary of the transport rate constants found with varying **2-27** concentrations is shown in Table 4-2.

Table 4-2. Comparison of rate constants for different concentrations of **2-27** calculated by pH and emission intensity ratio methods.

[2-27] Relative to Lipid (mol %)	**k [a] (x 10^4 s^{-1}) (pH method)**	**k [a] (x 10^4 s^{-1}) (emission intensity ratio method)**
0.067	7.3 ± 1.5	4.7 ± 0.9
1.3	5.7 ± 1.1	3.5 ± 0.7
6.7	17.0 ± 3.4	6.7 ± 1.3

[a] Errors calculated based on statistics of 20% error.

The calculated transport rate constants are similar within error for concentrations of 0.067 and 1.3 mol%. The rate constants derived by either method are very sensitive to where the slope is defined in the transport process. This would help explain why there are some large errors in the rate constants. The important point is that the relationship between transporter concentration and observed rate constant is consistent between methods (i.e. the observed rate constant increases with increasing transporter concentration).

There was always a steep jump in the normalized extent of transport (circle in Figure 4-11) when the pH gradient was generated. It is possible, but unlikely, that the jump is due to HPTS dye in the external buffer. The vesicles went through a GP-10 column (gel permeation column) so the dye was removed from the vesicle fraction collected. The jump might be due to a "pH shock" that splits a few vesicles and releases protons. However, in some cases the "jump" appears to be relatively slow and occurs over 20-100 seconds. Qualitatively this appears to be a fast step (circled region) followed by a slow step. The total height of the curve in Figure 4-11 after vesicle lysis is omitted so that the biphasic curve can be expanded.

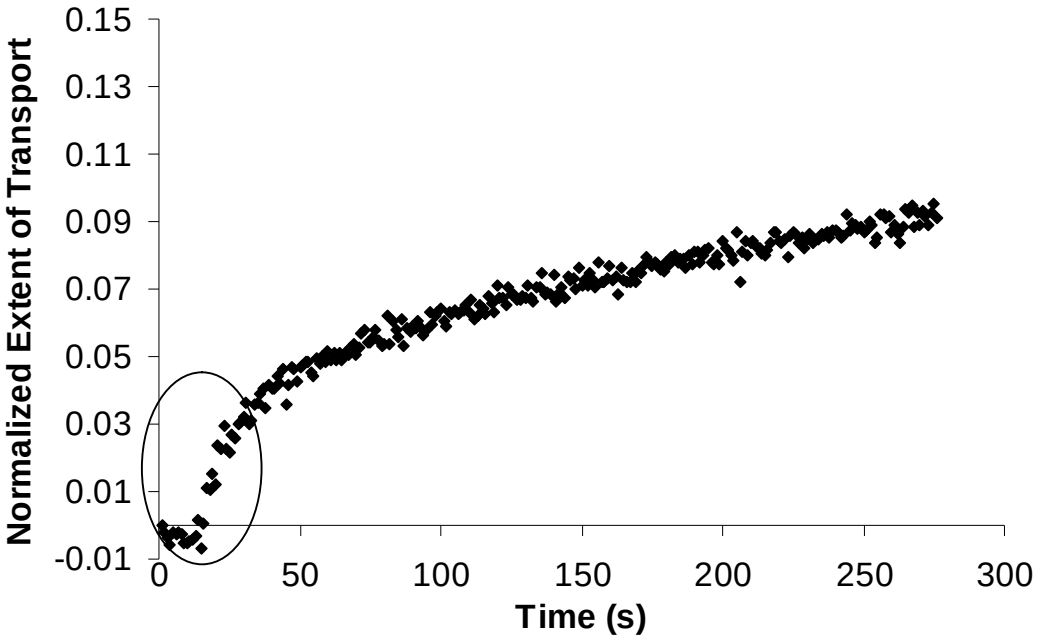

Figure 4-11. Methanol injected (25 µL) into a vesicle solution show a biphasic nature in proton leakage.

Chiu studied the proton permeability into uni- and multilamellar vesicles by measuring the quenching rate of encapsulated carboxyfluorescein dye fluorescence.[86] A large pH gradient of 5.5 pH units was induced with base. Similar to what we observed in Figure 4-11, Chiu observed a biphasic transport process (starting with a steep and short slope (rate constant) for the first 50 seconds and then decreasing to a shallower slope). He proposed that the steep jump was due to pores that randomly form in the membrane. This first process is the relief of the osmotic pressure (vesicles swelling from the influx of water because carboxyfluorescein was inside the vesicles) and electrical gradient (there was an ion concentration difference between inside and outside of the vesicles). The second process (called the solubility-diffusion stage[87]) is a much slower process and occurred after the first because it depends on the exchange of a proton from the external buffer with an alkali ion from the internal buffer to collapse the chemical gradient while

maintaining electrical neutrality. Therefore, in our observed "initial jump" in Figure 4-11, the initial steep slope was proposed as the result of the transient pore mechanism due mostly to the lipids on their own (between 50-100 seconds) followed by the solubility-diffusion mechanism of transport (between 100-490 seconds) related and altered by the action of the channel compound and other lipid leakage processes.

As a practical issue the first 100 seconds worth of data was ignored in the linear fits of all data. Whether the initial stage was due to transient pore formation, pH shock lysis, or due to a small amount of external HPTS, it had no bearing on the rates of the slower process discussed. Recall that the first process was usually over within the first 50 seconds and the slower process lasted for about 600-800 seconds. The one issue with the first process was when high transporter concentrations were used and the transport process was fast and therefore overlapped with the first process. This sets an upper limit on the rates that can be determined by the method.

4.2.2.1 Interpolating Rate Constants

All of the ion channel candidates are introduced in a methanol solution (30 µL). For most of the vesicle batches, this amount of methanol (without ion channels) will lead to a small rate of "background leakage". As a consequence, for every new batch of vesicles, a blank run (methanol only) was tested to determine the leakage rates.

In Figure 4-12 the transport period for various concentrations of **2-27** is shown and the determined transport rate constants are tabulated in Table 4-3.

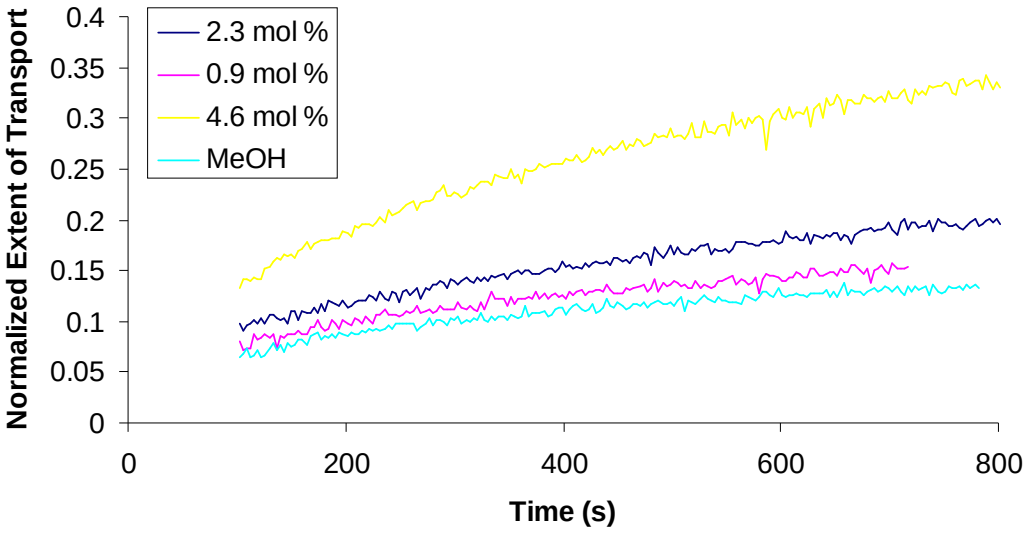

Figure 4-12. Plots to derive the transport rate constants for various concentrations of **2-27.**

Table 4-3. Tabulated rate constants from data in Figure 4-12.

[2-27] Relative to Lipid (mol %)	**k [a] (x 10^4 s^{-1})**
MeOH (0 mol %)	0.9 ± 0.2
0.9	1.2 ± 0.2
2.3	1.4 ± 0.3
4.6	2.5 ± 0.5

[a] Errors calculated based on about 20% error in the experiment.

In cases where relatively slow transport processes are observed, these are proposed to be a combination of transport by the transporter and the solubility-diffusion process. To test if this is that case, the rate constant for ion transport by methanol can be measured and compared with the transport by a low transporter concentration. If the hypothesis is valid, then at almost any transporter concentration, the observed rate constant should be larger than the leakage caused by the methanol.

Transport data was collected for various concentrations of **2-27** and the rate constants ($k_{[x]}$) at a particular concentration ([x]) were plotted in Figure 4-13. Figure 4-13 shows a trend line with an equation (4-7).

(4-7) $k_{[x]} = 0.34 \times [\mathbf{2\text{-}27}] + 0.84$

In the equation of the trend line, [**2-27**] is expressed as a mol % in lipid. However, there is some flexibility with this variable and it can also be expressed in μM of **2-27** in the bulk solution which can then change the slope. The intercept of 0.84 x 10^{-4} s^{-1} is very close to the transport rate constant for methanol for this batch of vesicles (0.9 x 10^{-4} s^{-1}). Therefore the conditions under 5 mol % are considered "low concentration conditions" and a linear relationship is found.

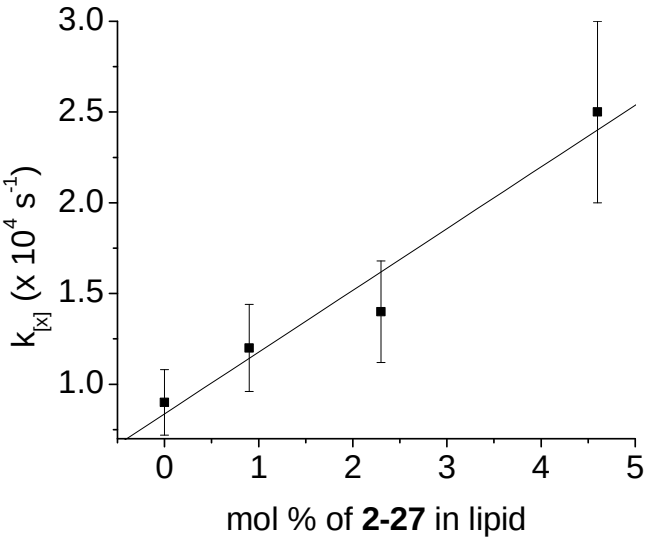

Figure 4-13. The linear relationship between transport rate constant ($k_{[x]}$) and [**2-27**].

The main differences in vesicles on a day-to-day basis were lipid concentration and the background leakage caused by methanol. Therefore in order to compare data from separate days and vesicle experiments, a method is required to be able to determine a consistent rate constant based on a concentration.

The linear relationship found for **2-27** can be generalized to equation (4-8) which is the relationship between the transport rate constant ($k_{[x]}$) and transporter concentration ([Tr]) and rate constant by methanol (k_{MeOH}). The value of this equation is that a slope (m_s) for the linear fit can be derived and hence it is possible to interpolate or extrapolate a rate constant for a specified concentration. Extrapolation should not be done because the data may not be linear at higher concentrations.

(4-8) $$k_{[x]} = m_s \times [Tr] + k_{MeOH}$$

If the intercept and slope are known in equation (4-8), then the rate constant at a transporter concentration can be derived. The slope is found by plotting at least two to three points on the $k_{[x]}$ vs. [Tr] curve. The y-intercept can either be found graphically, or if there are not enough data points, then it can be approximated as the rate constant caused by methanol (background leakage).

Due to the practical limitations of time and vesicle batch size resulted in only two or three different concentrations were examined for each ion channel candidate. In this case, the observed rate constant for methanol can be used for k_{MeOH}. When sufficient fluorescence data was available with several concentrations of transporter, then k_{MeOH} was determined as the intercept from plotting the various concentrations with the rate constants. On a given day the MeOH leakage rate determined at various times and varied from vesicle batch to batch; the average rate constant over eight batches spanning 15 months was $(2.4 \pm 1.1) \times 10^{-4}\ s^{-1}$.

The concentration of lipid also varied from batch to batch. In the vesicle experiments, the average concentration of lipid was 0.43 ± 0.05 mM as determined by the Bartlett assay.[2] For our experiments the span in the lipid concentration was only about

12%. For triplicate transport readings of the same channel candidate (at the same concentration), the reproducibility of the determination of k was typically ± 20%. Therefore given the poor precision of the transport results, the maximum 12% difference in lipid concentration really was not that concerning. Given the imprecision in rate constants, a transport rate constant of at least 1.5 times the k_{MeOH} would be considered marginally significant and at least 2 times the k_{MeOH} would it be considered significantly different from background.

In the vesicle assays, an equilibration time of 30-60 seconds was used for the mixing of the channel candidate with the vesicles. In comparing two different structures: **2-27** and **2-39**, the results showed that 30-60 seconds was sufficient for **2-27** to partition into the bilayer membrane and showed some activity (Figure 4-14).

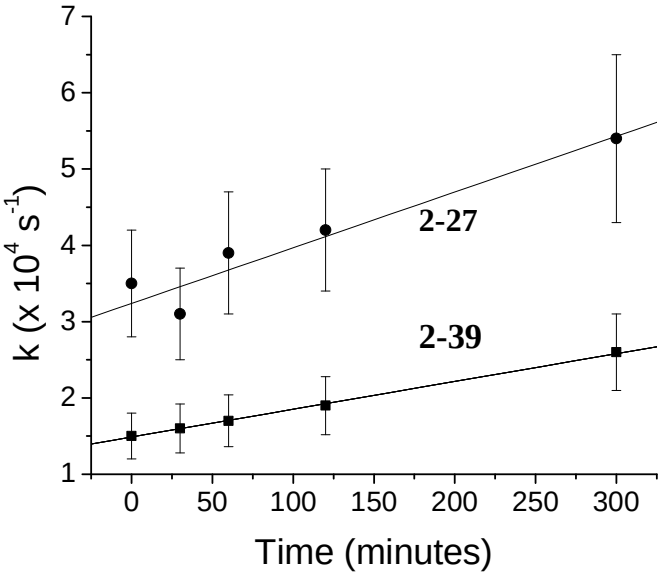

Figure 4-14. Comparison of transport activity as a function of equilibration time for channels **2-39** (1.8 mol %, 12 μM) and **2-27** (0.86%, 5.7 μM).

Within five hours, both compounds appear to increase proportionally in rate constant but are within the 20% error so really the increase may be marginally significant.

This result shows in effect the vesicles “dying” over time and is therefore more prone to leakage. Therefore on a given experiment day, the absolute rate constant for a compound varied depending on when the compound was tested. Therefore the comparison of the absolute rate constants may not be appropriate if the compounds were tested at different times.

Many of the ion channel candidates were made in a range of yields and low quantity, so it was not always practical to make a standard concentration for all the compounds. However since the normalized method of data analysis was used, then the stock concentration was irrelevant as long as there was a linear relationship of the bulk concentration to the rate constants.

There are advantages for the normalized extent of transport method over the pH method. There is no need to do as many mathematical transformations with the data, the ability to find a rate constant at a given concentration, and the background leakage caused by methanol is taken into account in the rate constants. It would be possible to normalize the pH data such that many of these advantages could carry over, but as noted above, the additional calculations are simply extra compared to the extent of transport method. Therefore we have adopted the more convenient approach of using the ratio of intensities to get normalized data.

4.3 Using Normalized Data Method for Ion Channel Candidates

Since most of the transport data was linearly proportional to concentration, the task of deriving a normalized transport rate constant ($k_{32\ uM}$) was relatively straight-forward once a concentration was decided upon for comparison. All of the normalized

data (Table 4-4) discussed in this section are the key numbers taken from section 7.2.5. Please consult section 7.2.5 for a complete dataset.

Table 4-4. Summary of transport rate constants found at certain concentrations using the normalized extent of transport method and a normalized transport rate constant at 32 μM.

Entry	Transporter	$[Tr]_{Bulk}$ (μM)		k (x 10^4 s^{-1})		average $k_{32\ \mu M}$ (x 10^4 s^{-1})
		[Low]	[High]	$k_{[low]}$	$k_{[high]}$	
1	**2-27**	8.4	53	3.6	10.1	6.1 ± 1.7
2	**2-35**	9.0	90	4.4	25.0	12 ± 4
3	**2-39**	26	127	0.8	7.5	1.5 ± 0.7
4	**2-25**	39	75	0.48	0.93	0.7 ± 0.1
5	**3-1**	17	49	4.7	6.2	6.3 ± 2.1
6	**3-2**	28	-	2.9	-	3.0
7	**3-3**	14	46	2.7	3.5	3.9 ± 1.4
8	**2-24**	7	66	4.7	10.0	29 ± 4
9	**3-4**	25	41	3.1	3.0	3.1 ± 0.5
10	**2-36**	19	49	3.0	3.9	3.6 ± 0.3
11	**3-8**	49	-	3.9	-	3.3
12	**2-38**	42	-	3.2	-	3.0
13	**3-9**	56	-	1.9	-	2.1
14	**3-7**	31	-	2.2	-	2.1
15	**2-48**	15	49	2.7	2.4	2.6 ± 0.2
16	**3-11**	16	41	6.8	6.4	6.7 ± 4.1
17	**3-16**	18	44	3.8	5.9	4.1 ± 1.7
18	**3-17**	17	42	2.7	4.5	3.9 ± 0.1
19	**3-12**	19	37	3.9	6.7	7.6 ± 2.2
20	**3-14**	27	32	2.0	2.0	2.0 ± 0.4
21	**1-18**	9	32	4.3	23	16 ± 6
22	Gramicidin	3.9e-3	-	1.9	-	>1000

The normalized transport rate constant ($k_{32\ \mu M}$) was calculated at 32 μM because on average all of the compounds tested are active at this concentration and there is sufficient concentration vs. k data to interpolate a $k_{32\ \mu M}$.

To demonstrate the use of the normalized data method, **2-27** is the example compound. The information needed to get to the normalized rate constant is tabulated in Table 4-4. The "rate constant" ($k_{[\mathbf{2\text{-}27}]}$) was the observed rate constant for the particular bulk ion channel concentration ($[\mathbf{2\text{-}27}]_{Bulk}$).

To calculate $k_{32\ uM}$, firstly three two-point lines are constructed using the methanol rate constant (k_{MeOH}) and the rate constant (k) for each concentration. The slope of these lines will give the variable "m_s". Mathematically this can also be calculated using equation (4-9).

(4-9) $$m_s = \frac{k_{[Tr]} - k_{MeOH}}{[Tr]}$$

Substitution of 32 μM into [Tr] of equation (4-9) when m_s and k_{MeOH} are known will leave only one variable, $k_{32\ uM}$. Solving for this variable will give the normalized rate constant, 6.6 ± 1.3 s^{-1}, at 32 μM.

The errors associated with any of the rate constants from the normalized method are about 20%, so some of the values for comparison are not significantly different.

With the many compounds made in the previous chapters, they can be grouped into categories to address general structure-activity related questions: short sequences, constitutional isomers, variations in lipophilicity on head group, variations in internal core length, effects by the number of esters, and appending another lipophilic head group.

Short sequences are shorter components such as dimers, trimers of a longer sequence (tetramer). Constitutional isomers have all the same building blocks but just modification of their locations within the structure. Variations in lipophilicity on head group are explored by changing the lipophilic tail on the glutaric acid head group. Variations in core length can probe for activity related to shortening and lengthening the three core units. The effects by the numbers of core esters are explored by varying the number of ester functionalities. Finally increasing the lipophilicity of the overall ion channel candidate by appending another head group with more lipophilic character is examined for transport activity.

For simplicity and clarity, the compound names have been changed from here onwards so that they better represent the structure (Table 4-5).

Table 4-5. Descriptive nomenclature for each compound discussed.

Transporter	New name	Transporter	New name
2-24	Oct_H-$G12_T$	**3-3**	Oct_H-Dod_C-Oct_C-$G16_T$
2-25	Oct_H-Dod_T	**3-4**	Oct_H-Oct_C-Dod_C-$G12_T$
2-27	Oct_H-Dod_C-Oct_C-$G12_T$	**3-7**	Dod_H-Dod_C-Dod_C-$G12_T$
2-35	Dod_H-Oct_C-$G12_T$	**3-8**	Dod_H-Dod_C-Oct_C-$G12_T$
2-36	Dod_H-Oct_C-Oct_C-$G12_T$	**3-9**	Oct_H-Dod_C-Dod_C-$G12_T$
2-38	Oct_H-Oct_C-Oct_C-$G12_T$	**3-11**	Hex_H-Oct_C-Hex_C-Oct_C-$G12_T$
2-39	Oct_H-Dod_C-Oct_T	**3-12**	Oct_H-Dod_C-Oct_C-Lau_T
2-48	$G12_H$-Oct_C-Dod_C-Oct_T	**3-14**	Oct_H-Dod_C-Oct_C-Oleic acid
3-1	Oct_H-Dod_C-Oct_C-$G10_T$	**3-16**	Lau_H-Oct_C-Dod_C-Oct_C-$G12_T$
3-2	Oct_H-Dod_C-Oct_C-$G14_T$	**3-17**	Ole_H-Oct_C-Dod_C-Oct_C-$G12_T$

4.3.1 Transport Results from Dimers and Trimers

One of the goals of thesis was to develop a method to generate ion channel candidates easily. The shorter sequences generated only had two or three building blocks coupled together. It was of interest to know if the shorter sequences (Oct_H-Dod_T (**2-25**), Oct_H-Dod_C-Oct_T (**2-39**), Dod_H-Oct_C-$G12_T$ (**2-35**), and Oct_H-$G12_T$ (**2-24**)) are active transporters on their own.

From Table 4-4 the shorter compounds of Oct_H-Dod_T (**2-25**) and Oct_H-Dod_C-Oct_T (**2-39**) are not active transporters. However the dimeric Oct_H-$G12_T$ (**2-24**) and trimer Dod_H-Oct_C-$G12_T$ (**2-35**) are much more active by comparison. The correlation between these two findings is presumed to be that the compounds must have some degree of lipophilicity in order to partition into the bilayer. Compounds Oct_H-Dod_T (**2-25**) and Oct_H-Dod_C-Oct_T (**2-39**) may not have enough lipophilicity and so they poorly partition into the bilayer membrane and therefore leading to poor transport activity.

Of interest is the activity for Oct_H-Dod_C-Oct_C-$G12_T$ (**2-27**) compared with shorter Oct_H-$G12_T$ (**2-24**) and Dod_H-Oct_C-$G12_T$ (**2-35**) because these three compounds differ in length yet the activity is comparable or even greater for the shorter compounds (Oct_H-$G12_T$ (**2-24**) and Dod_H-Oct_C-$G12_T$ (**2-35**)) than Oct_H-Dod_C-Oct_C-$G12_T$ (**2-27**). One key component is the $G12_T$ unit which is a component in all of the highly active compounds, once again suggesting that the lipophilic component plays a big role in the membrane partitioning and activity. Despite the activity observed for these shorter sequences, they are unlikely structures in the tetrameric products. Therefore they do not compromise the conclusions for longer sequences. In the purity analysis of some other tetramers, structures like Oct_H-Dod_C-Oct_T (**2-39**) were observed. These common impurities are not

very active, and therefore the activity of synthetic products can be assumed to reflect contributions from the targets unaffected by the contaminants.

4.3.2 Transport Results from Constitutional Isomers

Using the three building blocks Dod, Oct and G12 many isomers can be made in a tetrameric arrangement. When the dodecyl tail was kept constant in the structure, but the Dod_C/Dod_H unit was moved around to generate the isomers.

Table 4-6. Tabulated data for the ion transport abilities by constitutional isomers.

Transporter	**$k_{32\mu M}$ (x 10^4 s^{-1})**
Oct_H-Dod_C-Oct_C-$G12_T$ (**2-27**)	6.1 ± 1.7
Dod_H-Oct_C-Oct_C-$G12_T$ (**2-36**)	3.6 ± 0.3
Oct_H-Oct_C-Dod_C-$G12_T$ (**3-4**)	3.1 ± 0.5

The data in Table 4-6 shows that the order of increasing activity was Oct_H-Dod_C-Oct_C-$G12_T$ (**2-27**) > Dod_H-Oct_C-Oct_C-$G12_T$ (**2-36**) = Oct_H-Oct_C-Dod_C-$G12_T$ (**3-4**).

Tetramer Oct_H-Dod_C-Oct_C-$G12_T$ (**2-27**) is substantially more active than either of the two constitutional isomers and the rationale is related to the integrity of Dod_H-Oct_C-Oct_C-$G12_T$ (**2-36**) and Oct_H-Oct_C-Dod_C-$G12_T$ (**3-4**). The integrity of Oct_H-Dod_C-Oct_C-$G12_T$ (**2-27**) was much higher than either of the other two isomers (which are mostly contaminated with trifluoroesters of the deletion sequences). The transporter concentrations prepared for ion transport studies were based on mass recovery and assumed to be from the transporter only with no impurities present. Therefore the effective concentration of Dod_H-Oct_C-Oct_C-$G12_T$ (**2-36**) and Oct_H-Oct_C-Dod_C-$G12_T$ (**3-4**) was much lower than the effective concentration of Oct_H-Dod_C-Oct_C-$G12_T$ (**2-27**). The

integrity of Dod_H-Oct_C-Oct_C-$G12_T$ (**2-36**) and Oct_H-Oct_C-Dod_C-$G12_T$ (**3-4**) was about the same (60% and 67%, respectively) and so it was not surprising that the activities were about the same. The normalized rate constants were calculated again taking into account that Dod_H-Oct_C-Oct_C-$G12_T$ (**2-36**) and Oct_H-Oct_C-Dod_C-$G12_T$ (**3-4**) had integrity of about 60% and 67%, respectively. Assuming that the impurities had null activity, the transporter concentrations reported in Table 4-4 were multiplied by 82%, 60%, and 67% for Oct_H-Dod_C-Oct_C-$G12_T$ (**2-27**), Dod_H-Oct_C-Oct_C-$G12_T$ (**2-36**), and Oct_H-Oct_C-Dod_C-$G12_T$ (**3-4**), respectively. The rate constants at these concentrations do not change but the normalized rate constant at 32 μM varies from the calculated value before. These results are tabulated in Table 4-7.

Table 4-7. Normalized transport rate constants calculated for 32 μM transporter concentration using integrities increased integrity values.

Transporter	**Adjusted [Tr] (μM)**		**k (x 10^4 s^{-1})**		**Recalculated $k_{32\ \mu M}$ (x 10^4 s^{-1})**
	[Low]	[High]	$k_{[low]}$	$k_{[high]}$	
Oct_H-Dod_C-Oct_C-$G12_T$ (**2-27**)	6.9	44	3.6	10.1	7.0 ± 2.1
Oct_H-Oct_C-Dod_C-$G12_T$ (**3-4**)	17	28	3.1	3.0	3.7 ± 0.7
Dod_H-Oct_C-Oct_C-$G12_T$ (**2-36**)	11	29	3.0	3.9	4.7 ± 0.9

The errors associated with each normalized rate constant are based on the total variations in normalized rate constants calculated from the concentrations tested. At a 99% confidence level all three of the recalculated $k_{32\ \mu M}$ have no statistical differences. However, the reason for this is because the sampling size for Oct_H-Dod_C-Oct_C-$G12_T$ (**2-27**) is greater than that of the other two isomers. The precision for Oct_H-Dod_C-Oct_C-$G12_T$ (**2-27**) is also less than the other two isomers.

For a vesicle experiment where all three isomers were examined on the same day, the data is reported in Table 4-8. The reported transporter concentrations have been adjusted for the integrity. Two concentrations of transporter were available for some of the compounds and the calculated $k_{32\ \mu M}$ have not been averaged just to show the difference in calculated numbers.

Table 4-8. Normalized transport rate constants calculated for 32 μM transporter concentration from same day vesicle experiments.

Transporter	**Adjusted [Tr] (μM)**		**k (x 10^4 s^{-1})**		**Recalculated $k_{32\ \mu M}$[a] (x 10^4 s^{-1})**	
	[low]	[high]	$k_{[low]}$	$k_{[high]}$	Based on $k_{[low]}$	Based on $k_{[high]}$
Oct_H-Dod_C-Oct_C-$G12_T$ (**2-27**)	17	26	2.8	9.5	3.7 ± 0.7	11.3 ± 2.3
Oct_H-Oct_C-Dod_C-$G12_T$ (**3-4**)	17	28	3.1	3	3.2 ± 0.6	4.3 ± 0.9
Dod_H-Oct_C-Oct_C-$G12_T$ (**2-36**)	11		3.0		5.2 ± 1.0	

[a] Error calculated based on statistics of 20% error.

The data in Table 4-8 shows a small variation in $k_{32\ \mu M}$ for all isomers (if the large $k_{32\ \mu M}$ calculated for Oct_H-Dod_C-Oct_C-$G12_T$ (**2-27**) is excluded). The large $k_{32\ \mu M}$ for Oct_H-Dod_C-Oct_C-$G12_T$ (**2-27**) could be the result of unusually high k values for the 26 μM experiment. On the day of the experiment, this sample at 26 μM was examined last and therefore the vesicles may have aged by then and therefore were more susceptible to leakage. Assuming that the high $k_{32\ \mu M}$ from Oct_H-Dod_C-Oct_C-$G12_T$ (**2-27**) can be excluded from the comparison, then the variation in the location of the Dod_C/Dod_H unit has little effect on activity.

Another pair of constitutional isomers is made by placing the G12 unit in the $G12_H$ (to generate $G12_H$-Oct_C-Dod_C-Oct_T (**2-48**)) instead of $G12_T$. The length of $G12_H$-Oct_C-Dod_C-Oct_T (**2-48**) and Oct_H-Dod_C-Oct_C-$G12_T$ (**2-27**) are directly comparable based

on molecular computations (38 Å when measured from the carboxyl terminus to the alcohol in the extended conformation). The transport activity of $G12_H$-Oct_C-Dod_C-Oct_T (**2-48**) is at least a factor of 2 lower than Oct_H-Dod_C-Oct_C-$G12_T$ (**2-27**). The integrity of the $G12_H$-Oct_C-Dod_C-Oct_T (**2-48**) sample is not an issue here because it has an integrity >95% while Oct_H-Dod_C-Oct_C-$G12_T$ (**2-27**) is around 82%.

A potential explanation for the difference in activity between Oct_H-Dod_C-Oct_C-$G12_T$ (**2-27**) and $G12_H$-Oct_C-Dod_C-Oct_T (**2-48**) could be related to how the compounds insert into the bilayer membrane. An assumption is made that the threading of the compound into the bilayer favors one direction over another as shown in Figure 4-15. Chapter 5 discusses our method in exploring the orientation of the channel in the bilayer membrane.

If there is a preference in the ion channel orientation and Oct_H-Dod_C-Oct_C-$G12_T$ (**2-27**) and $G12_H$-Oct_C-Dod_C-Oct_T (**2-48**) insert into the membrane bilayer and orientate in a specific manner, then it would be expected that these two compounds would have different transport activities.

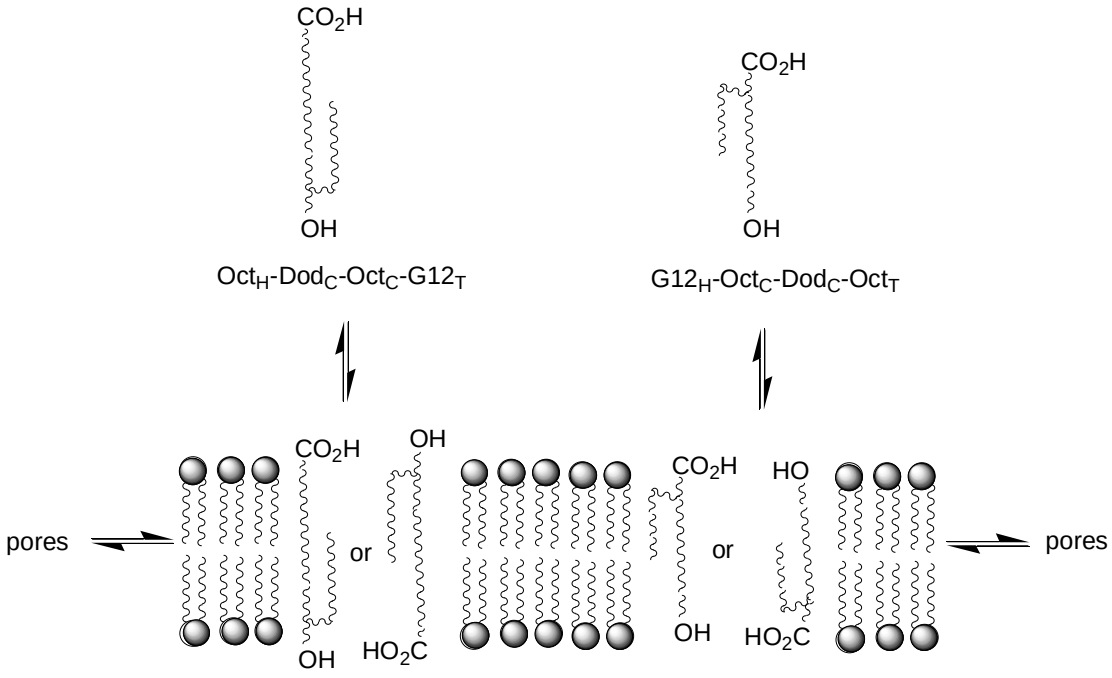

Figure 4-15. Hypothesis for the partitioning of Oct_H-Dod_C-Oct_C-$G12_T$ (**2-27**) and $G12_H$-Oct_C-Dod_C-Oct_T (**2-48**) into the membrane bilayer.

4.3.3 Transport Results from Varying the Core Length

The core length can be modified using only the Dod_C/Dod_H and Oct_C/Oct_H units. The data in Table 4-9 showed that Oct_H-Dod_C-Oct_C-$G12_T$ (**2-27**) was much more active than Oct_H-Dod_C-Dod_C-$G12_T$ (**3-9**), Dod_H-Dod_C-Dod_C-$G12_T$ (**3-7**), Dod_H-Dod_C-Oct_C-$G12_T$ (**3-8**), and Oct_H-Oct_C-Oct_C-$G12_T$ (**2-38**) (the last four compounds have approximately equivalent activity).

Table 4-9. Tabulated data for the ion transport abilities by compounds of varying core length.

Transporter	**$k_{32\mu M}$ (x 10^4 s^{-1})**
Oct_H-Dod_C-Oct_C-$G12_T$ (**2-27**)	6.1 ± 1.7
Oct_H-Dod_C-Dod_C-$G12_T$ (**3-9**)	2.1
Dod_H-Dod_C-Dod_C-$G12_T$ (**3-7**)	2.1
Dod_H-Dod_C-Oct_C-$G12_T$ (**3-8**)	3.3
Oct_H-Oct_C-Oct_C-$G12_T$ (**2-38**)	3.0

With the modification of core length, there appear to be a relationship between core length and activity. It can be postulated that lengthening the core length (four methylene units: Dod_H-Dod_C-Oct_C-$G12_T$ (**3-8**) and Oct_H-Dod_C-Dod_C-$G12_T$ (**3-9**), eight methylene units: Dod_H-Dod_C-Dod_C-$G12_T$ (**3-7**)) affects the monomer aggregation (favoring aggregates due to increased lipophilicity) and therefore these compounds are not as active. By shortening the core (Oct_H-Oct_C-Oct_C-$G12_T$ (**2-38**)) these structures are four methylenes shorter so they may not be long enough to span across a bilayer. To explain the difference in activity between the locations of the Dod_H/Dod_C unit, it was speculated that these compounds should have the same or very close rate constants; however, as mentioned in Chapter 3 the integrity of some of these compounds was under 90%.

The normalized rate constants at 32 μM were recalculated for the compounds in this section and are listed in Table 4-10.

Table 4-10. Recalculated normalized rate constants at 32 μM.

Transporter	Adjusted [Tr] (μM)		k (x 10^4 s^{-1})		Recalculated $k_{32\ \mu M}$ (x 10^4 s^{-1})
	[Low]	[High]	$k_{[low]}$	$k_{[high]}$	
Dod_H-Dod_C-Oct_C-$G12_T$ (**3-8**)	45	-	3.9	-	3.4
Oct_H-Oct_C-Oct_C-$G12_T$ (**2-38**)	17	-	3.2	-	4.0
Oct_H-Dod_C-Dod_C-$G12_T$ (**3-9**)	40	-	1.2	-	2.0
Dod_H-Dod_C-Dod_C-$G12_T$ (**3-7**)	27	-	2.2	-	2.1

In the recalculation of $k_{32\ \mu M}$ unfortunately not enough samples were tested to get an error associated with the values. However on first inspection, Oct_H-Oct_C-Oct_C-$G12_T$ (**2-38**) is more active than the longer analogues. Once again this might hint towards an aggregation issue for the longer compounds.

4.3.4 Transport Results from Varying Number of Esters

The Oct_H-Dod_C-Oct_C-$G12_T$ (**2-27**) structure can be used as the principal structure and the number of esters within the structure can be modified while maintaining roughly the same length. The transport activity of the compounds which were used to probe for the effects of varying the number of esters are summarized in Table 4-11

Table 4-11. Tabulated data for the ion transport abilities by compounds of varying the number of esters in the compound structure.

Transporter	**$k_{32\mu M}$ (x 10^4 s^{-1})**
Oct_H-Dod_C-Oct_C-$G12_T$ (**2-27**)	6.1 ± 1.7
Hex_H-Oct_C-Hex_C-Oct_C-$G12_T$ (**3-11**)	6.7 ± 4.1
Oct_H-Dod_C-Oct_C-Lau_T (**3-12**)	7.6 ± 2.2
Oct_H-Dod_C-Oct_C-Oleic acid (**3-14**)	2.0 ± 0.4

Pentamer Hex_H-Oct_C-Hex_C-Oct_C-$G12_T$ (**3-11**) has an additional ester unit but maintaining the same number of carbons it was found that Hex_H-Oct_C-Hex_C-Oct_C-$G12_T$ (**3-11**) was as active as Oct_H-Dod_C-Oct_C-$G12_T$ (**2-27**) within error. The additional ester functionality may act similarly to natural ion channels where the carbonyl aids in the transport of the ions through a membrane by coordination and solvating the cations which flow through the channel. The length of the core for Hex_H-Oct_C-Hex_C-Oct_C-$G12_T$ (**3-11**) is only one oxygen atom longer than Oct_H-Dod_C-Oct_C-$G12_T$ (**2-27**) so the bilayer membrane may be tolerant to this minor modification.

The structures of tetramers Oct_H-Dod_C-Oct_C-Lau_T (**3-12**) and Oct_H-Dod_C-Oct_C-Oleic acid (**3-14**) have the glutaric acid building block replaced by the lauric acid derivative and oleic acid unit. Comparing these two compounds with Oct_H-Dod_C-Oct_C-$G12_T$ (**2-27**), it was found that in order of decreasing activity: Oct_H-Dod_C-Oct_C-Lau_T (**3-12**) = Oct_H-Dod_C-Oct_C-$G12_T$ (**2-27**) > Oct_H-Dod_C-Oct_C-Oleic acid (**3-14**). This was an interesting finding because Oct_H-Dod_C-Oct_C-Oleic acid (**3-14**) does not have a hydroxyl group. Therefore there is nothing to define how long the core is relative to the lipophilic tail. Compound Oct_H-Dod_C-Oct_C-Oleic acid (**3-14**) may be acting more as a membrane

disrupter (like a detergent) rather than an actual ion channel if our design assumptions are correct. The activities of Oct_H-Dod_C-Oct_C-Lau_T (**3-12**) and Oct_H-Dod_C-Oct_C-$G12_T$ (**2-27**) are comparable and from Chapter 3 it was mentioned that the integrity of Oct_H-Dod_C-Oct_C-Lau_T (**3-12**) was about 75% whereas Oct_H-Dod_C-Oct_C-$G12_T$ (**2-27**) was about 82%. Therefore with a less pure sample of Oct_H-Dod_C-Oct_C-Lau_T (**3-12**) and relatively good activity is achieved, then for a sample with higher integrity should yield an even higher rate constant.

The conclusion from this section is that the ion channel candidate may not require ester functionalities. In fact, the transport activity appears to be enhanced with a decrease in the number of ester groups.

4.3.5 Transport Results from Appending Another Lipophilic Head Group

Tetramers and pentamers with Dod_C, Oct_C, $G12_T$, Ole_H, and/or Lau_H units were compared to study the effect of varying lipophilicity.

The compounds containing the lauric and oleic acid-derivative head groups were important from both a synthetic perspective (they showed that pentameric products Ole_H-Oct_C-Dod_C-Oct_C-$G12_T$ (**3-17**) and Lau_H-Oct_C-Dod_C-Oct_C-$G12_T$ (**3-16**) can be made and the stability of the primary alcohol) and an ion transporter perspective.

Lau_H-Oct_C-Dod_C-Oct_C-$G12_T$ (**3-16**) and Ole_H-Oct_C-Dod_C-Oct_C-$G12_T$ (**3-17**) are longer than Oct_H-Dod_C-Oct_C-$G12_T$ (**2-27**) and possess more lipophilic character but their activities are ranked in Oct_H-Dod_C-Oct_C-$G12_T$ (**2-27,** $6.1 \pm 1.7 \times 10^{-4}$ s^{-1}) > Lau_H-Oct_C-Dod_C-Oct_C-$G12_T$ (**3-16,** $4.1 \pm 1.7 \times 10^{-4}$ s^{-1}) = Ole_H-Oct_C-Dod_C-Oct_C-$G12_T$ (**3-17, ,** $3.9 \pm 0.1 \times 10^{-4}$ s^{-1}). In the synthesis of Lau_H-Oct_C-Dod_C-Oct_C-$G12_T$ (**3-16**) and Ole_H-Oct_C-Dod_C-Oct_C-$G12_T$ (**3-17**) only some addition sequences to Lau_H-Oct_C-Dod_C-Oct_C-$G12_T$ (**3-**

16) were observed and most of these addition sequences was an additional Lau_C unit, further increasing the lipophilic component.

The results of these two more lipophilic pentameric compounds show that increasing the lipophilic character may hinder the ability to transport ions. It is speculated that compound aggregation in solution may be an issue.

4.3.6 Effects of Transporter Lipophilic Tail Length on Transport Activity

A series of compounds with constant core and varying lipophilic tail on the glutaric acid-derivative head group was made Oct_H-Dod_C-Oct_C-$G10_T$ (**3-1**), Oct_H-Dod_C-Oct_C-$G12_T$ (**2-27**), Oct_H-Dod_C-Oct_C-$G14_T$ (**3-2**) and Oct_H-Dod_C-Oct_C-$G16_T$ (**3-3**). The data for the transport activity is presented in Table 4-12.

Table 4-12. Tabulated data for the ion transport abilities by compounds of varying lipophilic tail length on the head group.

Transporter	**$k_{32\mu M}$ (x 10^4 s^{-1})**
Oct_H-Dod_C-Oct_C-$G12_T$ (**2-27**)	6.1 ± 1.7
Oct_H-Dod_C-Oct_C-$G10_T$ (**3-1**)	6.3 ± 2.1
Oct_H-Dod_C-Oct_C-$G14_T$ (**3-2**)	3.0
Oct_H-Dod_C-Oct_C-$G16_T$ (**3-3**)	3.9 ± 1.4

The rate constants for the longer lipophilic tail (Oct_H-Dod_C-Oct_C-$G14_T$ (**3-2**) and Oct_H-Dod_C-Oct_C-$G16_T$ (**3-3**)) were lower on first inspection than the shorter lipophilic tail compounds (Oct_H-Dod_C-Oct_C-$G10_T$ (**3-1**) and Oct_H-Dod_C-Oct_C-$G12_T$ (**2-27**)).

The expected outcome of this experiment agreed with what was observed. With the pentameric oligoesters, the decrease in transport activity is thought to be due to the

increase in lipophilic character. This observation leads to the hypothesis that the "greasy" compounds may be aggregating in the aqueous solution and therefore not partition into the bilayer membrane to form the active ion channel structure.

4.3.7 Monomer Aggregation Studies

The ion transport results showed that the more lipophilic compounds were less active than the ones with less lipophilic character. Therefore it is believed that the more lipophilic compounds aggregate in solution such that there is poor partitioning into the bilayer membrane.

The carboxylate head group and lipophilic-tail character of the oligoester ion channel candidates show a strong structural resemblance to surfactants. Conventional surfactants form micelles in aqueous solution. Aggregates, like micelles, are colloidal particles which form in an aqueous environment. Under the influence of these particles, the aqueous solution would behave like a microheterogeneous medium, meaning that there were microphases within the solution (aqueous phase and the nonpolar phase within the micelle or aggregate).[88]

It is postulated that the inactive and lipophilic ion channel candidates preferentially aggregate in solution instead of partition into the bilayer. The aggregation process is spontaneous but there can be reversibility in the process. The presence of aggregates could potentially be detected experimentally. Normally micelle formation is studied using methods which focus on surface tension, light scattering, spectroscopy or conductivity. One of the easiest methods for measuring critical micelle concentrations (CMC) is a fluorescence/pyrene assay. Therefore this fluorescence assay was used to

probe for the existence of aggregates for the more lipophilic compounds in an aqueous environment.

Pyrene has electronic fine structure in which the fluorescence intensities are environment dependent.[88] Pyrene is a nonpolar molecule and therefore would prefer to be in a nonpolar over a polar environment. For a conventional surfactant at a concentration below the CMC, the fluorescence of the pyrene in solution shows vibrational bands which report the polar aqueous environment. However when the micelles are present, hydrophobic pyrene prefers to partition into the non-aqueous, apolar environment and the pyrene fluorescence spectrum would report this apolar environment. Pyrene is excited at 334 nm and the corresponding emission spectrum produced has five bands. The two bands which are most sensitive to the difference in environments are bands 1 (about 372 nm) and 3 (about 383 nm) (Figure 4-16).

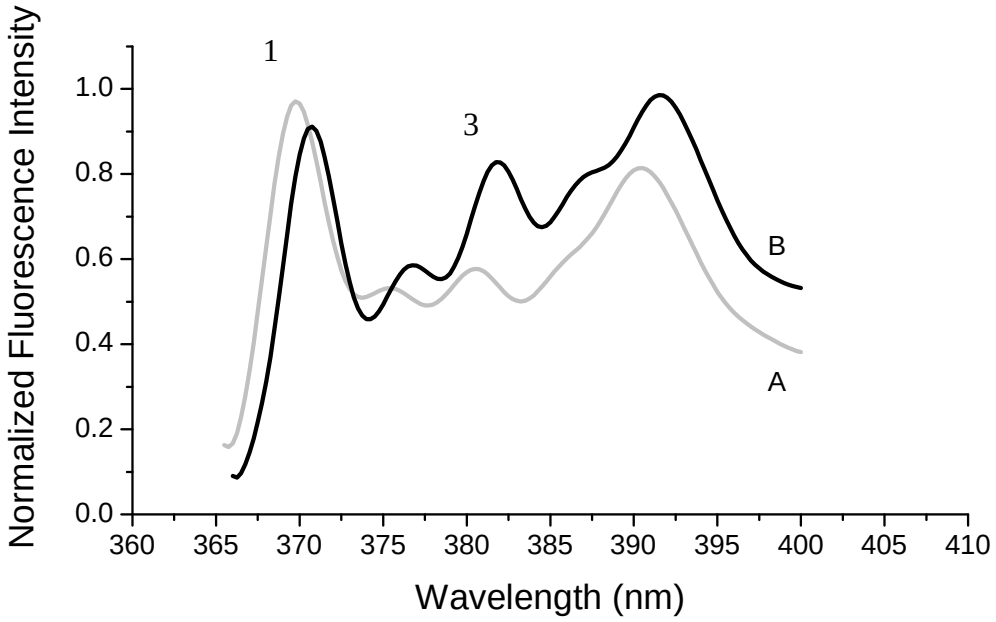

Figure 4-16. Pyrene environments and emission spectra with different surfactant concentrations (Oct_H-Dod_C-Oct_C-$G16_T$ (**3-3**)). Excitation at 331 nm. (A) Pyrene in a low surfactant concentration. (B) Pyrene in a high surfactant concentration.

For these spectroscopic experiments, the full pyrene emission spectra are recorded because the emission wavelength shifts by a few nanometers as the conditions change. Bands 1 and 3 (I_1 and I_3, respectively) are integrated for the 5 nm region centered at the observed maximum. The ratio of the integrated areas I_1/I_3 is the parameter of merit. Below the CMC, for a conventional surfactant, pyrene is in a polar environment and the ratio of I_1/I_3 is usually around 1.5; above the CMC the pyrene is in a predominantly hydrocarbon environment so the ratio drops to about 1.2. For ideal amphiphiles, there is an abrupt change in I_1/I_3 at the CMC.

Applying this method to compound Oct_H-Dod_C-Oct_C-$G16_T$ (**3-3**) yielded a graph shown in Figure 4-17. The graph of the surfactant concentration to the band intensity ratios follows a logistic function.

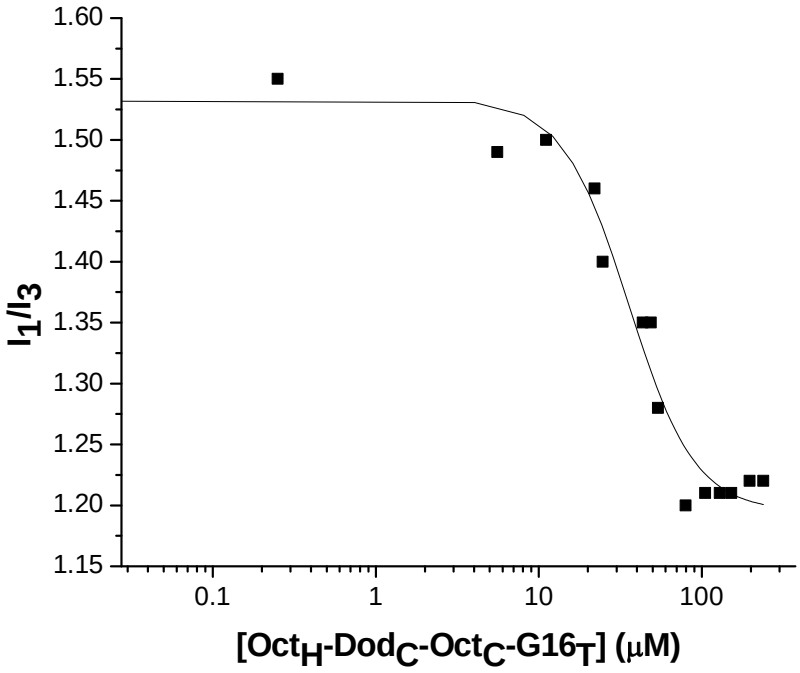

Figure 4-17. I_1/I_3 for 1.8 x 10^{-6} M pyrene as a function of total Oct_H-Dod_C-Oct_C-$G16_T$ (**3-3**) concentration.

Normally the pyrene method for determining CMCs is a reliable method for many surfactants which have CMCs in the millimolar range and a steep transition where the CMC occurs. As observed in Figure 4-17, the transition for pyrene in an aqueous environment to hydrophobic spans over 50 μM. The amount of pyrene used for these experiments was on the order of 1.8 μM. At very low concentrations of Oct_H-Dod_C-Oct_C-$G16_T$ (**3-3**) (less than 25 μM) pyrene responds to a change in environment as shown by the drop in I_1/I_3. The bands of pyrene report an increasing hydrophobic environment between 10 and 50 μM. This could be due to a CMC-like transition in which micelles form for Oct_H-Dod_C-Oct_C-$G16_T$ (**3-3**) in this range. Alternatively, the "true" CMC for Oct_H-Dod_C-Oct_C-$G16_T$ (**3-3**) could be at even lower concentration and the changes would then reflect only the pyrene: Oct_H-Dod_C-Oct_C-$G16_T$ (**3-3**) ratio.

At low concentrations of Oct_H-Dod_C-Oct_C-$G16_T$ (**3-3**) (<25 μM) the ratio of Oct_H-Dod_C-Oct_C-$G16_T$ (**3-3**):pyrene is roughly 10. The pyrene reports a predominantly hydrophobic environment when the ratio of Oct_H-Dod_C-Oct_C-$G16_T$ (**3-3**):pyrene was greater than 35.

There are a variety of ways to interpret the broad range in concentration for detection of the hydrophobic environment. One possibility is that a range of aggregation species might be present. These aggregates could be of various sizes and the size distribution could change as the concentration of Oct_H-Dod_C-Oct_C-$G16_T$ (**3-3**) increases. Alternatively, rather than various aggregate species being present, there may be one defined-size aggregate formed well below 10 μM. Only when there is enough Oct_H-Dod_C-Oct_C-$G16_T$ (**3-3**) present to generate many aggregates would it be possible to entrap all of the pyrene.

The collected pyrene fluorescence data was not the typical type observed for CMC determinations of common surfactants, which normally show much sharper transitions in the millimolar concentrations. This observed behavior was designated as aggregate rather than micelle formation and hence refer to critical aggregation concentrations rather than critical micelle concentrations.

For the oligoester ion channel candidates, it was of interest to see if the critical aggregation concentrations differ significantly as a function of lipophilic tail length. The monomer aggregation was determined for compounds Oct_H-Dod_C-Oct_C-$G10_T$ (**3-1**), Oct_H-Dod_C-Oct_C-$G12_T$ (**2-27**), Oct_H-Dod_C-Oct_C-$G14_T$ (**3-2**) and Oct_H-Dod_C-Oct_C-$G16_T$ (**3-3**) in which the glutaric acid tail increased in lipophilicity. The curves and slopes for all of the compounds tested for the critical aggregation concentrations followed the same shape and very similar inflection points. The aggregation concentrations that were observed for Oct_H-Dod_C-Oct_C-$G10_T$ (**3-1**), Oct_H-Dod_C-Oct_C-$G12_T$ (**2-27**), Oct_H-Dod_C-Oct_C-$G14_T$ (**3-2**) and Oct_H-Dod_C-Oct_C-$G16_T$ (**3-3**) were all in the 30-50 μM range. This similarity for compounds of clearly different lipophilicity suggests the aggregates form at concentrations below 10 μM. The concentrations that are used for most of the transport experiments range from 14 to 50 μM which can encompass the aggregation concentration. Concentrations lower than 14 μM have been used to try to avoid the aggregation issue; unfortunately the transport caused by the intrinsic methanol leakage is dominant so the rates are of marginal significance.

These aggregate concentration experiments are important for determining whether the concentrations that were used for the vesicle transport assays are too high, resulting in aggregates which limit the partition of the compounds into the vesicles. It is likely that

the ion transport process is initiated using conditions under which aggregates form as the dominant species of the transporter.

4.3.8 Channel Emigration

The significant difference in transport activity between the short lipophilic tail (Oct_H-Dod_C-Oct_C-$G12_T$ (**2-27**) and Oct_H-Dod_C-Oct_C-$G10_T$ (**3-1**)) and long lipophilic tail (Oct_H-Dod_C-Oct_C-$G14_T$ (**3-2**) and Oct_H-Dod_C-Oct_C-$G16_T$ (**3-3**)) may be a result of the difference in ability to partition from one vesicle to another or from an aggregate to the vesicle. The hypothesis for the mode of action for the channel in vesicles is shown in Figure 4-18. It is assumed that exchange between the aggregate and vesicle is via a monomer species. Monomers break off from the compound aggregates which then are responsible for the partitioning into Vesicle 1. At any point, the compound in Vesicle 1 may partition back into the external buffer and then into Vesicle 2. In Figure 4-18, two assumptions were made: 1) that aggregates cannot partition into a vesicle and 2) the compound cannot partition directly from one vesicle to another. The second of these assumptions is highly probable, given that the vesicles do not fuse under the condition of the experiment due to anionic surface charges. The former is also probable for the same reason. An aggregate is likely anionic and would not approach an anionic vesicle easily. As well, in Figure 4-18 the carboxylate head groups are drawn as extravesicular, but this is not essential. An alternative mechanism is for the monomer to partition into Vesicle 1 and then drive further partitioning into the vesicle. Then once in the vesicle the transporter may resist repartitioning back into the external buffer and therefore very few transporters end up in Vesicle 2.

The position of the overall equilibrium is not known. The aggregate might be the dominant species of the compound, or the compound might be predominantly incorporated in the vesicles.

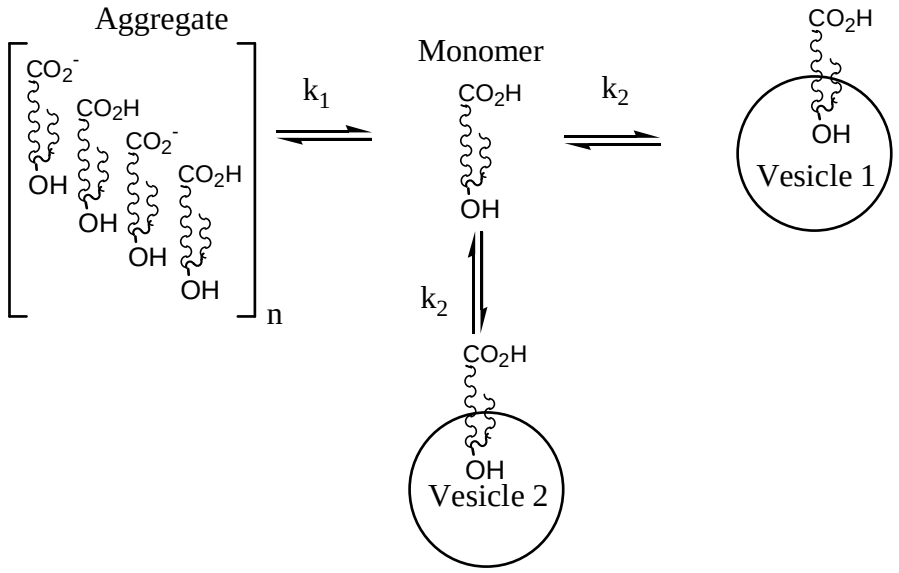

Figure 4-18. Mode of action for channel-forming compounds in vesicles.

One method to probe this system is by an experiment known as "add-back"[89,26,90]. In the add-back experiment a population of vesicles is equilibrated with the channel-forming compound, a pH gradient is induced and after the vesicles have equilibrated, a second set of vesicles (without channels) is added. If transport is observed for the second set of vesicles, then it can be assumed that the compounds can partition into the external buffer and then into the new vesicles. On the other hand, if no transport occurs for this second set, then the compound emigration from the initial vesicles must be slow, or only a very small proportion of compound is vesicle associated.

Table 4-4 shows that compounds with the shorter lipophilic tail (Oct_H-Dod_C-Oct_C-$G10_T$ (**3-1**) and Oct_H-Dod_C-Oct_C-$G12_T$ (**2-27**)) were more active than the longer tail analogues (Oct_H-Dod_C-Oct_C-$G14_T$ (**3-2**) and Oct_H-Dod_C-Oct_C-$G16_T$ (**3-3**)). According to

Figure 4-18 it would be expected that the more lipophilic compounds would be at one or the other extremes and have relatively low monomer concentrations relative to the less lipophilic compounds. As a result the migration from occupied to unoccupied vesicles should be slower for Oct_H-Dod_C-Oct_C-$G14_T$ (**3-2**) and Oct_H-Dod_C-Oct_C-$G16_T$ (**3-3**) relative to Oct_H-Dod_C-Oct_C-$G10_T$ (**3-1**) and Oct_H-Dod_C-Oct_C-$G12_T$ (**2-27**).

The graphical data for when Oct_H-Dod_C-Oct_C-$G16_T$ (**3-3**) was tested using the add-back experiment is shown in Figure 4-19 . Upon addition of the second batch of vesicles there is always a downward jump in the extent of transport due to the addition of vesicles which have a larger proportion of the acidic form of HPTS (HA) relative to the conjugate base (A^-).

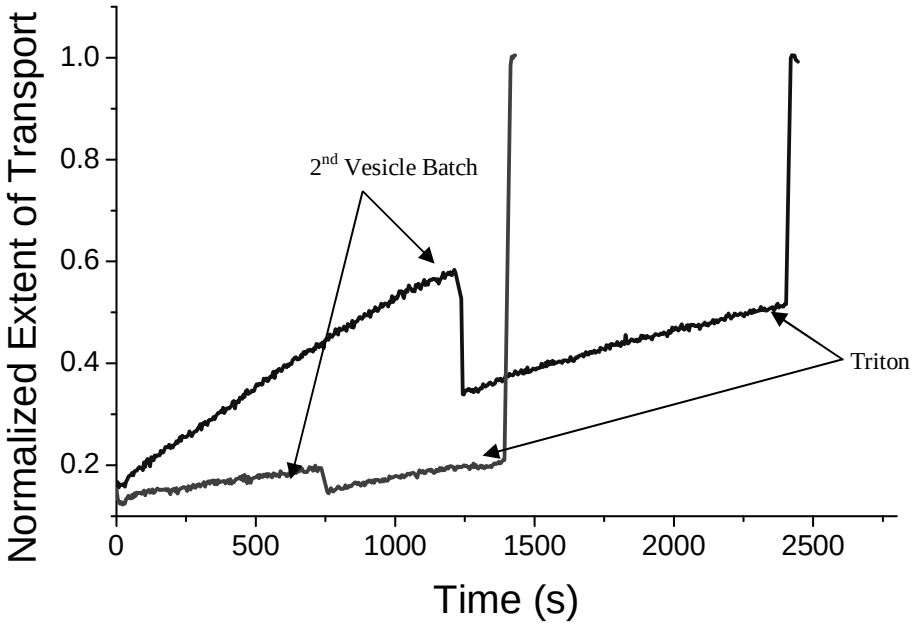

Figure 4-19. Add-back experiment for Oct_H-Dod_C-Oct_C-$G16_T$ (**3-3**) (black) and methanol (grey) (concentrations in compound:total lipid (after add-back) %, bulk concentrations after add-back): (5.6%, 44 μM).

The data collected from the add-back experiment has two slopes (one from the first batch of vesicles and then the second after the introduction of the second batch of vesicles). Rate constants were deduced for the first 100-800 seconds (100-500 seconds for MeOH) and 100-800 seconds after the introduction of the second batch of vesicles. The migration ratio is a ratio of the second to the first transport rate constant. A summary of the results are in Table 4-13.

Table 4-13. Add-back experiment results.

Tr	[Tr]: [total lipid] (mol %)	$[Tr]_{bulk}$ (μM)	k for 1st aliquot of vesicles[a] (x 10^4 s^{-1})	k for 2nd aliquot of vesicles[a] (x 10^4 s^{-1})	Migration ratio
MeOH	-		1.3 ± 0.3	1.5 ± 0.3	1.2±0.4
Oct_H-Dod_C-Oct_C-$G10_T$ (**3-1**)	6.0	47	3.6 ± 0.7	1.1 ± 0.2	0.31±0.8
Oct_H-Dod_C-Oct_C-$G12_T$ (**2-27**)	2.5	20	4.0 ± 0.8	2.8 ± 0.6	0.70±0.21
Oct_H-Dod_C-Oct_C-$G14_T$ (**3-2**)	6.2	48	3.6 ± 0.7	1.6 ± 0.3	0.44±0.12
Oct_H-Dod_C-Oct_C-$G16_T$ (**3-3**)	5.6	44	4.5 ± 0.9	1.6 ± 0.3	0.36±0.10

[a] Error calculated based on statistics of 20% error.

Methanol has a migration ratio of 1.2 which is expected as the background leakage should exist to the same extent for both sets of vesicles. The migration ratio for Oct_H-Dod_C-Oct_C-$G14_T$ (**3-2**) and Oct_H-Dod_C-Oct_C-$G16_T$ (**3-3**) (with more lipophilic tails) indicated that the transport activity for the second aliquot drops to less than 50% compared to the first aliquot. The migration ratio for Oct_H-Dod_C-Oct_C-$G12_T$ (**2-27**) was 0.70 indicating that the transport activity for the second batch of vesicles was about 70% as high as the first batch. In shortening the lipophilic tail, tetramer Oct_H-Dod_C-Oct_C-$G10_T$ (**3-1**) showed that the transport was not a first order reaction process. The non-first

order process is evident by the irregular S-shaped curve of Figure 4-20 between the injection time and 1000 seconds. This S-shaped curve is reproducible for this compound at approximately the same concentrations. In these non-first order processes, the initial rates within the first 200 seconds were measured for each aliquot of vesicles.

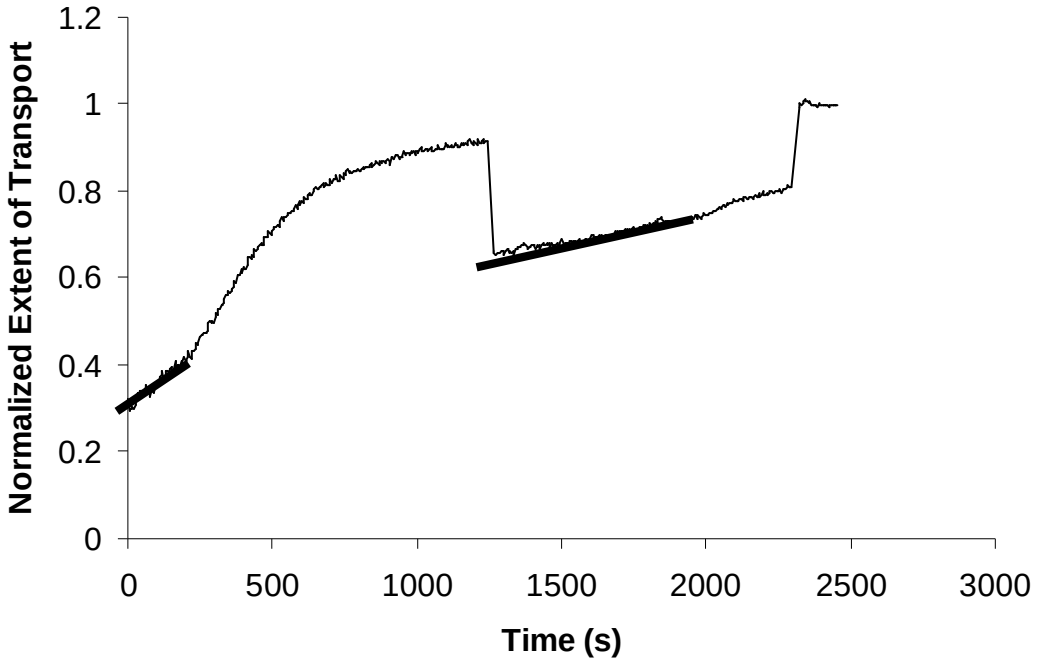

Figure 4-20. Add-back experiment for Oct_H-Dod_C-Oct_C-$G10_T$ (**3-1**) at 47 μM, 6.0 mol % relative to total lipid concentration.

The maximum migration ratio in the middle of the series (in Table 4-13) suggests the position of the overall equilibrium shifts along the series. For the lipophilic compounds the aggregates would be expected to dominate while the decyl derivative Oct_H-Dod_C-Oct_C-$G10_T$ (**3-1**) would be predominantly vesicle associated. Only the dodecyl compound has a sufficient reservoir of aggregates to allow relatively efficient migration between occupied and unoccupied vesicles.

4.3.9 Comparison of Transport Activity to known Ion Channels

To get some appreciation for how active some of the oligoester compounds are, two known ion channel compounds were tested using the HPTS assay, gramicidin D and **1-18**. The normalized rate constant at 32 μM for **1-18** and gramicidin were calculated to be 16±6 x 10^{-4} and >10000 x 10^{-4} s^{-1}, respectively.

Gramicidin D is a very effective channel and therefore requires very low concentrations to show significant activity. Compound **1-18** was synthesized by Hu and was shown to be an active transporter in pH-stat vesicle assays.[91] Compound **1-18** yields a higher rate constant compared to the solid-phase oligoester products. By simplifying the synthesis, there is a loss in the ion transport activity, yet end-differentiated products are made which is heading towards voltage-gated ion channels.

4.4 Bilayer Clamp Results

It was possible that the observed activities in vesicles occur by a membrane disruption mechanism as opposed to a channel type.

Planar bilayer voltage clamp experiments were conducted by Jonathan Chui for the constitutional isomers Oct_H-Dod_C-Oct_C-$G12_T$ (**2-27**) (Figure 4-21) and $G12_H$-Oct_C-Dod_C-Oct_T (**2-48**) (Figure 4-22). He found that both compounds showed "square-top" openings. The square-tops are indicative of ion channel formation and based on the duration of the average square-tops, the ion channels are regular and formed long-lived channel openings (seconds in duration). The two compounds have channel structures which have diameters of similar dimensions (as shown by the conductances at around 4 pA).

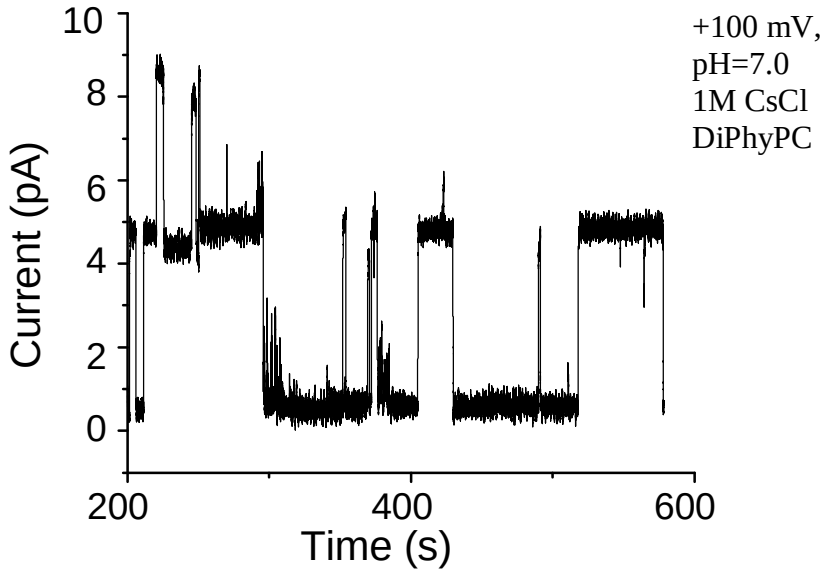

Figure 4-21. Ion channel behavior observed by planar bilayer clamp experiments for Oct_H-Dod_C-Oct_C-$G12_T$ (**2-27**).

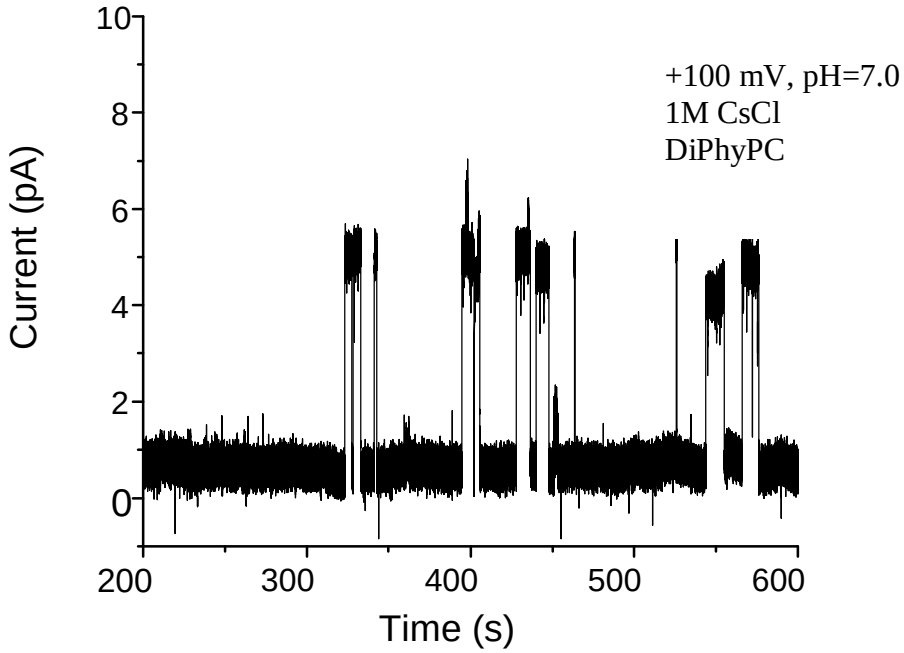

Figure 4-22. Ion channel behavior observed by planar bilayer clamp experiments for $G12_H$-Oct_C-Dod_C-Oct_T (**2-48**).

It was clear that at least Oct_H-Dod_C-Oct_C-$G12_T$ (**2-27**) and $G12_H$-Oct_C-Dod_C-Oct_T (**2-48**) would form channel structures, but whether these compounds will form voltage-gated ion channels or have any ion selectivity will require further mechanistic studies in planar bilayer clamp experiments.

4.5 Summary from Transport Assay

Various structure-activity relationships have been studied using the HPTS dye/ fluorescence method and it has been noted that the amount of lipophilicity in the oligoesters is very important in determining the ability to transport ions. The length of the core is also important because compounds that are too long are not active probably due to aggregation, or if they are too short, they may not be able to span across a bilayer. The rate constants observed for some of the oligoesters may not be totally representative of the compound at high integrity. It was noted that some of the compounds have low integrity (mixtures of some shorter or longer products) and therefore the observed rate constants are lower than expected for the compound with high integrity.

The pyrene experiments showed that some oligoesters may form reversible aggregates in solution. The add-back experiments showed that there may be poor partitioning between of compounds in vesicles. From these observations, the working hypothesis is proposed in Figure 4-23.

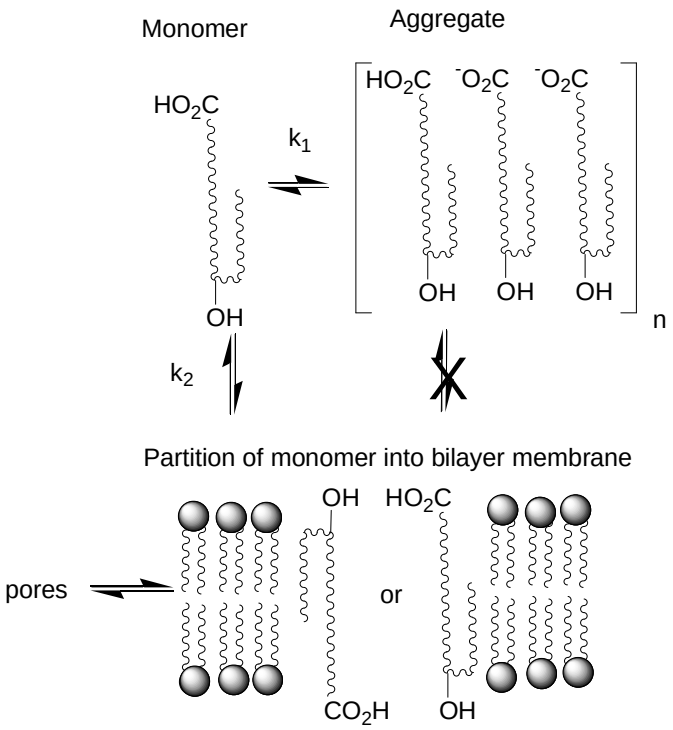

Figure 4-23. Proposed transport model.

It was interesting what a difference a pair of methylene groups added to or taken away from the lipophilic tail of Oct_H-Dod_C-Oct_C-$G12_T$ (**2-27**) can lead to in transport activity. To rationalize these results, consideration must be made for factors such as compound lipophilicity and overall molecular structure. In general the proposed schematic for generating the active ion channel is shown in Figure 4-23. Two generalized steps are mentioned: k_1 is the leaving of a monomer from an aggregate; k_2 is the partitioning of the monomer into the vesicle and creating an active structure. k_2 is probably at least a two-step process in reality: partitioning of compound into the bilayer and aggregating of the partitioned monomers to form the active structure. Since these processes cannot be observed separately under the vesicle assay, a collective rate constant was used. All of the proposed mechanisms are reversible but there may be preferential directionality for each mechanism.

When the methanol solution containing the ion channel candidate is injected into the external buffer solution, the compound exists in either a monomeric form or aggregate. The data for Oct_H-Dod_C-Oct_C-$G16_T$ (**3-3**) showed that as concentration increased the rate constant/compound concentration ratio decreased, which would show that as concentrations increased, then more aggregates formed, holding the monomer concentration approximately constant. Once in the membrane, the orientation of the compound is unclear and most likely these oligoester compounds cannot act as a unimolecular channel. Therefore monomers must aggregate in the membrane to form the active ion channel (pore).

The ability to transport ions by the oligoester compounds could act by one of several mechanisms. The present vesicle assays cannot distinguish between the mechanisms. However preliminary bilayer clamp studies have shown that two particular compounds act by ion channel mechanisms.

Chapter 5 Prospects for Simple Voltage-Gated Ion Channels

In the previous chapters the synthesis and evaluation of oligoester ion channel forming compounds were discussed. The oligoester compounds are terminated with carboxylic acid and alcohol functionalities. To further diversify the oligoester compounds, amino acids can be appended onto the structures. With 20 naturally occurring amino acids, a variety of functional groups can be attached to the structure. Depending on the pH of a solution, some amino acids can lead to charged structures (negatively charged: glutamic acids and aspartic acid; positively charged: lysine, arginine and histidine). Recall that a voltage-gated ion channel must possess a molecular dipole, so by taking advantage of coupling these amino acids to the oligoester, an end-differentiated product is made which could be a voltage-gated ion channel.

One of the inconveniences in the synthesis of oligoester ion channel candidates noted in previous chapters is that the purity cannot be assessed using conventional methods such as HPLC. It would be appropriate to try to find a way to incorporate a chromophore/fluorophore tag to the oligoester compounds so that the purity issue can be addressed directly. There are many tags which can fit this criterion but as well, this tag should also help with determining the location of the tagged ion channel in the bilayer membrane. The fluorescent indole ring of tryptophan provides a useful chromophore handle for various spectroscopic experiments. Commonly, tryptophan is particularly important in the fluorescence study of protein orientations in membrane bilayers.[92]

In order to append the amino acid to the oligoester, there has to be at least one amide linkage. Amide linkages are chemically more inert than ester linkages. However

in an ion channel structure related to **1-18** Hu found that the transport activities for oligoester ion channels were more active than amide-containing structures.[91] Despite his finding, amino acids provide a range of functionality and the advantages of using amino acids outweighed the potential decrease in ion transport activity.

In this chapter the incorporation of a tryptophan moiety into an oligoester ion channel-forming compound are discussed.

5.1 Structure-Design Considerations

Compound **2-27** was one of the most active tetrameric oligoester compounds made by SPOS; therefore it was selected as the basis for structural modifications. Tryptophan (Trp) derivatives were proposed (**5-1**, **5-2**, **5-3**, **5-4**, and **5-5**) having tryptophan groups inserted into various positions of **2-27**. Any of these structures can be synthesized but only some are of value in addressing targeted questions. One of the proposed issues that Hu and Fyles proposed for structures with amides is that there may be a rotational barrier with the amide bond and that might affect the ability to achieve an active ion channel.[25] Therefore having the amide linkage in the core units (**5-3** and **5-4**) may not be good targets because of this issue. What is desired is to have the Trp in a location where conformation of the rotamer does not affect the overall length of the structure.

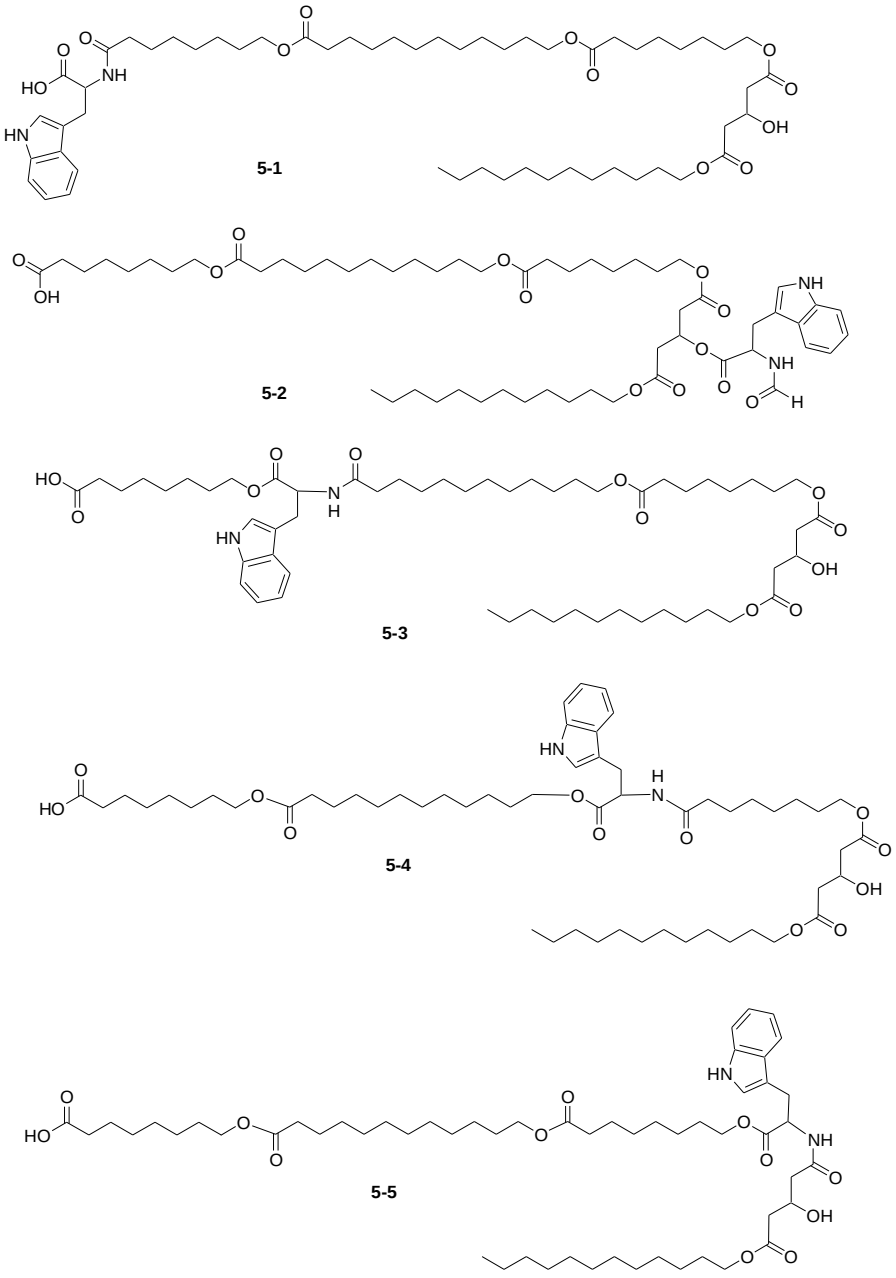

5-1

5-2

5-3

5-4

5-5

To simplify the number of targets down to two, the Trp unit can be placed at either ends of **2-27** (carboxy (**5-1**) or hydroxy terminus (**5-2**)) so that the orientation of the rotamers should not be an issue in the active structure.

Since the Trp fluorescence can be quenched, then the Trp label on compounds **5-1** and **5-2** is useful for addressing if the carboxylic acid head group resided intravesicular or extravesicular by the addition of a quencher. When the structure of **5-5** is extended, the

indole moiety would be located about the lipid mid-polar region in the bilayer membrane. The indole ring would be hidden away from the quencher all together and the quenching experiments would prove to be uninformative. This further suggests that the **5-5** is not a good target.

There are many commercially available amino acids with a range of amino-protecting group types. The building blocks were judiciously chosen such that the deprotection conditions did not affect the ester linking the amino acid to the Wang resin. For **5-1**, commercially available L-Fmoc-Trp could be used to introduce the Trp group whereas an N-formyl-Trp (**5-6**) was used for **5-2**.

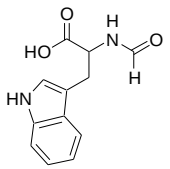

5-6

The Trp amino group is protected as an N-formyl group in **5-2**. The reason for this is three-fold: the formyl group provides an excellent handle in the ^{1}H NMR spectrum, the product **5-6** is commercially available, and the amine is protected as an amide which prevents intra or intermolecular cyclization of the amine with one of the four ester functionalities. The intramolecular cyclization to yield a morpholine-2,5-dione is expected to be particularly facile (Scheme 5-1).

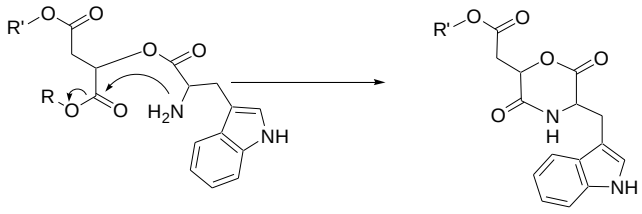

Scheme 5-1. Intramolecular cyclization of a free amine to yield a morpholine-2,5-dione.

5.1.1 Synthesis

For the synthesis of **5-1**, L-Fmoc-tryptophan was loaded onto Wang resin using the oligoester coupling conditions (DMAP/DIC coupling conditions) followed by capping any remaining hydroxyl sites on the resin with biphenylacetic acid. The Fmoc deprotection was achieved using a standard protocol[93] of 20% piperidine in DMF solution. The coupling of protected-hydroxy acids to the amine was done using our standard coupling and deprotection conditions (Table 2-4). The compound made would exist as diastereomers due to the presence of two chirality centers from the enantiomerically pure L-tryptophan configuration combined with the glutaric acid fragment which existed as both the R and S forms. These two centers are close in **5-2** so should be detectable, but they are remote in **5-1** so might be undetectable by ^{1}H NMR resonances. Pentamer **5-1** was recovered from Wang resin of mass 0.210 g (0.158 mmol) in 5.8% (6.2 mg , 6.0 μmol) yield.

Pentamer **5-1** was analyzed by ^{1}H NMR (in d_6-DMSO) and ^{13}C NMR (in $CDCl_3$) spectroscopy as well as by MALDI-MS. The ^{1}H NMR spectrum was originally collected in $CDCl_3$ but the broadness of the resonances indicated that aggregation in the solution was a problem; this issue was resolved by using d_6-DMSO (Figure 5-1 and Figure 5-2). As expected in the **5-1** product, there are proton resonances for the indole ring (between 6.8 ppm – 7.8 ppm). Many of the upfield signals from the indole resonances are rather complicated in pattern. The complexity of the ^{1}H NMR spectrum was due to diastereomers as well as amide-rotamers in the sample. Temperature variation studies (Figure 5-1) in the ^{1}H NMR spectrum were done and it was determined that only the two methine (H_a and H_b) protons shifted significantly (5.0 ppm at 301 K).

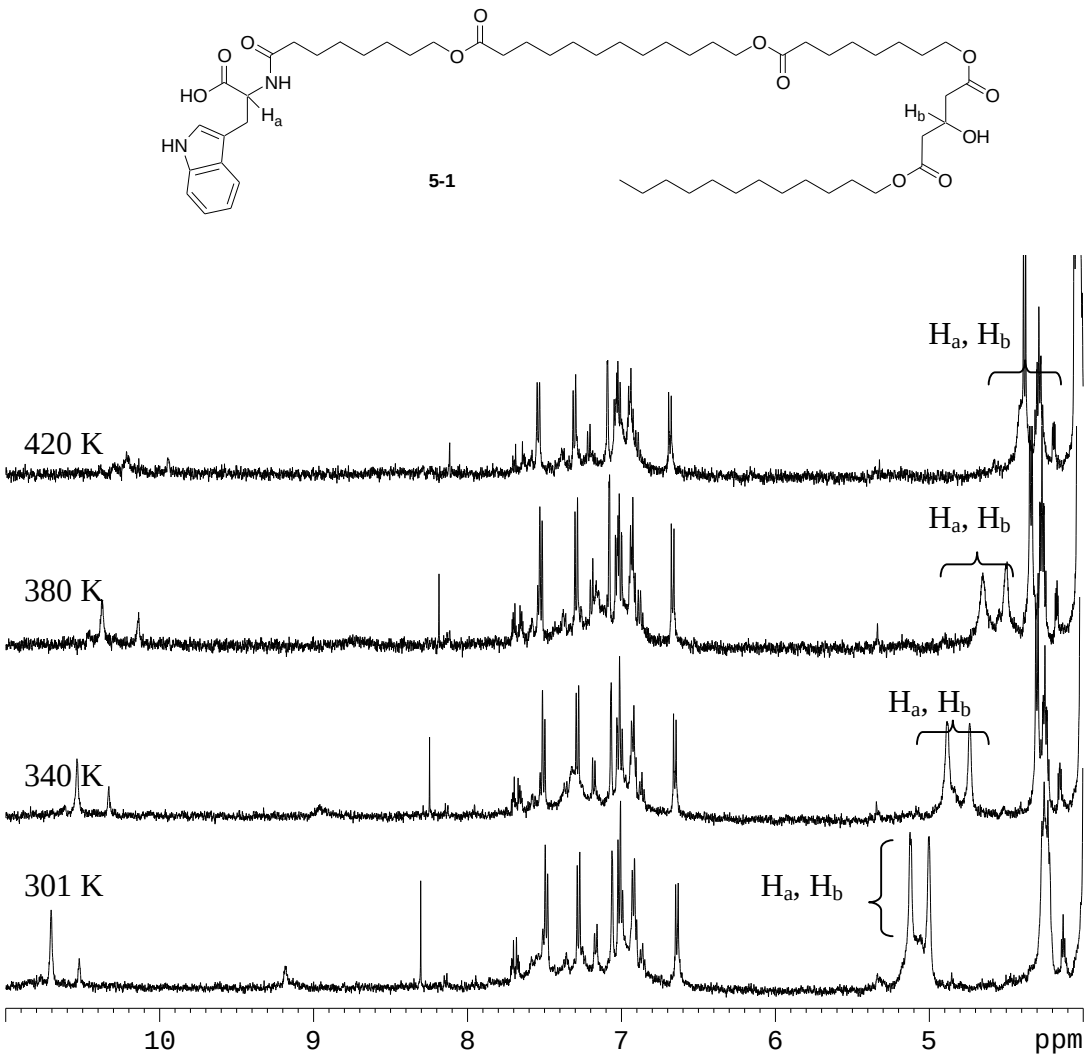

Figure 5-1. ^{1}H NMR temperature variation studies of **5-1** in d_6-DMSO.

In the ^{1}H NMR spectrum (Figure 5-2) of **5-1**, the proton integrations of the Trp methine proton (a) compared closely to the glutaric methine proton (b) which implied that the Trp and glutaric head group were in roughly equal amounts. The integration of the tryptophan aromatic protons (a) and the methylene (f) are about 10% short of what are expected for each of those types of protons. Since the methine protons (B) were calibrated as 2.00, then the calibration may be an overestimate if there were more $G12_T$ than the Trp block. The methylenes ($C\underline{H}_2OCO$: c, $C\underline{H}_2CO_2$: d) were each about 26% and 36%, respectively, lower than expected in integration which suggested that there was a

significant proportion of deletion sequences lacking the Dod or Oct building block in the product. Alternatively, the other explanation is that the resonance for H_b which is referenced to 2.00 has encompassed other impurities, leading to peak over-integration.

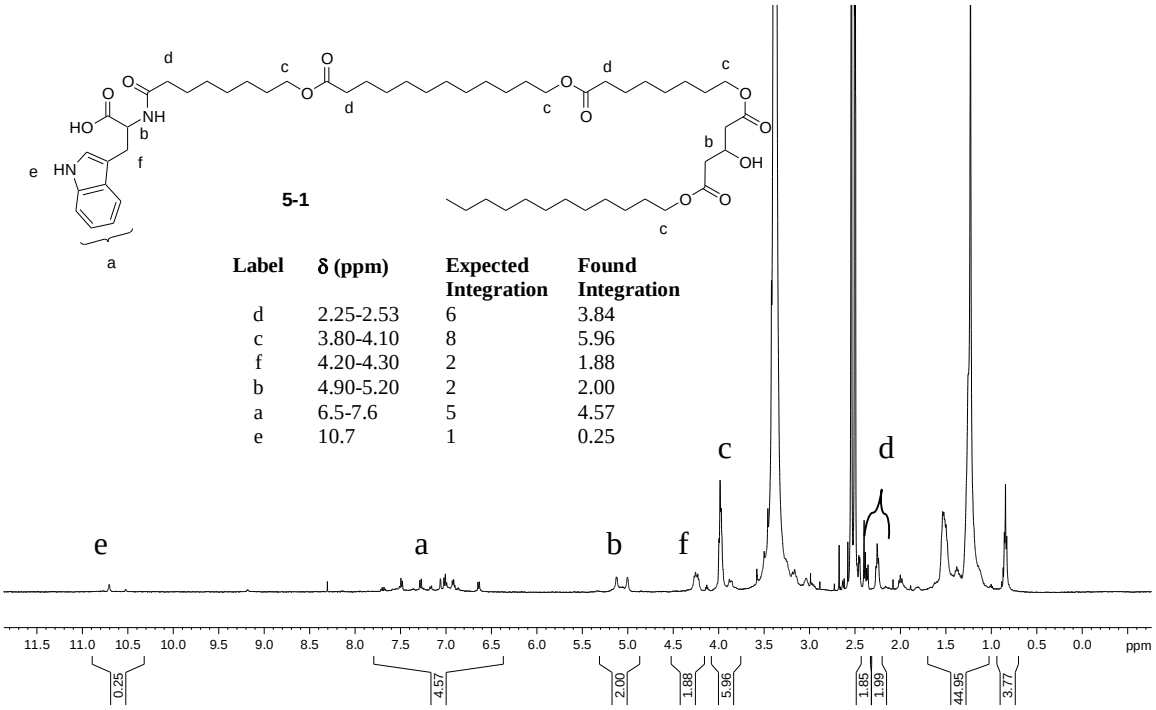

Figure 5-2. ^{1}H NMR spectrum of **5-1** in d_6-DMSO.

From integrations in the ^{1}H NMR spectrum, a mixture of some other shorter analogues (**5-7**, **5-8**, **5-9**, and **5-10**) was present. Diastereomers were known to be present because enantiomerically pure starting materials were not used however with the large distance between the stereocenters it was not anticipated that the chemical shifts from the diastereomers would be very different from each other.

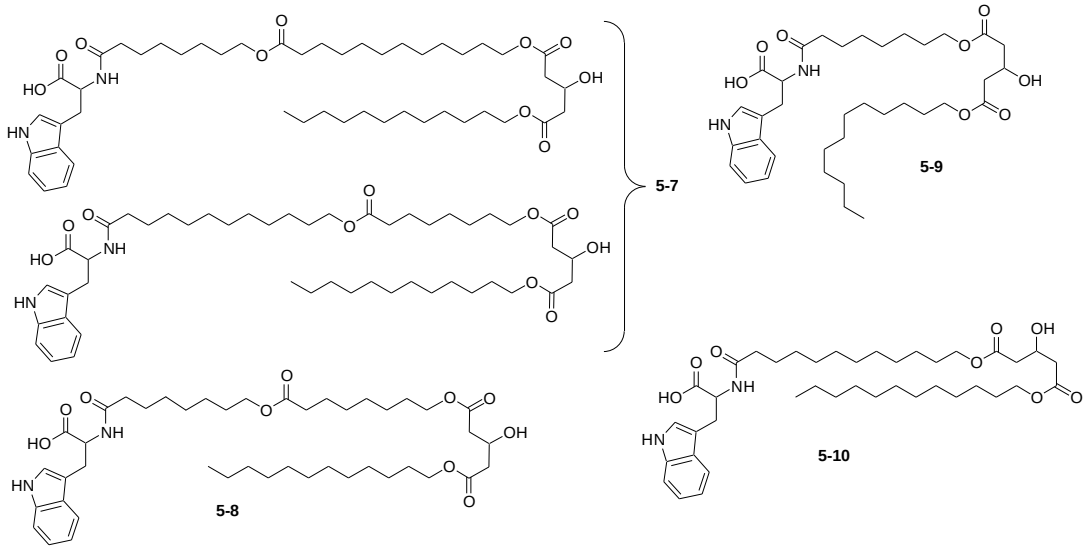

The quantity of shorter analogues cannot be determined using ^{1}H NMR spectroscopy, but the presence of these compounds was also confirmed by MALDI MS (Figure 5-3). In the previous chapters the oligoester compounds were characterized mostly by the LSIMS technique. MALDI MS is a soft ionization technique which is typically used for characterizing the molecular weights of large molecules such as proteins. Therefore fragments are not as likely to be observed in the MALDI MS. The peaks at *m/z* 1029.6 and 1007.6 in Figure 5-3 are consistent with the $[M+2Na-H]^+$ and $[M+Na]^+$ ions, respectively of **5-1**. The peaks observed at *m/z* 887.5 and 865.5 are consistent with $[M+2Na-H]^+$ and $[M+Na]^+$ ions, respectively of **5-7**. Compound **5-8** was assumed to be present because the $[M+2Na-H]^+$ and $[M+Na]^+$ ions may be observed at *m/z* 831.4 and 809.5, respectively. Finally the peaks at *m/z* 723.4 and 667.4 were consistent with the $[M+Na]^+$ ion of the trimeric products of **5-9** and **5-10**, respectively. These peaks give some evidence that they result from the deletion sequences from the synthesis as opposed to fragments from an intact precursor. The observed deletion sequence peaks have both the Trp and $G12_T$ fragments intact but they lack either the

Dod_C or Oct_C fragments. As well, many of the shorter analogues in the MALDI MS showed both a peak to represent the ions $[M+Na]^+$ and $[M+2Na-H]^+$. In Chapters 2 and 3, some compounds also showed the presence of the sodiated sodium salt ($[M+2Na-H]^+$ ion) in the MS which suggested that the lower molecular weight species are not fragments in the mass spectrometer, but are deletion sequences. In the MALDI MS there was no evidence of addition sequences present but the intensities were quite low so they may be hidden in the baseline if they did exist.

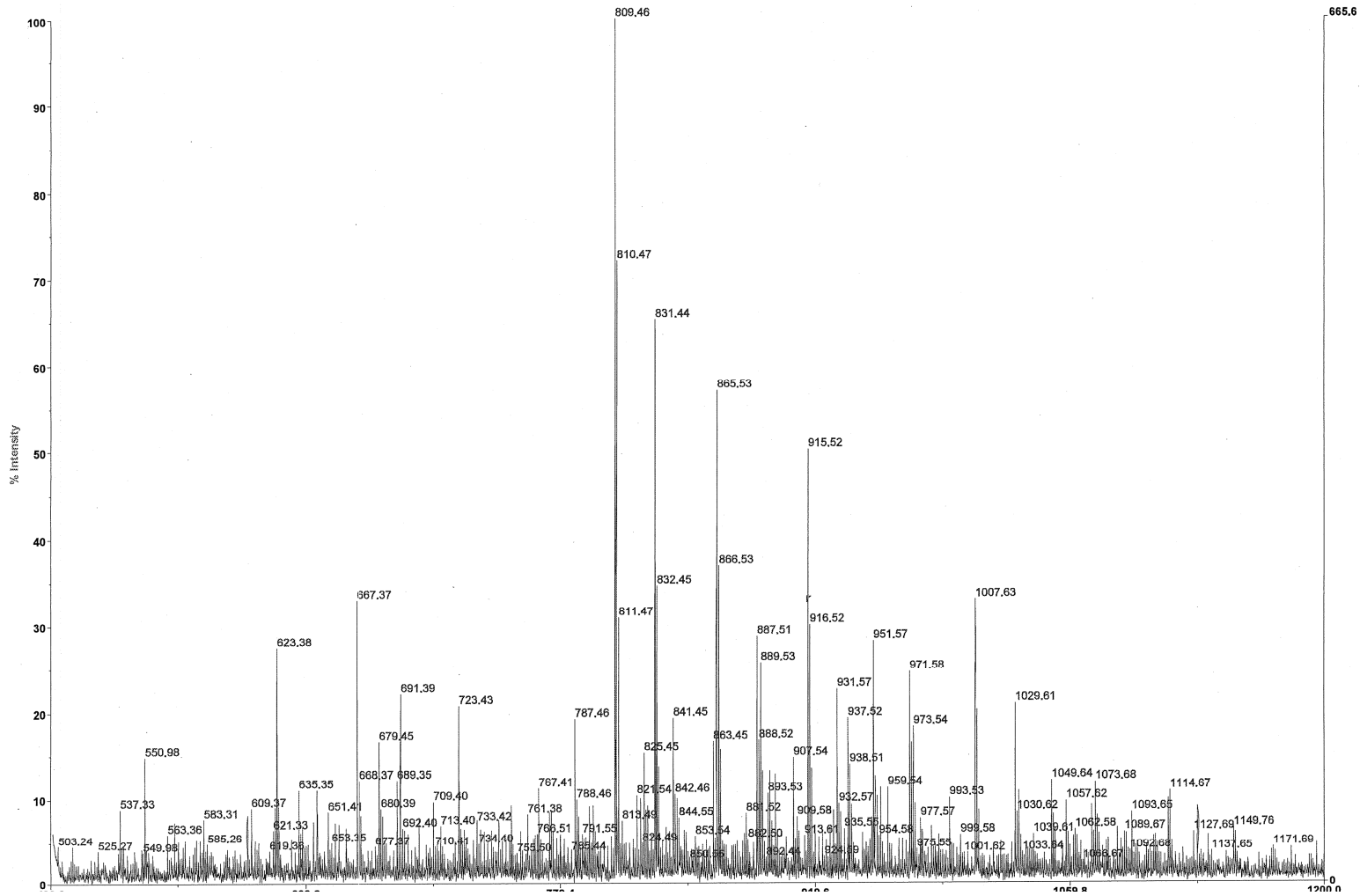

Figure 5-3. MALDI MS of **5-1**. 100% = 666 mV.

The presence of the fluorescent tryptophan chromophore on **5-1** allowed for the analysis of purity using HPLC. In the chromatogram (Figure 5-4), four distinct peaks with retention times of I: 6.08 min, II: 6.63 min, III: 7.11 min, and IV: 7.84 min were apparent. A gel permeation column (GPC) column was used for the separation and it was assumed that the elution order corresponded to decreasing molecular weight. If this assumption were true, then the peak at I was **5-1**, peak at II was the **5-7** (there was uncertainty in the Oct_C and Dod_C location in the structure), peak III was the tetramer **2-27** and finally IV was the trimer **5-10** and **5-9**. A summary of the data collected from the MALDI MS and HPLC is given in Table 5-1; note that the intensities observed in the MS reflect the ratio of peaks in the HPLC.

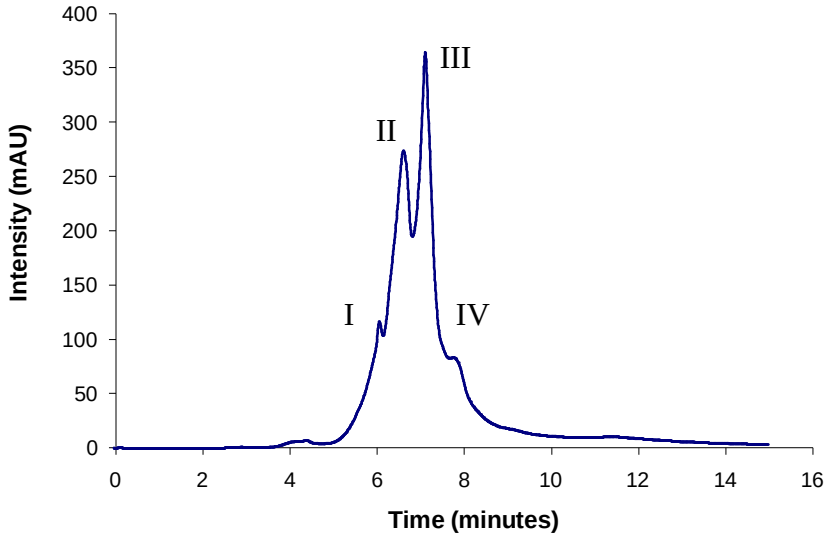

Figure 5-4. HPLC chromatogram of **5-1** eluting with MeOH:$CHCl_3$ (1:1) through a GPC column. Flow rate = 2.0 ml/min and UV_{282} for detection.

Table 5-1. Summary of the MALDI MS and HPLC data for a sample of **5-1.**

		MALDI MS		HPLC	
Label in HPLC	**Label in MS**	**Mass unit**	**Identification**	**Retention time (min)**	**Fraction of chromatogram**
I	A	1007.6	Na^+·**5-1**	6.08	13.7%
		1029.6	$2Na^+$·**5-1**-H^+		
II	B	865.5	Na^+·**5-7**	6.63	33.0%
		887.5	$2Na^+$·**5-7**-H^+		
III	C	787.5	**5-8**	7.11	44.0%
		809.5	Na^+·**5-8**		
		831.4	$2Na^+$·**5-8**-H		
IV	D	667.4	Na^+·**5-9**	7.84	9.3%
		723.4	Na^+·**5-10**		

The presence of the shorter analogues was of concern because it indicated incomplete coupling or incomplete deprotection. The coupling and deprotection of L-Fmoc-tryptophan on Wang resin was not optimized in the synthesis. Although after loading L-Fmoc-tryptophan onto the resin, the free hydroxyl sites on the resin were capped with BPAA, so the generation of **2-27** from incomplete Trp coupling would not be of concern. It is possible that the incomplete coupling was due to the persistence of piperidine from the Fmoc deprotection. Piperidine is a secondary amine which can couple to DIC-activated carboxylic acids. For the Fmoc deprotection, a 10 mL solution of 20% piperidine in DMF was used, so if the washing steps were not adequate then there would be residual piperidine. There was no evidence of shorter analogues missing the $G12_T$ fragment, which further supported the notion that the piperidine may have all reacted during the first two Dod and Oct couplings. Addition sequences involving just the oligoesters with the Oct_C and Dod_C units were not observed.

The synthesis of **5-2** was proposed to be a straightforward reaction of the resin precursor **2-27** with an activated N-formyl tryptophan (**5-6**) onto the hydroxy terminus using the standard amino acid coupling procedures (Scheme 5-2).

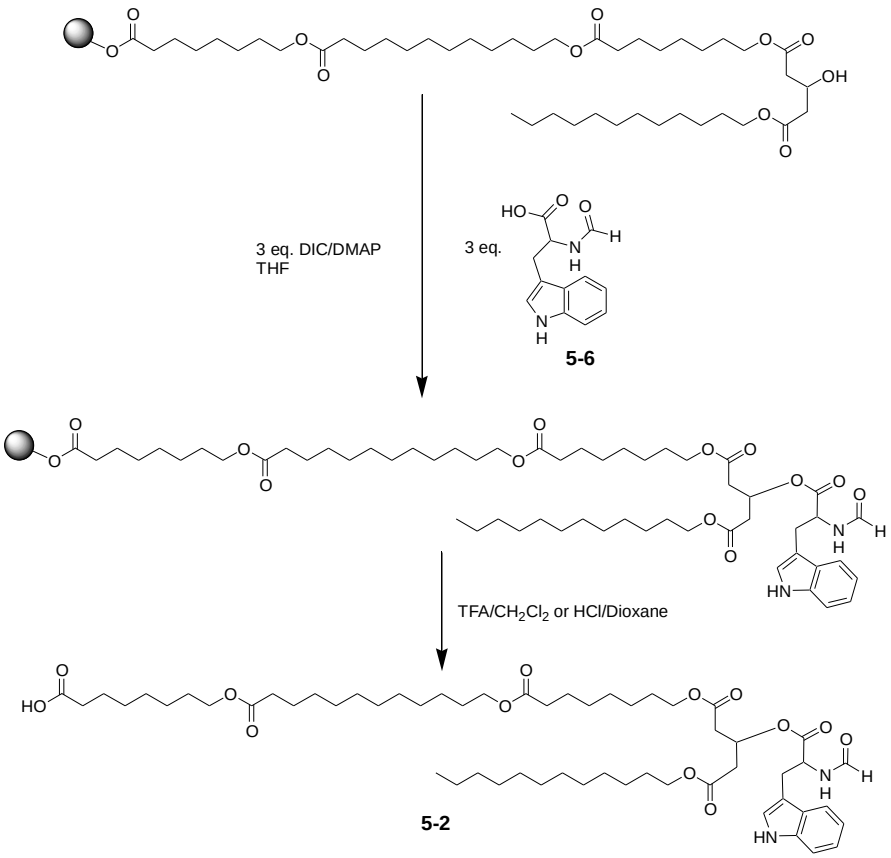

Scheme 5-2. Proposed synthesis of **5-2**.

It was noted that the ^{1}H NMR spectrum of the product as proposed by Scheme 5-2 did not show a downfield shift of the $G12_C$ methine proton to about 5.5 ppm, which would be evidence of the successful coupling of **5-6** onto $G12_T$.

An alternate solution phase approach was attempted as well to generate **5-2** (Scheme 5-3). A very large excess of **5-6** was used so that the flood of activated amino acid would overwhelm the secondary alcohol on the $G12_T$ such that self-dimerization of **2-27** would be reduced. The crude product was purified using gel permeation chromatography.

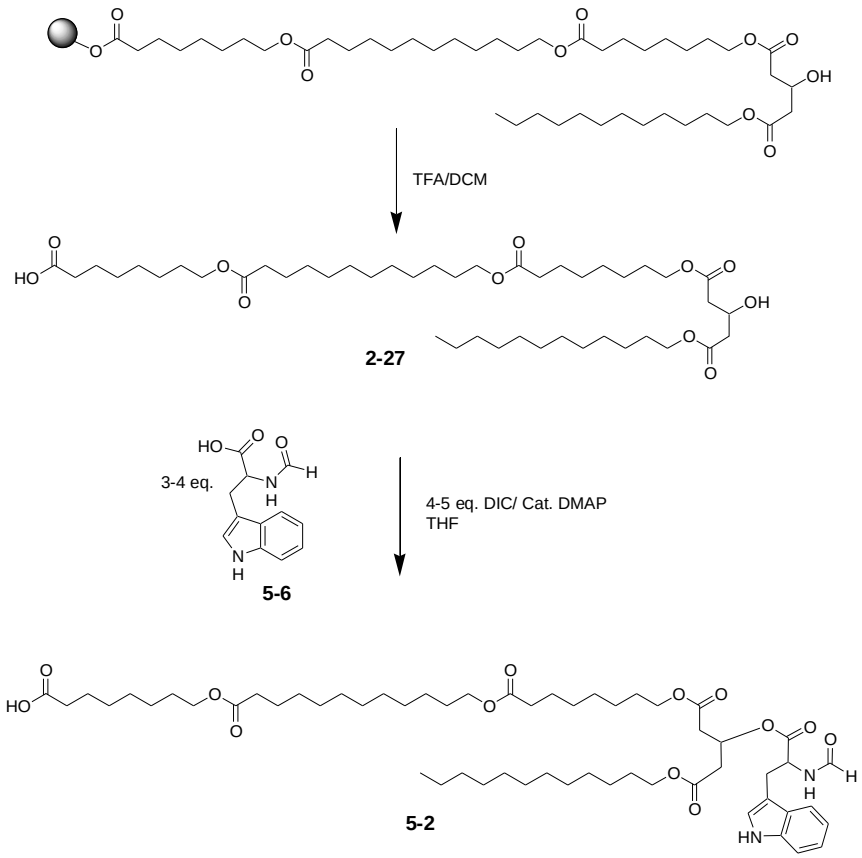

Scheme 5-3. Attempted synthesis of **5-2** by first cleaving **2-27** from the resin and coupling **5-6** in solution.

The MALDI MS in Figure 5-5 showed a peak at *m/z* 1035.7 consistent with the $[M+Na]^+$ of **5-2**, but this signal is not very intense and lower molecular weight fragments under *m/z* 700 were not searched for. From the MALDI MS the expected molecular ion for **5-2** is observed.

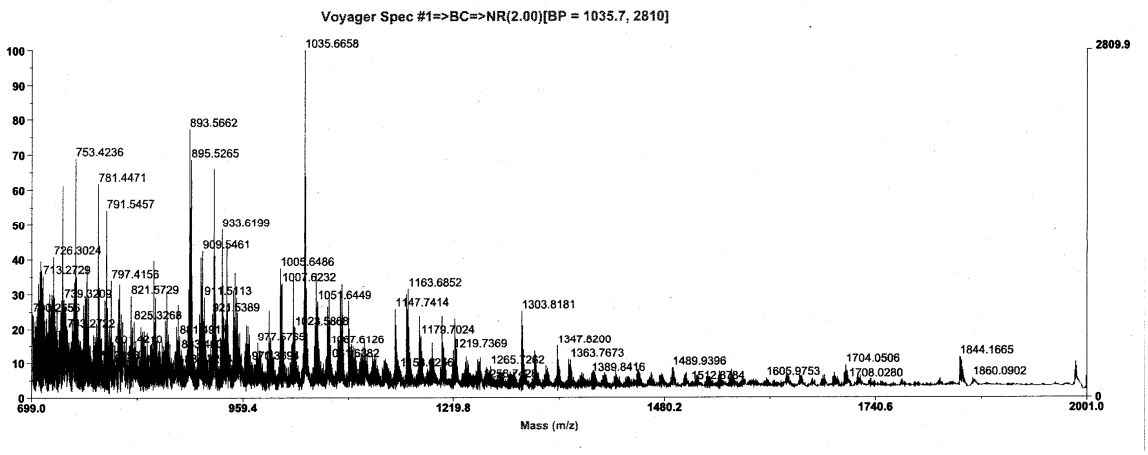

Figure 5-5. MALDI MS of **5-2** from Scheme 5-3. 100% = 2810 mV.

The ^{1}H NMR for this **5-2** sample is in Figure 5-6. In the ^{1}H NMR spectrum there is evidence of some incomplete coupling by **5-6** (circled area). The coupling reaction of **5-6** and **2-27** yielded a product which had a methine with a chemical shift downfield at about 5.5 ppm (thought to have been the product (**5-2**)); however, this product could be isolated by chromatography (neutral alumina and $CHCl_3$ eluent) and the ^{1}H NMR spectrum revealed that no tryptophan proton signals were present (Figure 5-7); suggesting that the coupling of **2-27** and **5-6** did not occur but instead **2-27** may have lactonized or dimerized to give the downfield methine chemical shift.

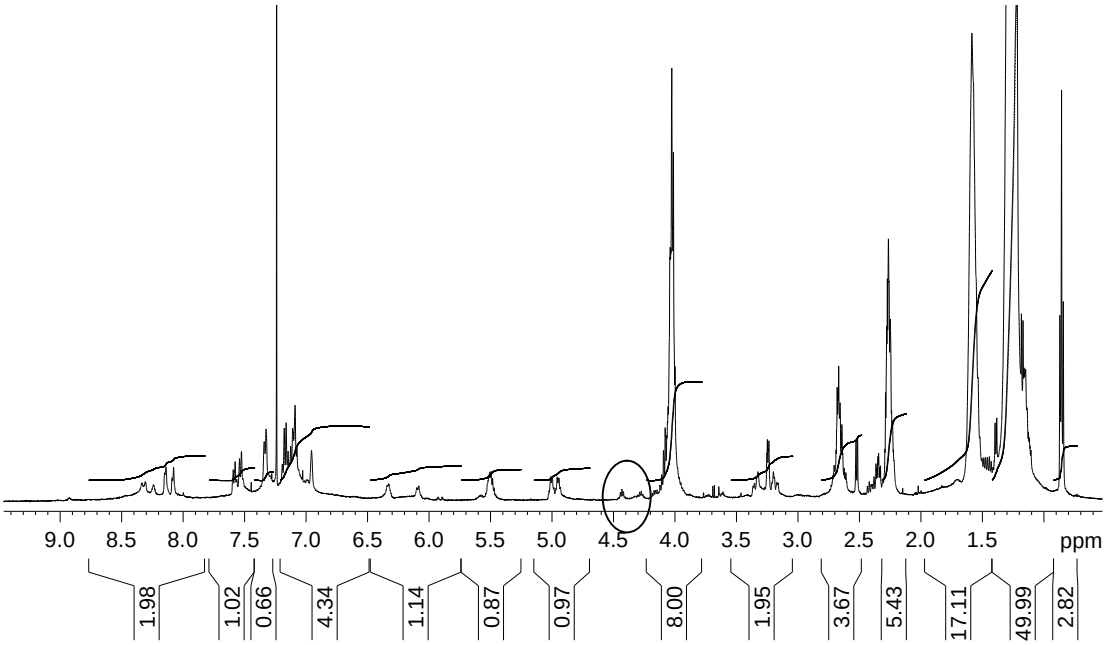

Figure 5-6. ^{1}H NMR spectrum of the product from Scheme 5-3 in $CDCl_3$

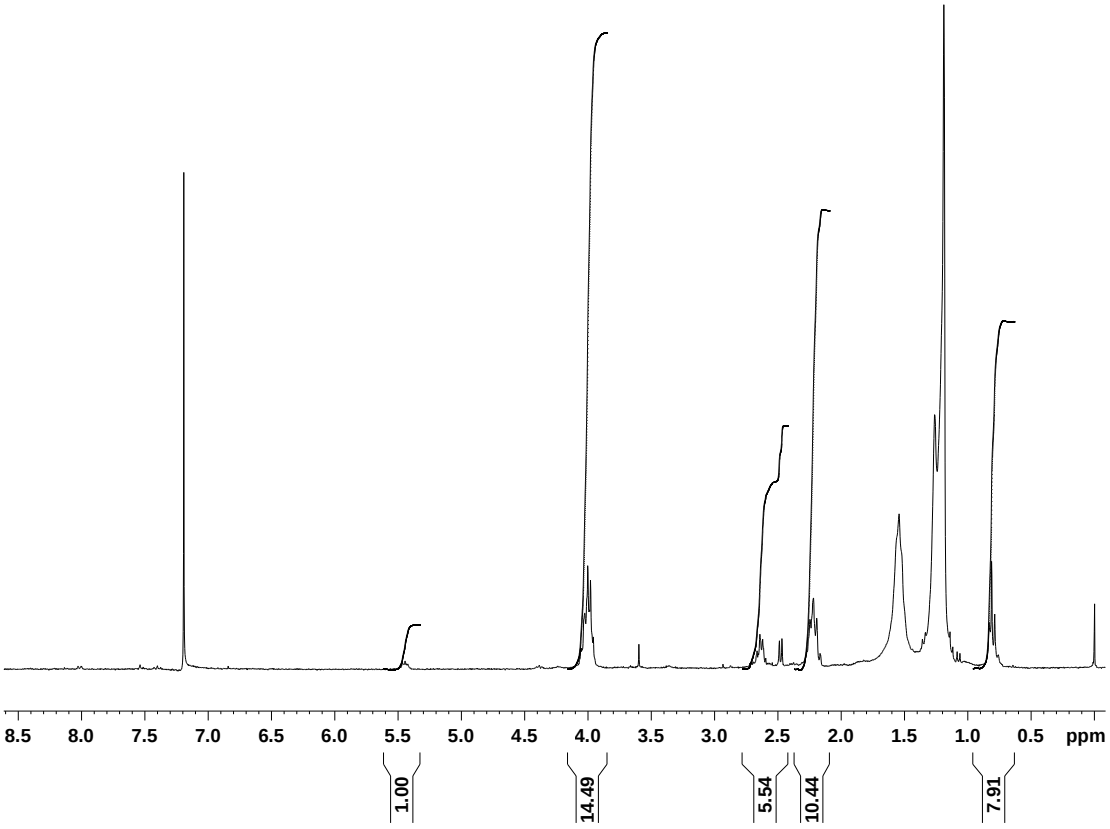

Figure 5-7. ^{1}H NMR spectrum (in $CDCl_3$) of the product from Scheme 5-3 after further purification on an alumina column with $CHCl_3$ as the eluent.

Therefore the solution phase synthesis of **5-2** by coupling **5-6** onto **2-27** is not a good approach. Even though some of the desired product was made (supported by the MALDI MS), there is a significant amount of some other product.

It was important to understand why the coupling of **5-6** and **2-27** failed because **5-2** was an appropriate comparison to **5-1**. Two model compounds were prepared as a proof of principle for the feasibility of coupling the Trp group to a primary alcohol (**5-11**) and a secondary alcohol (**5-12**).

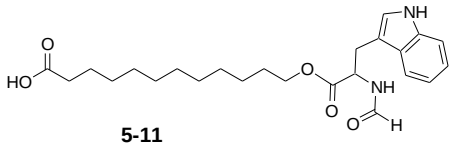

5-11

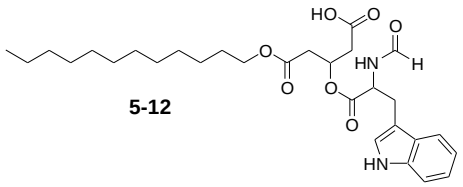

5-12

The synthesis of **5-11** started with the coupling of a Dod block onto Wang resin, deprotecting the alcohol and then coupling with three equivalents of **5-6** (Scheme 5-4).

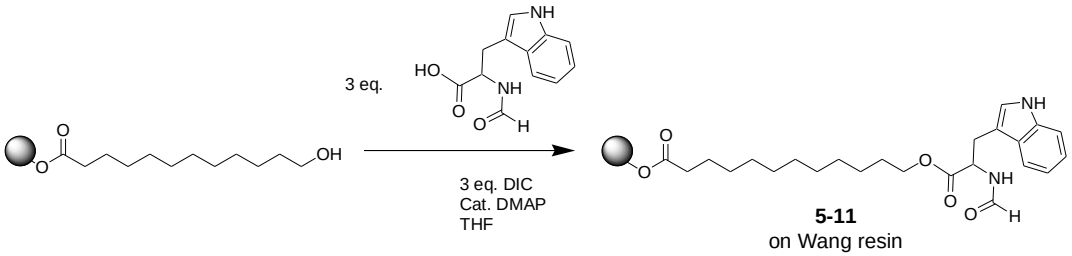

5-11
on Wang resin

Scheme 5-4. Synthesis of **5-11**.

The resin with the proposed **5-11** was cleaved with a solution of TFA:CH_2Cl_2. The ^1H NMR spectrum (Figure 5-8) from this crude product showed a small ratio of the ester methylene (of **5-11**) to the methylene of the primary alcohol, which implied minimal coupling occurred despite three cycles of coupling. The circled area is the expected resonance of the tryptophan methine (H_a).

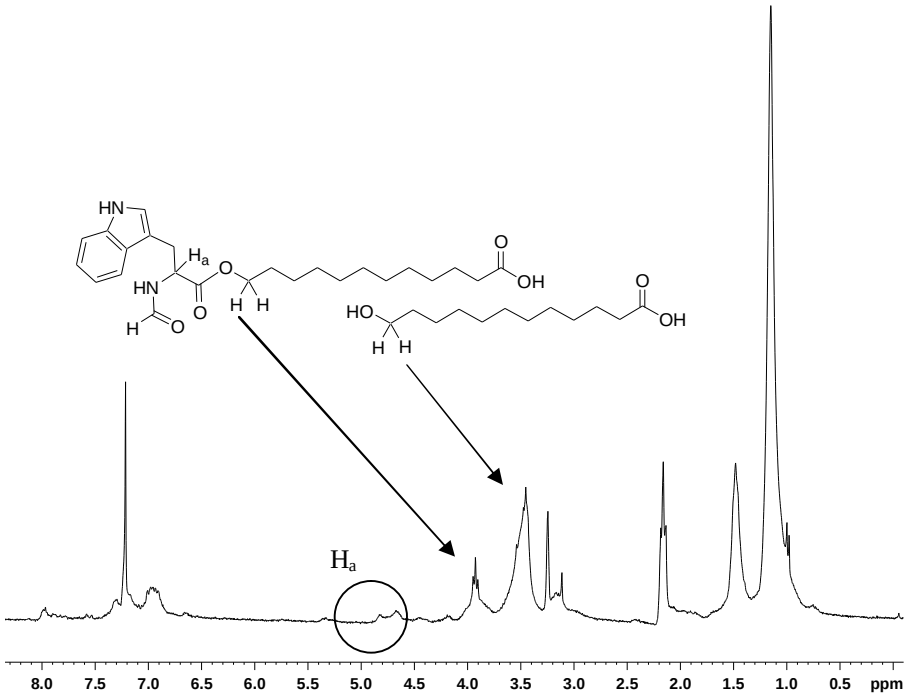

Figure 5-8. ^{1}H NMR spectrum of the crude product from the synthesis of **5-11** in $CDCl_3$.

In the synthesis of **5-12**, **2-3** was coupled onto Wang resin; the secondary alcohol was deprotected by a fluoride treatment; and then a DIC/DMAP-activated solution of **5-6** was introduced (Scheme 5-5).

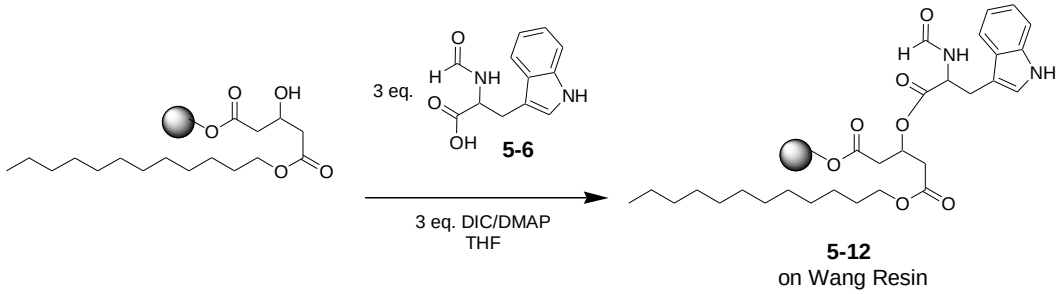

Scheme 5-5. Proposed synthesis of **5-12** on Wang resin.

The ^{1}H NMR spectrum (Figure 5-9) of the crude product cleaved from the resin using TFA:CH_2Cl_2 did not show the Trp indole protons, as well there was no evidence of a downfield shift for the methine next to the ester if **5-12** (H_a) was made (circled region in the figure).

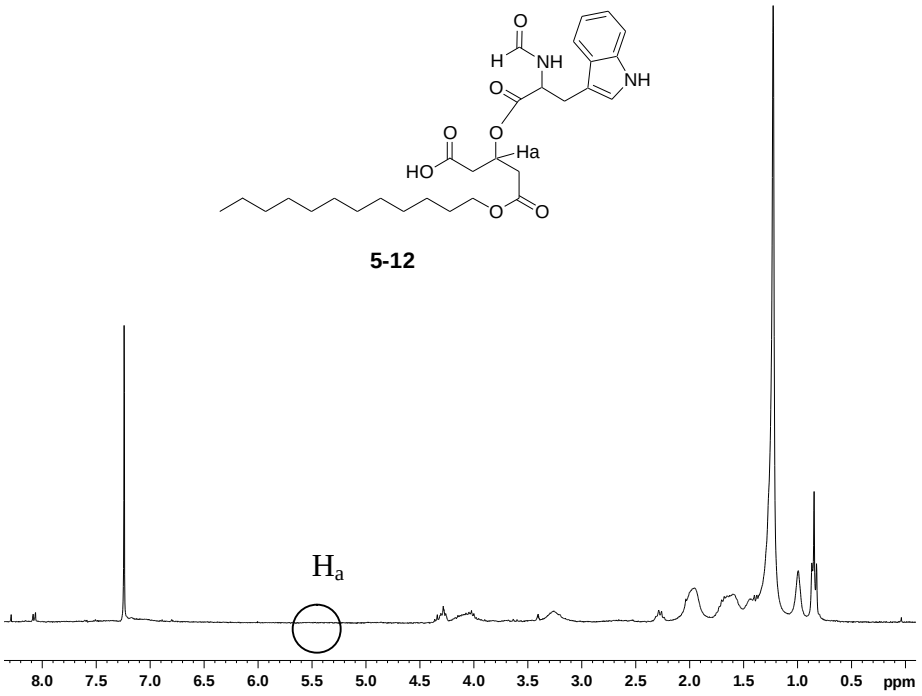

Figure 5-9. ^{1}H NMR spectrum (in $CDCl_3$) of an attempt to synthesize **5-12**.

Attempts to synthesize models **5-12** and **5-11** using DIC/DMAP coupling conditions showed that it was very difficult to couple **5-6** to either the primary or secondary alcohol. From the failed attempts at synthesizing **5-12** and **5-11**, it was not surprising that **5-2** could not be made efficiently by the DIC/DMAP coupling conditions.

5.2 Transport Studies of 5-1

The transport of **5-1** was measured in vesicles with encapsulated HPTS. The rate constant observed for **5-1** is reported in Table 5-2.

Table 5-2. Transport data for **5-1** from HPTS vesicles assay.

$[\mathbf{5\text{-}1}]_{bulk}$ (mM)	**[5-1]** (mol % in lipid)	k (x 10^4 s^{-1})	Methanol rate constant (x 10^4 s^{-1})	$k_{32\ \mu M}$ (x 10^4 s^{-1})
0.11	10	7.0 ± 1.4	1.0 ± 0.2	2.1 ± 0.4

The normalized rate constant for **5-1** at 32 μM is about a third of the calculated value for **2-27** (6.1 x 10^{-4} s^{-1}). The difference in rate constants was not unexpected

because a head group modification has been made to the **2-27** structure. Recall as well that based on the MS and HPLC data, deletion sequences are also present in the **5-1** product. Therefore the actual reported bulk concentration would be an overestimate of the amount of **5-1** in solution. Since the normalized rate constants were derived from the bulk concentration, then these rate constants would be an underestimate of the true value.

5.3 Fluorescence Studies

Compound **5-1** was found to be an active ion channel-forming compound. Therefore there was no doubt that the compound partitioned into a bilayer membrane. As mentioned before, the indole ring of the Trp unit is fluorescent and like many fluorophores, the fluorescence can be quenched. Since compound **5-1** can partition into a lipid membrane and we are interested in determining the orientation of the compound in a bilayer membrane, then the fluorescence of the indole ring can be used to probe for orientation preference within the bilayer membrane.

One literature example of orientation studies of synthetic ion channels was by Gokel.[94] Gokel was interested in determining the location of the hydraphile (**5-13**) head group within a membrane bilayer.

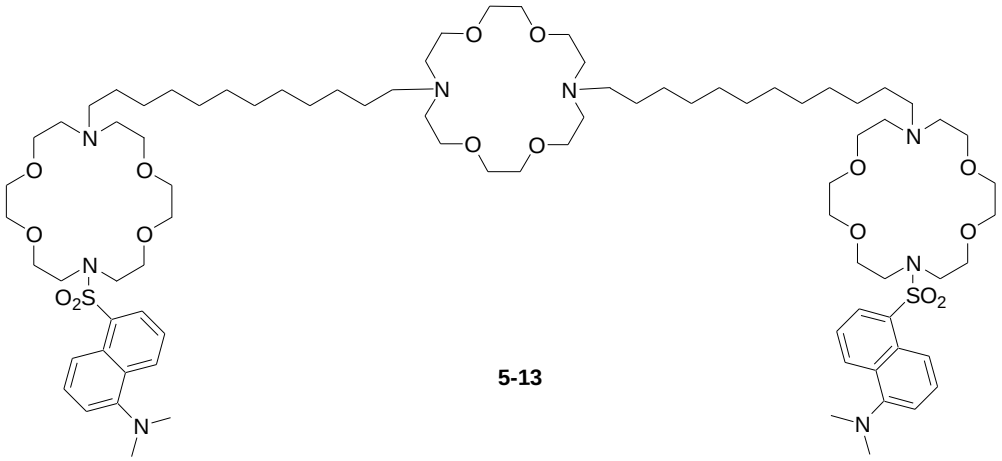

5-13

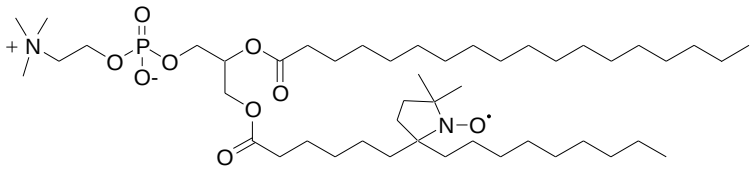

5-14

The hydraphile **5-13** is different from previously synthesized hydraphiles because it possessed a fluorescent dansyl head group. The dansyl fluorescence can be quenched by the radical center on doxyl heterocycles. Gokel used a mixture of lipids, some with attached doxyl groups (for example **5-14**) and some without, to prepare the lipid vesicles. The doxyl group on the lipid quenches the dansyl fluorescence as a function of distance between the fluorophore and quencher. From these studies, he found that the hydraphile was located in the membrane as a monomer and that the dansyl groups at either end of the molecule were distant from the doxyl label near the center of the bilayer by about 14 Å. This distance implied that the head groups were in the vicinity of the mid-polar region.

In comparison to the dansyl group, the tryptophan (Trp) residue is important for studying protein structure and function because of the fluorescent nature of the indole. By incorporating a Trp residue to the channel-forming compound it can be possible to infer where the Trp resides via the addition of a fluorescence quencher. Several

possibilities are illustrated in Figure 5-10. As previously mentioned, compound insertion into the bilayer could occur using one or both of the hydroxy terminus and carboxylic acid terminus. If the hydroxy terminus inserts through the bilayer membrane, then the Trp head group would be extravesicular. Should the carboxylic acid end partitions through the bilayer membrane, then the Trp head group is intracellular. If the Trp residue existed on the external surface of the vesicle, then upon the addition of a quencher in the extravesicular phase, the fluorescence intensity would decrease. On the other hand, if the Trp partitions into the interior of the vesicle, then the Trp fluorescence should not change with the addition of quencher to the external buffer.

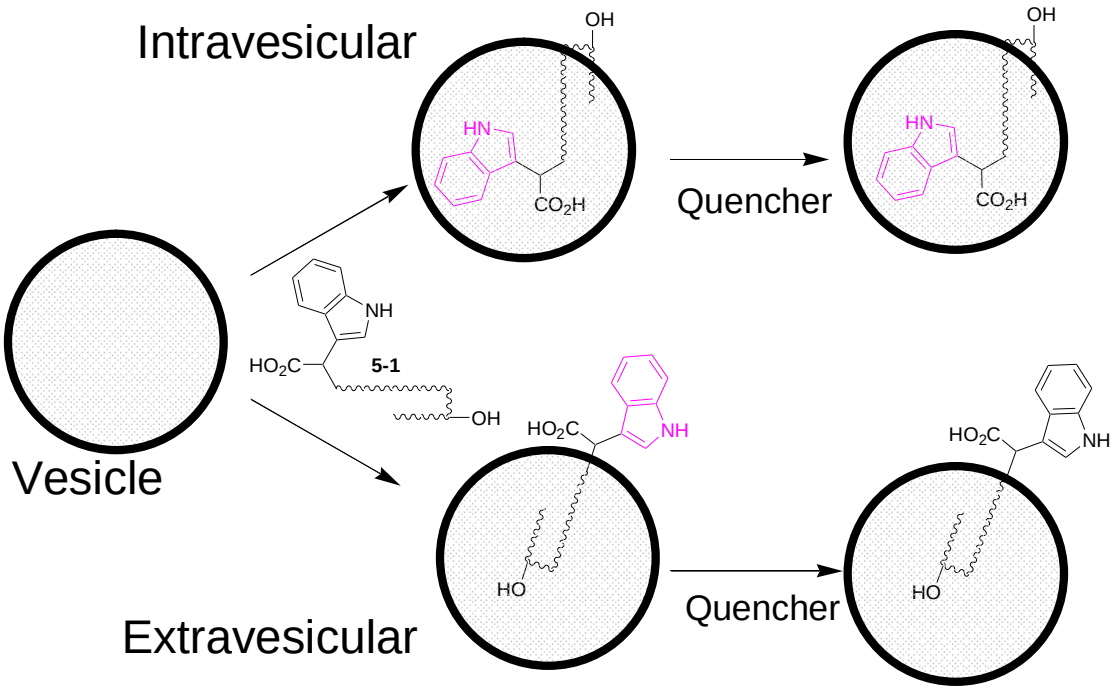

Figure 5-10. Partition studies of the Trp head group by fluorescence quenching experiments. Pink indole moiety represents Trp in the electronic excited state.

Tryptophan fluorescence is quenched with a variety of molecules such as acrylamide, hydrogen peroxide, succinimide, imidazole and iodide.[92] For these studies it was important that the chosen quencher does not pass through the bilayer membrane easily. The transported ions by the oligoester ion channel-forming compounds were not

established, but common quenchers such as Cs^+ and I^- should be avoided as these are potentially transported. A small molecule, acrylamide, was used as the quencher in this experiment because of its availability and relatively high purity (>99.9%). Assumptions were made that hydrophilic acrylamide would not diffuse through the membrane easily. The assumption will be verified shortly.

The excitation scan was measured to ensure that the excitation of the chromophore on **5-1 (**Figure 5-11**)** was the same as any other tryptophan derivative represented by **5-6** (Figure 5-12). The remarkable similarity between the peak shapes of **5-1** and **5-6** indicated that the Trp moiety functioned appropriately. The concentrations used to perform the excitation scan were about the same (33-38 μM) but the overall absorption by **5-1** (Figure 5-11) was about twice that of **5-6** (Figure 5-12). When the solutions were prepared for the fluorescence assays, the mass of the product was thought to have been strictly **5-1**. Based on the analysis of the HPLC and MALDI MS data, deletion sequences were present in **5-1** which yielded more Trp-containing molecules in solution than anticipated if the product was only **5-1**. For example, two equivalents of **5-1** have roughly the same molecular weight as three equivalents of **5-9**; so at equal masses, there is 50% more Trp-chromophore.

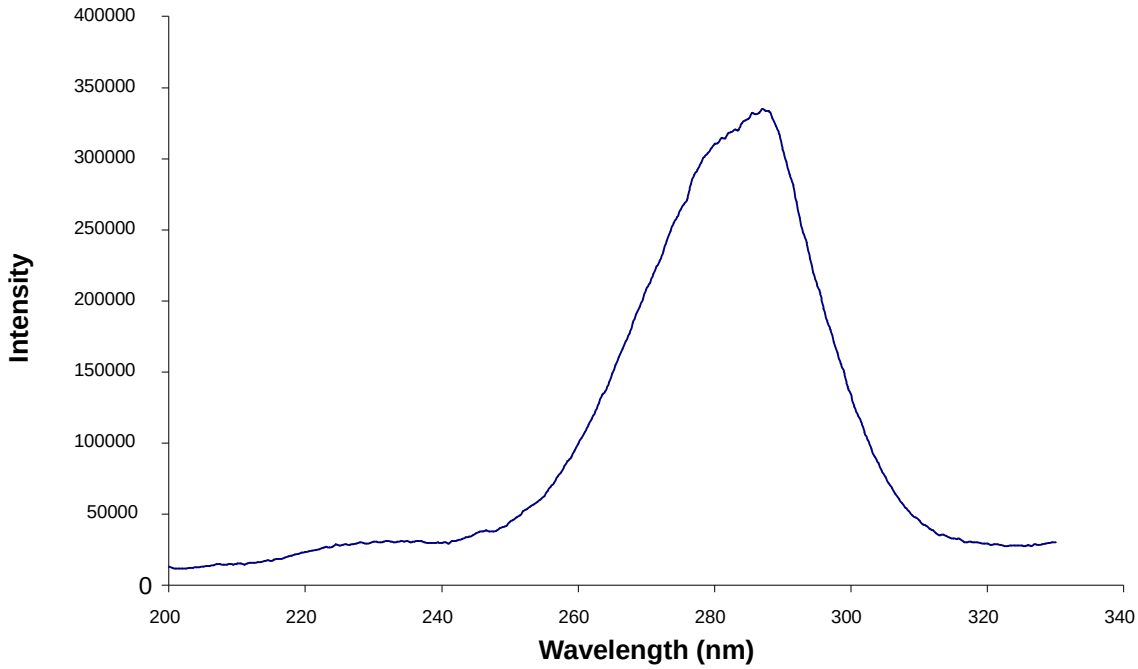

Figure 5-11. Excitation scan spectrum of **5-1** (38 µM) in external buffer (background corrected) with emission at 351 nm.

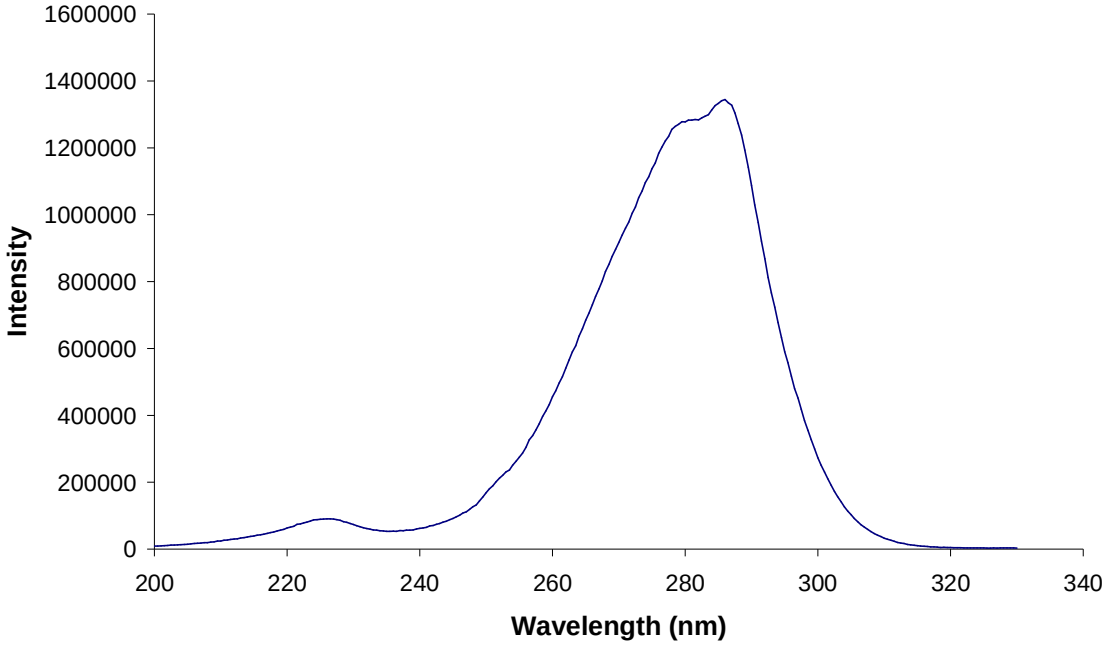

Figure 5-12. Excitation scan spectrum of **5-6** (33 µM) in external buffer (background corrected) with emission at 351 nm.

It was necessary to establish how the location of the Trp can be determined. For these studies the control compound of choice was the N-formyl tryptophan (**5-6**) because the lack of lipophilic groups on **5-6** was thought to prevent it from partitioning into the membrane bilayer.

The relationship between the concentrations of quencher added versus the quenched intensity is usually related linearly by an equation known as the Stern-Volmer equation (5-1):

(5-1) $$\left(\frac{1}{F}\right)\left(\frac{F_i \times V_i}{V_t}\right) = \frac{F_o}{F} = 1 + K_s[Q]$$

In equation (5-1), F_i is the initial Trp fluorescence intensity in the buffer and vesicles solution prior to the addition of the quencher; F is the observed Trp fluorescence intensity at a particular [Q]; V_i is the initial volume; V_t is the total volume at the end of the experiment; K_s is a constant; and [Q] is the quencher concentration in the overall solution (ranging in quencher concentration of 0 to 0.12 M). Together the terms F_i, V_i, and V_t combine to give F_o which is what the unquenched Trp fluorescence intensity should be taking solution dilution into account. Normally a plot of (F_o/F) vs. [Q] is linear for a simple quenching mechanism (either dynamic or static quenching). When the linearity fails then this is usually a sign that there are different fluorophores in different environments and that several quenching mechanisms exist.[95] Dynamic quenching is the result of the collisions that occur between the fluorophore and the quencher during the excited state lifetime, whereas static quenching is the result of a complex formed between the quencher and fluorophore to give a non-fluorescent ground-state.[95]

Two scenarios were designed: 1) **5-6** was encapsulated into vesicles and quencher was injected into the external buffer (external vesicle environment) and 2) **5-6**

was introduced to the external buffer and then quencher added. Two types of vesicles were made to demonstrate the Trp quenching principle: 1) vesicles with a diameter of about 217 ± 27 nm were made with **5-6** encapsulated (0.86 mM) and 2) vesicles with a diameter of 254 ± 29 nm with no **5-6** encapsulated. In the fluorescence experiments for the vesicles without **5-6**, a background subtraction of the external buffer and vesicles was done. The external and internal buffers are the same in these tryptophan experiments and consist of a sodium phosphate (10.05 mM) and sodium sulfate buffer (75.22 mM) at pH 6.4. The excitation of the Trp group was done at 288 nm and the emission scan was collected between 320 – 400 nm.

In the Trp quenching experiments it was first necessary to establish the Stern-Volmer plot for a solution of just quencher and Trp containing compound in external buffer without vesicles (Figure 5-13). The Stern-Volmer plot for the model **5-6** gave a slope of 10.8 M^{-1} calculated from a linear function. The y-intercept is normally 1 for a Stern-Volmer plot, but the y-intercept is 0.89 which suggests that the function is not linear but may be a positive (upward) deviation. The upward deviation is usually evidence for a combination of static and dynamic quenching mechanisms.[92]

The data appeared more linear for compound **5-1** which had a slope of 9.1 M^{-1} and a y-intercept of 1.05. If the data for **5-6** was treated by linear regression, then the slopes by both compounds were approximately the same.

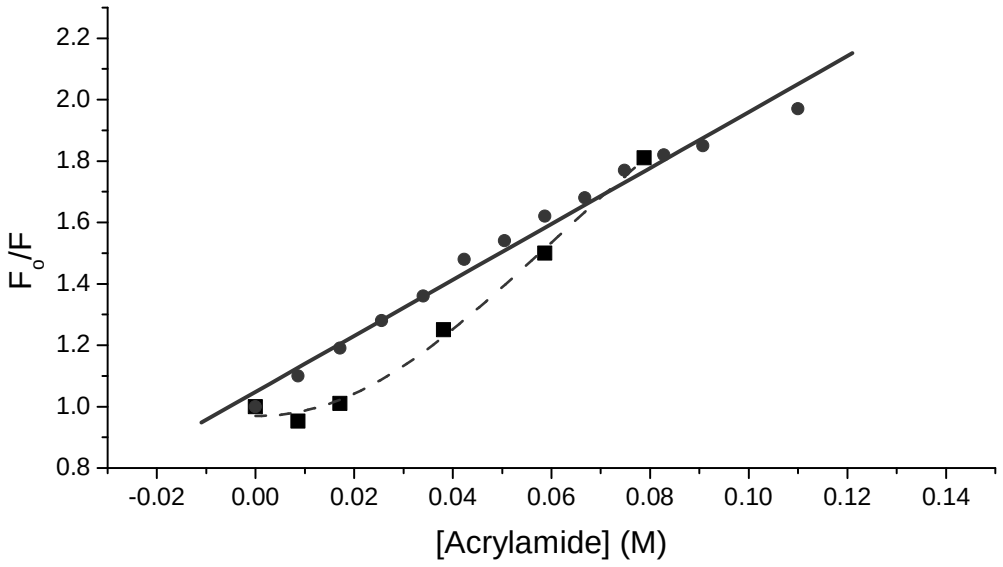

Figure 5-13. Stern-Volmer plot for (■) **5-6** and (•) **5-1** in external buffer. Excitation at 288 nm; emission at 320-400 nm.

Vesicles were made which had either intravesicular or extravesicular **5-6**.

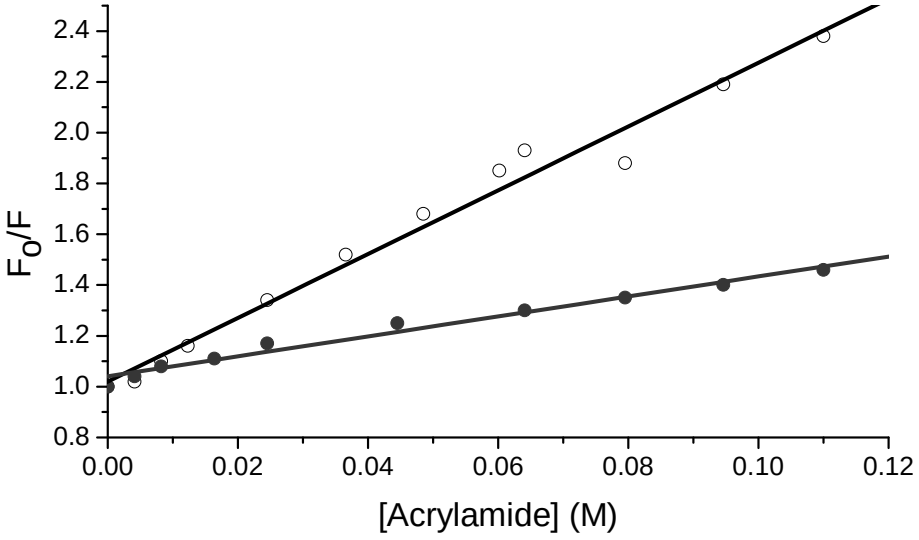

Figure 5-14. Stern-Volmer plot for (o) vesicles with extracellular **5-6** and (•) vesicles with intracellular **5-6**.

Linear fits were placed through the data in Figure 5-14 for extravesicular **5-6** and intravesicular **5-6**. The slopes of these lines are 12.6 M^{-1} and 4.0 M^{-1}, respectively. The

corresponding y-intercept for extravesicular 5-6 and intravesicular 5-6 are 1.02 and 1.04, respectively.

The differences in slopes of the entrapped and external **5-6** suggested that this assay was sensitive to the location of the Trp with respect to the membrane. The slope for the vesicles with entrapped **5-6** was expected to be zero because no quenching should occur. However, a low slope was observed and this suggested that acrylamide can diffuse through the membrane to quench some of the entrapped **5-6**. Alternatively some **5-6** could partition to the vesicle surface and their fluorescence quenched.

The quenching of **5-1** and **5-6** in the absence of vesicles are similar (Figure 5-13), so it was assumed that the response of **5-1** in vesicles would be similar to **5-6** in vesicles (Figure 5-14).

To determine the fluorescence response of **5-1** in vesicles, vesicles in external buffer were equilibrated with **5-1** (36 μM) for about 30 seconds. Increasing concentrations of acrylamide were added to the solution and the fluorescence of Trp was measured. The data collected were plotted in a Stern-Volmer plot (Figure 5-15).

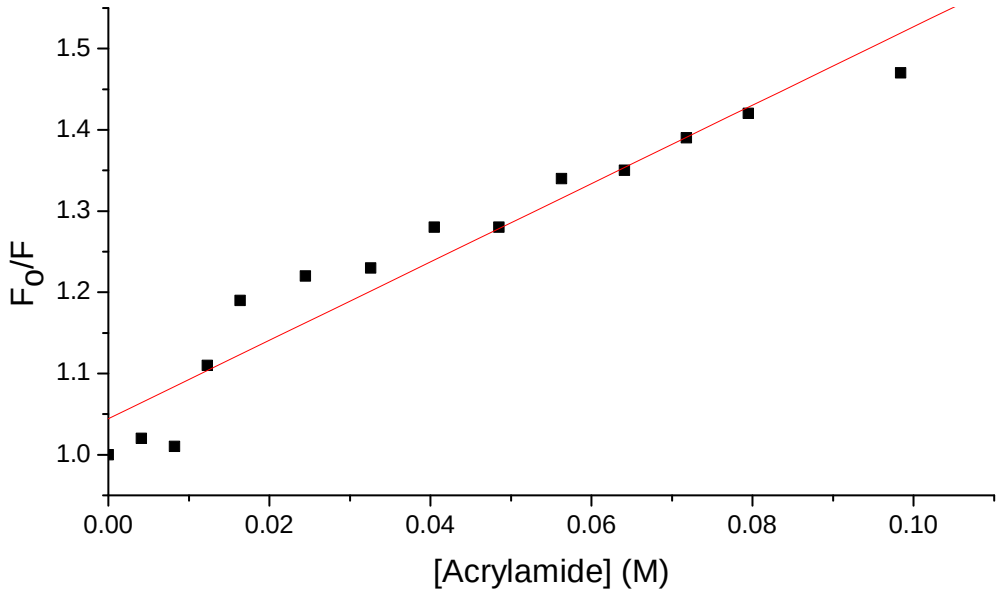

Figure 5-15 Stern-Volmer plot of **5-1** in the presence of vesicles.

The data in Figure 5-15 fits a linear function and the slope from the Stern-Volmer plot is 4.8 M^{-1} which is exceedingly close to the slope from the Stern-Volmer plot of intravesicular **5-6** (4.0 M^{-1}) (Figure 5-15). A y-intercept of 1.04 from the Stern-Volmer plot is similar to the other intercepts found in the other examples.

A summary of the Stern-Volmer data is shown in Table 5-3.

Table 5-3. Summary of Stern-Volmer data for **5-1** and **5-6**.

Condition	Slope (M^{-1})	Intercept
External buffer with only **5-1**	9.1	1.05
External buffer with only **5-6**	10.8	0.89
Vesicles entrapped with **5-6**	4.0	1.04
5-6 injected extravesicular	12.6	1.02
5-1 injected extravesicular	4.8	1.04

Since the fluorescence quenching of **5-1** in vesicles was not very efficient, then this data suggested that the Trp head group of **5-1** partitions into the vesicle interior. Presently this data implied that a majority of the Trp head group was hidden from the

quencher. It is possible that the Trp is completely partitioned into the intravesicular volume. Alternatively the head group may simply be buried in the hydrophobic region of the bilayer membrane (Figure 5-16).

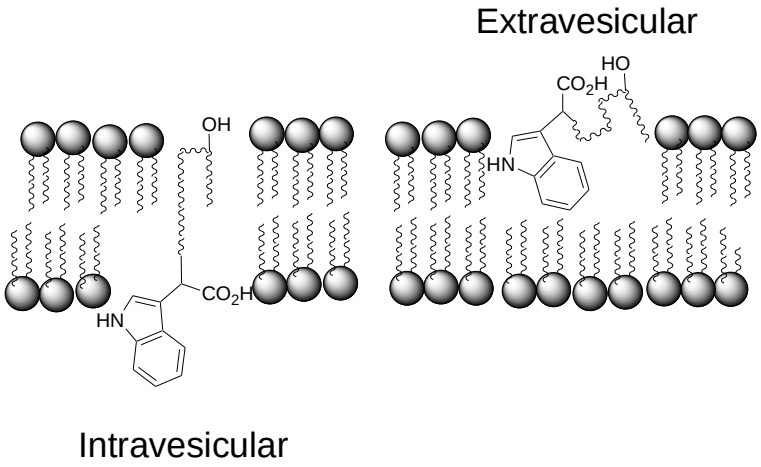

Figure 5-16. Diagram depicting possible orientations for **5-1** in a bilayer membrane.

Past research by Fyles[68] proposed that certain functional groups on an ion channel would pass through a bilayer membrane (such as a monoanionic acetate head group). In their cases the channel was anchored to one side of the membrane by a dianionic head group while the monoanionic head group partitioned through the membrane. In the Trp example, there is no divalent head group and the "anchoring group" is neutral. In contrast to the Fyles example, one of the driving forces for the carboxylic acid of the amino acid derivative to pass through the bilayer membrane was an electrical potential. In the tryptophan quenching experiments a pH gradient was not induced; therefore under the pH of external and internal buffer (about 6.4), the carboxylate anion is dominant over the carboxylic acid for the ion channel candidate form. Hence, the migration of the carboxylic head group through to the interior membrane cannot be driven by electrochemical potential. It can be driven by

hydrophobic partitioning and by voids in the bilayer membrane where the indole ring can fit appropriately such that the indole is buried.

In this chapter the Trp building block was shown to be a useful group to append to the oligoester ion channels. Using unoptimized amino acid coupling conditions an oligoester ion channel was made containing a Trp group. The fluorescent nature of the Trp indole ring provided a handle for monitoring chromatographic separation. The Trp indole fluorescence was also used for examining the orientation of the oligoester ion channels in the bilayer membrane. Evidence from the Trp quenching experiments showed that the Trp moiety was hidden from the acrylamide quencher. Therefore two possible orientations for the ion channel is either to have the fluorescent Trp head group buried in the membrane or have the head group diffuse through the membrane and end up intravesicular. Either way, the finding that there is a preferential molecular orientation within the bilayer is important for heading towards voltage-gated ion channels.

Chapter 6 Conclusions and Future Work

The goals of this thesis were to optimize a way to generate simple asymmetric ion channel-forming compounds and to develop a way to evaluate their ability to transport ions through a membrane bilayer. Eventually the asymmetric compounds can lead to structures which can be voltage-gated in a bilayer membrane.

The optimized syntheses of oligoester ion channel-forming compounds have been proposed in this thesis. It was found that up to pentameric oligoesters can be made using hydroxy acid building blocks containing as many as 12-carbon long chains. The coupling reactions between building blocks have been optimized to show that many of the compounds made showed very few impurities containing sequences missing greater than one monomeric unit. However, it was found that there were sequences which had an extra monomer unit. These addition sequences are suspected to arise due to the impurities present in the building blocks. The impurities may be a relatively minute amount, undetectable by ^{1}H NMR spectroscopy, but over several coupling cycles on the solid they do add up.

The oligoester compounds made were tested for ion transport activity using a fluorescence vesicle assay. Many of the oligoester compounds were found to be active ion transporters but there was a dependence on the oligoester structure for relatively high activity. There needed to be a certain amount of lipophilicity in the overall structure to yield high ion transport activity. Yet it was also found that too much lipophilicity lead to transport inactive compounds. It is proposed that the inactivity of these more lipophilic compounds is due to either the compounds aggregate in solution or partitioning

efficiently into the bilayer membrane but once they are in the bilayer membrane repartitioning back into the aqueous phase is unfavored.

In order to generate a voltage-gated ion channel, a large dipole must be present in the ion channel. One way of generating a large dipole is to have structural ionic units. Amino acids exist with a variety of functionalities and therefore the ability to append these groups onto a structure can lead to a diverse library of compounds. The fluorescent amino acid tryptophan was incorporated into the structure of one of the most transport active oligoester ion channel-forming compounds to generate **5-1**. The ability to do this demonstrated that we can extend our methodologies of making oligoester compounds to containing amide linkages as well by coupling on amino acids.

The synthesis of these amide containing oligoesters has not been optimized so several shorter sequences exist in the product mixture. The tryptophan derivatized compound (**5-1**) forms ion channels. The orientation of **5-1** was studied using fluorescence quenching experiments by comparing the Stern-Volmer plot results to the quenching results of encapsulated and nonencapsulated **5-6** in vesicles. The comparison showed that **5-1** was either oriented with the head group located intravesicular or it may have been buried within the membrane and therefore prevented fluorescence quenching.

The goal of generating asymmetric oligoester ion channel-forming compounds has been met. The structure-activity relationship of these compounds has been examined and provides insight in the design of future oligoester compounds synthesized by SPOS.

Many doors have been opened for future experiments pertaining to this dissertation. Similar to many simple ion channel-forming compounds, the synthesized oligoesters are expected to aggregate in the membrane to form an active structure for ion

conduction. It would be interesting to determine how many molecules are required to form an active structure (the kinetic order) and whether there is only one active structure available. Normally using a pH-stat titration method of evaluating transport activity, a kinetic order can be calculated from the relationship of the initial transport rates to the transporter concentrations.[25] Planar bilayer clamp experiments can be done to determine how many channel types are present. If there is only one conducting channel type, then there is a linear relationship between the conductance and level number in the bilayer clamp traces. If varying conducting states are present, then the relationship between conductance and level number will deviate from linearity.[96]

Vesicles with entrapped CF can be used as an estimate of the channel structure size. If the formed ion channels are relatively large and stable, then perhaps atomic force microscopy may be used to measure the dimensions.

The ion selectivity of the channel-forming compounds is also important and the oligoester compounds should be tested for ion selectivity using either vesicle assays[54] or planar bilayer clamp experiments.[23]

The Trp fluorescence quenching experiments showed that **5-1** was buried in the membrane with either the Trp head group in the outer or inner bilayer leaflet. Regardless, the indole moiety is not at the extravesicular surface of the vesicle. Further research using these preliminary results would be to place a fluorescence quencher in the internal buffer to see if the Trp head group can be quenched which can confirm compound unidirectional insertion into the membrane (Trp on the surface of the inner leaflet).

Eventually, these voltage-gated ion channels may be found in applications where a network has been made for demonstrating artificial nerves and signal propagation.

Chapter 7 Experimental

7.1 Apparatus

All reagents were obtained from commercial sources and were used without further purification unless noted otherwise. Dry THF was dried over sodium and benzophenone and distilled. Pyrene was purified by column chromatography using silica gel and cyclohexane as eluent.

All NMR spectra were recorded on a Bruker Advance 500 (500 MHz ^{1}H and 125 MHz ^{13}C) or Bruker AC300 (300 MHz ^{1}H and 75.47 MHz ^{13}C). Chemical shifts are reported relative to tetramethylsilane in ppm (δ). FT-IR spectra were recorded on a Perkin-Elmer Spectrum One FT-IR spectrometer. Liquid secondary ion mass spectra (LSIMS) and EI were recorded on a Kratos Concept double focusing magnetic instrument. MALDI MS were recorded by the UVic Genome Proteomics Centre on a Voyager DE STR MALDI-TOF (Voyager) mass spectrometer and using a α–cyano-4-hydroxycinnamic acid (CHCA) or 2,5-dihydroxybenzene (DHB) (CH_2Cl_2) matrix. Samples for MALDI MS were dissolved in 50 μL $CHCl_3$, 1-2 μL of sample spotted onto stainless steel MALDI target plates, allowed to dry, 1 μL of matrix spotted overtop of sample and allowed to dry prior to MS analysis.

Elemental analyses were performed by Canadian Microanalytical Services Ltd., Delta, BC, Canada.

Thin layer chromatography was performed on Macherey-Nagel polygram sil /UV_{254} for TLC plate. Column chromatography was performed on silica gel (grade 60, 60-200 mesh). Size exclusion separation was performed on a column packed with

Lipophilic Sephadex LH-20 (Sigma). High performance liquid chromatography (HPLC) was performed on a Jordi gel DVB GPC column (500 A, 5 micron, 250 mm x 10 mm).

The injector port on the fluorimeter was made from an aluminum cylinder long enough to span the distance from the lid on the fluorimeter to the top of the cuvette. A hole was bore through the center of the aluminum cylinder. The NaOH solution was injected from a syringe attached to a piece of Tygon tubing and threaded through the aluminum bore.

7.2 Procedures

7.2.1 Synthesis of Building Blocks

3-(*tert*-butyl dimethylsiloxy)-5-oxo-5-(decyloxy) pentanoic acid (2-2). To a stirred toluene solution (20 mL) of 3-(*tert*-butyldimethylsilyloxy)glutaric anhydride (0.97 g, 3.96 mmol) was added 1-decanol (0.75 mL, 3.92 mmol). The solution was stirred at reflux overnight and the solvent was removed under reduced pressure to give a crude product. The crude product was dissolved in pentane (80 mL) and cooled in a dry ice/ethanol bath for 10 minutes before filtration. The filtrate was cooled again in a dry ice/ethanol bath for 10 minutes and then filtered. This crystallization was repeated until no more solids were produced. The filtrate was concentrated under reduced pressure to afford a colorless oil identified as **2-2** (1.49 g, 93%). ^{1}H NMR (500 MHz, $CDCl_3$): 0.04-0.06 (m, 6H), 0.82-0.89 (m, 12H), 1.24 (br, 14H), 1.57-1.61 (m, 2H), 2.53-2.64 (m, 4H), 4.01-4.07 (m, 2H), 4.52 (quintet, 1H, J = 6 Hz); ^{13}C NMR (125.77 MHz, $CDCl_3$): -4.8, -4.7, 14.3, 18.1, 22.9, 25.8, 26.1, 28.8, 29.45, 29.50, 29.71, 29.73, 32.1, 42.4, 42.6, 65.1, 66.3, 171.2, 177.0. IR: 1736 cm^{-1} (s), 1711 cm^{-1} (s). HRLSIMS: Calcd for $C_{21}H_{42}O_5SiNa^+$ [M+Na^+]: 425.2699 Found: 425.2717.

3-(*tert*-Butyl dimethylsiloxy)-5-oxo-5-(dodecyloxy) pentanoic acid (2-3). To a stirred toluene solution (20 mL) of 3-(*tert*-butyldimethylsilyloxy)glutaric anhydride (1.9 g, 7.79 mmol) was added 1-dodecanol (1.40 g, 7.49 mmol). The solution was stirred at reflux overnight and the solvent was removed under reduced pressure to give a crude product. The crude product was dissolved in pentane (80 mL) and cooled in a dry ice/ethanol bath for 10 minutes before filtration. The filtrate was cooled again in a dry ice/ethanol bath for 10 minutes and then filtered. This crystallization was repeated until no more solids were produced. The filtrate was concentrated under reduced pressure to afford a colorless oil identified as **2-3** (3.18 g, quantitative yield). ^{1}H NMR (300 MHz, $CDCl_3$): 0.05 and 0.06 (2 singlets, 6H), 0.82-0.88 (m, 12H), 1.24 (br, 18H), 1.50-1.63 (m, 2H), 2.51-2.66 (m, 4H), 3.95-4.10 (m, 2H), 4.52 (quintet, 1H, J = 6 Hz); reported ^{1}H NMR resonances from reference ([25]): 0.00 and 0.01 (2 singlets, 6H), 0.76-0.79 (m, 12H), 1.05-1.32 (br, 18H), 1.52-1.58 (m, 2H), 2.42-2.70 (m, 4H), 3.78-4.26 (m, 2H), 4.47 (qu, 1H); ^{13}C NMR (75 MHz, $CDCl_3$): -4.8, -4.7, 14.3, 18.1, 22.9, 25.8, 26.1, 28.8, 29.5, 29.6, 29.71, 29.77, 29.84, 32.1, 42.4, 42.6, 65.1, 66.3, 171.2, 177.0. reported ^{13}C NMR resonances from reference ([25]): -4.9, 14.1, 17.8, 22.7, 25.6, 25.9, 28.5, 29.2, 29.3, 29.4, 29.5, 29.6, 31.9, 64.8, 66.1, 170.9, 176.7. IR: 1738 cm^{-1} (s), 1713 cm^{-1} (s). HRLSIMS: Calcd for $C_{23}H_{47}O_5Si^{+}$ [$M+H^{+}$]: 431.319 Found: 431.320.

3-(*tert*-Butyl dimethylsiloxy)-5-oxo-5-(tetradecyloxy) pentanoic acid (2-4). To a stirred toluene solution (20 mL) of 3-(*tert*-butyldimethylsilyloxy)glutaric anhydride (1.92 g, 7.86 mmol) was added 1-tetradecanol (1.65 g, 7.68 mmol). The solution was stirred at reflux overnight and the solvent was removed under reduced pressure to give a crude product. The crude product was dissolved in pentane (80 mL) and cooled in a dry

ice/ethanol bath for 10 minutes before filtration. The filtrate was cooled again in a dry ice/ethanol bath for 10 minutes and then filtered. This crystallization was repeated until no more solids were produced. The filtrate was concentrated under reduced pressure to afford a colorless oil identified as **2-4** (2.514 g, 71%). ^{1}H NMR (500 MHz, $CDCl_3$): 0.04-0.08 (m, 6H), 0.82-0.89 (m, 12H), 1.23 (br, 22H), 1.57-1.62 (m, 2H), 2.53-2.64 (m, 4H), 4.01-4.08 (m, 2H), 4.52 (quintet, 1H, J = 6 Hz); ^{13}C NMR (125.77 MHz, $CDCl_3$): -4.8, -4.7, 14.3, 18.1, 22.9, 25.9, 26.1, 28.8, 29.5, 29.6, 29.72, 29.79, 29.86, 29.88, 29.9, 32.1, 42.4, 42.6, 65.1, 66.3, 171.2, 177.0. IR: 1738 cm^{-1} (s), 1713 cm^{-1} (s). HRLSIMS: Calcd for $C_{25}H_{50}O_5SiNa^+$ [M+Na^+]: 481.3325 Found: 481.3307.

3-(*tert*-Butyl dimethylsiloxy)-5-oxo-5-(hexadecyloxy) pentanoic acid (2-5). To a stirred toluene solution (20 mL) of 3-(*tert*-butyldimethylsilyloxy)glutaric anhydride (1.9 g, 7.9 mmol) was added 1-hexadecanol (1.48 g, 6.10 mmol). The solution was stirred at reflux overnight and the solvent was removed under reduced pressure to give a crude product. The crude product was dissolved in pentane (80 mL) and cooled in a dry ice/ethanol bath for 10 minutes before filtration. The filtrate was cooled again in a dry ice/ethanol bath for 10 minutes and then filtered. This crystallization was repeated until no more solids were produced. The filtrate was concentrated under reduced pressure to afford a colorless oil identified as **2-5** (0.977 g, 33%). ^{1}H NMR (500 MHz, $CDCl_3$): 0.04-0.08 (m, 6H), 0.82-0.89 (m, 12H), 1.23-1.32 (m, 26H), 1.57-1.63 (m, 2H), 2.54-2.65 (m, 4H), 4.01-4.08 (m, 2H), 4.52 (quintet, 1H, J = 6 Hz); ^{13}C NMR (125.77 MHz, $CDCl_3$): -4.8, -4.7, 14.3, 18.1, 22.9, 25.9, 26.1, 28.8, 29.5, 29.6, 29.73, 29.80, 29.88, 29.89, 29.92, 32.2, 42.3, 42.5, 65.1, 66.4, 171.2, 176.2. IR: 1738 cm^{-1} (s), 1713 cm^{-1} (s). HRLSIMS: Calcd for $C_{27}H_{55}O_5SiNa^+$ [M+Na^+]: 487.3813 Found: 487.3813.

Trifluoroacetyl-L-aspartic acid 5-dodecyl ester (2-10). The anhydride (**2-8**) was made from L-aspartic acid (2.09 g, 15.2 mmol) and trifluoroacetic anhydride (10 mL) according to a literature procedure.[74] **2-8** was isolated as a solid by removing the solvent in vacuo. To the crude product, 20 mL pentane and 1-dodecanol (3.6 mL, 15.7 mol) were added and stirred for three hours at room temperature followed by addition of 50 mL toluene and stirred for another three hours. The solvent was removed in vacuo to yield a wax, **2-10**. (4.85 g, 80% from L-aspartic acid). ^{1}H NMR (300 MHz, $CDCl_3$): 0.86 (t, *J*=6.8 Hz, 3H), 1.22-1.71 (overlapping signals, 24H), 2.83-3.19 (multiplet, 2H), 4.17 (t, *J*=6.8 Hz, 2H), 4.78-4.84 (m, 1H), 6.29 (m, 1H). 7.41 (d, J=7.8, 1H). ^{13}C NMR (75.47 MHz, $CDCl_3$): 14.3, 22.9, 25.9, 26.0, 28.5, 28.7, 29.3, 29.6, 29.7, 29.75, 29.83, 32.1, 35.4, 35.6, 49.0, 49.2, 66.0, 66.9, 67.1, 115.8 (q, *J*=287 Hz), 157.4 (q, *J*=38 Hz), 169.4, 171.0, 175.0.

Trifluoroacetyl-DL-glutamic acid 5-dodecyl ester (2-11). The dodecyl ester glutamic acid (**2-6**) was made in 28% yield according to a proposed literature procedure (reported yield of 48.5%).[97] The reported melting temperature for the pure product was 177-177.4 ºC while we found a decomposition temperature of 110-129ºC for the crude product. **2-6** was dissolved in 1 mL of trifluoroacetic anhydride and stirred for 1 hour. The solvent was removed in vacuo to yield a white solid identified as **2-11** (0.345 g, 92%). ^{1}H NMR (300 MHz, $CDCl_3$): 0.83 (t, 4H, *J*=6.5 Hz), 1.22-1.57 (m, 29H), 2.1-2.5 (m, 4H), 4.04 (t, 3H, *J*=6.7 Hz), 4.5-4.6 (m, 1H), 7.93 (d, 1H, *J*= 7.3 Hz), 9.24 (br s, 2H); ^{13}C NMR (75 MHz, $CDCl_3$): 14.2, 22.8, 23.7, 26.0, 26.1, 26.4, 28.6, 29.4, 29.5, 29.66, 29.74, 29.8, 30.4, 32.1, 52.5, 53.2, 65.7, 65.9, 115.8 (t, *J*=287 Hz), 157.9 (t, *J*=38 Hz), 173.7, 174.2.

2-(*tert*-Butyl dimethylsilanyloxymethyl)-dodecanoic acid (**2-13**). To a stirred solution under a dry ice and ethanol bath of THF (180 mL) and disopropylamine (8.2 mL) was added butyl lithium (39 mL, 1.6 M). The solution was stirred for 10 minutes at 0ºC. A THF solution (30 mL) of lauric acid (5.86 g, 29.2 mmol) was added dropwise such that the solution was below 0ºC. Upon the full addition the mixture was heated to 35ºC for 1.5 hours while formaldehyde was bubbled in (by a thermal decomposition of 13.6 g of paraformaldehyde). The mixture was then cooled below 10ºC and then 100 mL of 1 M HCl was added. To the mixture 500 mL of THF was added and the aqeous layer was removed. The organic layer was then washed with 300 mL water dried with Na_2SO_4 and concentrated *in vacuo*. The crude product was purified on a silica gel column (53 g, 3 cm ID x 30 cm) using petroleum ether: ethyl acetate (4:1) to yield a clear, colorless oil (0.617 g, 9%). The pure oil was dissolved in 50 mL DCM and imidazole (0.73 g, 4 eq.), *tert*-butylchlorodimethylsilane (0.81 g, 2 eq.) was added. The mixture was stirred for 18 hours. To the mixture, a 2 M K_2CO_3 solution (16 mL) was added with 16 mL THF and 64 mL MeOH and stirred for 5 hours. DCM (400 mL) was then added and washed with 100 mL HCl (1M) and water (100 mL). The organic layer was dried with $MgSO_4$ and *in vacuo*. The crude product was purified on a silica gel column (53 g, 3 cm ID x 30 cm) using petroleum ether: ethyl acetate (4:1) to yield **2-13** as a clear, colorless oil (0.603 g, 6%). ^{1}H NMR (500 MHz, $CDCl_3$): 0.04 and 0.05 (2 singlets, 6H), 0.84-0.98 (m, 12H), 1.23-1.33 (m, 16H), 1.39-1.64 (m, 2H), 2.52-2.57 (m, 1H), 3.70-3.78 (m, 2H); ^{13}C NMR (126 MHz, $CDCl_3$): -5.34, -5.29, 14.3, 18.4, 22.9, 26.0, 27.4, 28.4, 29.5, 29.6, 29.76, 29.79, 29.8, 32.1, 48.3, 64.0, 179.7. IR: 1710 cm^{-1} (s). HRLSIMS: Calcd for $C_{19}H_{39}O_3Si^+$ [M-H+Na^+]: 366.2566 Found: 366.2545.

2-(*tert*-Butyl dimethylsilanyloxymethyl)-octadec-9-enoic acid (**2-15**). To a stirred solution under a dry ice and ethanol bath of THF (180 mL) and disopropylamine (8.2 mL) was added butyl lithium (39 mL, 1.6 M). The solution was stirred for 10 minutes at 0ºC. A THF solution (30 mL) of lauric acid (8.26 g, 29.2 mmol) was added dropwise such that the solution was below 0ºC. Upon the full addition the mixture was heated to 35ºC for 1.5 hours while formaldehyde was bubbled in (by a thermal decomposition of 13.8 g of paraformaldehyde). The mixture was then cooled below 10ºC and then 100 mL of 1 M HCl was added. To the mixture 500 mL of THF was added and the aqueous layer was removed. The organic layer was then washed with 3 x 100 mL water dried with 100 mL brine and concentrated *in vacuo*. The crude product was purified on a silica gel column (323 g) using petroleum ether: ethyl acetate (4:1) to yield a clear, colorless oil (0.471 g, 5%). The pure oil was dissolved in 50 mL DCM and imidazole (0.41 g, 4 eq.), *tert*-butylchlorodimethylsilane (0.454 g, 2 eq.) was added. The mixture was stirred for 17 hours. To the mixture, a 2 M K_2CO_3 solution (8 mL) was added with 8 mL THF and 32 mL MeOH and stirred for 7 hours. DCM (450 mL) was then added and washed with 100 mL HCl (1M) and water (200 mL). The organic layer was dried with $MgSO_4$ and *in vacuo*. The crude product was purified on a silica gel column (53 g, 3 cm ID x 30 cm) using petroleum ether: ethyl acetate (4:1) to yield **2-15** as a clear, colorless oil (0.901 g, 7%). ^{1}H NMR (500 MHz, $CDCl_3$): 0.035 and 0.039 (2 singlets, 6H), 0.73-0.98 (m, 12H), 1.21-1.41 (m, 18H), 1.43-1.49 (m, 1H), 1.57-1.62 (m, 1H), 2.00-2.03 (m, 4H), 2.52-2.57 (m, 1H), 3.70-3.78 (m, 2H), 5.29-5.36 (m, 2H); ^{13}C NMR (126 MHz, $CDCl_3$): -5.34, -5.29, 14.3, 18.4, 22.8, 22.9, 25.9, 26.0, 27.36, 27.38, 28.4, 29.3, 29.4, 29.6, 29.67, 29.7,

29.8, 29.9, 30.0, 31.8, 32.1, 48.3, 64.0, 129.9, 130.2, 179.8. IR: 1709 cm^{-1} (s). HRLSIMS: Calcd for $C_{25}H_{50}O_3SiNa^+$ [M+Na^+]: 449.3427 Found: 449.3435.

6-(Tetrahydro-pyran-2-yloxy)-hexanoic acid (2-17). To a stirred solution of caprolactone (20 mL, 0.18 mol) in dioxane (80 mL) under an ice bath 30 mL NaOH (8 M) was added. Allow the solution to warm to room temperature over 2.5 hours and then quenched with 40 mL HCl (6 M). The aqueous solution was extracted with $CHCl_3$ (2 x 100 mL). The organic layer was washed with 100 mL water, dried with Na_2SO_4 and concentrated *in vacuo* to yield an oil (8.83 g) (partial ^{1}H NMR (300 MHz) consistent with **2-16**: 3.61 t, *J*=6.63 Hz; 2.32, t, *J*=6.63 Hz). The crude product and *p*-TsOH (1.27 g, 7.4 mmol) was dissolved in THF (200 mL). While this solution was stirred under an ice bath, DHP (6.4 mL, 0.07 mol) was added. The resulting solution was stirred for four hours and allowed to warm to ambient temperature afterwhich ether (200 mL) was added. The organic solution was then washed with water (2 x 100 mL) and dried with $MgSO_4$. The crude product was purified on a silica gel column (810 g, 5 cm ID x 85 cm) with the eluent DCM:ether (3:1) to yield a clear, colorless oil identified as **2-17** (9.07 g, 22% yield from caprolactone).^{1}H NMR (500 MHz, $CDCl_3$): 1.38-1.83 (m, 14H), 2.34 (t, 2H, *J*=7.4 Hz), 3.35-3.39 (m, 1H), 3.46-3.50 (m, 1H), 3.69-3.74 (m, 1H), 3.82-3.86 (m, 1H), 4.55-4.56 (m, 1H); ^{13}C NMR (125.75 MHz, $CDCl_3$): 19.8, 24.7, 25.7, 26.0, 29.6, 31.0, 34.1, 62.6, 67.5, 99.1, 179.5. HREI: Calcd for $C_{11}H_{19}O_4^+$ [M-H^+]: 215.1283 Found: 215.1278.

8-(Tetrahydro-2H-pyran-2-yloxy)octanoic acid (2-21). To a solution of cyclooctanone (65.42 g, 0.518 mol) and TFA (3 mL) in dichloroethane (2 L), *m*-CPBA (192.8 g, 1.117 mol) was added. The mixture was heated at 70°C for 2 days and then the temperature was lowered to 60°C for an additional 3 days. The mixture was allowed to cool to 50°C

at which point a saturated aqueous Na_2SO_3 solution (500 mL) was added. A solution of concentrated NaOH was added until the pH was about 12, which resulted in a biphasic separation (deep orange, brown aqueous layer and a yellow organic layer). The biphasic mixture was stirred overnight. CH_2Cl_2 (200 mL) was added and acidified with conc. HCl until the pH was 1-2. The aqueous layer was removed and then the organic layer was washed with $NaHCO_3$ (saturated) (3 x 1 L) and 1 M NaOH (3 x 1L) to yield a yellow organic layer. The organic layer was dried over $MgSO_4$ and concentrated *in vacuo* to yield a dark yellow oil (51.22 g) (partial ^{1}H NMR consistent with **2-20**: 4.27, t, *J*=5.89 Hz; 2.38, t, *J*=6.62 Hz). The crude product was dissolved in dioxane (200 mL) and a NaOH solution (300 mL, 2 M) was added with stirring and cooling with an ice bath. The mixture was stirred and warmed to ambient temperature over 5 hours. The solution turned orange and was diluted with CH_2Cl_2 (300 mL). The aqueous layer was isolated and acidified to pH 1-2 with concentrated HCl and then extracted with 100 mL CH_2Cl_2. The organic layer was washed with saturated NaCl (150 mL) and then dried over Na_2SO_4. The organic layer was concentrated *in vacuo* to yield a yellow oil (partial ^{1}H NMR consistent with **2-19**: 3.65, t, *J*=6.62 Hz; 2.35, t, *J*=7.72 Hz). The crude product was dissolved in THF (160 mL) and with stirring under an ice bath, a solution of DHP (32.9 mL, 360 mmol) and *p*-TsOH (3.766 g, 19.8 mmol) in THF (40 mL) was added slowly. The resulting solution was stirred for 3 hours and then diluted with ether (600 mL) and washed with water (3 X 200 mL) and saturated NaCl (200 mL). The organic layer was then dried over Na_2SO_4. The crude product was purified on a silica gel column (380 g, 7 cm ID x 30 cm) with the eluent $CHCl_3$:MeOH (95:5) to yield a clear, colorless oil identified as **2-21** (28.26 g, 22% yield from **2-20**).^{1}H NMR (300 MHz, $CDCl_3$): 1.10-

1.85 (m, 16H), 2.19 (t, 2H, *J*=7.4 Hz), 3.20-3.28 (m, 1H), 3.34-3.41 (m, 1H), 3.54-3.62 (m, 1H), 3.69-3.76 (m, 1H), 4.47 (t, 1H, *J*=3.3 Hz), 10.9 (br s); reported ^{1}H NMR resonances from reference[25]: 1.31-1.85 (m, 17H), 2.30 (t, 2H, *J*=7.4 Hz), 3.31-3.38 (m, 1H), 3.44-3.51 (m, 1H), 3.65-3.73 (m, 1H), 3.80-3.87 (m, 1H), 4.55 (t, 1H, J=4.4 Hz). ^{13}C NMR (75 MHz, $CDCl_3$): 19.8, 24.8, 25.7, 26.2, 29.17, 29.24, 29.8, 30.9, 34.2, 62.5, 67.8, 99.0, 179.9.); reported ^{13}C NMR resonances from reference[25]: 19.6, 24.6, 25.4, 26.0, 28.9, 29.6, 30.7, 34.0, 62.2, 67.5, 98.8, 179.7. IR: 1736 cm^{-1} (s), 1709 cm^{-1} (s). HRLSIMS: Calcd for $C_{13}H_{23}O_4^+$ [M-H$^+$]: 243.1596 Found: 243.1597.

12-(Tetrahydro-2H-pyran-2-yloxy)dodecanoic acid (2-22). To a stirred suspension of 12-hydroxydodecanoic acid (9.180 g, 42.4 mmol) in THF (75 mL) under an ice bath, a solution of DHP (5.4 ml, 59 mmol) and *p*-TsOH (0.263 g, 1.24 mmol) in THF (10 mL) was added dropwise. The resulting solution was stirred for an additional 4.5 hours at 5°C. The solution was diluted with ether (120 mL) and washed with water (3 x 40 mL). The organic layer was dried over $MgSO_4$ and concentrated under reduced pressure to give a crude product. The crude product was purified on a silica gel column (1.1 kg, 10 cm ID x 90 cm) using $CHCl_3$ as eluent to afford a clear colorless oil identified as **2-22** (12.104 g, 95% yield). ^{1}H NMR (300MHz, $CDCl_3$): 1.20-1.90 (m, 25H), 2.31 (t, 2H, *J*=7.7 Hz), 3.31-3.39 (m, 1H), 3.45-3.51 (m, 1H), 3.66-3.74 (m, 1H), 3.81-3.88 (m, 1H), 4.56 (t, 1H, *J*= 3.3 Hz); reported ^{1}H NMR resonances from reference[25]: 1.15-1.41 (14H), 1.42-1.88 (m, 10H), 2.31 (t, 2H, *J*=7.3 Hz), 3.32-3.39 (m, 1H), 3.45-3.52 (m, 1H), 3.66-3.74 (m, 1H), 3.81-3.92 (m, 1H), 4.56 (t, 1H, J=4.5 Hz). ^{13}C NMR (75 MHz, $CDCl_3$): 19.8, 24.9, 25.7, 26.4, 29.2, 29.4, 29.57, 29.65, 29.68, 29.71, 29.9, 30.9, 34.3, 62.5, 67.9, 98.99, 180.02. reported ^{13}C NMR resonances from reference[25]: 19.6, 24.7, 25.5, 26.2, 29.0, 29.2,

29.3, 29.4, 29.5, 29.7, 30.7, 62.3, 98.8, 179.7. IR: 1736 cm^{-1} (s), 1709 cm^{-1} (s). HREIMS: Calcd for $C_{17}H_{31}O_4^+$ [M-H^+]: 299.222 Found: 299.222. Anal. Calcd for $C_{17}H_{32}O_4$: C, 67.96; H, 10.74; O, 21.30. Found: C, 67.82; H, 10.80; O, 21.33.

7.2.2 General Procedure for Solid-Phase Reactions

All reactions were conducted in standard fritted peptide synthesis vessels shaken at ambient temperature. The vessels were sealed under nitrogen during the reaction period. The standard conditions used roughly 0.2 g of Wang resin (Anaspec; 0.75 mmole/g).

A) Ester coupling conditions: A solution of DIC (3 equivalent), DMAP (0.3 equivalent), THP or TBDMS -protected hydroxy acid (3 equivalent), in THF (5 mL) was shaken with resin for three cycles of 5 hours, 5 hours, and overnight duration. The resin was washed between reaction cycles by mixing with solvent for 1 minute, followed by vacuum filtration. Three successive cycles of THF (10mL), ether (10mL), and CH_2Cl_2 (10 mL) were done. With the building blocks of **2-13** and **2-15**, two cycles of eight hours and one overnight (16 hours) and were required to couple them onto resin

B) THP deprotection conditions: A solution of *p*-TsOH (5 mg) in CH_2Cl_2:MeOH (97:3, 10 mL) was shaken with resin for two cycles of 2 hrs each. The resin was washed between reaction cycles by mixing with solvent for 1 minute, followed by vacuum filtration. Three successive cycles of THF (10mL), ether (10mL), and CH_2Cl_2 (10 mL) were done.

C) TBDMS deprotection conditions: Acetic acid (100 uL) was added to TBAF (1 M in THF, 10 mL), and the resin was shaken in this mixture for two cycles of 2 hrs and 2.5 hrs. The resin was washed between reaction cycles by mixing with solvent for 1 minute

with THF (10 mL), followed by a mixture of acetone and 1.9 mM NaI (aq) (95:5 v/v; 10mL) followed by vacuum filtration. The iodide treated resin was then using washed with three successive cycles of 10 mL THF (10mL), ether (10mL), and CH_2Cl_2 (10mL).

D) Cleavage from the support: A solution of HCl in dioxane solution was prepared for the cleavage by gently bubbling gaseous HCl into dioxane under an ice bath for 15 minutes. The HCl concentration varied between 5-7 M as determined by titration with 1.0 M NaOH. The freshly prepared HCl solution, diluted as appropriate to 5 M, was added to the solid support and shaken for 1 hour. The filtrate was collected and then the resin was washed with CH_2Cl_2 (10 mL). The washings were combined and concentrated *in vacuo.* The crude product was purified on a LH-20 column (23 cm x 1.8 cm ID) with $CHCl_3$:MeOH (3:4) as eluent. The samples were collected in 8 mL fractions. The solvents from the fractions were evaporated and the resulting products were examined by NMR to identify the desired product. Products were typically found in fractions 8 -10 dependent somewhat on the size of the product. Normally the first fraction containing the product also contained resin degradation products. These contaminants can be removed from the product by passing a chloroform solution through a short silica column (pipette size) and then washing the product immobilized on the column with about 3 mL of chloroform. The product was then released from the silica column by washing with methanol.

7.2.3 Solid Phase Products

The solid phase products were synthesized according to standard conditions listed in Table 2-4.

Dimer 2-23 was prepared using the standard conditions on Wang resin (0.234 g, 0.18 mmol) to produce **2-23** (14 mg; 0.027 mmole, yield 15%). ^{1}H NMR (500 MHz, $CDCl_3$): 0.86 (t, *J*=7.0 Hz, 3H), 1.20-1.65 (m, 41H), 2.25 (t, *J*=7.5 Hz, 2H), 2.67-2.78 (m, 4H), 3.64 (t, *J*=6.5 Hz, 2H), 4.05 (t, *J*=6.8 Hz, 2H), 5.48 (quintet, *J*=6.0 Hz, 1H). ^{13}C NMR (125.75 MHz, $CDCl_3$): 14.3, 22.9, 25.0, 25.8, 26.1, 28.8, 29.1, 29.3, 29.4, 29.47, 29.52, 29.6, 29.7, 29.80, 29.84, 29.9, 32.1, 32.8, 34.5, 38.1, 38.6, 63.3, 65.3, 66.7, 170.2, 173.0, 173.7. HRLSIMS: Calcd for $NaC_{29}H_{54}O_7^+$ [M+Na^+]: 537.3767 Found: 537.3764.

Dimer 2-24 was prepared using the standard conditions on Wang resin (0.202 g, 0.15 mmol) to produce **2-24** (10 mg; 0.022 mmole, yield 15%). ^{1}H NMR (500 MHz, $CDCl_3$): 0.86 (t, *J*=7 Hz, 3H), 1.19-1.70 (m, 30H), 2.20-2.35 (m, 2H), 2.50-2.60 (m, 4H), 4.08 (t, *J*= 6.8 Hz, 4H), 4.41-4.46 (m, 1H). ^{13}C NMR (125.75 MHz, $CDCl_3$): 14.3, 22.9, 25.0, 25.8, 26.1, 28.6, 28.8, 29.0, 29.2, 29.5, 29.6, 29.7, 29.8, 29.85, 29.86, 32.1, 40.9, 40.9, 65.0, 65.1, 65.3, 172.3. HRLSIMS: Calcd for $NaC_{25}H_{46}O_7^+$ [M+Na^+]: 481.3141 Found: 481.3139.

Dimer 2-25 was prepared using the standard conditions in the sequence on Wang resin (.259 g, .19 mmol) to produce **2-25** (8 mg; 0.022 mmole, yield 12%). ^{1}H NMR (500 MHz, $CDCl_3$): 1.20-1.65 (m, 28H), 2.27 (t, *J*=7.5 Hz, 2H), 2.33 (t, *J*=7.5, 2H), 3.62 (t, *J*=6.6 Hz, 2H), 4.04 (t, *J*=6.6 Hz, 2H). ^{13}C NMR (125.75 MHz, $CDCl_3$): 24.9, 25.1, 25.8, 26.1, 28.8, 29.1, 29.22, 29.24, 29.3, 29.37, 29.45, 29.54, 29.60, 29.63, 29.7, 32.85, 32.91, 33.9, 34.6, 63.2, 64.5, 64.7, 174.2, 177.9. HRLSIMS: Calcd for $NaC_{20}H_{38}O_5^+$ [M+Na^+]: 381.2617 Found: 381.2523.

Tetramer 2-27 was prepared using the standard conditions on Wang resin (0.227 g, 0.17 mmol) to produce **2-27** (66 mg; 0.083 mmole, yield 49%). ^{1}H NMR (500 MHz, $CDCl_3$):

0.85 (t, *J*=6.9 Hz, 3H), 1.20-1.65 (m, 60H), 2.26 (t, *J*=7.5 Hz, 4H), 2.32 (t, *J*=7.5 Hz, 2H), 2.52 (d, *J*=6.6 Hz, 4H), 4.03 (t, *J*=6.7 Hz, 4H), 4.07 (t, *J*=6.7 Hz, 4H), 4.43 (quintet, *J*=6.3 Hz, 1H). ^{13}C NMR (125.75 MHz, $CDCl_3$): 14.3, 22.9, 24.8, 25.05, 25.08, 25.2, 25.88, 25.94, 26.07, 26.11, 28.65, 28.73, 28.77, 28.83, 29.0, 29.06, 29.11, 29.16, 29.20, 29.3, 29.43, 29.44, 29.5, 29.6, 29.7, 29.75, 29.81, 29.82, 32.1, 34.0, 34.5, 34.6, 40.9, 64.47, 64.51, 64.7, 65.0, 65.1, 65.2, 172.09, 172.11, 174.1, 174.2, 179.0, 179.1. HRLSIMS: Calcd for $NaC_{45}H_{82}O_{11}^+$ $[M+Na]^+$: 821.5755 Found: 821.5760. Anal. Calcd for $C_{45}H_{82}O_{11}$: C, 67.62; H, 10.63. Found: C, 71.77; H, 11.09.

Trimer 2-35 was prepared using the standard conditions on Wang resin (0.202 g, 0.15 mmol) to produce **2-35** (44 mg; 0.067 mmole, yield 45%). ^{1}H NMR (500 MHz, $CDCl_3$): 0.84 (t, *J*=7.0, 3H), 1.20-1.40 (m, 40H), 1.51-1.65 (m, 10H), 2.26 (t, *J*=7.5 Hz, 2H), 2.31 (t, *J*=7.5 Hz, 2H), 2.51-2.53 (m, 4H), 4.01-4.08 (m, 6H), 4.40-4.45 (m, 1H). ^{13}C NMR (125.75 MHz, $CDCL_3$): 14.3, 22.9, 24.9, 25.0, 25.86, 25.93, 26.05, 26.08, 28.6, 28.7, 28.76, 28.81, 29.0, 29.1, 29.15, 29.19, 29.22, 29.4, 29.5, 29.55, 29.59, 29.63, 29.68, 29.74, 29.80, 29.81, 32.1, 34.2, 34.5, 40.9, 64.6, 65.0, 65.1, 65.2, 172.07, 172.11, 174.1, 179.4. HRLSIMS: Calcd for $NaC_{37}H_{68}O_9^+$: 679.4761 Found: 679.4781.

Tetramer 2-36 was prepared using the standard conditions on Wang resin (0.22 g, 0.50 mmol) to produce **2-36** (3.7 mg; .015 mmole, yield 3%). ^{1}H NMR (500 MHz, $CDCl_3$): 0.86 (t, *J*=7.0 Hz, 3H), 1.24-1.72 (overlapping signals, 60H), 2.25-2.69 (m, 8H), 4.03, 4.04, and 4.08 (overlapping t, *J*=6.7 Hz each, 8H), 4.40-4.46 (m, 1H). ^{13}C NMR (125.75 MHz, $CDCl_3$): 14.3, 22.9, 24.9, 25.07, 25.12, 25.2, 25.91, 25.98, 26.10, 26.12, 28.70, 28.77, 28.81, 28.86, 29.06, 29.11, 29.20, 29.23, 29.38, 29.40, 29.45, 29.56, 29.63, 29.7, 29.8, 29.85, 29.93, 31.1, 32.1, 33.65, 33.67, 34.5, 34.6, 40.9, 64.6, 64.7, 65.0, 65.1, 65.3,

172.11, 172.15, 174.1. HRLSIMS: Calcd for $NaC_{45}H_{82}O_{11}^{+}$ [M+Na^{+}]: 821.5755 Found: 821.5766.

Tetramer 2-38 was prepared using the standard conditions on Wang resin (0.319 g, 0.24 mmol) to produce **2-38** (12 mg; 0.019 mmole, yield 8%). ^{1}H NMR (500 MHz, $CDCl_3$): 0.86 (t, *J*=7.0 Hz, 3H), 1.20-1.70 (m, 50H), 2.20-2.35 (overlapping signals, 10H), 2.5 (d, 4H), 4.04 and 4.08 (overlapping t, *J*=6.5 Hz, 8H), 4.42-4.46 (m, 1H). ^{13}C NMR (125.75 MHz, $CDCl_3$): 14.3, 22.9, 24.8, 25.08, 25.13, 25.91, 25.97, 26.1, 28.69, 28.77, 28.79, 29.06, 29.09, 29.12, 29.2, 29.5, 29.6, 29.7, 29.79, 29.86, 29.94, 32.1, 33.6, 34.5, 34.6, 40.9, 64.5, 64.6, 65.0, 65.1, 65.3, 172.1, 174.1, 174.2. HRLSIMS: Calcd for $NaC_{41}H_{74}O_{11}^{+}$ [M+Na^{+}]: 765.5129 Found: 765.5121.

Trimer 2-39 was prepared using the standard conditions in the sequence on Wang resin (.225 g, 0.17 mmol) to produce **2-39** (19 mg; 0.038 mmole, yield 23%). ^{1}H NMR (500 MHz, $CDCl_3$): 1.20-1.40 (m, 26H), 1.50-1.70 (m, 12H), 2.25-2.32 (m, 6H), 3.61 (t, *J*=6.6 Hz, 2H), 4.03 (t, *J*=6.6 Hz, 4H). ^{13}C NMR (125.75 MHz, $CDCl_3$): 24.9, 25.1, 25.2, 25.7, 26.0, 26.1, 28.79, 28.84, 29.08, 29.15, 29.2, 29.28, 29.34, 29.42, 29.44, 29.6, 29.7, 32.8, 34.57, 34.59, 63.2, 64.5, 64.7, 174.20, 174.23, 174.3, 178.9. HRLSIMS: Calcd for $NaC_{28}H_{52}O_{7}^{+}$ [M+Na^{+}]: 523.3611 Found: 523.3606.

Tetramer 2-48 was prepared using the standard conditions on Wang resin (0.304 g, .228 mmol) to produce **2-48** (67 mg; 0.084 mmole, yield 37%). ^{1}H NMR (300 MHz, $CDCl_3$): 0.84 (t, *J*=6.6 Hz, 3H), 1.10-1.68 (m, 61H), 2.15-2.35 (m, 6H), 2.60-2.80 (m, 4H), 3.50-3.65 (m, 2H), 3.95-4.10 (m, 6H), 5.46 (quintet, J=5.9 Hz, 1H), 5.2 (br s, 1H). ^{13}C NMR (125.75 MHz, $CDCl_3$): 29.1, 29.18, 29.21, 29.23, 29.3, 29.36, 29.41, 29.50, 29.55, 29.58, 29.6, 29.68, 29.75, 29.79, 29.80, 31.02, 31.06, 32.07, 32.69, 34.2, 34.4, 34.43, 34.52,

34.55, 38.2, 38.4, 38.5, 38.6, 45.3, 63.0, 63.1, 64.5, 64.53, 64.6, 65.2, 66.8, 66.9, 170.2, 172.9, 173.0, 174.1, 174.2, 174.3, 174.4. HRLSIMS: Calcd for $NaC_{45}H_{82}O_{11}^{+}$ [M+Na^{+}]: 821.5755 Found: 821.5745.

Tetramer 3-1 was prepared using the standard conditions on Wang resin (0.23 g, 0.17 mmol) to produce **3-1** (18 mg; 0.023 mmole, yield 13%). ^{1}H NMR (500 MHz, $CDCl_3$): 0.85 (t, *J*=7.0 Hz, 3H), 1.20-1.70 (m, 56H), 2.26, 2.27, and 2.32 (overlapping t, *J*=7.5 Hz, 6H), 2.50-2.53 (m, 4H), 4.03, 4.075 and 4.078 (overlapping t, *J*=6.7 Hz, 8H), 4.40-4.46 (m, 1H). ^{13}C NMR (125.75 MHz, $CDCl_3$): 14.3, 22.9, 24.8, 25.1, 25.2, 25.9, 25.96, 26.08, 26.13, 28.68, 28.75, 28.8, 28.9, 29.05, 29.07, 29.1, 29.2, 29.36, 29.43, 29.45, 29.5, 29.6, 29.70, 29.72, 32.1, 34.0, 34.5, 34.6, 40.9, 64.5, 64.7, 65.0, 65.1, 65.2, 172.10, 172.13, 174.2, 174.2, 178.7. HRLSIMS: Calcd for $NaC_{43}H_{78}O_{11}^{+}$ [M+Na^{+}]: 793.5442 Found: 793.5451.

Tetramer 3-2 was prepared using the standard conditions on Wang resin (0.20 g, 0.20 mmol) to produce **3-2** (63.1 mg; 0.076 mmole, yield 38%). ^{1}H NMR (500 MHz, $CDCl_3$): 0.85 (t, *J*=7.0 Hz, 3H), 1.20-1.70 (m, 64H), 2.253, 2.26, and 2.31 (overlapping t, *J*=7.5 Hz each, 6H), 2.50-2.53 (m, 4H), 4.02, 4.066, and 4.069 (overlapping t, *J*=6.7 Hz each, *J*=1.0 Hz, 8H), 4.40-4.46 (m, 1H). ^{13}C NMR (125.75 MHz, $CDCl_3$): 14.3, 22.9, 24.8, 25.0, 25.2, 25.86, 25.93, 26.06, 26.10, 28.65, 28.73, 28.77, 28.83, 29.02, 29.05, 29.11, 29.15, 29.3, 29.4, 29.5, 29.6, 29.67, 29.68, 29.75, 29.82, 29.84, 29.86, 32.1, 34.1, 34.5, 34.6, 40.9, 64.5, 64.7, 65.0, 65.1, 65.2, 172.08, 172.10, 174.1, 174.2, 179.1. HRLSIMS: Calcd for $NaC_{47}H_{86}O_{11}^{+}$ [M+Na^{+}]: 849.6068 Found: 849.6085.

Tetramer 3-3 was prepared using the standard conditions on Wang resin (0.20 g, 0.21 mmol) to produce **3-3** (58.7 mg; 0.071 mmole, yield 34%). ^{1}H NMR (500 MHz, $CDCl_3$):

0.86 (t, *J*=7.0 Hz, 3H), 1.18-1.70 (m, 76H), 2.26, 2.27, and 2.32 (overlapping t, *J*=7.5 Hz, 6H), 2.51-2.53 (m, 4H), 4.03 (t, *J*=6.7 Hz, 4H), 4.08 (t, *J*=6.7 Hz, 4H), 4.40-4.46 (m, 1H). ^{13}C NMR (125.75 MHz, $CDCl_3$): 14.3, 22.9, 24.8, 25.1, 25.2, 25.9, 25.96, 26.09, 26.13, 28.69, 28.76, 28.80, 28.86, 29.06, 29.08, 29.14, 29.19, 29.23, 29.4, 29.5, 29.57, 29.63, 29.70, 29.72, 29.79, 29.88, 29.91, 32.1, 33.9, 34.5, 34.6, 40.9, 64.5, 64.7, 65.0, 65.1, 65.3, 172.11, 172.14, 174.17, 174.23, 178.1. HRLSIMS: Calcd for $NaC_{49}H_{90}O_{11}^+$ [M+Na^+]: 877.6381 Found: 877.6374.

Tetramer 3-4 was prepared using the standard conditions on Wang resin (0.23 g, 0.53 mmol) to produce **3-4** (6 mg; 7.5 μmole, yield 1%). ^{1}H NMR (500 MHz, $CDCl_3$): 0.86 (t, *J*=7.0 Hz, 3H), 1.22-1.72 (overlapping signals, 58H), 2.265 and 2.267 (overlapping t, *J*=7.5 Hz each, 4H), 2.33 (t, *J*=7.5 Hz, 2H), 2.50-2.57 (m, 4H), 4.030 and 4.032 (overlapping t, *J*=6.7 Hz each, 4H), 4.08 (t, *J*=6.8 Hz, 4H), 4.40-4.46 (m, 1H). ^{13}C NMR (125.75 MHz, $CDCl_3$): 14.3, 22.9, 24.8, 25.07, 25.10, 25.11, 25.9, 25.96, 26.09, 28.6, 28.69, 28.76, 28.79, 29.06, 29.09, 29.13, 29.18, 29.22, 29.44, 29.48, 29.6, 29.72, 29.78, 29.8, 29.9, 32.1, 33.9, 34.51, 34.54, 40.9, 64.5, 64.6, 65.0, 65.1, 65.3, 172.11, 172.14, 174.10, 174.17, 177.96. HRLSIMS: Calcd for $NaC_{45}H_{82}O_{11}^+$ [M+Na^+]: 821.5755 Found: 821.5753.

Tetramer 3-7 was prepared using the standard conditions on Wang resin (0.242 g, 0.55 mmol) to produce **3-7** (39 mg; 0.13 mmole, yield 24%). ^{1}H NMR (500 MHz, $CDCl_3$): 0.85 (t, *J*=7.0 Hz, 3H), 1.22-1.70 (m, 70H), 2.25 and 2.30 (overlapping t, J=7.5 Hz each, 6H), 2.50-2.57 (m, 4H), 4.02 and 4.07 (overlapping t, *J*=6.8 Hz,, 8H), 4.40-4.45 (m, 1H). ^{13}C NMR (125.75 MHz, $CDCl_3$): 14.3, 22.9, 24.9, 25.2, 26.06, 26.11, 28.7, 28.8, 29.2, 29.3, 29.41, 29.43, 29.52, 29.57, 29.60, 29.65, 29.67, 29.68, 29.75, 29.80, 29.82, 32.1,

34.1, 34.6, 40.9, 64.6, 65.0, 65.20, 65.21, 172.1, 174.2, 179.2. HRLSIMS: Calcd for $NaC_{53}H_{98}O_{11}^{+}$ [M+Na^{+}]: 933.7007 Found: 933.7019.

Tetramer 3-8 was prepared using the standard conditions, on Wang resin (0.24 g, 0.54 mmol) to produce **3-8** (27 mg; .097 mmole, yield 18%). ^{1}H NMR (500 MHz, $CDCl_3$): 0.85 (t, *J*=7.0 Hz, 3H), 1.23-1.70 (overlapping signals, 60H), 2.261, 2.264, and 2.32 (overlapping t, *J*=7.5 Hz each, 6H), 2.51-2.58 (m, 4H), 4.03 and 4.08 (overlapping t, *J*=6.7 Hz each, 8H), 4.40-4.46 (m, 1H). ^{13}C NMR (125.75 MHz, $CDCl_3$): 14.3, 22.9, 24.9, 25.1, 25.2, 25.9, 26.08, 26.13, 28.68, 28.75, 28.85, 29.05, 29.18, 29.26, 29.36, 29.43, 29.45, 29.54, 29.58, 29.63, 29.66, 29.70, 29.77, 29.82, 29.84, 32.1, 34.1, 34.5, 34.6, 40.9, 64.6, 64.7, 65.0, 65.1, 65.2, 172.09, 172.11, 174.14, 174.3, 179.0. HRLSIMS: Calcd for $NaC_{49}H_{90}O_{11}^{+}$ [M+Na^{+}]: 877.6381 Found: 877.6384.

Tetramer 3-9 was prepared using the standard conditions on Wang resin (0.305 g, 0.23 mmol) to produce **3-9** (17 mg; 0.020 mmole, yield 9%). ^{1}H NMR (500 MHz, $CDCl_3$): 0.85 (t, *J*=6.8 Hz, 3H), 1.20-1.63 (m, 62H), 2.26 and 2.31 (overlapping t, *J*=7.5 Hz each, 4H), 2.49-2.56 (m, 4H), 4.02 and 4.07 (overlapping t, *J*=6.8 Hz, 8H), 4.40-4.46 (m, 1H). ^{13}C NMR (125.75 MHz, $CDCl_3$): 14.3, 22.9, 24.8, 24.9, 25.2, 25.9, 26.07, 26.12, 28.73, 28.78, 28.8, 29.06, 29.1, 29.21, 29.25, 29.34, 29.41, 29.44, 29.53, 29.58, 29.61, 29.66, 29.68, 29.69, 29.76, 29.81, 29.82, 32.1, 34.06, 34.13, 34.51, 34.58, 34.60, 40.9, 64.5, 64.6, 65.0, 65.21, 65.22, 172.2, 174.22, 174.3, 179.1, 179.2. HRLSIMS: Calcd for $NaC_{49}H_{90}O_{11}^{+}$ [M+Na^{+}]: 877.6381 Found: 877.6382.

Pentamer 3-11 was prepared using the standard conditions on Wang resin (0.214 g, 0.16 mmol) to produce **3-11** (11.3 mg; 13.3 μmole, yield 8%). ^{1}H NMR (500 MHz, $CDCl_3$): 0.86 (t, *J*=7.0 Hz, 3H), 1.24-1.68 (overlapping signals, 52H), 2.25-2.37 (m, 8H), 2.52-

2.53 (m, 4H), 4.01-4.11 (m, 10H), 4.40-4.46 (m, 1H). ^{13}C NMR (125.75 MHz, $CDCl_3$): 14.3, 22.9, 24.1, 24.4, 24.5, 24.6, 24.7, 24.8, 25.1, 25.5, 25.5, 25.6, 25.69, 25.72, 25.75, 25.82, 25.90, 25.94, 25.97, 26.1, 28.41, 28.45, 28.55, 28.68, 28.76, 28.96, 29.07, 29.1, 29.2, 29.4, 29.6, 29.7, 29.78, 29.84, 29.85, 32.1, 33.8, 33.9, 34.4, 34.5, 40.9, 41.0, 64.2, 64.3, 64.4, 64.6, 64.7, 64.8, 65.0, 65.1, 65.3, 172.05, 172.1, 172.2, 173.8, 173.8, 173.9, 174.1, 174.2, 177.8. HRLSIMS: Calcd for $NaC_{45}H_{80}O_{13}^+$ [M+Na^+]: 851.5497 Found: 851.5481.

Tetramer 3-12 was prepared using the standard conditions on Wang resin (0.105 g, 0.11 mmol) to produce **3-12** (64 mg , 89.8 μmole, yield 81%). ^{1}H NMR (500 MHz, $CDCl_3$): 0.86 (t, *J*=7.0 Hz, 3H), 1.12-1.80 (overlapping signals, 51H), 2.25-2.45 (m, 8H), 2.52-2.58 (m, 1H), 3.71-3.90 (m, 2H), 4.01-4.2 (overlapping signals, 8H). ^{13}C NMR (125.75 MHz, $CDCl_3$): 13.9, 14.3, 20.0, 22.9, 24.2, 24.9, 25.0, 25.08, 25.12, 25.2, 25.8, 25.9, 26.0, 26.1, 26.6, 27.2, 27.5, 28.5, 28.75, 28.77, 28.8, 28.9, 29.0, 29.1, 29.17, 29.20, 29.24, 29.37, 29.47, 29.54, 29.65, 29.71, 29.75, 29.78, 29.80, 29.81, 29.92, 31.1, 32.1, 32.9, 33.9, 34.3, 34.5, 34.55, 34.6, 45.2, 47.8, 59.2, 63.4, 64.50, 64.53, 64.7, 64.9, 173.7, 174.18, 174.22, 175.86, 177.5. HRLSIMS: Calcd for $NaC_{41}H_{76}O_9^+$ [M+Na^+]: 735.5387 Found: 735.5374.

Tetramer 3-14 was prepared using the standard conditions, on Wang resin (0.105 g, 1.1 mmol) to produce **3-14** (2 mg, 3 μmole, yield 0.2%). ^{1}H NMR (500 MHz, $CDCl_3$): 0.86 (t, *J*=7.0 Hz, 3H), 1.12-1.80 (overlapping signals, 66H), 1.99 (q, 3H), 2.25-2.35 (overlapping signals, 8H), 4.02-4.05 (overlapping signals, 6H), 5.31-5.33 (overlapping signals, 2H). ^{13}C NMR (125.75 MHz, $CDCl_3$): 14.3, 22.9, 24.8, 25.1, 25.2, 26.0, 26.1, 26.6, 27.4, 27.5, 28.8, 28.9, 29.08, 29.12, 29.24, 29.34, 29.37, 29.40, 29.46, 29.47, 29.55,

29.65, 29.71, 29.74, 29.92, 30.0, 31.1, 32.1, 33.7, 34.55, 34.61, 64.49, 64.54, 64.7, 64.9, 96.4, 130.0, 130.2, 174.18, 174.22, 174.3. HRLSIMS: Calcd for $NaC_{46}H_{84}O_8^+$ [M+Na^+]: 787.6064 Found: 787.6042.

Pentamer 3-15 was prepared using the standard conditions on Wang resin (0.227 g, 0.17 mmol) to produce **3-15** (64 mg; 0.068 mmole, yield 40%). ^{1}H NMR (500 MHz, $CDCl_3$): 0.82 (t, *J*=6.5 Hz, 3H), 1.10-1.70 (m, 68H), 2.15-2.35 (m, 8H), 2.65 (d, *J*= 6.2 Hz, 4H), 3.58 (t, *J*=6.4 Hz, 2H), 3.90-4.10 (m, 8H), 5.45 (quintet, *J*=6.1 Hz, 1H), 5.5 (br s, 1H). ^{13}C NMR (125.75 MHz, $CDCl_3$): 14.2, 22.8, 24.73, 24.88, 24.94, 25.00, 25.03, 25.1, 25.7, 25.8, 25.9, 26.0, 26.1, 26.5, 28.4, 28.6, 28.7, 28.7, 28.8, 28.96, 29.03, 29.06, 29.09, 29.15, 29.20, 29.3, 29.4, 29.46, 29.54, 29.60, 29.64, 29.70, 29.74, 29.8, 31.0, 32.0, 32.7, 34.0, 34.1, 34.3, 34.4, 34.5, 38.6, 45.25, 51.6, 63.0, 64.5, 64.6, 65.0, 65.1, 66.9, 170.08, 170.10, 172.7, 174.1, 174.2, 178.5. HRLSIMS: Calcd for $NaC_{53}H_{96}O_{13}^+$ [M+Na^+]: 963.6749 Found: 963.6765.

Pentamer 3-16 was prepared using the standard conditions on Wang resin (0.222 g, 0.17 mmol) to produce **3-16** (6.7 mg; 6.6 μmole, yield 4%). ^{1}H NMR (500 MHz, $CDCl_3$): 0.86 (t, *J*=7.0 Hz, 12H), 1.12-1.71 (overlapping signals, 153H), 2.25-2.34 (m, 10H), 2.52-2.54 (m, 4H), 2.67-2.80 (m, 2H), 4.01-4.3 (overlapping signals, 14H), 4.40-4.45 (m, 1H). ^{13}C NMR (125.75 MHz, $CDCl_3$): 14.3, 22.9, 24.8, 25.0, 25.09, 25.14, 25.21, 25.76, 25.85, 25.92, 26.0, 26.10, 26.14, 26.6, 27.2, 28.5, 28.70, 28.74, 28.77, 28.81, 28.87, 28.92, 28.98, 29.05, 29.07, 29.15, 29.20, 29.24, 29.30, 29.36, 29.46, 29.57, 29.60, 29.64, 29.67, 29.71, 29.73, 29.80, 29.85, 29.86, 31.1, 32.1, 32.8, 33.7, 34.27, 34.32, 34.5, 34.6, 34.7, 40.9, 44.6, 45.2, 63.2, 64.49, 64.53, 64.62, 64.7, 65.03, 65.13, 65.3, 172.1, 172.2, 173.7, 174.2,

174.6, 176.2. HRLSIMS: Calcd for $NaC_{45}H_{82}O_{11}^{+}$ [M+Na^{+}]: 1033.7531 Found: 1033.7584.

Pentamer 3-17 was prepared using the standard conditions on Wang resin (0.232 g, 0.17 mmol) to produce **3-17** (13.5 mg; .015 mmole, yield 7%). ^{1}H NMR (500 MHz, $CDCl_3$): 0.85 (t, *J*=7.0 Hz, 6H), 1.22-1.71 (overlapping signals, 80H), 1.96-2.00 (overlapping signals, 4H), 2.25-2.34 (m, 7H), 2.52-2.54 (m, 4H), 2.6-2.8 (m, 1H), 4.01-4.09 (overlapping signals, 8H), 4.16-4.23 (m, 2H), 4.40-4.45 (m, 1H), 5.29-5.35 (m, 1H). ^{13}C NMR (125.75 MHz, $CDCl_3$): 14.3, 22.9, 24.8, 25.0, 25.1, 25.2, 25.9, 25.96, 26.09, 26.14, 26.56, 27.2, 27.4, 27.4, 28.5, 28.7, 28.76, 28.80, 28.86, 28.99, 29.06, 29.08, 29.15, 29.19, 29.23, 29.29, 29.36, 29.45, 29.47, 29.53, 29.55, 29.57, 29.64, 29.71, 29.78, 29.84, 29.85, 29.98, 31.1, 32.1, 34.0, 34.29, 34.37, 34.5, 34.60 34.2, 40.9, 44.8, 45.4, 64.4, 64.5, 64.6, 64.7, 65.0, 65.1, 65.3, 129.9b, 130.3, 172.11, 172.13, 173.8, 174.16, 174.23, 174.5, HRLSIMS: Calcd for $NaC_{64}H_{116}O_{13}^{+}$ [M+Na^{+}]: 1115.8314 Found: 1115.8287.

Pentamer 5-1 was prepared using the standard conditions on Wang resin (0.203 g, 0.205 mmol) to produce **5-1** (6.2 mg; 6.0 µmol, 5.8%). ^{1}H NMR (500 MHz, CD_2Cl_2): 0.88 (t, 6*H*), 1.00-1.71 (m, 77*H*), 2.25-2.29 (m, 6*H*), 2.47-2.53 (m, 4*H*), 3.1-3.65 (m, 2*H*) 4.00-4.10 (m, 8H), 4.39-4.42 (m, 1H), 6.50-7.80 (m, 5H). ^{13}C NMR (125.75 MHz, CD_2Cl_2): 14.5, 14.6, 23.3, 25.5, 26.27, 26.34, 26.5, 26.9, 28.9, 29.06, 29.14, 29.25, 29.43, 29.54, 29.8, 29.9, 30.1, 30.2, 30.3, 30.4, 30.6, 31.2, 31.4, 32.5, 34.8, 41.4, 45.6, 53.6, 53.8, 54.0, 54.2, 54.4, 60.8,b64.9, 65.4, 65.5, 172.4, 174.3, 176.1. MALDIMS: Calcd for $NaC_{56}H_{92}N_2O_{12}^{+}$ [M+Na^{+}]: 1007.65 Found: 1007.68.

7.2.4 Vesicle preparation

The general procedure for vesicle preparation and the HPTS fluorescence assay has been described elsewhere[83] and our procedure employed minor modifications. A chloroform solution containing PC:PA:cholesterol (8:1:1 mole ratio) was dried *in vacuo* and then left on the vacuum line overnight. The approximately 60 mg lipid film was hydrated with 1 mL of internal buffer solution (9.9 μM HPTS, 10.1 mM Na_3PO_4, 74.7 mM Na_2SO_4, pH adjusted to 6.4 using H_3PO_4) and transferred into a small test tube. The suspension was frozen under liquid nitrogen and subsequently thawed at room temperature over ten minutes. This cycle was repeated three times. The mixture was then equilibrated in an ice bath and sonicated with a 13 mm tip probe (Heat Systems) for 20 seconds with 2 second pulses (at 50% duty cycle and 20% power output), the sonicator was switched off for 30 seconds and the sonication cycle was repeated until a total sonication time of two minutes was reached. The liposomes were then allowed to anneal overnight. The vesicle solution was then sized 19 times through a 400 nm polycarbonate nucleopore filter using a LiposoFast membrane extrusion apparatus (Avestin) and purified using an external buffer solution (10.1 mM Na_3PO_4, 74.7 mM Na_2SO_4, pH adjusted to 6.4 using H_3PO_4) equilibrated PD-10 Sephadex G-25 column. The first three cloudy drops were discarded but thereafter the cloudy fraction was collected and diluted to 5.00 mL using the external buffer solution. A typical preparation of this vesicle stock solution contained 340 nm diameter vesicles (Nicomp dynamic light scattering) and a lipid concentration of typically 7 mg/mL as determined by the Barlett assay.[2,58,98,99] The vesicle solution was used within 24 hours of preparation.

7.2.5 HPTS Ion Transport Assay – General Method

In a fluorimetric cell was added a magnetic stir bar, 2.00 mL of the external buffer solution, 100 μL of the stock vesicle solution and 30 μL of a 0-4.3 mM MeOH solution of the oligoester compound. HPTS emission was monitored at 510 nm and excitation wavelengths of 403 and 460 nm were used concurrently. Raman emission artifacts were not an issue based on the examination of fluorescence spectra of vesicles made without the HPTS dye. After a 30 second equilibration time, 50 μL of 0.5 M NaOH was added (time = zero) through an injector port. After about 500 seconds, the vesicles were lysed with a 50 μL 5% Triton® X-100 solution. The data was imported into a Microsoft Excel worksheet and all data after 100 seconds from the introduction of NaOH was ignored. The relative intensity of E_{403nm}/ E_{460nm} (F) was calculated. The adjusted mean time was determined from the difference of the actual time and about 60-100 seconds (t_o) after the NaOH injection. The extent of transport was calculated using $(F_i-F_o)/(F_f-F_o)$; F is the relative emission intensity at time i, F_o is the relative emission intensity at t_o, F_f is the relative emission intensity when vesicles are lysed. The extent of transport is plotted against time and the slope of the resulting line was the rate constant for the particular concentration tested. The error in the rates assessed from duplicates was ± 20% within one batch of vesicles.

Table 7-1. Summary of all transport data (1).

Tr	$[Tr]_{Bulk}$ (μM)	Tr/lipid mol %	k (x 10^4 s^{-1})	k adjusted for MeOH leakage (x 10^4 s^{-1})	$k_{32\ \mu M}$ (x 10^4 s^{-1})	S.D.
1-18	31.6	3.5	23.0	22.5	23.3	4.7
1-18	9.9	1.1	3.8	3.3	11.2	2.2
1-18	9.0	1.0	4.3	3.8	14.0	2.8
2-24	66.0	7.3	54.0	53.5	26.4	5.3
2-24	6.6	0.7	6.9	6.4	31.5	6.3
2-24	1.4	0.2	4.7	4.2	96.5	19.3
2-25	38.9	4.3	0.48	0.0	0.5	0.1
2-25	75.0	8.3	1	0.5	0.7	0.1
2-25	75.0	8.3	0.7	0.2	0.6	0.1
2-25	75.0	8.3	1.1	0.6	0.8	0.2
2-27	8.4	2.0	3.6	1.0	6.4	1.3
2-27	21.0	4.6	2.8	1.0	3.3	0.7
2-27	21.0	4.9	3.7	2.8	5.2	1.0
2-27	21.0	4.9	4.8	3.9	6.9	1.4
2-27	21.0	4.9	4.8	3.9	6.9	1.4
2-27	21.0	4.9	3.9	1.6	4.7	0.9
2-27	21.0	4.9	4.5	2.2	5.7	1.1
2-27	21.0	4.9	3.8	1.5	4.6	0.9
2-27	21.0	4.9	5.2	2.6	6.6	1.3
2-27	31.5	6.8	9.5	7.7	9.6	1.9
2-27	53.0	7.5	10.1	7.5	7.1	1.4
2-27	32.0	7.5	9.0	6.4	9.0	1.8
2-35	0.1	0.0	1.3	0.8	283.7	56.7
2-35	9.0	1.0	4.1	3.6	13.3	2.7
2-35	9	1.0	5.1	4.6	16.9	3.4
2-35	9.0	1.0	4	3.5	12.9	2.6
2-35	90.4	10.0	25.0	24.5	9.2	1.8
2-36	18.9	4.1	3.0	1.2	3.8	0.8
2-36	49.4	11.6	3.9	1.6	3.3	0.7
2-38	42.0	9.8	3.2	0.9	3.0	0.6
2-39	26.2	2.9	0.8	0.3	0.9	0.2
2-39	64.2	7.1	2.4	1.9	1.4	0.3
2-39	126.6	14.1	7.5	7.0	2.3	0.5
2-48	14.6	3.4	2.7	0.1	2.8	0.6
2-48	49.4	11.6	1.7	-0.6	1.9	0.4
2-48	49.4	11.6	2.4	0.1	2.4	0.5

Table 7-2. Summary of all transport data (2).

Tr	$[Tr]_{Bulk}$ (μM)	Tr/lipid mol %	k (x 10^4 s^{-1})	k adjusted for MeOH leakage (x 10^4 s^{-1})	$k_{32\ \mu M}$ (x 10^4 s^{-1})	S.D.
3-1	17.0	4.0	4.7	2.1	6.6	1.3
3-1	25.9	5.6	9.1	7.3	10.8	2.2
3-1	26.0	6.1	4.6	2.0	5.1	1.0
3-1	34.0	7.4	6.9	4.5	6.6	1.3
3-1	34.0	7.9	5.1	2.5	5.0	1.0
3-1	43.2	9.4	6.4	4.6	5.2	1.0
3-1	49.4	11.6	6.2	3.9	4.8	1.0
3-2	28.0	6.1	2.9	0.5	3.0	0.6
3-3	14.0	3.1	2.7	0.3	3.1	0.6
3-3	15.4	4.1	4.1	1.4	5.6	1.1
3-3	45.7	10.7	3.5	1.2	3.1	0.6
3-4	24.7	5.4	3.1	1.3	3.5	0.7
3-4	41.2	8.9	3.0	1.2	2.7	0.5
3-7	30.7	7.2	2.2	-0.1	2.2	0.4
3-7	30.7	7.2	2.1	-0.2	2.1	0.4
3-8	49.4	11.6	3.9	1.6	3.3	0.7
3-9	55.6	13.0	1.9	-0.4	2.1	0.4
3-11	16.0	3.8	6.8	4.5	11.3	2.3
3-11	24.7	5.4	3.1	1.3	3.5	0.7
3-11	41.2	8.9	6.4	4.6	5.4	1.1
3-12	18.5	4.0	3.9	2.1	5.4	1.1
3-12	11.2	3.0	5.2	2.6	9.9	2.0
3-12	22.2	5.9	6.9	4.3	8.8	1.8
3-12	36.7	8.0	6.7	4.9	6.1	1.2
3-14	26.7	5.8	2.0	0.2	2.0	0.4
3-14	32.1	7.5	2.0	1.1	2.0	0.4
3-16	17.7	4.1	3.8	2.9	6.2	1.2
3-16	26.5	5.8	2.7	0.9	2.9	0.6
3-16	35.4	7.7	2.6	0.8	2.5	0.5
3-16	44.2	9.6	5.9	4.1	4.8	1.0
3-17	16.9	3.7	2.8	1.0	3.7	0.7
3-17	17.0	4.0	2.5	1.6	3.9	0.8
3-17	25.3	5.5	3.5	1.7	3.9	0.8
3-17	42.2	9.2	4.5	2.7	3.8	0.8
5-1	110.0	10.0	7.0	6.0	2.1	0.4
MeOH				2.3		
MeOH				1.6		
MeOH				3.7		
MeOH				4.0		
MeOH				2.4		
MeOH				2.6		
MeOH				1.8		
MeOH				0.5		
Gram-icidin	3.90E-03		1.9	1.4	11487.7	

7.2.6 HPTS Ion Transport Assay – Equilibration Time

To 20.0 mL of external buffer, 1.00 mL of the vesicle solution was added as well as 300 μL of the methanol solution of Trimer **2-39** (.858 mM) or Tetramer **2-27** (.403 mM)**.** Aliquots of 2.13 mL were taken at intervals of initial, 0.5 hour, 1 hour, 2 hours and 5 hours from this mixture and injected with 50 μL of NaOH (0.5 M) and monitored the fluorescence intensity ratios at 510 nm of the excitation at 403 and 460 nm. Finally the vesicles were lysed with 50 uL 5% Triton® X-100.

7.2.7 Compound Aggregation Studies

Pyrene was purified by column chromatography through a silica gel column and using cyclohexane as the eluent. The high purity of the pyrene was determined by Effie Li using lifetime measurements, where a mono-exponential decay for aqueous solutions is obtained for pure samples. In a low-volume fluorescence cell various volumes of the ion channel solution (mM in concentrations) in methanol (1-30 μL) were injected and methanol was added so that the total volume of methanol was 30 μL. A 5 μL aliquot of a methanoic pyrene solution (0.025 mg/mL) was injected and 0.3 mL external buffer. The solution was vigorously shaken and waited three minutes before measurements were taken. The measurements were recorded at 20.0±0.1 °C with an excitation of 331 nm (slit width of 3 nm) and emission spectra were collected between 365-400 nm (slit width of 1 nm). The spectra were collected with a background subtraction of a solution containing all components excluding pyrene. The method of determining the 1 and 3 band ratio is reported in the literature.[100]

7.2.8 Tryptophan Fluorescence Studies

The vesicles used for addressing the head group orientation were prepared similarly as the HPTS assay vesicles. The exception is that the internal buffer does not contain HPTS, but instead external buffer was used internally. For vesicles with **5-6** entrapped, an external buffer solution with 0.86 mM of **5-6** was used to prepare the vesicles. The vesicles made with entrapped **5-6** were 217 ± 27 nm in diameter while the vesicles without were 254 ± 29 nm in diameter.

The tryptophan chromophore was excited at 288 nm and the emission spectra were collected between 320-400 nm. The excitation and emission slits were open to 4 nm each.

A background scan was collected for a nitrogen purged (for 20 minutes) mixture of 2.3 mL external buffer, 100 µL vesicles (without **5-6**). Acrylamide is injected as a solution of increasing volumes (from 5- 200 µL) from a methanoic solution (1.995 M) using an airtight syringe. The collected background fluorescence data was subtracted from the collected scans from the tryptophan containing data. A dilution factor (V_i (the initial volume)/V_t (total volume)) was applied to the observed initial fluorescence (F_i) by using the equation to yield the corrected initial fluorescence (F_o):

$$F_o = Fi \times V_i/V_t$$

The Stern-Volmer plot is achieved by plotting the ratio of the corrected initial fluorescence (F_o) and the observed fluorescence versus the total quencher concentration:

$$F_o/F = 1 + K_s[Q]$$

For the tryptophan experiments with **5-1**, 10 μL of a methanoic **5-1** solution (8.7 mM) was injected and equilibrated with the vesicles for about 30 seconds before addition of the quencher.

Appendix

PERMISSION REQUEST FORM

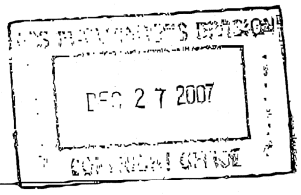

Date: Dec 20, 2007

FROM ~~To~~: Copyright Office
Publications Division
American Chemical Society
1155 Sixteenth Street, N.W.
Washington, DC 20036

FAX: 202-776-8112

TO
~~From~~: Horace Luong
Department of Chemistry
University of Victoria
P.O. Box 3065
Victoria, BC
V8W3V6

Your Phone No. 250-721-7197
Your Fax No. 250-721-7147

I am preparing a paper entitled:
Solid-phase Synthesis of Ion Channels
to appear in a **(circle one)** book, magazine, journal, proceedings, other Ph.D Thesis
entitled:

to be published by: University of Victoria

I would appreciate your permission to use the following ACS material in print and other formats with the understanding that the required ACS copyright credit line will appear with each item and that this permission is for only the requested work listed above:

From ACS journals or magazines (for ACS magazines, also include issue no.):

ACS Publication Title	Issue Date	Vol.	No.	Page(s)	Material to be used*
J.Am.Chem. Soc.	04/15/1999	121	17		figure 1

From ACS books: include ACS book title, series name and number, year, page(s), book editor=s name(s), chapter author's name(s), and material to be used, such as Figs. 2 & 3, full text, etc.*

* If you use more than three figures/tables from any article and/or chapter, the author's permission will also be required.

Questions? Please call Arleen Courtney at (202) 872-4368 or use the FAX number above.

This space is reserved for ACS Copyright Office Use

PERMISSION TO REPRINT IS GRANTED BY THE AMERICAN CHEMICAL SOCIETY

ACS CREDIT LINE REQUIRED. Please follow this sample: Reprinted with permission from (reference citation). Copyright (year) American Chemical Society.

12/3/99

APPROVED BY: *C. Arleen Courtney* 12/28/07
ACS Copyright Office

☐ **If box is checked, author permission is also required. See original article for address.**

1-04 now
1-05

01/03/2008 THU 13:18 [TX/RX NO 7637]

Bibliography

(1) Fyles, T. M. *Chemical Society Reviews* **2007**, *36*, 335-347.
(2) New, R. R. C. *Liposomes: a practical approach*; IRL Press: Oxford, 1990;64-66.
(3) Ashkenasy, N.; Sanchez-Quesada, J.; Bayley, H.; Ghadiri, M. R. *Angewandte Chemie-International Edition* **2005**, *44*, 1401-1404.
(4) Cornell, B. A.; BraachMaksvytis, V. L. B.; King, L. G.; Osman, P. D. J.; Raguse, B.; Wieczorek, L.; Pace, R. J. *Nature* **1997**, *387*, 580-583.
(5) Gu, L. Q.; Braha, O.; Conlan, S.; Cheley, S.; Bayley, H. *Nature* **1999**, *398*, 686-690.
(6) Martin, C. R.; Siwy, Z. S. *Science* **2007**, *317*, 331-332.
(7) Matile, S.; Som, A.; Sorde, N. *Tetrahedron* **2004**, *60*, 6405-6435.
(8) Yamnitz, C. R.; Gokel, G. W. *Chemistry & Biodiversity* **2007**, *4*, 1395-1412.
(9) Doyle, D. A.; Cabral, J. M.; Pfuetzner, R. A.; Kuo, A. L.; Gulbis, J. M.; Cohen, S. L.; Chait, B. T.; MacKinnon, R. *Science* **1998**, *280*, 69-77.
(10) Woolley, G. A.; Wallace, B. A. *Journal of Membrane Biology* **1992**, *129*, 109-136.
(11) Burkhart, B. M.; Gassman, R. M.; Langs, D. A.; Pangborn, W. A.; Duax, W. L.; Pletnev, V. *Peptide Science* **1999**, *51*, 129-144.
(12) MacKinnon, R. *Science (Washington, DC, United States)* **2004**, *306*, 1304-1305.
(13) Zhou, Y.; Morals-Cabral, J. H.; Kaufman, A.; MacKinnon, R. *Nature (London, United Kingdom)* **2001**, *414*, 43-48.
(14) Tabushi, I.; Kuroda, Y.; Yokota, K. *Tetrahedron Letters* **1982**, *23*, 4601-4604.
(15) Tabushi, I.; Yuan, L. C.; Shimokawa, K.; Yokota, K.; Mizutani, T.; Kuroda, Y. *Tetrahedron Letters* **1981**, *22*, 2273-6.
(16) Gokel, G. W.; Carasel, I. A. *Chemical Society Reviews* **2007**, *36*, 378-389.
(17) Koert, U. *Chemie in Unserer Zeit* **1997**, *31*, 20-26.
(18) Sakai, N.; Mareda, J.; Matile, S. *Molecular BioSystems* **2007**, *3*, 658-666.
(19) Sisson, A. L.; Shah, M. R.; Bhosale, S.; Matile, S. *Chemical Society Reviews* **2006**, *35*, 1269-1286.
(20) Fyles, T. M.; Van Straaten-Nijenhuis, W. F. In *Comprehensive Supramolecular Chemistry* Reinhoudt, D. N., Ed.; Elsevier Science: Amsterdam/New York, 1996; Vol. 10, p 53-77.
(21) Gokel, G. W.; Mukhopadhyay, A. *Chemical Society Reviews* **2001**, *30*, 274-286.
(22) Baumann, G.; Mueller, P. *Journal of Supramolecular Structure* **1974**, *2*, 538-57.
(23) Matile, S.; Sakai, N. In *Analytical Methods in Supramolecular Chemistry*; Schalley, C., Ed.; Wiley-VCH: Weinbeim, Germany, 2007, p 391-418.
(24) Kleinsmith, L. J.; Kish, V. M. *Principles of Cell and Molecular Biology*; 2nd ed.; HarperCollins College Publishers: New York, 1995
(25) Hu, C.-W. Doctoral Thesis, University of Victoria, 2002.
(26) Fyles, T. M.; James, T. D.; Kaye, K. C. *Journal of the American Chemical Society* **1993**, *115*, 12315-12321.
(27) Williams, A. J. In *Ion Channels: A Practical Approach*; Ashley, R. H., Ed.; Oxford University Press: USA, 1996.

(28) Venegas, B.; Gonzalez-Damian, J.; Celis, H.; Ortega-Blake, I. *Biophys. J.* **2003**, *85*, 2323-2332.
(29) Hartsel, S. C.; Bolard, J. *Trends Pharmacol. Sci.* **1996**, *17*, 445-449.
(30) Bratjtburg, J.; Powderly, W. G.; Kobayashi, S.; Medoff, G. *Antimicrob. Agents Chemother.* **1990**, *34*, 183-188.
(31) Meyer, C. E.; Reusser, F. *Experientia* **1967**, *23*, 85-6.
(32) Fernandez-Lopez, S.; Kim, H. S.; Choi, E. C.; Delgado, M.; Granja, J. R.; Khasanov, A.; Kraehenbuehl, K.; Long, G.; Weinberger, D. A.; Wilcoxen, K. M.; Ghadiri, M. R. *Nature* **2001**, *414*, 329-329.
(33) Biron, E.; Otis, F.; Meillon, J. C.; Robitaille, M.; Lamothe, J.; Van Hove, P.; Cormier, M. E.; Voyer, N. *Bioorganic & Medicinal Chemistry* **2004**, *12*, 1279-1290.
(34) Leevy, W. M.; Donato, G. M.; Ferdani, R.; Goldman, W. E.; Schlesinger, P. H.; Gokel, G. W. *Journal of the American Chemical Society* **2002**, *124*, 9022-9023.
(35) Gokel, G. W. *Chemical Communications* **2000**, 1-9.
(36) Rostovtseva, T. K.; Bashford, C. L.; Lev, A. A.; Pasternak, C. A. *Journal of Membrane Biology* **1994**, *141*, 83-90.
(37) Jullien, L.; Lehn, J. M. *Journal of Inclusion Phenomena and Molecular Recognition in Chemistry* **1992**, *12*, 55-74.
(38) Jullien, L.; Lehn, J. M. *Tetrahedron Letters* **1988**, *29*, 3803-3806.
(39) Pregel, M. J.; Jullien, L.; Canceill, J.; Lacombe, L.; Lehn, J. M. *Journal of the Chemical Society-Perkin Transactions 2* **1995**, 417-426.
(40) Carmichael, V. E.; Dutton, P. J.; Fyles, T. M.; James, T. D.; Swan, J. A.; Zojaji, M. *Journal of the American Chemical Society* **1989**, *111*, 767-769.
(41) Fyles, T. M.; James, T. D.; Pryhitka, A.; Zojaji, M. *Journal of Organic Chemistry* **1993**, *58*, 7456-7468.
(42) Fyles, T. M.; Kaye, K. C.; Pryhitka, A.; Tweddell, J.; Zojaji, M. *Supramolecular Chemistry* **1994**, *3*, 197-209.
(43) Fyles, T. M.; Loock, D.; vanStraatenNijenhuis, W. F.; Zhou, X. *Journal of Organic Chemistry* **1996**, *61*, 8866-8874.
(44) Sansom, M. S. P. *Progress in Biophysics & Molecular Biology* **1991**, *55*, 139-235.
(45) Hernandez, J. C.; Trafton, J. E.; Gokel, G. W. *Tetrahedron Letters* **1991**, *32*, 6269-6272.
(46) Nakano, A.; Xie, Q. S.; Mallen, J. V.; Echegoyen, L.; Gokel, G. W. *Journal of the American Chemical Society* **1990**, *112*, 1287-1289.
(47) Murillo, O.; Watanabe, S.; Nakano, A.; Gokel, G. W. *Journal of the American Chemical Society* **1995**, *117*, 7665-79.
(48) Gokel, G. W. *Cell Biochemistry and Biophysics* **2001**, *35*, 211-231.
(49) Murray, C. L.; Shabany, H.; Gokel, G. W. *Chemical Communications (Cambridge)* **2000**, 2371-2372.
(50) Leevy, W. M.; Gokel, M. R.; Hughes-Strange, G. B.; Schlesinger, P. H.; Gokel, G. W. *New Journal of Chemistry* **2005**, *29*, 205-209.
(51) Sakai, N.; Majumdar, N.; Matile, S. *Journal of the American Chemical Society* **1999**, *121*, 4294-4295.
(52) Sakai, N.; Brennan, K. C.; Weiss, L. A.; Matile, S. *Journal of the American Chemical Society* **1997**, *119*, 8726-8727.
(53) Sakai, N.; Matile, S. *Chemical Communications* **2003**, 2514-2523.

(54) Sakai, N.; Matile, S. *Journal of Physical Organic Chemistry* **2006**, *19*, 452-460.
(55) Sakai, N.; Mareda, J.; Matile, S. *Accounts of Chemical Research* **2005**, *38*, 79-87.
(56) Litvinchuk, S.; Sorde, N.; Matile, S. *Journal of the American Chemical Society* **2005**, *127*, 9316-9317.
(57) Litvinchuk, S.; Bollot, G.; Mareda, J.; Som, A.; Ronan, D.; Shah, M. R.; Perrottet, P.; Sakai, N.; Matile, S. *Journal of the American Chemical Society* **2004**, *126*, 10067-10075.
(58) Fyles, T. M.; Knoy, R.; Mullen, K.; Sieffert, M. *Langmuir* **2001**, *17*, 6669-6674.
(59) Kobuke, Y.; Ueda, K.; Sokabe, M. *Journal of the American Chemical Society* **1992**, *114*, 7618-7622.
(60) Durkin, J. T.; Koeppe, R. E.; Andersen, O. S. *Journal of Molecular Biology* **1990**, *211*, 221-234.
(61) Bandyopadhyay, P.; Janout, V.; Zhang, L. h.; Regen, S. L. *Journal of the American Chemical Society* **2001**, *123*, 7691-7696.
(62) Bandyopadhyay, P.; Janout, V.; Zhang, L. h.; Sawko, J. A.; Regen, S. L. *Journal of the American Chemical Society* **2000**, *122*, 12888-12889.
(63) Zhang, J.; Jing, B.; Regen, S. L. *Journal of the American Chemical Society* **2003**, *125*, 13984-13987.
(64) Goto, C.; Yamamura, M.; Satake, A.; Kobuke, Y. *Journal of the American Chemical Society* **2001**, *123*, 12152-12159.
(65) Ruiz-Perez, C.; Rodriguez, M. L.; Martin, J. D.; Perez, C.; Morales, P.; Ravelo, J. L. *Acta Crystallographica Section C* **1990**, *46*, 1507-1509.
(66) Perez, C.; Espinola, C. G.; Foces-Foces, C.; Nunez-Coello, P.; Carrasco, H.; Martin, J. D. *Organic Letters* **2000**, *2*, 1185-1188.
(67) Fyles, T. M.; Hu, C. W.; Knoy, R. *Organic Letters* **2001**, *3*, 1335-1337.
(68) Fyles, T. M.; Loock, D.; Zhou, X. *Journal of the American Chemical Society* **1998**, *120*, 2997-3003.
(69) Kuisle, O.; Quinoa, E.; Riguera, R. *Journal of Organic Chemistry* **1999**, *64*, 8063-8075.
(70) Brown, A. R.; Hermkens, P. H. H.; Ottenheijm, H. C. J.; Rees, D. C. *Synlett* **1998**, 817-827.
(71) Fruchtel, J. S.; Jung, G. *Angewandte Chemie-International Edition in English* **1996**, *35*, 17-42.
(72) US6500089, 1965, (Merck & Co., Inc.).
(73) Carpino, L. A.; Han, G. Y. *Journal of Organic Chemistry* **1972**, *37*, 3404-9.
(74) Gong, B.; Lynn, D. G. *Journal of Organic Chemistry* **1990**, *55*, 4763-5.
(75) Boger, D. L.; Yohannes, D. *Journal of Organic Chemistry* **1989**, *54*, 2498-502.
(76) Brown, P.; Eggleston, D. S.; Haltiwanger, R. C.; Jarvest, R. L.; Mensah, L.; O'Hanlon, P. J.; Pope, A. J. *Bioorganic & Medicinal Chemistry Letters* **2001**, *11*, 711-714.
(77) Zervas, L.; Theodoropoulos, D. M. *J. Am. Chem. Soc.* **1956**, *78*, 1359.
(78) Applegate, H. E.; Cimarusti, C. M.; Dolfini, J. E.; Funke, P. T.; Koster, W. H.; Puar, M. S.; Slusarchyk, W. A.; Young, M. G. *Journal of Organic Chemistry* **1979**, *44*, 811-818.
(79) Mohrbacher, R. J.; Ho, W.; Tutwiler, G. F. 78-897971 4132719, 1979, (McNeil Laboratories, Inc., USA).

(80) Liebman, J. F.; Greenberg, A. *Chemical Reviews (Washington, DC, United States)* **1976**, *76*, 311-65.
(81) Dalla Cort, A. *Synthetic Communications* **1990**, *20*, 757-60.
(82) Gottlieb, H. E.; Kotlyar, V.; Nudelman, A. *Journal of Organic Chemistry* **1997**, *62*, 7512-7515.
(83) Sidorov, V.; Kotch, F. W.; Abdrakhmanova, G.; Mizani, R.; Fettinger, J. C.; Davis, J. T. *Journal of the American Chemical Society* **2002**, *124*, 2267-2278.
(84) Fyles, T. M.; Hu, C. W.; Luong, H. *Journal of Organic Chemistry* **2006**, *71*, 8545-8551.
(85) Haugland, R. P.; Spence, M. T. Z. *The Handbook. A Guide to Fluorescent Probes and Labelling Technologies* 10th ed.; Molecular Probes: Eugene, Or, 2005
(86) Kuyper, C. L.; Kuo, J. S.; Mutch, S. A.; Chiu, D. T. *Journal of the American Chemical Society* **2006**, *128*, 3233-3240.
(87) Paula, S.; Deamer, D. W. In *Current Topics in Membranes*; Deamer, D. W., Kleinzeller, A., Fambrough, D. M., Eds.; Academic Press: Burlington, MA, 1999; Vol. 48, p 77.
(88) Dominguez, A.; Fernandez, A.; Gonzalez, N.; Iglesias, E.; Montenegro, L. *Journal of Chemical Education* **1997**, *74*, 1227-1231.
(89) Kaye, K. C. Master's Thesis, University of Victoria, 1991.
(90) Herve, M.; Cybulska, B.; Garybobo, C. M. *European Biophysics Journal with Biophysics Letters* **1985**, *12*, 121-128.
(91) Fyles, T. M.; Hu, C. W. *Journal of Supramolecular Chemistry* **2001**, *1*, 207-215.
(92) Lakowicz, J. R. *Principles of Fluorescence Spectroscopy*; third ed. Singapore, 2006
(93) Kerr, J. M.; Banville, S. C.; Zuckermann, R. N. *J. Am. Chem. Soc.* **1993**, *115*, 2529-2531.
(94) Abel, E.; Maguire, G. E. M.; Meadows, E. S.; Murillo, O.; Jin, T.; Gokel, G. W. *Journal of the American Chemical Society* **1997**, *119*, 9061-9062.
(95) Cooper, A. *Biophysical Chemistry*; Royal Society of Chemistry: Cambridge, 2004;184.
(96) Loock, D. Doctoral Thesis, University of Victoria, 1997.
(97) Wasserman, D.; Garber, J. D.; Meigs, F. M. US 3285953, 1966,
(98) Renkes, T.; Schäfer, H. J.; Siemens, P. M.; Neumann, E. *Angewandte Chemie International Edition* **2000**, *39*, 2512-2516.
(99) Menger, F. M.; Aikens, P. *Angewandte Chemie-International Edition in English* **1992**, *31*, 898-900.
(100) Chang, Y.; Kellermann, M.; Becherer, M.; Hirsch, A.; Bohne, C. *Photochemical & Photobiological Sciences* **2007**, *6*, 525-531.